NTNU – Trondheim
Norwegian University of
Science and Technology

Backcalculation of Plate Loading Tests using PLAXIS 2D and the Hardening Soil Model

Santosh Khanal

Geotechnics and Geohazards
Submission date: June 2013
Supervisor: Steinar Nordal, BAT

Norwegian University of Science and Technology
Department of Civil and Transport Engineering

NORWEGIAN UNIVERSITY OF SCIENCE AND TECHNOLOGY
DEPARTMENT OF CIVIL AND TRANSPORT ENGINEERING

Report Title:	Date: 09/06/2013			
BACKCALCULATION OF PLATE LOADING TESTS USING PLAXIS 2D AND THE HARDENING SOIL MODEL	Number of pages (incl. appendices): 139			
	Master Thesis	√	Project Work	

Name:

Santosh Khanal

Professor in charge/supervisor:

Steinar Nordal

Other external professional contacts/supervisors:

Abstract:
Shallow foundations are extensively used to support structures of all sizes in order to safely transmit the structural load to the ground without exceeding the bearing capacity of the ground and causing excessive settlement. They are typically embedded up to a few meters into the soil profile. While designing foundations, two requirements need to be satisfied: complete failure of the foundation must be avoided with adequate margin of safety (bearing capacity) and relative settlement should be within limits that can be tolerated by superstructure. Foundation is that part of the structure which is in direct contact with soil and involves the footing and the ground influenced by the footing. The master thesis aims to back-calculate the load tests using advanced soil models in PLAXIS 2D in order to gather experience on soil behavior and constitutive models. For this, extensive study of literature with full-scale load tests was carried out. Both tests on clay and sand were the theme interest.

To examine the plate loading tests, three case studies were selected. In this report, the load-settlement responses of vertically loaded footings placed on both sands and clay were analysed using the finite element method. The numerical analysis was performed using PLAXIS 2D. The soil profiles and parameters used in the analysis were based on either in situ tests or laboratory tests. The Hardening Soil model was used as a material model to analyse the soil behavior. Finally, the load-settlement curves obtained from finite element analysis were compared with those from plate-load tests and see whether they are well fitted.

The first case study was on clay till from Sweden. In this case, the back-calculated results showed that c'_{ref} = 11.45 to 14.45 kPa and ϕ = 30^0. The second case was on saprolitic soil from Portugal. In this case, c'_{ref} = 8 to 13 kPa and ϕ = 37^0 to 38^0. The third case was on sand from Texas A&M, USA. In this case, sand shows some varying behavior in stiffness. The stiffness from laboratory tests and back-calculated vary by a factor of 3 to 8. The angle of friction was from 36^0 to 39^0.

Keywords:

1. Shallow foundations
2. Footings
3. Plate loading tests
4. Finite element analysis

NTNU
Fakultet for ingeniørvitenskap og teknologi
Institutt for bygg, anlegg og transport

MASTER DEGREE THESIS

Spring 2013

for

MSc candidate: Santosh Khanal

Backcalculation of plate loading tests using Plaxis 2D and the Hardening Soil Model

Prediction of bearing capacity and settlements of shallow foundations is essential in geotechnical engineering. Shallow foundations may be circular, quadratic or rectangular and placed at the terrain surface or below the terrain surface. The foundations support columns or walls in buildings or other structures. Prediction is in classical soil mechanics based on bearing capacity formulas and a separate settlement calculation. Nowadays the finite element method (FEM) provides an efficient and more refined alternative, but the programs need many input parameters and may be complicated to use. It is importance to collect information on how the parameters should be selected and to gather experience on how the FEM works by comparing predictions to observations.

The aim of the current MSc thesis is to contribute to collecting information and experience on how to best use FEM and a relevant soil model in predicting the behavior of shallow foundations.

For this purpose the candidate shall search for high quality, relevant, well documented plate loading tests with recorded load deformation curves and back calculate selected tests using reported soil data. The study shall be limited to vertically loaded foundations. The FEM program Plaxis and the Hardening Soil Model are to be used.

The selected field tests shall be described and soil data given. It shall be shown how soil parameters are obtained. The field tests are to be simulated in an axisymmetric model on an equivalent circular foundations using Plaxis 2D. The results of the simulations shall be well documented and discussed in view of the selected soil parameters.

Department of Civil an Transport Engineering, NTNU

Trondheim, 2013

Steinar Nordal
Professor

ACKNOWLEDGEMENT

This technical report has been written as a part of the Master in Geotechnics program at NTNU, Trondheim, and was written over a course of 20 weeks from January to June.

I would like to express my gratitude to my advisor, Professor Steinar Nordal, for his worthy guidance, priceless advice, well-built support, suggestions and encouragement throughout the study. As well as sincere appreciation goes to my advisor for his constructive critics.

I would like to express profound appreciation to Professor A. Viana da Fonseca from University of Porto, Portugal for providing me data and journals for my study.

Sincere appreciation goes to NTNU for providing me admission to pursue master degree in Geotechnics and Geohazards.

I would like to express thanks to Mr. Pankaj Baral, Mr. Anup Khanal and Mr. Chhatra Bahadur Basnet for their moral support and encouragement.

Last but not the least; I would like to express deep gratitude to my parents and brothers for their love, care and support during my study at NTNU.

ABSTRACT

Shallow foundations are extensively used to support structures of all sizes in order to safely transmit the structural load to the ground without exceeding the bearing capacity of the ground and causing excessive settlement. They are typically embedded up to a few meters into the soil profile. While designing foundations, two requirements need to be satisfied: complete failure of the foundation must be avoided with adequate margin of safety (bearing capacity) and relative settlement should be within limits that can be tolerated by superstructure. Foundation is that part of the structure which is in direct contact with soil and involves the footing and the ground influenced by the footing. The master thesis aims to back-calculate the load tests using advanced soil models in PLAXIS 2D in order to gather experience on soil behavior and constitutive models. For this, extensive study of literature with full-scale load tests was carried out. Both tests on clay and sand were the theme interest.

To examine the plate-load tests, three case studies were selected. In this report, the load-settlement responses of vertically loaded footings placed on both sands and clay were analysed using the finite element method. The numerical analysis was performed using PLAXIS 2D. The soil profiles and parameters used in the analysis were based on either in situ tests or laboratory tests. The Hardening Soil model was used as a material model to analyse the soil behavior. Finally, the load-settlement curves obtained from finite element analysis were compared with those from plate-load tests and see whether they are well fitted.

The first case study was on clay till from Sweden. In this case, the back-calculated results showed that c'_{ref} = 11.45 to 14.45 kPa and ϕ = 30^0. The second case was in saprolitic soil from Portugal. In this case, c'_{ref} = 8 to 13 kPa and ϕ = 37^0 to 38^0. The third case was on sand from USA. In this case, sand shows some varying behavior in stiffness. The stiffness from laboratory tests and back-calculated vary by a factor of 3 to 8. The angle of friction was from 36^0 to 39^0.

TABLE OF CONTENTS

LIST OF FIGURES

LIST OF TABLES

1 INTRODUCTION

1.1 Background

Due to rapid growth of urbanization, constructions of civil structures are increasing tremendously. For the civil structures, design and analysis of foundation plays a vital role. The bearing capacity calculation of foundations is one of the most interesting problems for geotechnical engineers and researchers. Over the course of many decades, the bearing capacity of footings has been widely investigated both theoretically and experimentally. In addition, the designer must ensure the superstructure does not suffer from excessive displacements.

Different researches have been made in determining ultimate bearing capacity of shallow foundations. The ultimate bearing capacity of shallow strip footings is generally determined by Terzaghi in 1943. In 1948, Terzaghi proposed a well-conceived theory to determine the ultimate bearing capacity of a shallow rough rigid continuous (strip) foundation supported by a homogeneous soil layer extending to a great depth. Terzaghi's equation is an approximate solution which uses the superposition technique to combine the effects of cohesion c, soil weight γ and surcharge q. These contributions are expressed through three factors of bearing capacity, N_c, N_γ and N_q. These bearing capacity factors are functions of angle of internal friction ϕ. Later, assuming a different failure mechanism, Meyerhof obtained approximate solution of shallow and deep foundations. The solution was expressed in the form of bearing capacity factors like Terzaghi and these factors are functions of internal friction ϕ. Nilmar Janbu, the senior Professor at NTNU, also obtained the solution of total foundation pressure expressing the results in the form of bearing capacity factors N_q and N_γ but no N_c term was included in the solution. N_q and N_γ are functions of the shear mobilization $tan\rho$ and the roughness ratio r in the foundation plane.

This master thesis aims to back-calculate the plate load tests using advanced soil models in PLAXIS 2D in order to gather experience on soil behavior and constitutive models. Different relevant reports of investigations and load tests are collected and studied. The appropriate parameters required are identified and extracted to be used in Hardening Soil Model which is the constitutive model used for back-calculation. The plate load tests for shallow foundations on both sand and clay are of interest.

1.2 Objectives of the study

The main objectives of this thesis are listed below:

- To look after extensive literature study and search relevant tests those are suitable for back-calculations. The tests aiming for the bearing capacity and tests focusing on deformations of the plate or footing are of concentration.
- To identify relevant soil profile and soil parameters to be used in Advanced soil model, that is, Hardening Soil Model from field and laboratory tests.

- To back-calculate the tests using PLAXIS 2D.
- To compare the load-settlement curves obtained from PLAXIS 2D with those from plate load tests.

1.3 Thesis outline

The report is composed of five chapters and five appendices.

In chapter 2, the literature review is established. Theory on bearing capacity is described briefly as well as bearing capacity on Janbu's principle is also pointed out. The settlement of shallow foundation on clay and silt, and on sand is also reviewed. The brief description of plate load tests as well as Finite Element method is also carried out.

Chapter 3 contains methodology. In this chapter, the discussion is done on which of the case studies are selected. The PLAXIS software and procedure is described how the analysis is done for each case.

Chapter 4 includes numerical modeling of three case studies. In this chapter, numerical analysis is performed using geological and geotechnical studies of each case, and comparison is done between load-settlement curves obtained numerically with measured curves.

Chapter 5 contains conclusion and recommendation. Finally, appendices are included which consists of some additional soil data for each case study. CD included here contains the work of master thesis.

2 LITERATURE REVIEW

2.1 Theory on Bearing capacity

Foundation is that part of the structure which is in direct contact with soil. Foundation transfers the forces and moments from the super structure to the soil below such that the stresses in soil are within permissible limits and it provides stability against sliding and overturning to the super structure. It is a transition between the super structure and foundation soil. The job of a geotechnical engineer is to ensure that both foundation and soil below are safe against failure and do not experience excessive settlement.

The bearing capacity calculation of foundations is one of the most interesting problems for geotechnical engineers and researchers. Over the course of many decades, the bearing capacity of footings has been widely investigated both theoretically and experimentally. While designing foundations, engineers and researchers must satisfy two requirements, such as, complete failure of the foundation must be avoided with adequate margin of safety and relative settlement should be within limits that can be tolerated by superstructure. The ultimate bearing capacity of a foundation is defined as the maximum load that the ground can sustain (general shear failure); where the load-settlement curve does not exhibit a peak load, the bearing capacity is taken as the load at which the curve passes into a steep and fairly straight tangent (local shear failure) Terzaghi (1943) (Meyerhof 1951).

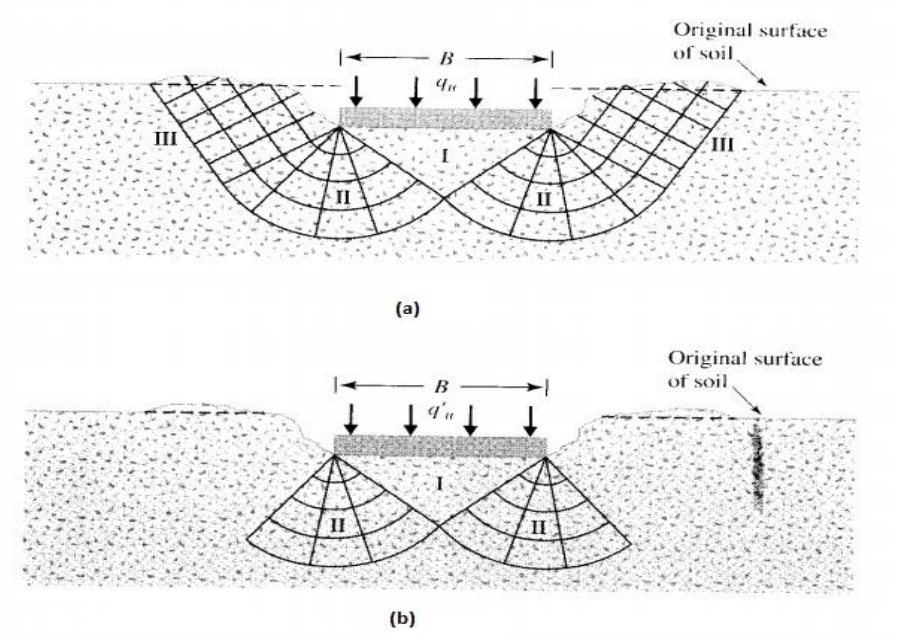

Figure 2.1 Modes of bearing capacity of failure in soil: (a) general shear failure of soil; (b) local shear failure of soil.

2.1.1 Modes of shear failure

Depending on the stiffness of foundation soil and depth of foundation, three principal modes of shear failure may be defined:

a) General shear failure
This type of failure is seen in dense and stiff soil which is associated with low compressibility soil. Since soil above failure surface is in state of plastic equilibrium with heaving on either side, failure is sudden and catastrophic and accompanied by tilting of the footing.

b) Local shear failure
This type of failure is seen in relatively loose and soft soil, that is, moderately compressible soil. There is partial development of plastic equilibrium. Failure is not sudden and there is no tilting of footing. There may be some minor heaving at ground level but no catastrophic failure.

c) Punching shear failure
This type of failure is seen in loose and soft soil and at deeper elevation, that is, in a soil of very high compressibility. There is no heaving, tilting or catastrophic failure. Compression increases the density of soil.

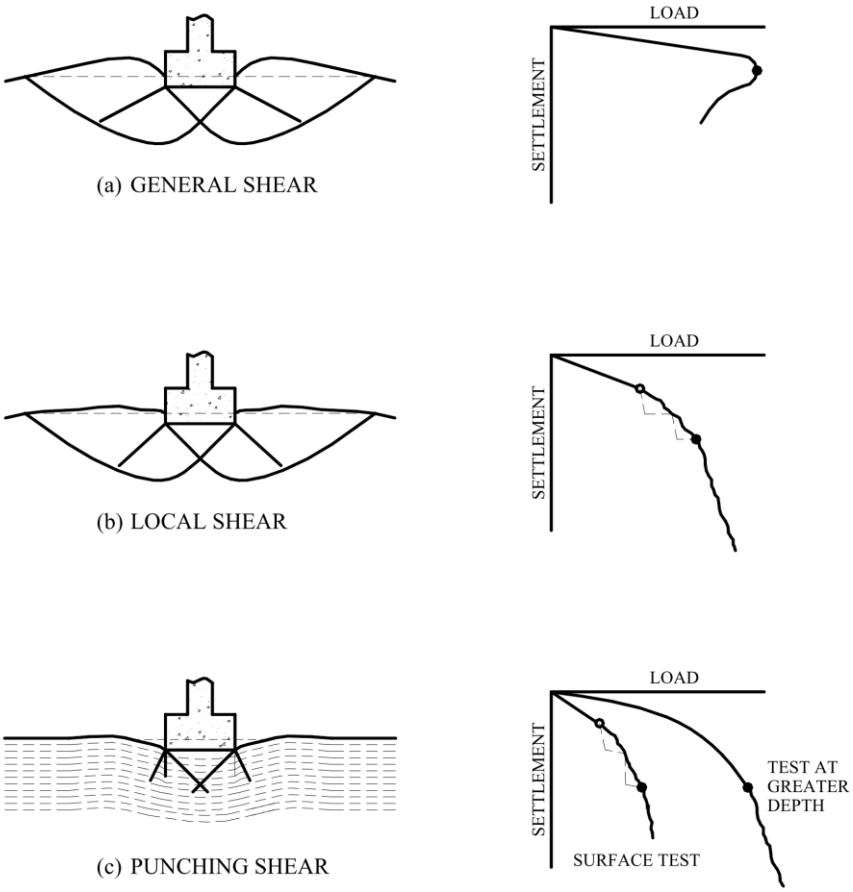

Figure 2.2 Modes of bearing capacity failure.

2.2 Bearing capacity of shallow foundation

The evaluation of the bearing capacity of a shallow foundation is an important problem in foundation engineering, and a number of analytical, numerical and empirical methods have been proposed for various cases of single-layered and multi-layered soil by different authors. Some of the general theories for evaluating the supporting capability of shallow foundations are included in this master thesis. A foundation is said to be shallow, if they are placed at a shallow depth, that is, D < B or where D is less than about 3 m (i.e. within reach of normal excavation plant). Footings should be placed at least deep enough to avoid soil volume changes due to moisture change or freezing and thawing.

In designing shallow foundations, two possible failure mechanisms must be considered (Dunn, Anderson et al. 1980);

- A shear failure in the soil
- Excessive settlement leading to differential settlement in excess of that tolerable for the supported structures

The cases considered in this report assume that the foundation is subjected to centric vertical loading. For determining the ultimate bearing capacity of a horizontal footing with a vertical load, the following factors are included;

- The unit weight, shear strength, and deformation characteristics of the soil,
- The size, shape, depth, and roughness of the footing, and
- The water table conditions and initial stresses in the foundation soil

Most methods of analysis are based on the assumptions of zones of plastic equilibrium in the soil supporting the footing. Theoretical methods for predicting ultimate footings loads are generally based only on the general shear failure case. For the other two failure modes a reduction in the ultimate load due to compressibility effects is applied to the solution for the general shear case(Dunn, Anderson et al. 1980).

Terzaghi (1943) proposed a bearing capacity theory based on the superposition method. The theory was originated from the pioneering work given by Prandtl (1920) and Reissner(1924). In the bearing capacity estimation, the contribution of different loading and soil strength parameters (cohesion, friction angle, surface surcharge and self-weight) expressed in the form of non-dimensional bearing capacity factors N_c, N_q and N_γ are summed. Different analytical solutions have been proposed for computing these factors. After the development of bearing capacity solution, the great effort was given to find more realistic methods of bearing capacity and various correction factors by numerous investigators (Meyerhof 1951, Skempton 1951, Meyerhof 1955, Meyerhof 1963, Meyerhof 1965, Hansen 1970, Vesic 1973, Taiebat and Carter 2000, Erickson and Drescher 2002, Griffiths, Fenton et al. 2002).

2.2.1 Ultimate bearing capacity

In 1921, Prandtl published the results of his study on the penetration of hard bodies, such as metal punches, into as softer material. (Terzaghi 1943) extended the plastic failure theory of Prandtl to evaluate the bearing capacity of soils for shallow strip footings. In 1948, Terzaghi proposed a well-conceived theory to determine the ultimate bearing capacity of shallow rough rigid continuous (strip) foundation supported by a homogeneous soil layer extending to a greater depth. Terzaghi defined a shallow foundation as a foundation where the width, B, is equal to or less than its depth, D. The failure surface in a soil at ultimate load assumed by Terzaghi is shown in Figure 2.3. The general bearing capacity formula derived by Terzaghi for an infinitely long strip foundation of width B for a *c-ϕ* soil is given by;

$$q_u = cN_c + qN_q + \frac{1}{2}\gamma BN_\gamma$$

or

$$q_u = cN_c + \gamma D_f N_q + \frac{1}{2}\gamma BN_\gamma$$

where:

c = cohesive strength of soil

q = overburden pressure = γD_f

B = width of foundation

γ = unit weight of soil

N_c = bearing capacity factor (cohesion)

N_q = bearing capacity factor (surcharge and friction)

N_γ = bearing capacity factor (self-weight and friction)

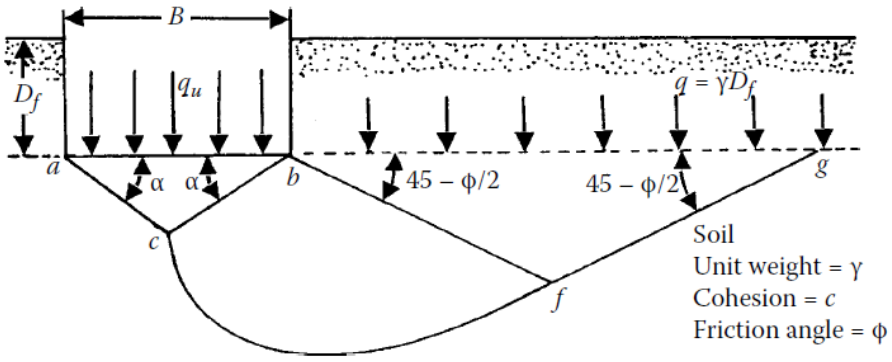

Figure 2.3 Failure surface in soil at ultimate load for a continuous rough rigid foundation as assumed by Terzaghi (Das 2009).

A proper assessment of the bearing factors N_c, N_q, and N_γ is essential for the correct evaluation of bearing capacity. The bearing capacity factors are expressed by the following equations;

$$N_q = \frac{e^{2(\frac{3\Pi}{4}-\frac{\Phi}{2})\tan\Phi}}{2\cos^2(45+\frac{\phi}{2})}$$

$$N_c = \cot\Phi(N_q - 1)$$

$$N_\gamma = \tfrac{1}{2}K_{P\gamma}\tan^2\phi - \frac{\tan\phi}{2}$$

where, $K_{p\gamma}$= passive earth pressure coefficient

Table 2.1 gives the values of N_c, N_q and N_γ for various values of ϕ and Figure 2.4 gives the same in a graphical form.

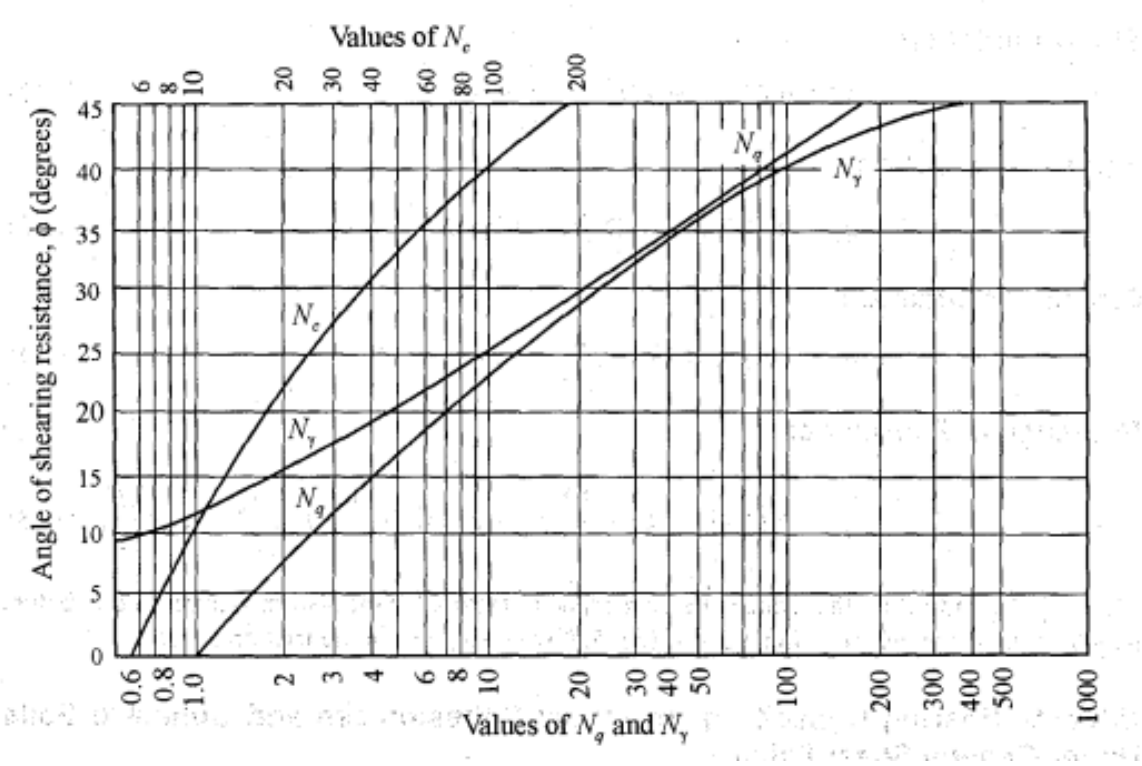

Figure 2.4 Terzaghi's bearing capacity factors for general shear failure (Murthy 2007).

Table 2.1 gives the values of N_c, N_q and N_γ for various values of ϕ and Figure 2.4 gives the same in a graphical form.

Table 2.1 Bearing capacity factors of Terzaghi (Murthy 2007).

ϕ^o	N_c	N_q	N_γ
0	5.7	1.0	0.0
5	7.3	1.6	0.5
10	9.6	2.7	1.2
15	12.9	4.4	2.5
20	17.7	7.4	5.0
25	25.1	12.7	9.7
30	37.2	22.5	19.7
35	57.8	41.4	42.4
40	95.7	81.3	100.4
45	172.3	173.3	297.5
50	347.5	415.1	1153.0

For square and circular footings, Terzaghi suggested the following equations for ultimate soil – bearing capacity:

$$q_u = 1.3cN_c + qN_q + 0.4\gamma BN_\gamma \qquad \text{(square foundation; plan B X B)}$$

and

$$q_u = 1.3cN_c + qN_q + 0.3\gamma BN_\gamma \qquad \text{(circular foundation; diameter B)}$$

Numerous experimental studies have been done to estimate the ultimate bearing of shallow foundations. Hence, it is concluded that the Terzaghi's assumption of the failure surface in soil at ultimate load is essentially correct. However, the angle α in Figure 2.3 that make with the horizontal is close to 45 + ϕ/2 and not ϕ, as assumed by Terzaghi. Figure 2.5 shows the nature of the soil surface for that case (Das 2009).

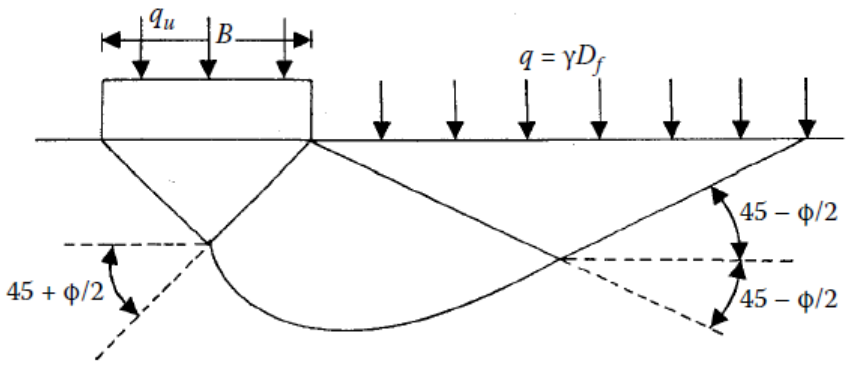

Figure 2.5 Modified failure surface in soil supporting a shallow foundation at ultimate load(Das 2009).

The above equation of ultimate bearing capacity given by Terzaghi was derived on the assumption that the bearing capacity failure of soil takes place by general shear failure. When a soil fails by local shear, the actual shear parameters *c* and ϕ are to be reduced as per (Terzaghi 1943). The lower limiting values of *c* and ϕ are;

$c' = 0.67c$

and

$\tan\phi' = 0.67\tan\phi$ or $\phi' = \tan^{-1}(0.67\tan\phi)$

Terzaghi suggested the following relationships for local shear failure in soil (Das 2009):

Strip foundation (B/L = 0; L = length of foundation);

$$q_u = c' N_c' + qN_q' + \frac{1}{2}\gamma B N_\gamma'$$

Square foundation (B = L);

$$q_u = 1.3c' N_c' + qN_q' + 0.4\gamma B N_\gamma'$$

Circular foundation (B = diameter);

$$q_u = 1.3c' N_c' + qN_q' + 0.4\gamma B N_\gamma'$$

where,

N_c', N_q' and N_γ' = modified bearing capacity factors

Table 2.2 Modified bearing capacity factors by Terzaghi (Das 2009).

ϕ°	N_c	N_q	N_γ
0	5.7	1.0	0.0
5	6.74	1.39	0.074
10	8.02	1.94	0.24
15	9.67	2.73	0.57
20	11.85	3.88	1.1
25	14.8	5.6	2.25
30	18.99	8.31	4.39
35	25.18	12.75	8.35
40	34.87	20.5	17.22
45	51.17	35.11	36
50	81.31	65.6	85.8

General Bearing capacity equation:

The bearing capacity equation developed by Terzaghi is for a strip footing under general shear failure. After Terzaghi developed the bearing capacity equation, several investigators worked on this area to get the refined solution (Meyerhof 1951, Meyerhof 1955, Hansen 1970, Vesic 1973). Different solutions show that there is no much difference in the bearing capacity factors N_c and N_q. However, for the value of ϕ', the values of N_γ vary over a wide range depending primarily on the shape of the assumed failure surface used.

Prandtl (1921) first developed a solution for N_c, assuming a weightless cohesive material with a shear strength c. Reissner (1924) first provided the solution for N_q, which defines the component of bearing capacity due to friction of a weightless material on which a surcharge γD_f is acting (Dunn, Anderson et al. 1980). All three investigators use the equations proposed by Prandtl (1921) and Reissner (1924) for computing the values of N_c and N_q. However, the equations used by them for computing the values are different.

The equations for N_q and N_c as founded by Prandtl and Reissner are as follows;

$$N_q = e^{\pi \tan\phi \left[\tan^2\left(45+\frac{\phi}{2}\right)\right]}$$

$$N_c = (N_q - 1)\cot\phi$$

The equations for N_γ developed by Vesic, Brinch Hansen and Meyerhof are as follows;

$$N_\gamma = 2\left(N_q + 1\right)\tan\left(\phi\right) \qquad \text{(Vesisc)}$$

$$N_\gamma = 1.5\left(N_q - 1\right)\tan\left(\phi\right) \qquad \text{(Brinch Hansen)}$$

$$N_\gamma = \left(N_q - 1\right)\tan\left(1.4\phi\right) \qquad \text{(Meyerhof)}$$

The general bearing capacity equation is given by;

$$q_u = cN_c + \gamma D_f N_q + \frac{1}{2}\gamma B N_\gamma$$

This equation is same as Terzaghi's bearing capacity equation but the difference is that the bearing capacity factors are different. The general bearing capacity equation has been modified for other types of foundations such as square, circular and rectangular by introducing the following factors;

1. Depth factor: to account for the shearing resistance developed along the failure surface in soil above the base of the footing;
2. Shape factor: to determine the bearing capacity of rectangular and circular footings; and
3. Inclination factor: to determine the bearing capacity of a footing on which the direction of load application is inclined at a certain angle to the vertical.

(Meyerhof 1963) presented a general bearing capacity equation which takes into account the shape and inclination of load. Thus, the general ultimate bearing capacity equation can be written as;

$$q_u = cN_c s_c d_c i_c + q_o' N_q s_q d_q i_q + \frac{1}{2}\gamma B N_\gamma s_\gamma d_\gamma i_\gamma$$

where,

c = unit cohesion

q_o' = effective overburden pressure at the base level of the foundation = $\gamma' D_f$

γ' = effective unit weight above the base level of foundation

γ = effective unit weight of soil below the foundation base

D_f = depth of foundation

s_c, s_q, s_γ = shape factors

d_c, d_q, d_γ = depth factors

i_c, i_q, i_γ = load inclination factors

B = width of foundation

N_c, N_q, N_γ = bearing capacity factors

Table 2.3 The values of N_c, N_q, and Meyerhof (M), Hansen (H) and Vesic (V) N_γ Factors (Murthy 2007).

ϕ	N_c	N_q	N_γ (H)	N_γ (M)	N_γ (V)
0	5.14	1.0	0.0	0.0	0.0
5	6.49	1.6	0.1	0.1	0.4
10	8.34	2.5	0.4	0.4	1.2
15	10.97	3.9	1.2	1.1	2.6
20	14.83	6.4	2.9	2.9	5.4
25	20.71	10.7	6.8	6.8	10.9
26	22.25	11.8	7.9	8.0	12.5
28	25.79	14.7	10.9	11.2	16.7
30	30.13	18.4	15.1	15.7	22.4
32	35.47	23.2	20.8	22.0	30.2
34	42.14	29.4	28.7	31.1	41.0
36	50.55	37.7	40.0	44.4	56.2
38	61.31	48.9	56.1	64.0	77.9
40	72.25	64.1	79.4	93.6	109.4
45	133.73	134.7	200.5	262.3	271.3
50	266.50	318.50	567.4	871.7	762.84

Table 2.4 Shape, depth and load inclination factors of Meyerhof, Hansen and Vesic (Murthy 2007).

Factors	Meyerhof	Hansen	Vesic
s_c	$1+0.2N_\phi \frac{B}{L}$	$1+\frac{N_q}{N_c}\frac{B}{L}$	
s_q	$1+0.1N_\phi \frac{B}{L}$ for $\phi>10^\circ$	$1+\frac{B}{L}\tan\phi$	
s_γ	$s_\gamma = s_q$ for $\phi>10^\circ$ $s_\gamma = s_q = 1$ for $\phi=0$	$1-0.4\frac{B}{L}$	The shape and depth factors of Vesic are the same as those of Hansen.
d_c	$1+0.2\sqrt{N_\phi}\frac{D_f}{B}$	$1+0.4\frac{D_f}{B}$	
d_q	$1+0.1\sqrt{N_\phi}\frac{D_f}{B}$ for $\phi>10^\circ$	$1+2\tan\phi(1-\sin\phi)^2\frac{D_f}{B}$	
d_γ	$d_\gamma = d_q$ for $\phi>10^\circ$ $d_\gamma = d_q = 1$ for $\phi=0$	1 for all ϕ Note; Vesic's s and d factors = Hansen's s and d factors	
i_c	$1-\frac{\alpha^\circ}{90}^2$ for any ϕ	$i_q-\frac{1-i_q}{N_q-1}$ for $\phi>0$	Same as Hansen for $\phi>0$
		$0.5\left(1-\frac{Q_h}{A_f c_a}\right)^{\frac{1}{2}}$ for $\phi=0$	$1-\frac{mQ_h}{A_f c_a N_c}$
i_q	$i_q = i_c$ for any ϕ	$1-\frac{0.5Q_h}{Q_u + A_f c_a \cot\phi}^5$	$1-\frac{Q_h}{Q_u + A_f c_a \cot\phi}^m$
i_γ	$1-\frac{\alpha^\circ}{\phi^\circ}^2$ for $\phi>0$ $i_\gamma = 0$ for $\phi=0$	$1-\frac{0.7Q_h}{Q_u + A_f c_a \cot\phi}^5$	$1-\frac{Q_h}{Q_u + A_f c_a \cot\phi}^{m+1}$

Bearing capacity on cohesive soil:

For saturated cohesive soils (clay and silt) with low permeability, the ultimate bearing capacity is most critical immediately after construction until the excess porewater pressure need time to dissipate, that is, undrained condition. As time proceeds, there will be consolidation process and the soil becomes stiffer and has more strength. Therefore, design of foundations on fine grained soils should be in terms of undrained or total stress.

For saturated clay soils, (Skempton 1951) proposed the following equation for a strip foundation;

$$q_u = cN_c + \gamma D_f$$

or,

$$q_{nu} = q_u - \gamma D_f = cN_c = \frac{q_{uc}}{2} N_c$$

where, q_{uc} = unconfined compressive strength of clay

The N_c values for strip and square (or circular) foundations as a function of the D_f / B ratio are given in Figure 2.6.

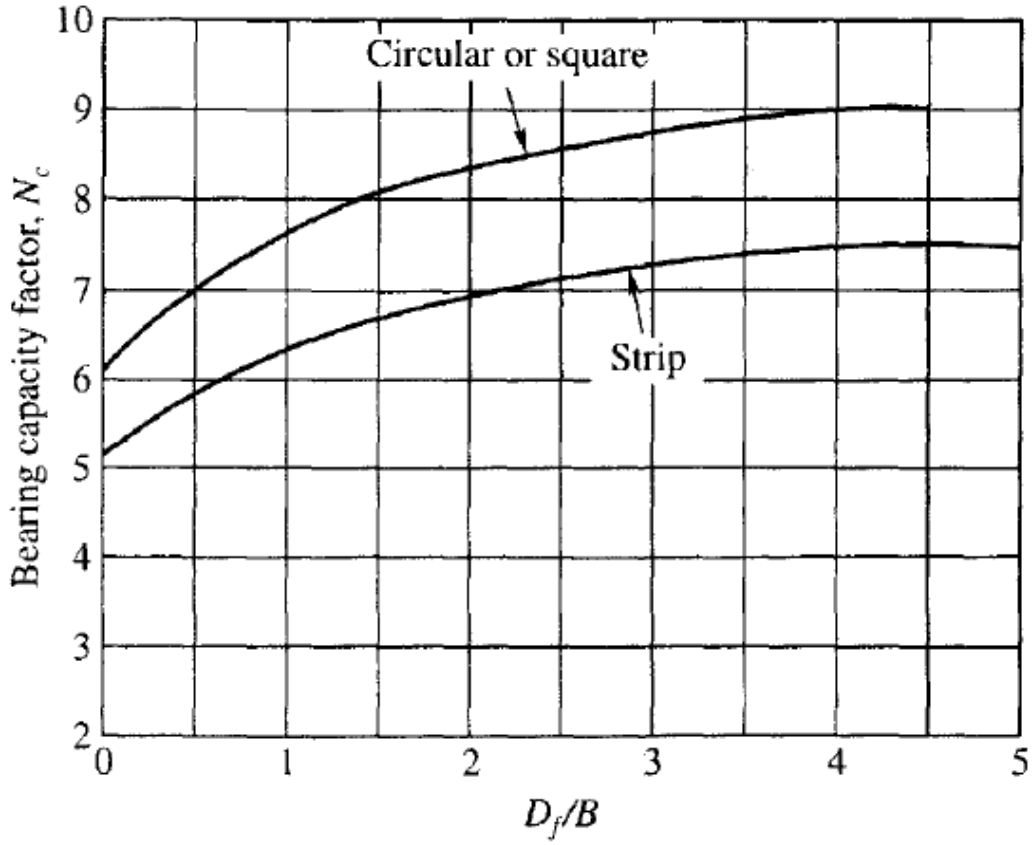

Figure 2.6 Skempton's bearing capacity factor N_c for clay soils (Murthy 2007).

Bearing capacity on cohesionless soil:

The settlement is almost immediate and an allowable or permissible settlement of 25mm is usually applied, when the case of sand comes. The allowable bearing capacity, q_{all} is used for foundation design which satisfies the settlement condition and provides Factor of Safety between 3 and 4. In-situ test results are used to determine the allowable bearing capacity and to make settlement predictions because obtaining undisturbed specimens of cohesionless sand during a soil exploration is usually difficult.

In-situ tests:

1. Plate bearing test
2. Standard penetration test (SPT)
3. Cone penetration test (CPT)

Based on the SPT (N) values:

According to (Meyerhof 1956) and (Bowles 1988):

The net allowable bearing pressure for foundations with the corrected standard penetration resistance, N_{cor} was proposed by (Meyerhof 1956). The net allowable bearing capacity was defined as;

$$q_{all(net)} = \frac{q_{u(net)}}{F_s} = \frac{q_u - q}{F_s}$$

where,

q_{all} = $\frac{q_u}{F_s}$ = gross allowable bearing pressure

F_s = Factor of safety, where F_s of 3 or more is not too conservative

$q_{u(net)}$ = $q_u - q$ = net ultimate load

According to Meyerhof's theory, for 25 mm of estimated maximum settlement,

$q_{all(net)}$ = 11.98 N_{cor} (for $B \leq$ 1.22 m)

and

$$q_{all(net)} = 7.99\, N_{cor} \left(\frac{3.28B+1}{3.28B}\right)^2 \quad \text{(for } B > 1.22 \text{ m)}$$

where,

N_{cor} = corrected standard penetration number

Though the original correlation was proposed by Meyerhof, researchers have observed that its results are rather conservative. Later, (Meyerhof 1965) suggested that the net allowable bearing pressure should be increased by 50%. The equation of bearing pressure was later again modified by (Bowles) (Bowles 1988) which can be expressed as;

$$q_{all(net)} = 19.16 N_{cor} F_d \left(\frac{S_e}{25}\right) \quad \text{(for } B \leq 1.22 \text{ m)}$$

and

$$q_{all(net)} = 11.98 N_{cor} \left(\frac{3.28B+1}{3.28B}\right)^2 F_d \left(\frac{S_e}{25}\right) \quad \text{(for } B > 1.22 \text{ m)}$$

where,

F_d = depth factor = $1 + 0.33(D_f / B) \leq 1.33$

S_e = tolerable elastic settlement, in mm

According to (Peck, Hanson et al. 1974):

The relation between N and ϕ established by Peck et al., (1974) is given in a graphical form in Figure 2.7. The value of N to be used for getting ϕ is the corrected value for standard energy. The angle ϕ obtained by this method can be used for obtaining the bearing capacity factors, and hence the ultimate bearing capacity of soil.

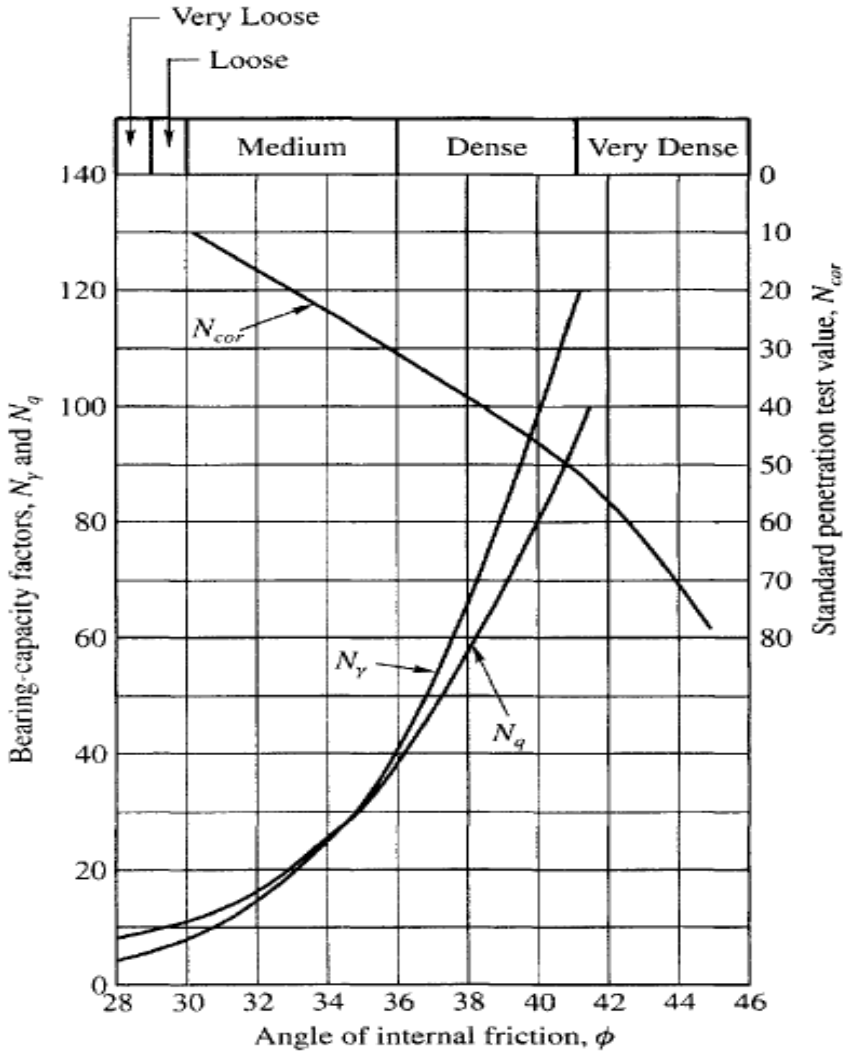

Figure 2.7 Terzaghi's bearing capacity factors which take care of mixed state of local and general shear failures in sand(Murthy 2007).

2.2.2 Janbu's bearing capacity principle

When the load is applied on the soil surface, the stresses in the soil get changed. If a high load is applied to the foundation of limited dimensions, a bearing capacity failure occurs with a shear failure in the soil beneath the foundation. The foundation penetrates the soil and the masses will be squeezed up on the sides of the foundation. Figure 2.8 shows principle sketch of a bearing capacity problem.

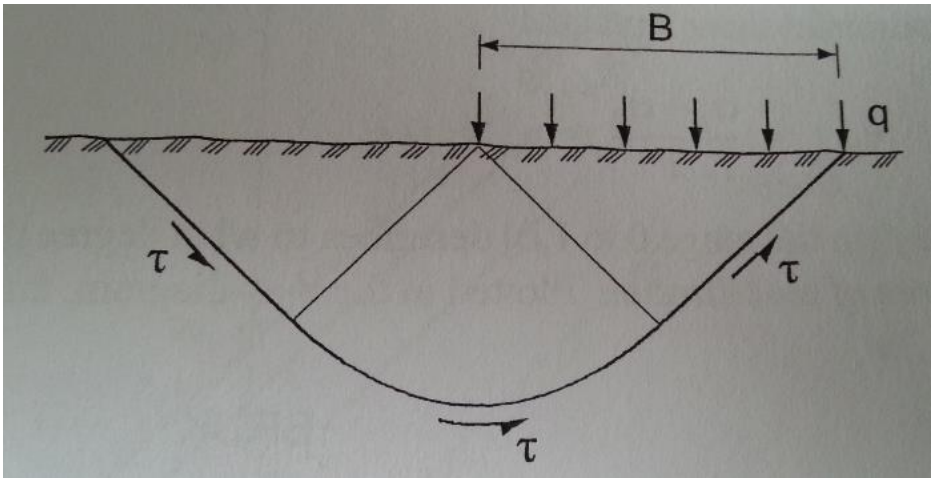

Figure 2.8 Principle sketch of a bearing capacity problem.

The total foundation pressure can be computed as the sum of the solution for weightless soil and the solution for the soil density effect(Janbu, Hjeldnes et al.);

$$\sigma'_{vn} = (N_q - 1)(p' + a) + \frac{1}{2}\gamma' N_\gamma B_o$$

where,

N_q = bearing capacity factor for weightless soil (a and p')

N_γ = bearing capacity factor for the density effect

B_0 = foundation width

p' = overburden pressure

a = attraction

The ground pressure thus obtained is based on the principles launched by Nilmar Janbu, who was a senior Professor at NTNU.

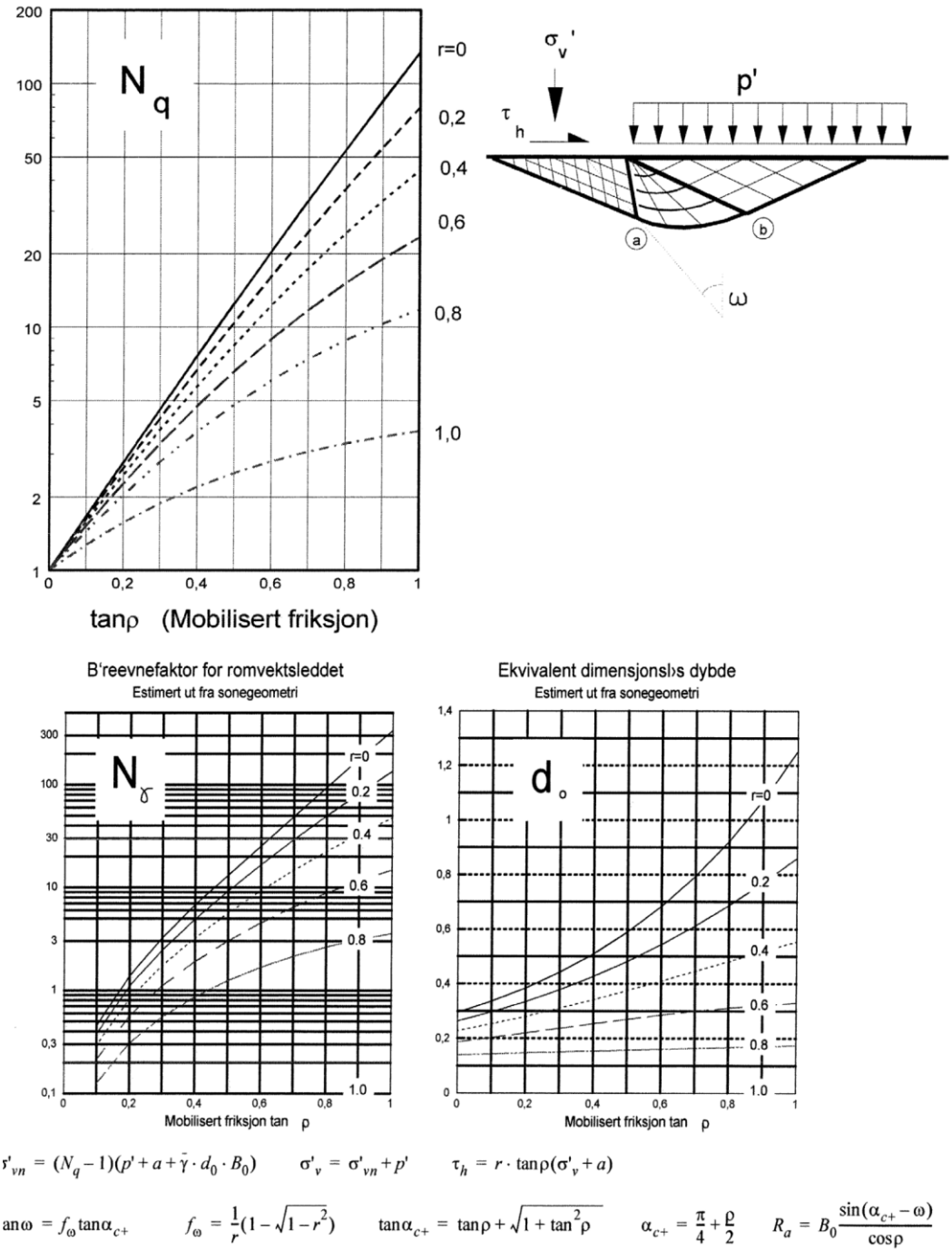

$$\sigma'_{vn} = (N_q - 1)(p' + a + \bar{\gamma} \cdot d_0 \cdot B_0) \qquad \sigma'_v = \sigma'_{vn} + p' \qquad \tau_h = r \cdot \tan\rho(\sigma'_v + a)$$

$$\tan\omega = f_\omega \tan\alpha_{c+} \qquad f_\omega = \frac{1}{r}(1 - \sqrt{1 - r^2}) \qquad \tan\alpha_{c+} = \tan\rho + \sqrt{1 + \tan^2\rho} \qquad \alpha_{c+} = \frac{\pi}{4} + \frac{\rho}{2} \qquad R_a = B_0 \frac{\sin(\alpha_{c+} - \omega)}{\cos\rho}$$

Figure 2.9 Bearing capacity factors N_q and N_γ effective stress analysis(Janbu, Hjeldnes et al.).

2.3 Effects of water table

The ultimate bearing capacity, q_u, of soil is based on the theory that the presence of a water table is at a depth equal to or greater than (D_f + B) from the ground surface. The water table when lies at an intermediate depth less than the depth (D_f + B), the effective shear strength is reduced and hence, bearing capacity get affected.

For the effect of water table, two cases can be considered;

Case 1: When the water table lies above the base of the foundation

Case 2: When the water table lies within depth B below the base of the foundation

The bearing capacity equation becomes as follow, when the position of water table is within the depth ($D_f + B$);

$$q_u = cN_c + \gamma D_f N_q R_{w1} + \frac{1}{2}\gamma B N_\gamma R_{w2}$$

where;

R_{w1} = reduction factor for water table above the base level of the foundation

R_{w2} = reduction factor for water table below the base level of the foundation

$\gamma = \gamma_{sat}$

For case 1, that is, $D_{w1} / D_f \leq 1$, the equation of R_{w1} becomes;

$$R_{w1} = \frac{1}{2}\left(1 + \frac{D_{w1}}{D_f}\right)$$

For case 2, that is, $D_{w2} / B \leq 1$, the equation of R_{w2} becomes;

$$R_{w2} = \frac{1}{2}\left(1 + \frac{D_{w2}}{B}\right)$$

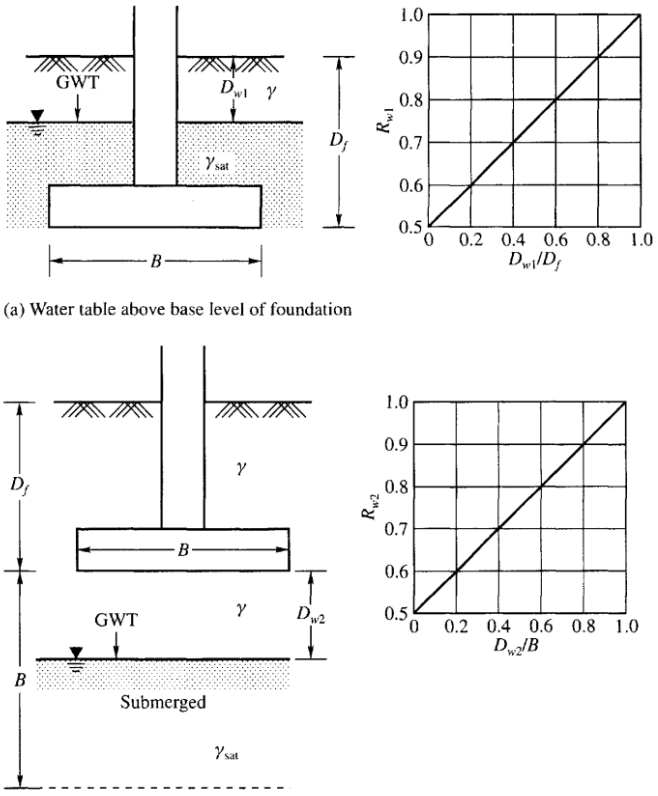

Figure 2.10 Effect of water table on bearing capacity(Murthy 2007).

2.4 Plate loading tests

The plate load test is a semi-direct method to determine the soil-bearing capacity of foundations. Plates, round or square, varying in size and thickness are employed for the test. The load on the plate is applied by making use of a hydraulic jack. The reaction of the jack load is taken by a cross beam or a steel truss anchored suitably at both the ends. The settlement of the plate is measured by a set of three dial gauges of sensitivity 0.02 mm placed 120^{o} apart. The dial gauges are fixed to independent supports which remain undisturbed during the test(Murthy 2007).

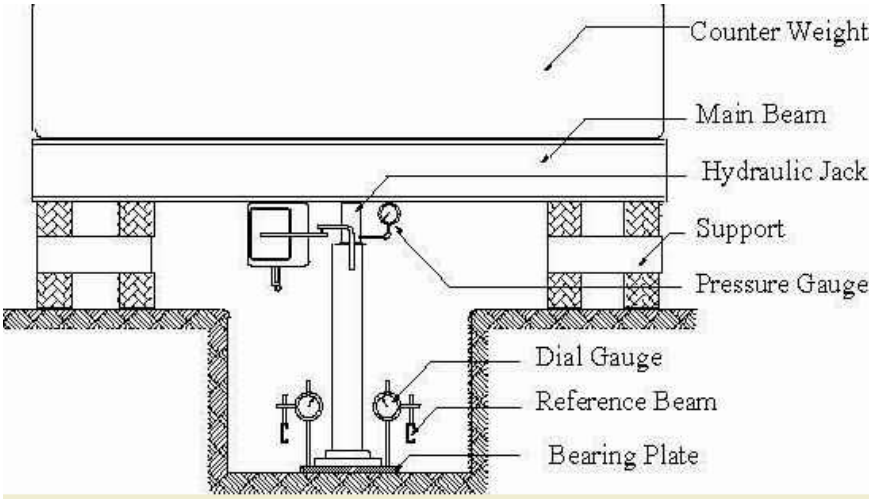

Figure 2.11 Diagram of plate load test.

A diagram of plate load test is shown in Figure 2.11. For the load test to be performed, a ditch of depth D_f is excavated which should be not less than 4 to 5 times the size of the plate. If the water table is above the level of the foundation, the water is carefully pumped out and kept it at the level of the foundation. A suitable bearing plate is selected and placed on the soil at the bottom of the pit, and incremental load on the bearing plate is applied. After the application of an incremental load, enough time is allowed for settlement to occur. When the settlement of the bearing plate becomes negligible, another incremental load is applied. In this manner a load-settlement plot can be obtained as shown in Figure 2.12.

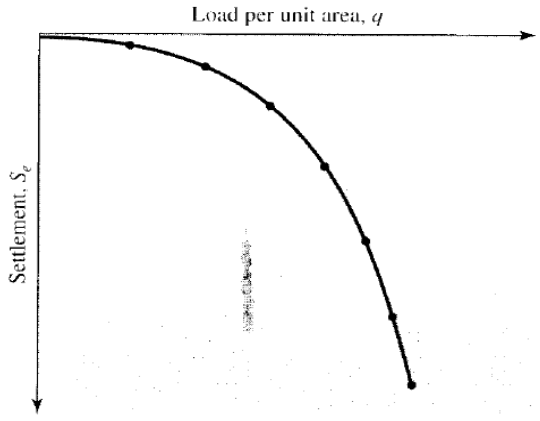

Figure 2.12 Load-settlement curve of a plate load test.

The permissible settlement suggested by (Terzaghi, Peck et al. 1996) for square footing in granular soils is given by equation;

$$S_f = S_p \left(\frac{B\left(b_p + 0.3\right)}{b_p \left(B + 0.3\right)} \right)^2$$

for clay soils,

$$S_f = S_p \times \frac{B}{b_p}$$

where,

S_f = permissible settlement of foundation in mm

S_p = settlement of plate in mm

B = size of foundation in meters

b_p = size of plate in meters

The stresses induced by a plate load test do not penetrate very deep into the soil, so its load-settlement behavior is not the same as that of a full-sized footing.

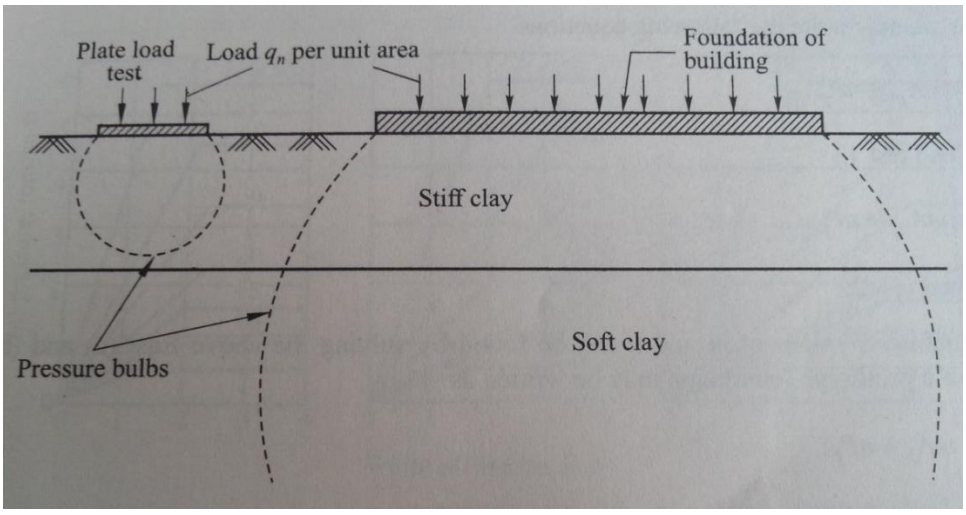

Figure 2.13 The stresses induced by a plate load test(Murthy 2007).

2.5 Settlement of shallow foundations

When the load from the structure is applied on a foundation consisting of soil, the soil mass deforms. The ground surface where the structure is laid can undergo compression leading to structural settlement. This structural settlement occurs even if the conditions of structural integrity or bearing capacity of a foundation are satisfied.

2.5.1 Settlement of shallow foundation in clay and silt

When settlement calculation of foundation under load comes to clay and silt, the consolidation of a material is usually linked. The consolidation process takes place which is followed by occurrence of settlement. The settlement in clay and silt can be determined based on lab tests. Then the settlement of a foundation can have three components:

a) Elastic settlement, S_e
b) Primary settlement, S_c, and
c) Secondary consolidation settlement, S_s

The total settlement can be expressed as;

$$S_t = S_e + S_c + S_s$$

Elastic settlement, S_e:

This is also referred to as the 'distortion settlement' or 'contact settlement' and is usually taken to occur immediately on application of the foundation load. The theory of elasticity is used to estimate the immediate settlement. Janbu, Bjerrum and Kjaernsli (1956) published a monograph, in Norwegian, on the application of soil mechanics to several problems of foundation engineering. For computing elastic settlement of circular or rectangular foundations embedded at various depths, charts were included in it (Christian and David Carrier III 1978). The settlement can be determined from the equation;

$$S_e = \mu_0 \mu_1 \frac{qB}{E}$$

where,

q = average applied vertical pressure

B = width of the foundation

E = Young's Modulus

S_e =elastic settlement

μ_0 = dimensionless parameter that describes the effect of the depth of embedment

μ_1 = dimensionless parameter that describes the effect of the depth of the layer itself

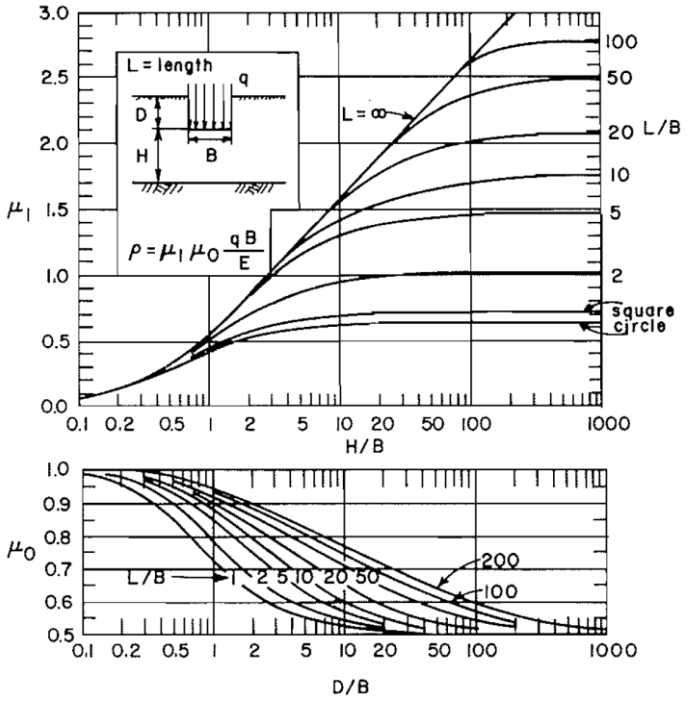

Figure 2.14 Original Janbu, Bjerrum and Kjaernsli (1956) chart for μ_0 and μ1 with captions translated into English(Christian and David Carrier III 1978).

For a flexible and rigid foundation, the profile of elastic settlement may vary as shown in Figure 2.15.

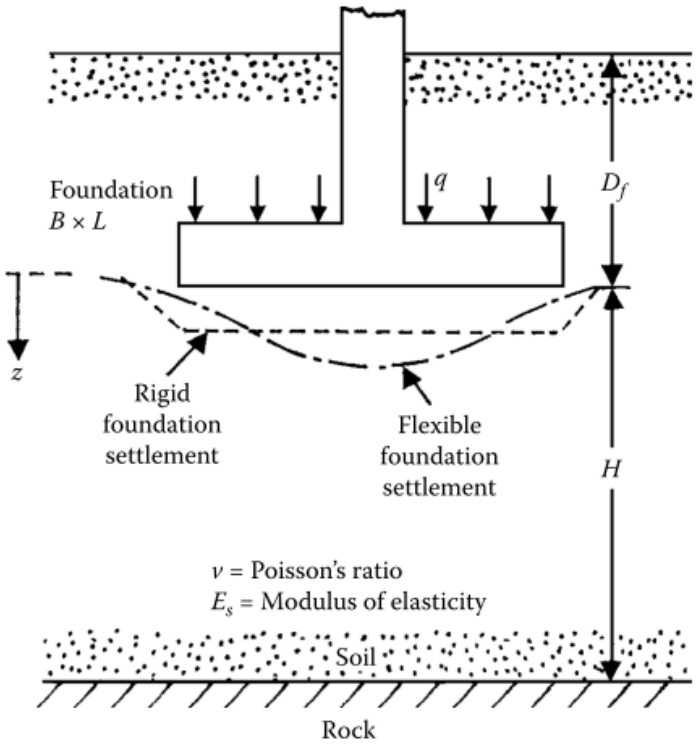

Figure 2.15 Settlement profile for shallow flexible and rigid foundations(Das 2009).

Primary settlement, S_c:

The phenomenon of consolidation occurs in clays because the initial excess pore water pressures cannot be dissipated immediately owing to the low permeability. The theory of one-dimensional consolidation, advanced by Terzaghi, can be applied of dissipation of excess pore pressures and hence the time-rate of settlement. The settlement computed by this procedure is known as that due to primary compression since the process of consolidation as being the dissipation of excess pore pressures alone is considered.

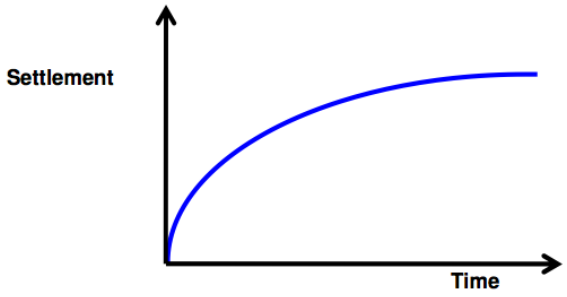

Figure 2.16 Primary settlement.

Primary settlement can be calculated using oedometer tests. The primary settlement can be determined by the equation;

$$S_c = H_o \left\{ \frac{C_c}{1+e_o} \log\left(\frac{\sigma'_{vm}}{\sigma'_{vo}} \right) + \frac{C_r}{1+e_o} \log\left(\frac{\sigma'_{vf}}{\sigma'_{vo}} \right) \right\}$$

where,

S_c = primary settlement

C_c = compression coefficient

C_r = recompression coefficient = 1/3 to 1/5 C_c

e_o = initial void ratio

σ'_{vo} = initial effective vertical stress

$\sigma'_{vm} = \sigma'_{vo} + \Delta\sigma'$ = maximum path pressure throughout its history

σ'_{vf} = final pressure

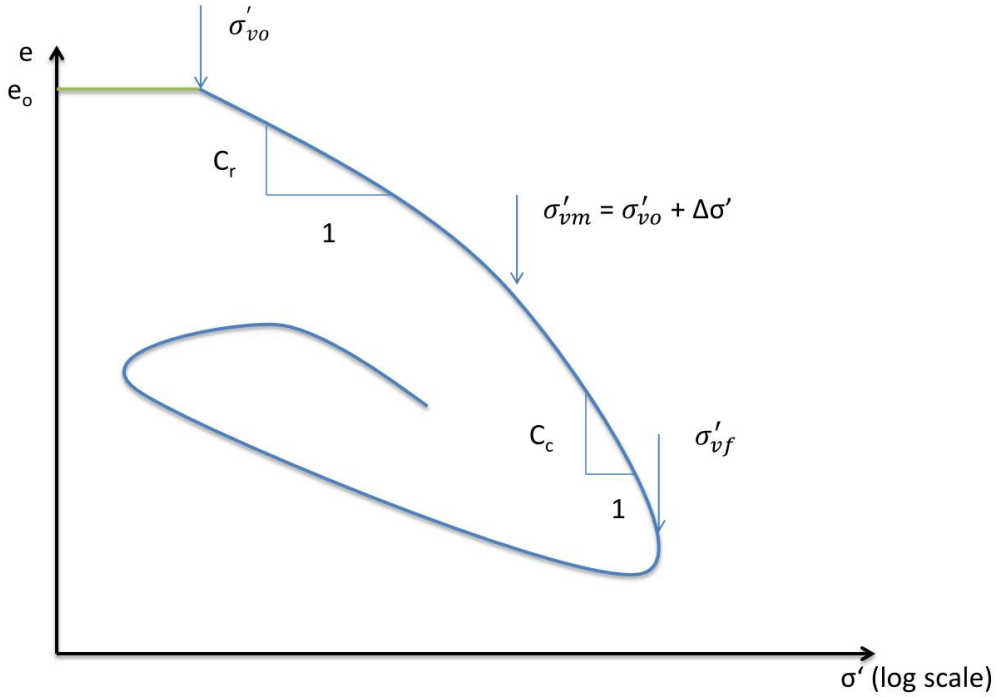

Figure 2.17 Typical void ratio vs effective stress graph in oedometer.

Secondary consolidation settlement, S_s:

Settlement due to secondary compression is believed to occur during and mostly after the completion of primary consolidation or complete dissipation of excess pore pressure. A few theories have been advanced to explain this phenomenon, known as 'secondary consolidation'.

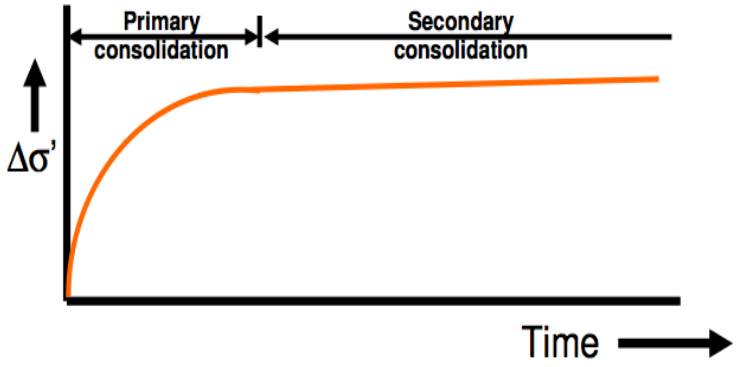

Figure 2.18 Secondary settlement.

These settlements are time-dependent and will never fully stop. They are dominated by creep and occur due to gradual changes in the particle structure of the soil. The rate of the secondary consolidation is much slower than for the primary consolidation, and depending on the material, many years will go by before the structure is considered to be "fully" settled.

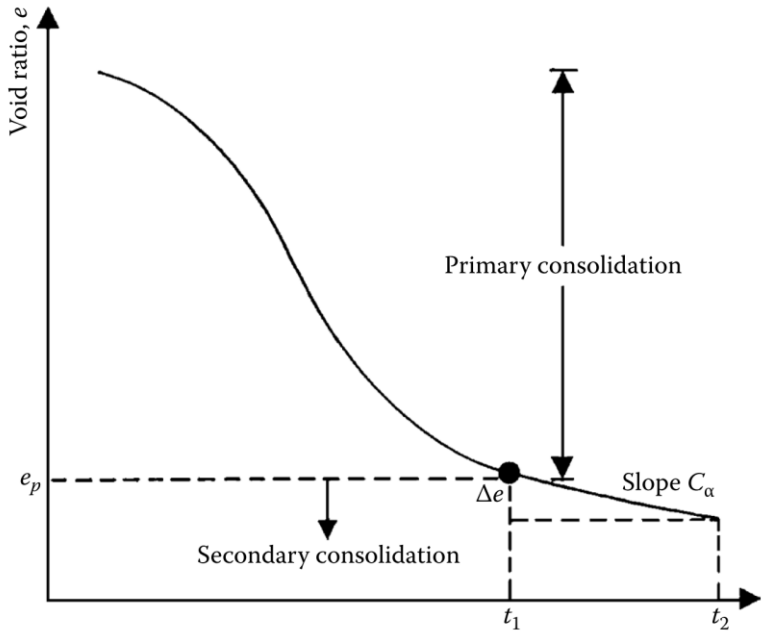

Figure 2.19 Secondary consolidation settlement (Das 2009).

The secondary consolidation settlement can be expressed as;

$$S_s = \frac{C_\alpha H_o}{1+e_p}\log\left(\frac{t_2}{t_1}\right)$$

where,

C_α = secondary compression index = $\frac{\Delta e}{\log\left(\frac{t2}{t1}\right)}$

e_p = void ratio at the end of primary consolidation

t_2, t_1 = time

2.5.2 Settlement of shallow foundation in sand

The settlement in sand does not behave as in clay and silt. Settlement criterion governs the allowable bearing capacity for footings on sand. Settlement in sand occurs rapidly. Footing settlement in sand deposits is often estimated using in situ tests, that is, mainly the standard penetration test (SPT) and the cone penetration test (CPT).

2.5.2.1SPT-based methods

There are several methods available to calculate the settlement of footings on sand using SPT results. (Meyerhof 1965) suggested the following relationship for the settlement of spread footings on sand(Lee and Salgado 2002);

$$S = \frac{0.203L_R}{N_{45}}\left(\frac{q_b}{p_A}\right) \qquad \text{for } B \le 1.2L_R$$

$$S = \frac{0.203 L_R}{N_{45}} \left(\frac{q_b}{p_a} \right) \left(\frac{B}{B + L_R / 3.28} \right)^2 \qquad \text{for } B > 1.2L_R$$

where,

S = footing settlement

q_b = unit load at base of footing

N_{45} = SPT blow count corrected for an energy ratio of 45%

B = footing width

L_R = reference length = 1 m

P_a = reference pressure = 100 kPa

Peck and Bazaraa method:

The following equation is used for estimating the settlements of footings on sand(Lee and Salgado 2002):

$$S = C_w C_d \frac{0.051 L_R}{N_B} \left(\frac{q_b}{p_a} \right) \left(\frac{B}{B + L_R / 3.28} \right)^2$$

$$N_B = \left(\frac{4 N_{45}}{1 + 4\sigma_v^{'} / p_a} \right) \frac{\sigma_v^{'}}{p_a} \qquad \text{for } \sigma_v^{'} \leq 0.75 p_a$$

$$N_B = \left(\frac{4 N_{45}}{3.25 + 4\sigma_v^{'} / p_a} \right) \frac{\sigma_v^{'}}{p_a} \qquad \text{for } \sigma_v^{'} > 0.75 p_a$$

where,

C_w = groundwater correction factor

C_d = depth correction factor

q_b = unit load at base of footing

N_{45} = SPT blow count corrected for an energy ratio of 45%

N_B = stress-normalized SPT N value

B = footing width

L_R = reference length = 1 m

P_a = reference pressure = 100 kPa

Burland and Burbidge method:

The following equation proposed by is used for estimating the settlements of footings on sand(Lee and Salgado 2002):

$$S = f_s \cdot f_I \cdot f_t \cdot I_c \left(q_b - \frac{2}{3}\sigma'_{v,p} \right) \left(\frac{100}{p_a} \right) \left(\frac{B}{L_R} \right)^{0.7}$$

where,

S = footing settlement

f_s = shape factor

f_I = depth factor for the sand or gravel layer

f_t = time factor

q_b = unit load at base of footing

$\sigma'_{v,p}$ = maximum previous vertical stress

B = footing width

p_a = reference pressure = 100 kPa

2.5.2.2 CPT-based methods

Schmertmann's method is one most common method for the estimation of settlement using CPT results. In this method, the soil profile beneath the footing is divided into several sub layers. For each sub layer, using CPT results the soil stiffness is calculated. For the settlement calculation, the influence zone for square footing goes down to 2B and for strip footing to 4B which is shown in Figure 2.20. The contribution of settlement in shallower layers is greater than the deeper layers. The reason behind this is due to the stiffness increment with depth, and the stresses induced by the applied load decrease with depth(Lee and Salgado 2002). The settlement calculation of footing on sand by Schmertmann's method is done using the following equations;

$$S = C_1 \cdot C_2 \cdot (q_b - \sigma'_v|_d) \cdot \sum \left(\frac{I_z \cdot \Delta z_i}{E_i} \right)$$

$$C_1 = 1 - 0.5 \left(\frac{\sigma'_v|_d}{q_b - \sigma'_v|_d} \right)$$

$$C_2 = 1 + 0.2 \log \left(\frac{t}{0.1 \cdot t_R} \right)$$

where,

S = settlement caused by applied load

C_1 and C_2 = depth and time factors

q_b = unit load on footing base

$\sigma'_v\big|_d$ = vertical effective stress at footing base level

I_z = depth influence factor

Δz_i = thickness of each sublayer

E_i = representative elastic modulus of each sublayer

t = time

t_R = reference time = 1 year = 365 days

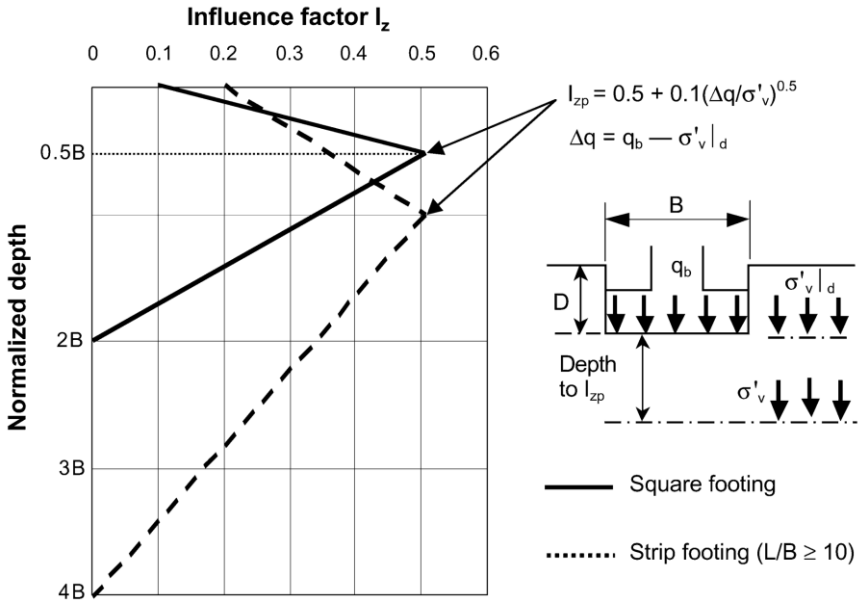

Figure 2.20 Influence factor I_z vs. depth(Lee and Salgado 2002).

The elastic modulus E_i of each sublayer is obtained from the representative cone resistance q_c for that layer. From different researchers, the q_c can be summarized as;

$$E_i = \begin{cases} 2.5q_c & \text{for yound normally consolidated silica sand} \\ 3.5q_c & \text{for aged normally consolidated silica sand} \\ 6.0q_c & \text{for overconsolidated silica sand} \end{cases}$$

2.5.3 Janbu's modulus concept for settlement calculation

Janbu's modulus concept can be used to determine the deformation of soil subjected to external load, typically to find settlements as a function of surcharge on soil surface or from ground water drawdown. For a soil element and a soil profile, the total settlement calculation is determined as follow taking the reference of Figure 2.21.

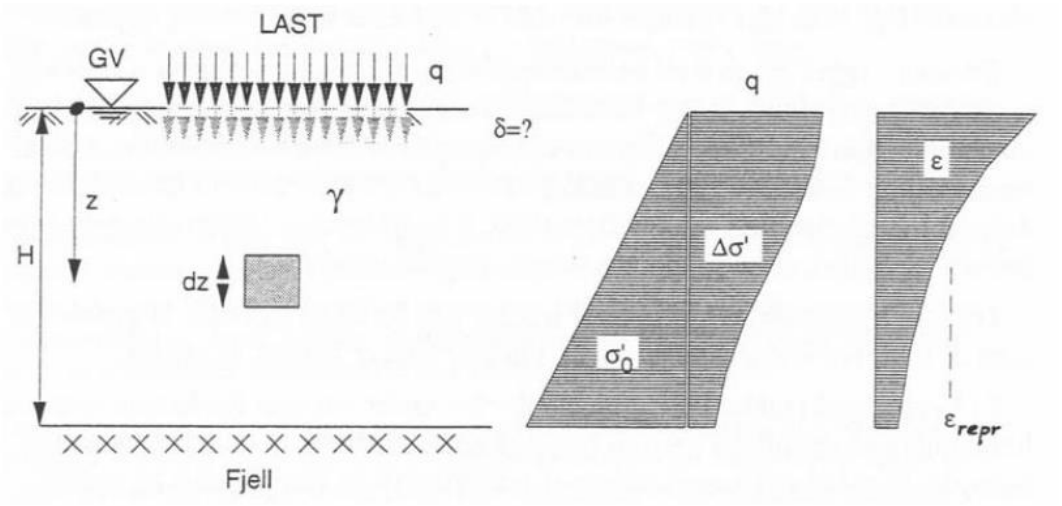

Figure 2.21 Principle sketch of settlement calculation.

1. Calculation of initial vertical stress, σ_o'.
2. Determination of total stress increase from external load q. After long time: $\Delta u \rightarrow 0$ $\Rightarrow \Delta\sigma' = \Delta\sigma$, that is, at the end of the primary consolidation.
3. One-dimensional confined modulus is determined from oedometer tests. The modulus is the ratio of strain vs. stress and can be written as equation; $d\sigma' = M \cdot d\varepsilon$

Integration of above equation from σ_o' to $(\sigma_o' + \Delta\sigma')$ gives,

$$\varepsilon = \int_{\sigma_o'}^{\sigma_o'+\Delta\sigma'} \frac{d\sigma'}{M}$$

For the settlement contribution from the element, $d\delta = \varepsilon \cdot dz$

Hence, total settlement can be obtained by;

$$\delta = \int_0^H \varepsilon \cdot dz$$

where, H = thickness of layer

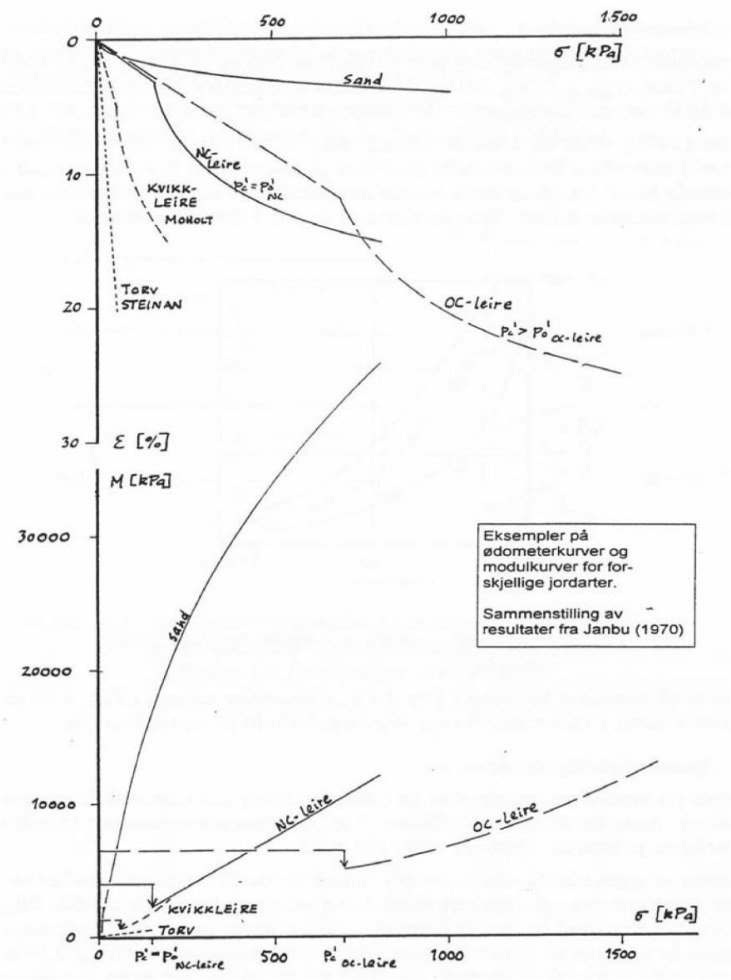

Figure 2.22 Oedometer tests on soil with large variation in stiffness.

The soil behavior when studied taking into three types, the following description is stated;

1. Constant stiffness with effective stress, valid for any material that behaves like this, typical for overconsolidated clays.
2. Linearly increasing with effective stress. Typical for normally consolidated clays, i.e. clays in the stress range above p_c'.
3. Parabolic increase with effective stress. Valid for sands and coarse silts, or any granular material.

For the determination of confined modulus Janbu has given the following equation;

$$M = m \cdot \sigma_a \left(\frac{\sigma'}{\sigma_a} \right)^{1-a}$$

where,

m = modulus number

σ' = actual effective stress level

σ_a = stress equivalent to one atomosphere

$$M = \frac{d\sigma'}{d\varepsilon} = m \cdot \sigma_a \left(\frac{\sigma'}{\sigma_a} \right)^{1-a}$$

$$d\varepsilon = \frac{1}{m\sigma_a} \left(\frac{\sigma'}{\sigma_a} \right)^{a-1} d\sigma'$$

$$\varepsilon = \frac{1}{m\sigma_a} \int_{\sigma_o'}^{\sigma'} \left(\frac{\sigma'}{\sigma_a} \right)^{a-1} d\sigma'$$

$$\varepsilon = \frac{1}{m\sigma_a} \left[\left(\frac{\sigma'}{\sigma_a} \right)^{a} \frac{\sigma_a}{\sigma} \right]_{\sigma_o'}^{\sigma'}$$

$$\varepsilon = \frac{1}{am} \left[\left(\frac{\sigma'}{\sigma_a} \right)^{a} - \left(\frac{\sigma_o'}{\sigma_a} \right)^{a} \right]$$

According to soil types the value of modulus number, m varies. In case of constant stiffness, the stress exponent a is equal to 1. For granular soil, a is equal to 0.5 is chosen and for clays, it is equal to 0. The calculation of strain is performed using above equations and finally the settlement estimation can be done for different types of soil.

2.6 Finite Element Method

It allows modeling complicated nonlinear soil behavior through constitutive model, various geometrics with different boundary conditions & interfaces. It can predict the stresses, deformations and pore pressures of a specified soil profile.

2.6.1 PLAXIS

According to (Burd 1999), the initiation of this Finite Element Program was held at Delft University of Technology Netherland by Pieter Vermeer in 1974. PLAXIS name was derived from PLasticity AXISymmetry, a computer program developed to solve the cone pentrometer problem by Pieter Vermeer and De borst. The development of the PLAXIS began in. Earlier version of PLAXIS was in DOS interface. In 1998, the first PLAXIS 2D for Windows was released. The new versions and modifications were carried out for the analysis of soil behavior for geotechnical engineers.

Advanced soil model

Hardening Soil Model:

The Hardening Soil model is an advanced model which was originally proposed for sand. It is now further developed for simulating the behavior of different types of soil, both soft soils and stiff soils. When subjected to primary deviatoric loading, soil shows a decreasing stiffness and simultaneously irreversible plastic strains develop. In the special case of a

drained triaxial test, the observed relationship between the axial strain and the deviatoric stress can be well approximated by a hyperbola. The well-known hyperbolic model was developed by (Duncan and Chang 1970). This model captures soil behavior in a very tractable manner on the basis of only two stiffness parameters. Though it is very appreciated among consulting geotechnical engineers, the major inconsistency of this type of model is that in contrast to the elasto-plastic type of model, a purely hypo-elastic model cannot consistently distinguish between loading and unloading. The model is also not suitable for collapse load computations in the fully plastic range (Schanz, Vermeer et al. 1999).

Due to these restrictions a model was formulated in an elasto-plastic framework called "Hardening Soil" with so-called isotropic hardening. The Hardening Soil model, however, supersedes the hyperbolic model by far: firstly by using the theory of plasticity rather than the theory of elasticity, secondly by including soil dilatancy and thirdly by introducing a yield cap.

The basic parameters that are used in HS Model are:

Stiffness parameters

E_{50}^{ref} = Secant stiffness in standard drained triaxial test

E_{oed}^{ref} = Tangent stiffness for primary oedometer loading

E_{ur}^{ref} = Unloading / reloading stiffness (default E_{ur}^{ref} =3 E_{50}^{ref})

Strength parameters

$c_{ref}^{'}$ = Effective cohesion

ϕ' = Effective angle of internal friction

ψ = Angle of dilatancy

"Hardening Soil" model is built in formulation that makes the stiffness dependent on the effective stress level. Several stiffness parameters are introduced, controlling loading in shear (deviatoric loading), volumetric loading and unloading. The stress dependency for all stiffness moduli can be expressed by the equation below for deviatoric loading.

$$E_{50} = E_{50}^{ref}\left(\frac{\sigma_3^{'} + a}{p_{ref} + a}\right)^m$$

or

$$E_{50} = E_{50}^{ref}\left(\frac{c\cos\phi - \sigma_3^{'}\sin\phi}{c\cos\phi + p_{ref}\sin\phi}\right)^m$$

where,

p_{ref} = p_a = 100 kPa is the atmospheric pressure

$a = \frac{c}{\tan \phi}$ is the attraction

m is normally equal to 1 for clay and 0.5 for sand.

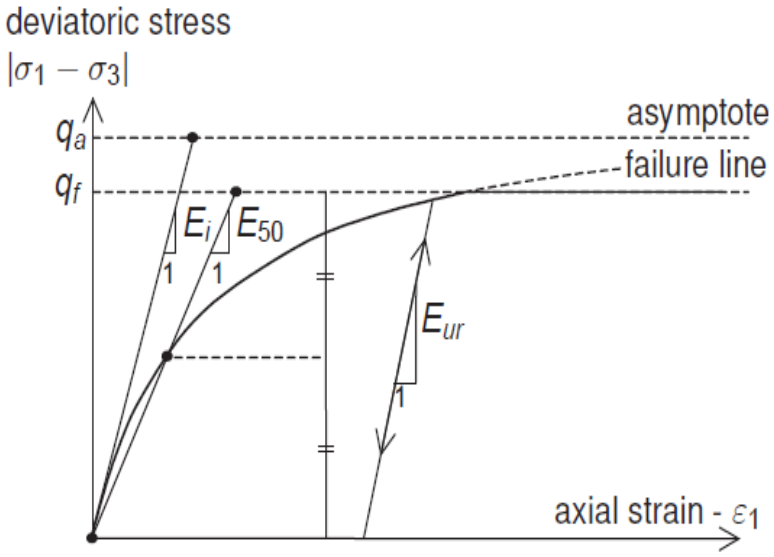

Figure 2.23 Hyperbolic stress strain relation in primary loading for a standard drained triaxial test(Brinkgreve, Broere et al. 2012).

3 METHODOLOGY

3.1 Introduction

The aim of this master work is to back-calculate the load tests using advanced soil models in PLAXIX 2D in order to gather experience on soil behavior and constitutive models. For this purpose, extensive relevant literature study is carried out and identifies high quality bearing capacity load tests in the literature. The relevant soil profiles and soil parameters are identified from field and laboratory tests. The Soil Test is also carried out when relevant. The back-calculation was done using PLAXIS 2D. The Advanced soil model, that is, Hardening soil model is used as a material model for simulation. Finally, the results of load-settlement curve are compared between PLAXIS 2D results with field measurements.

3.2 Reports used for the study and analysis

From the extensive literature review, some bearing capacity load tests are found. For this master work, three case studies with high quality bearing capacity load tests are identified for the study and analysis.

The first case study is of Tornhill, Sweden on Clay Till. The test field was located in southern Sweden north of the city of Lund where there square plate loading tests were conducted, that is, 0.5 X 0.5 m footing , 1.0 X 1.0 m footing and 2.0 X 2.0 m footing.

The second case study is of Portugal on Saprolitic soil. The greenfield site chosen was to be for a hospital where plate load tests (PLT) were made with circular steel plates 30 and 60 cm in diameter and the main test was on a 1.2 m diameter reinforced concrete foundation 0.5 m thick. This type of soil is common in the northern part of Portugal.

The third case study is of Texas A & M University on sand. At the sand site on the Texas A & M University National Geotechnical Experimentation Site (NGES) five spread footings were built, that is, two 3.0 X 3.0 m footings (south and north sides), one 2.5 X 2.5 m footings, one 1.5 X 1.5 m footing, and one 1.0 X 1.0 m footing.

Geological and geotechnical studies were done for all of the cases. The characteristics of the soil were measured by a range of in situ tests including standard penetration tests (SPT), static cone penetration tests (CPT), dynamic probing (DP), Menard pressuremeter tests (PMT), Marchetti dilatometer tests (DMT), self-boring pressuremeter tests (SBPT), and cross-hole seismic tests (CH). In addition, the laboratory tests such as oedometer and triaxial tests were conducted. The relevant soil profiles and soil parameters are identified to be used in Advanced soil model, that is, Hardening Soil model from field and laboratory tests.

3.3 PLAXIS Software and Procedure

3.3.1 Introduction of PLAXIS Software

The two-dimensional finite element program PLAXIS is used to simulate the bearing capacity and settlement of footing or plate on shallow foundation. During the modeling in PLAXIS, various trial analyses are performed to assess the model behavior. The variation in strength parameters c'_{ref} and ϕ' was done since the bearing capacity of soil depends on strength parameters. To carry out a finite analysis using PLAXIS, a finite element mesh has been created and the material properties and boundary conditions are specified. To set up a FEM, geometry model composed of points, lines and other components has been created in the XY-plane for PLAXIS 2D. The finite element mesh was generated in PLAXIS 2D after the material properties and boundary conditions are assigned.

3.3.2 Models of shallow foundation

Foundation soil:

In this project, three case studies was done from different places. For the first case from Sweden, it is clay till; for second case from Portugal, it is saprolitic soil; and for third case from United States, it is sand. The advanced soil model, that is, Hardening Soil model will be used to represent the soil for all cases.

Footing:

The footing or plate is modeled for axisymmetric conditions. The PLAXIS 2D program allows for elastic or elasto-plastic material behavior in plate elements. In these cased, elastic plate elements are used. Different sizes of footings are used according to the case studies.

Loading:

The distributed load A is applied vertically in the footing for the simulation of bearing capacity and settlement of the footing. The PLAXIS 2D is used to model the materials.

Interfacial strength:

The purpose of interface element is to simulate the relative friction between footing and soil. The roughness of the interaction is modeled by selecting an appropriate value for the strength reduction factor (R_{inter}) in the interface. If there is no relative sliding between the soil and footing, $R_{inter} = 1$. If the deformation or sliding of footing is more than the soil body, $R_{inter} < 1$. $R_{inter} = 1$ is used in the model.

3.3.3 Procedure and Simulation

The procedures in numerical simulation for reinforced concrete footings as well as steel plates from different case studies are done by excavating to the foundation level and placing the footing above it. During construction stage, the footing and load are activated. The

incremental load is applied on the footing and different results are taken from the output. Finally, the load-settlement curves are drawn.

3.4 Comparison between PLAXIS 2D results with field measurements

The output obtained from numerical simulation of the footing using PLAXIS 2D is analysed and plotted in load-settlement curve and this is compared with measured load-settlement curve in the field.

4 NUMERICAL MODELING USING PLAXIS 2D

The bearing capacity and settlement for both strip and circular footings have already been one of the most highly interesting areas in geotechnical engineering for researchers and practical engineers. Describing the correct bearing capacity of the footing is a very important factor in economic terms. In order to calculate the bearing capacity of strip and circular footings, there have been a lot of investigations using limit equilibrium method (Terzaghi 1943, Meyerhof 1951). The study of numerical methods to solve geotechnical problems are increasing tremendously such as finite element method (FEM)(Sloan and Randolph 1982, Griffiths 1989) and the finite difference method(Frydman and Burd 1997, Erickson and Drescher 2002) have been widely used to compute the bearing capacity of strip and circular footings.

Because of the complex nature of soil, the development of constitutive models capable of capturing 'real' soil behavior is a key aspect of analyses of geotechnical structures. The developments of the constitutive models implemented in commercial codes are PLAXIS, STRAUS-7, FLAC-3D, ABACUS. There is much effort increasing day by day to develop more precise and accurate constitutive models in commercial codes to allow geotechnical designers to solve practical problem considering more realistic soil behavior(Abate, Caruso et al. 2008).

As recently stressed by (Wood 2004), "*Numerical analysis tools should be used much more as part of the routine of geotechnical design, incorporating the constitutive models of today and recognizing the inadequacy of some of the simplifying assumptions that have been imposed in the past for reasons of calculation expediency".*

Numerical simulations were carried out using an axisymmetric, two-dimensional finite-element program. An elasto-plastic model called "Hardening Soil Model" with so-called isotropic hardening used as a material model in PLAXIS. From the literature review studies, the three case studies were selected for the analysis. First, second and third case studies included in this report are of Tornhill, Sweden on clay Till, Portugal on saprolitic soil and Texas A & M University on sand respectively. The Hardening Soil model parameters are derived from the results of conventional laboratory and field tests found in the existing geotechnical reports for each of the case studies.

4.1 A case study of Tornhill, Sweden on Clay Till

4.1.1 Geological and geotechnical studies

The test site is located in the south-western part of the province of Skåne, where several different types of clay till have been deposited on top of each other during different periods of the last glaciation. The test field was made available by the Department of Soil Mechanics and Foundation Engineering at Lund University, which is responsible for its administration.

The test field is named Tornhill. The geological soil profile at the site is varied and contains three major types of clay till in the area: Baltic clay till, Mixed clay till and North-east clay till. The North-east clay till is so coarse and stiff and penetration to it was quite difficult. The focus of the investigations therefore lies on the upper two types of clay till. Since it is a heterogeneous soil and the composition within these main layers varies considerably both with depth and laterally, the classification of the profile was done in detail. In the test field, the thickness of the Baltic clay till is about 3 meters and the intermediate layer is also about 3 meters thick. The thickness of the North-east till and the depth to the bedrock varies, that is, about 8 meters thick and the depth to the bed-rock was thus about 14 meters (Larsson 2001).

To determine the geotechnical conditions in the test field, different types of field and laboratory tests including cone penetration tests, dynamic probing tests, dilatometer tests, pressuremeter tests, oedometer tests, triaxial tests were carried out. After the investigations, a series of three large-scale plate load tests was performed in the test field. The plates were excavated to the normal foundation level. Nevertheless, the zone of influence from these tests was also confined to the upper two types of clay till. Although the results were unanimous in certain respects, the variation both vertically and laterally in the upper soil layers was so great that a detailed evaluation of the different design methods cannot be made from this limited number of load tests. The detail description of the field tests, field investigations, laboratory tests and plate loading test is given in the report 'Investigations and Load Tests in Clay Till' (Larsson 2001).

Classification and a detailed description of the soil profile were made during routine tests. The classification of the samples taken with the tube sampler gave relevant explanation regarding layering found in the profile. The classification for the sample was as follows;

Table 4.1 Classification of samples taken by tube sampler at Tornhill site on clay till(Larsson 2001).

Depth, m	Classification
0.8-1.1	Fine **sand**
1.1-2.8	Sandy silty **clay till** with grains of limestone
2.8-3.3	Silty **clay till** with grains of limestone and infusions of small sand pockets
3.3-3.4	Silty **sand** with infusions of clay
3.4-3.7	Silty **clay till** with thin layers and small pockets of silt
3.7-3,85	Sandy silty **clay till**
3.85-4.25	Sandy silty **clay till** mixed with layers of gravelly silty sand
4.24-5.1	Silty **clay till** with grains of limestone
5.1-5.4	Sandy **clay till**
5.4-5.7	Sandy **clay till** with coarse gravel size particles

From the study of this classification, the soil profile for the study was determined. The test site consists of stiff to very stiff clay till. The water table was observed a depth of 1.5 m from the ground surface. The soil profile at the site is shown in Figure 4.1.

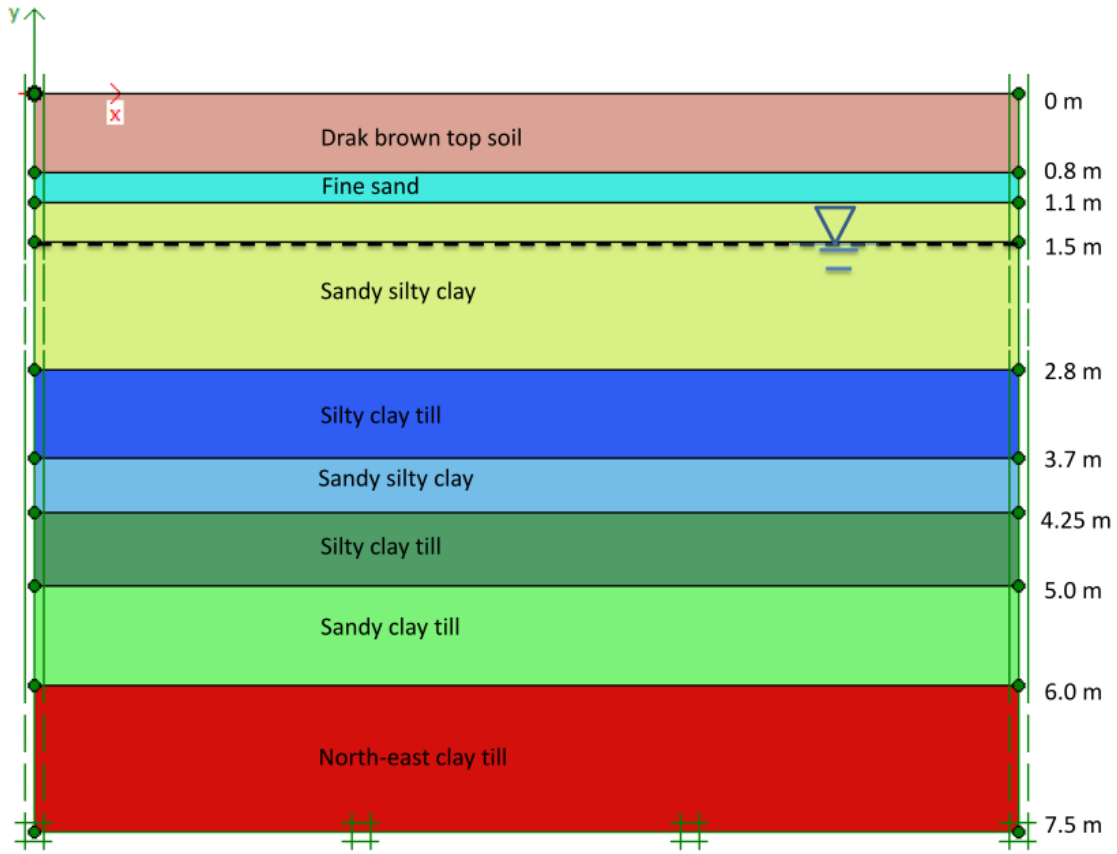

Figure 4.1 Soil profile at the Tornhill footing load test site.

The Clay till is heterogeneous soil and vary in composition and stiffness. Due to deposition of different types of clay till on top of each other during different periods of the last glaciation, the soil is very stiff and the stiffness increases with depth. Hence, the stiffness parameters in the soil profile may increase with depth. These also show that the soil is overconsolidated.

4.1.1.1 Laboratory tests

Determination of the preconsolidation pressure and oedometer modulus has been performed in oedometer tests in the laboratory. A result of an oedometer test on clay till, Tornhill at depth 1.25 m was illustrated in the report. The oedometer moduli evaluated were in good agreement.

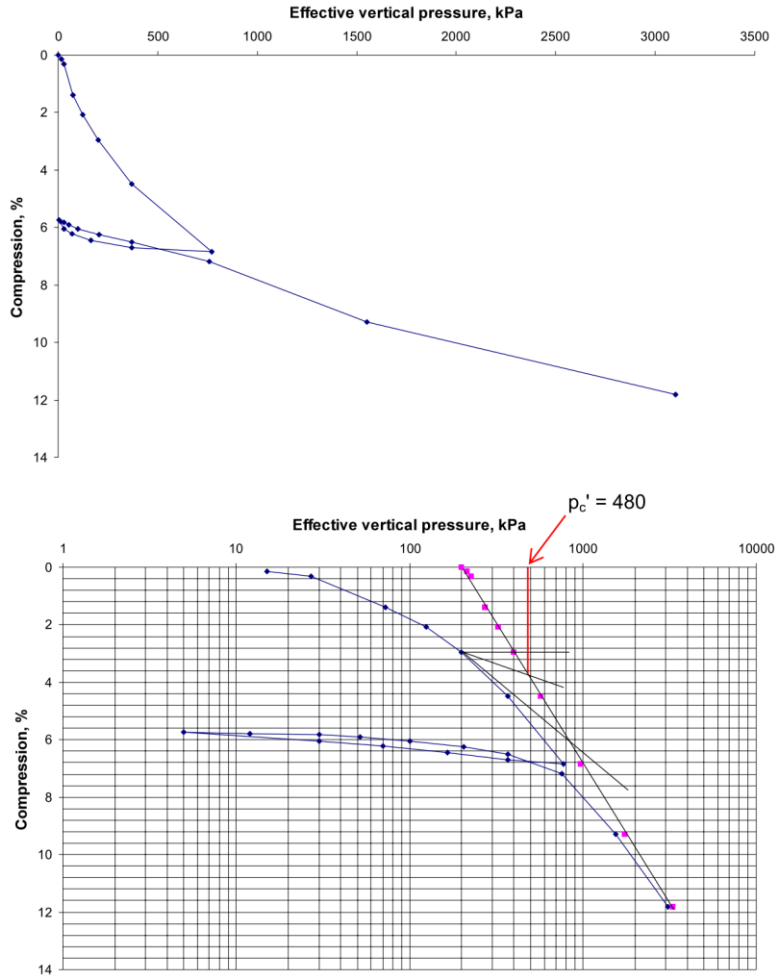

Figure 4.2 Results of an oedometer test at Tornhill footing load test site, 1.25 m depth(Larsson 2001).

Figure 4.2 show that the preconsolidation pressure, p_c', determined from oedometer test is in average of 480 kPa. Evaluation of preconsolidation pressures for the soil profile at Tornhill is shown in Figure 4.3.

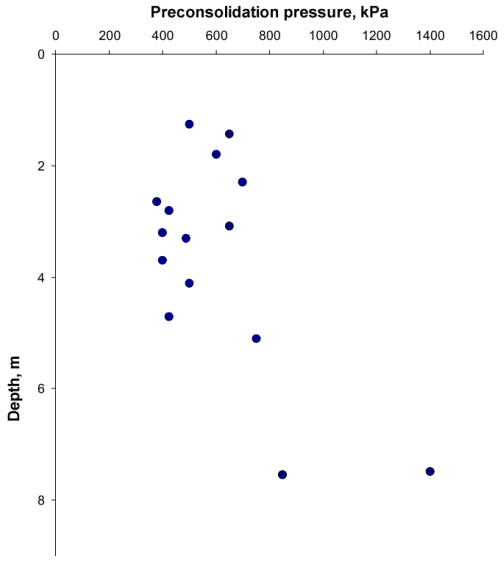

Figure 4.3 Preconsolidation pressures with depth at Tornhill footing load test site(Larsson 2001).

The unloading-reloading modulus, M_{url} is in the range of 50 to 100 MPa which is indicated in Figure 4.4.

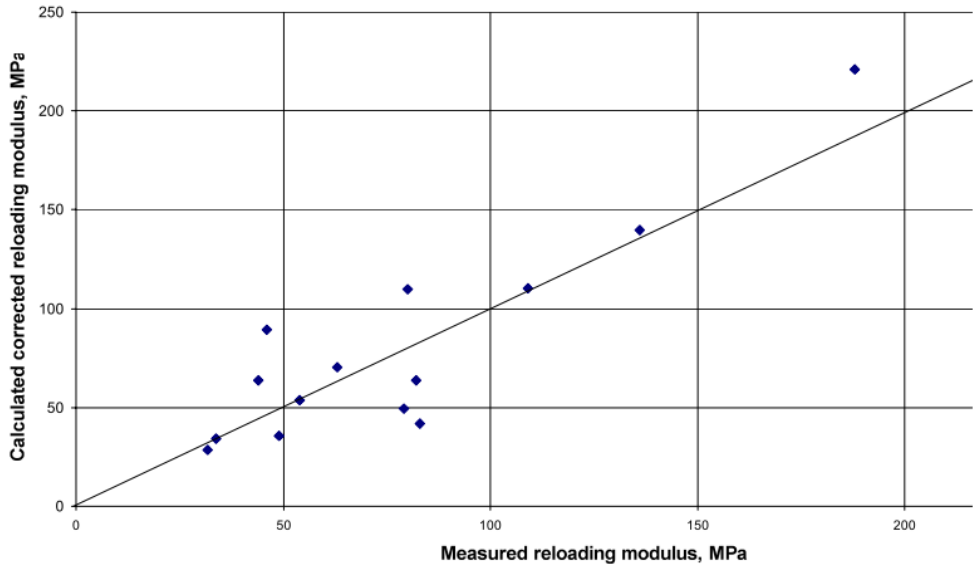

Figure 4.4 Comparison of measured and calculated reloading moduli at Tornhill(Larsson 2001).

Through a result from an undrained triaxial test on clay till from Tornhill, E_{50}^{ref} was determined as follow;

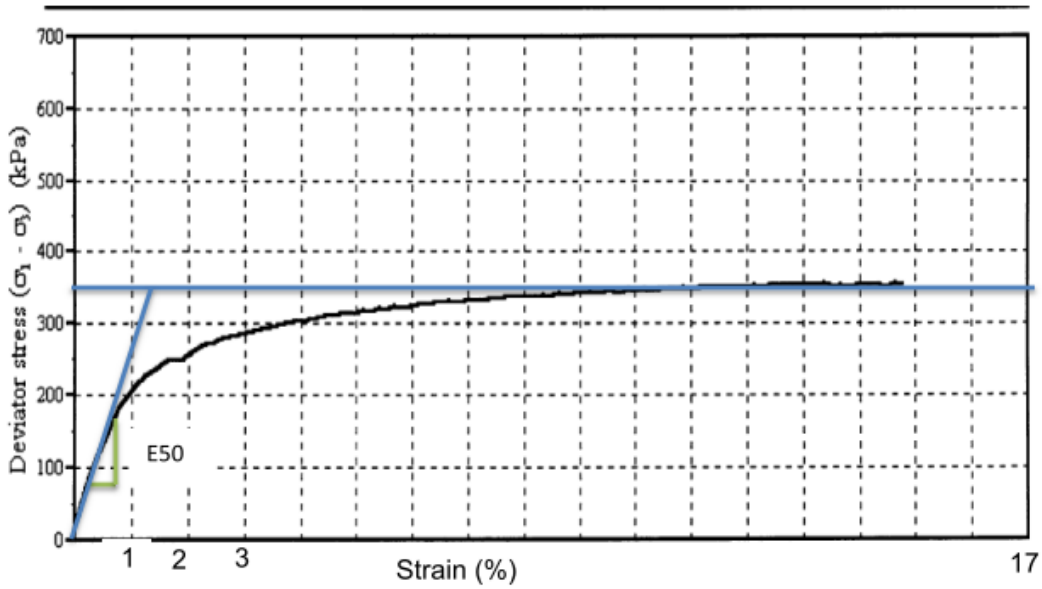

Figure 4.5 Determination of E_{50} from the triaxial test at Tornhill footing load test site(Larsson 2001).

E_{50} = 350/0.014 = 25000 kPa = 25 MPa

$$E_{50} = E_{50}^{ref}\left(\frac{\sigma_3^{'} + a}{p^{ref} + a}\right)^{0.8} \qquad @\ \sigma_3^{'} = 50 \text{ kPa}$$

where, $a = \frac{c}{\tan\phi} = \frac{16}{\tan 30} \approx 28$

In this case, the clay is sandy silty clay so m = 0.8 is assumed.

$$E_{50} = E_{50}^{ref}\left(\frac{50+28}{100+28}\right)^{0.8} = 0.67 * E_{50}^{ref}$$

Therefore,

E_{50}^{ref} = 1.48 * E_{50} = 1.48 * 25 = 37 MPa @ 2.2 m depth

The calculation result of triaxial test as well as unloading-reloading modulus from oedometer test is used as the reference to estimate the stiffness parameters for the Hardening soil model.

After extensive study of the geotechnical report of Tornhill, determination for the parameters required for Hardening Soil Model are shown in Table 4.2.

Table 4.2 Parameters of the soil at Tornhill footing load test site.

S/N	Soil Type	E_{50}^{ref}	E_{oed}^{ref}	E_{ur}^{ref}	m	c'	ϕ	Ψ	K_o^a	OCR[a]	γ	Model	Type
		MPa	MPa	MPa		kPa					kN/m^2		
1	Drak brown top soil	28	28	84	0.5	13.45	30	0	2.5	11.46	18	HS	Drained
2	Fine sand	30	30	90	0.5	13.45	30	0	3.7	17.5	17	HS	Drained
3	Sandy silty clay	32.5	32.5	99	0.5	16.14	30	0	4.4	23	17.6	HS	Drained
4	Silty clay till	35.75	35.75	108.90	1	9.08	30	0	2.2	7.8	17.2	HS	Drained
5	Sandy silty clay till	34	34	102	0.5	6.63	30	0	1.9	6.12	18.5	HS	Drained
6	Silty clay till	37.00	37.00	111.00	1	9.52	30	0	1.9	6	19.2	HS	Drained
7	Sand clay till	40.70	40.70	122.10	0.5	28.90	30	2	0.96	2.38	20.5	HS	Drained
8	North-east clay till	44.77	44.77	134.31	1	26.97	32	2	1.60	5	21.4	HS	Undrained

a = dilatometer test

Table 4.3 Material properties of the footing at Tornhill footing load test site.

Parameters	Name	Reinforced concrete footing	Unit
Thickness	d	0.5	m
Weight	w	12.5	kN/m/m
Poisson's ratio	υ	0.15	
Type of behavior	Type	Elastic, isotropic	-
Normal stiffness	EA	1.50E+07	kN/m
Flexural rigidity	EI	3.13E+05	kNm^2/m

The drained and effective shear strength parameters, c'_{ref} and ϕ' are determined by studying the triaxial tests as well as field investigations from the report. The dry density with depth can be found in the geotechnical report of Tornhill, with an average value of

approximately in the range 17 to 20.4 kN/m^2. Coefficient of horizontal earth pressure and overconsolidation ratio is taken from the dilatometer tests at Tornhill.

4.1.1.2 Plate loading tests

Three plate load tests were performed at Tornhill site in order to check the bearing capacity and settlement for shallow foundations on clay till. The plane dimensions of the plates are 0.5 X 0.5 m, 1.0 X 1.0 m and 2.0 X 2.0 m which were installed in a row along the main beams without significant interference in terms of the same soil mass being affected by the different load tests. The distance between the plates and the loading sequence were also adjusted so that there is no influence of previous load test results to the next one. For this reason, the smallest plate was placed at the one end of the row, the largest was in the middle and the intermediate plate was placed at the other end of the row.

Installation of plates and instrumentation:

The reinforced concrete plates were casted at the bottom of the excavated pits. The groundwater level would normally be at 2 m below the ground surface in summertime. However, when the test was conducted in that period the water level was at the ground surface. Though the great effort was given to lower the groundwater level, the attempt was not successful. The excavation was carried out maintaining the water level to preserve the soil properties.

The excavation was carried out to a depth of 1.3 m with base dimensions of 13 X 5 m in which 1:1 slope was made in one of the longer side but on the other side it was steeper. At two opposite corners of the excavation, holes were dug to 2 meters depth and the pumps were lowered into these. The further 0.2 m of the excavation for the test plates was carried out manually as shown in Figure 4.6.

After the excavation work, instrumentation below each of the plates was carried out which consist of three settlement gauges placed at different depths and one piezometer. Only one settlement gauge was installed under the smallest plate. The settlement gauges were installed close to three corners of the plates at a perpendicular distance of 0.13B from adjacent sides of the plate for the settlement and stresses (where B is the width of the plate). On gauge for each plate was placed with its center at a depth of about 0.15 m below the base to check the possible deformations. The other two gauges were placed at depths within the depth interval down to 2B below the plates.

Figure 4.6 Excavation for the plates at Tornhill footing load test site(Larsson 2001).

After installation of the instrumentation, reinforcing bars were placed in the moulds and concrete was pumped in. Apart from the settlement gauges below the plates, the total settlements of the plates were measured on rods fixed in the concrete at each corner of the plate. Piezometers were installed beneath the plates in order to check that the tests were drained and that all excess pore pressures had dissipated at the end of each load step. The piezometers were electrical and were intended to be installed at depths where the pore pressures could be expected to be highest with consideration to stress increases and drainage paths. The concrete plates were 0.5 m thick.

Installation of the reaction system and the loading system:

The eight ground anchors had been installed by PEAB Grundteknik about one month in advance. The ground surface was leveled and wooden rafts were stacked and placed horizontally on the leveled surfaces. The three railways bridge beams were then placed side by side with ends resting on stacks and bolted together. Their common center line was aligned with center of plates. Two short beams were placed on top and across the ends of large beams, and were connected to the tie rods from the ground anchors. Above the center of the largest plate, two other beams were placed on top of and across the railway bridge beam with their ends resting on the two stacks of excavator mats at the sides of the excavation. These beams were connected to tie rods which are pre-stressed and the whole reaction system was fixed which can be seen in Figure 4.7.

Figure 4.7 Reaction system being mounted at Tornhill footing load test site(Larsson 2001).

The plate loading tests were loaded hydraulically which consisted of a hydraulic pump and electronically operated regulation valves. In addition, two hydraulic jacks for different load ranges corresponding load cells for measuring the load and providing the signal for regulating the hydraulic pressure, and a computer for data collection and regulation of the loading process were also used. A back-up system for the hydraulic pressure was also installed. For the two smaller plates, circular stress distribution plate was centered directly on the concrete and further plates were put to fill the gaps whereas for the larger plate, square stress distribution plate was used covering a larger part of the top surface. In order to distribute the load on the reaction beams evenly, a short beam was fixed under and across them at the loading point. For the measurement of loading system, the computerized data collection and load regulation system, the load cells, the piezometers and the displacement transducers were used (Larsson 2001).

Plate load tests:

While performing load tests constant load steps were maintained. The tests were the drained and all the pore pressure was dissipated. The load step was given for duration of 2, 4 and 6 hours for small, middle and largest plate respectively. The detail of the plate load test can be studied in (Larsson 2001).

Results of plate load tests:

The loading of the 0.5 X 0.5 m plate was performed with an initial step of 10 kN, a second of 15 kN up to 25 kN and thereafter in steps of 25 kN. The unloading-reloading cycle was also performed in steps of 25 kN from the end of the step with 150 kN load down to 25 kN and then to 10 kN with the duration of each step on only 12 minutes. After initial as well as unloading-reloading cycle the duration of loading steps was 2 hours. After the last load steps

of 250 kN, the settlement continued with constant rate for half an hour where the failure was obtained but was slow.

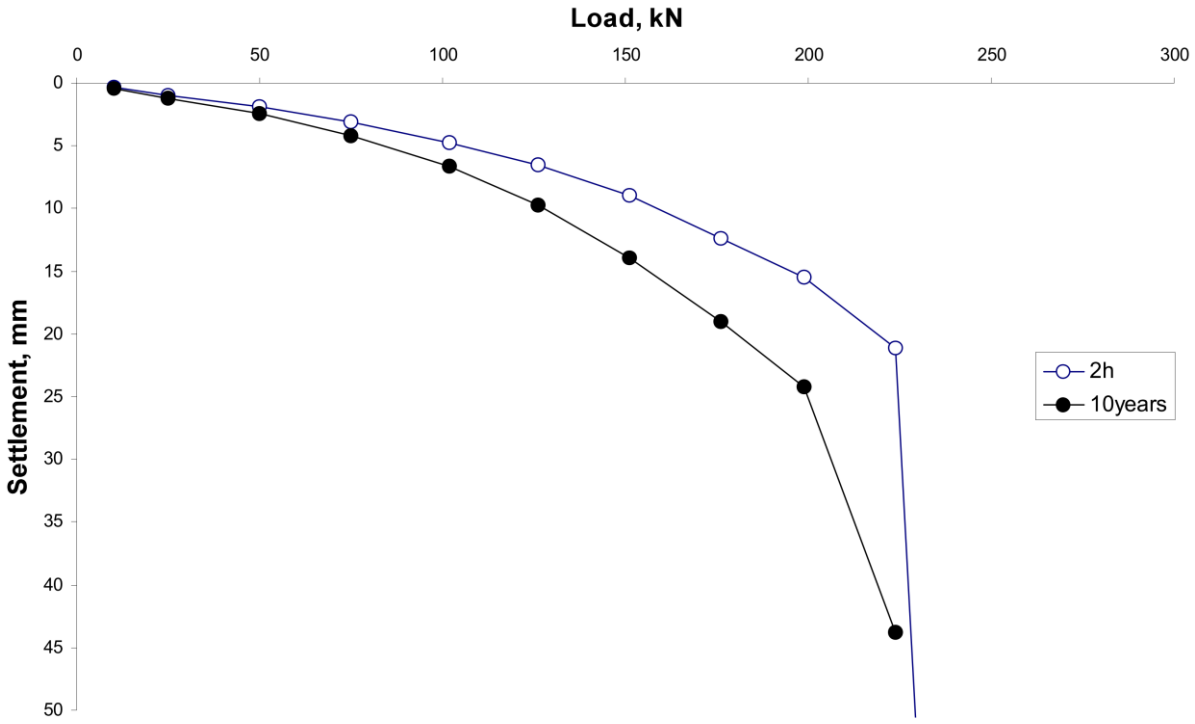

Figure 4.8 Measured and extrapolated load-settlement curves in the load test on the 0.5 X 0.5 m plate at Tornhill footing load test site(Larsson 2001).

The time-settlement curve was measured during each load steps. The 2 hours load-settlement curve was extrapolated to 10 years which is the time perspective normally considered in settlement predictions. Both the measured 2 hours and 10 year curves are smooth without any sign of a bearing capacity failure for load up to 200 kN which can be seen in Figure 4.8. Above this load, the creep settlements increase considerably and the extrapolated 10-year settlements almost reach the failure criterion for settlements, amounting to 10 % of the plate width as early as at a load of 225 kN.

The 1.0 X 1.0 m plate was performed in steps of 75 kN up to load of 300 kN and unloading was performed with a duration of 12 minutes. The loading was further done after unloading steps to load of 1350 kN and was terminated when the average settlement was 88 mm. The load-settlement curve of both the measured average 4 hours and extrapolated 10 years was plotted as in Figure 4.9. The failure criterion for a settlement, amounting to 10% of the plate width, had been passed at a load of 1200 kN for the 10 year settlements.

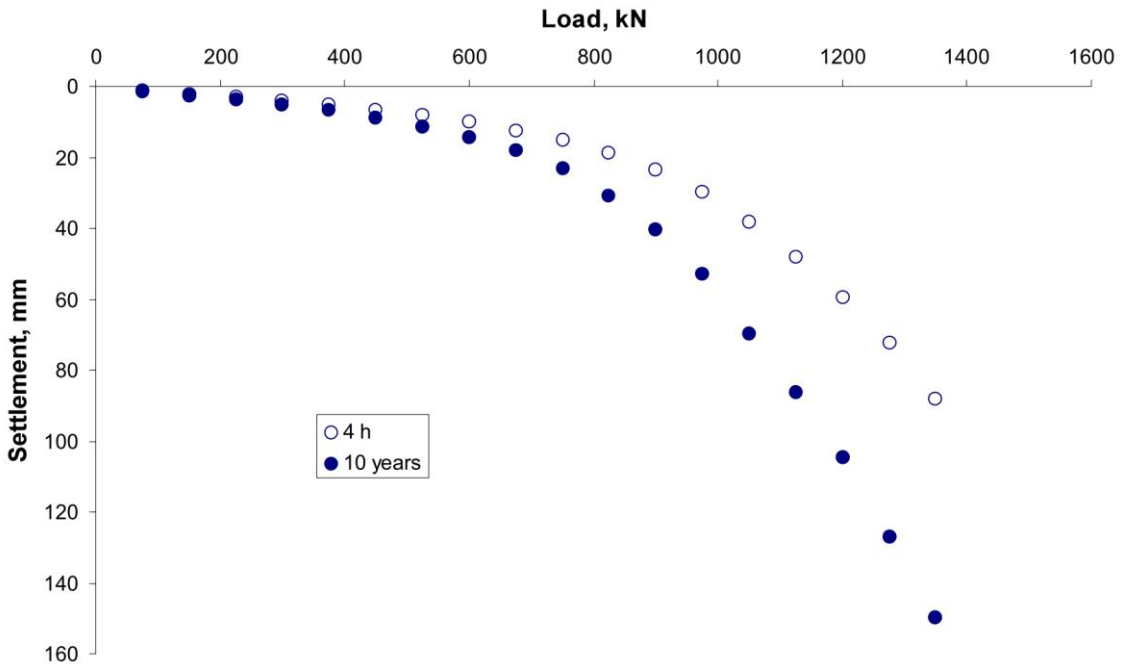

Figure 4.9 Measured and extrapolated load-settlement curves in the load test on the 1.0 X 1.0 m plate at Tornhill footing load test site(Larsson 2001).

For the 2.0 X 2.0 m load test, the load steps of 200 kN was performed at a duration of 6 hours without unloading-reloading cycle. The test was terminated at load of 2800 kN with settlement of 56 mm. The load-settlement curve of both the measured average 4 hours and extrapolated 10 years was plotted as in Figure 4.10.

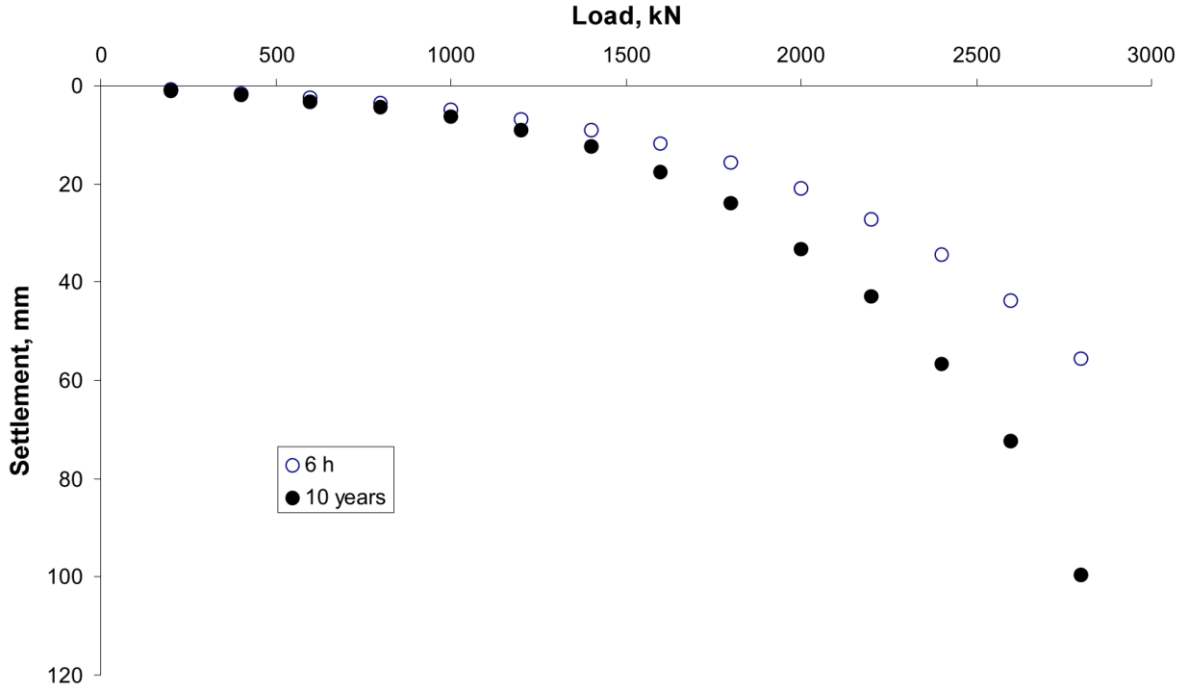

Figure 4.10 Measured and extrapolated load-settlement curves in the load test on the 2.0 X 2.0 m plate at Tornhill footing load test site(Larsson 2001).

The calculated load-settlement curves are compared to the results from the plate load tests which are shown in Figure 4.11 Figure 4.12 and Figure 4.13.

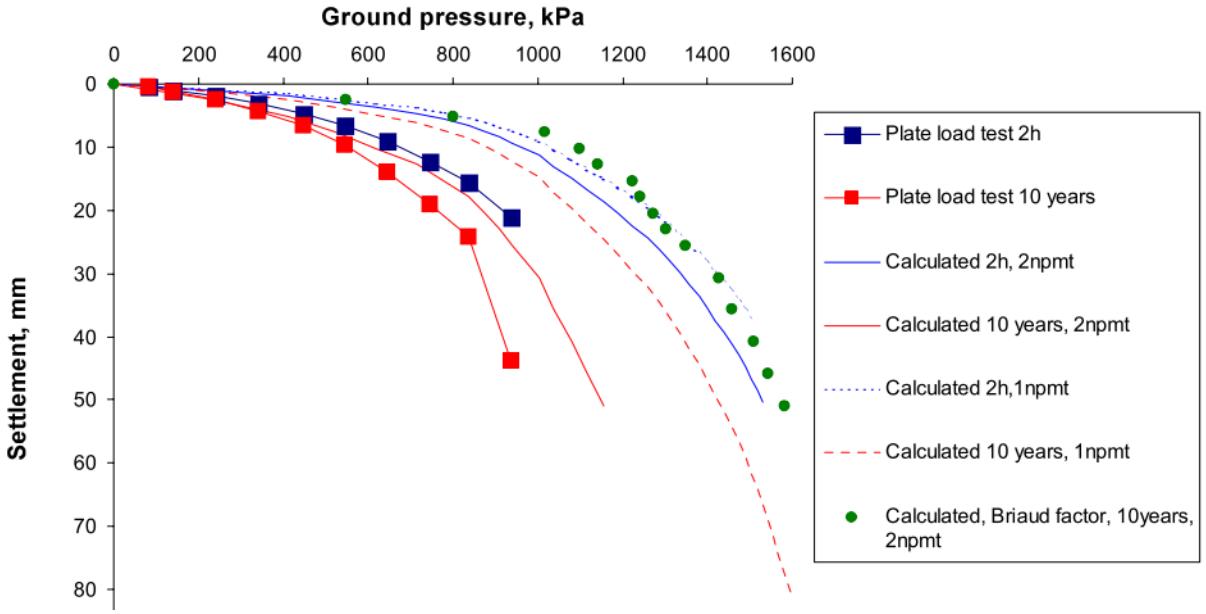

Figure 4.11 Comparison of calculated load-settlement curves to the results of plate load tests for 0.5 X 0.5 m plate at Tornhill footing load test site(Larsson 2001).

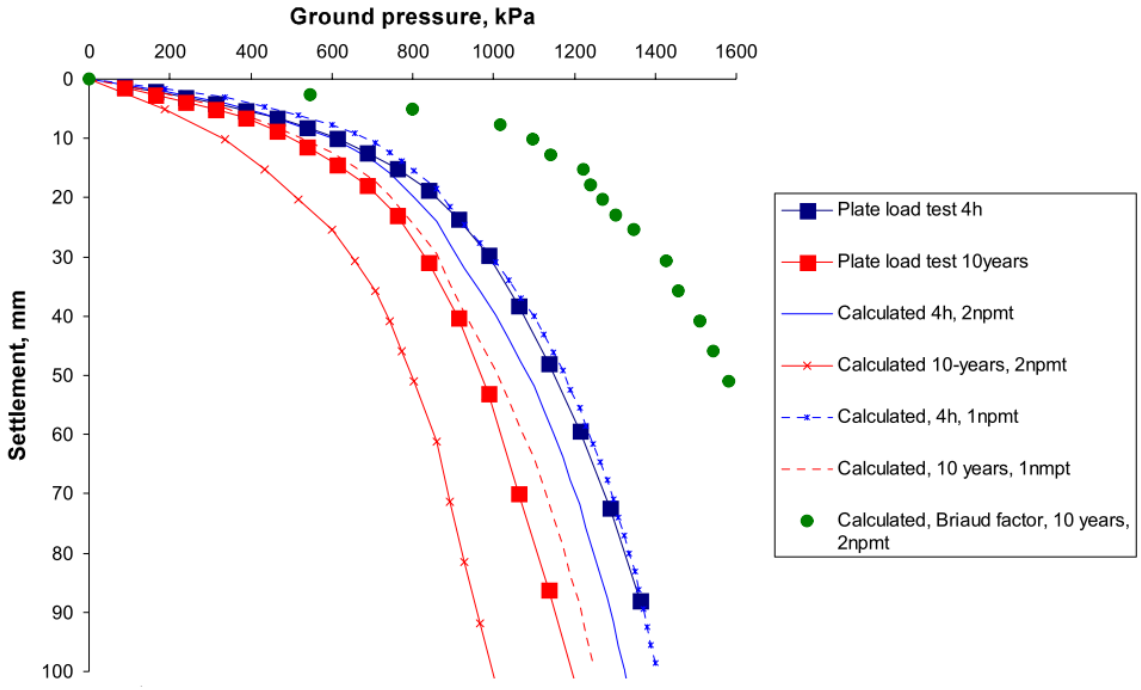

Figure 4.12 Comparison of calculated load-settlement curves to the results of plate load tests for 1.0 X 1.0 m plate at Tornhill footing load test site(Larsson 2001).

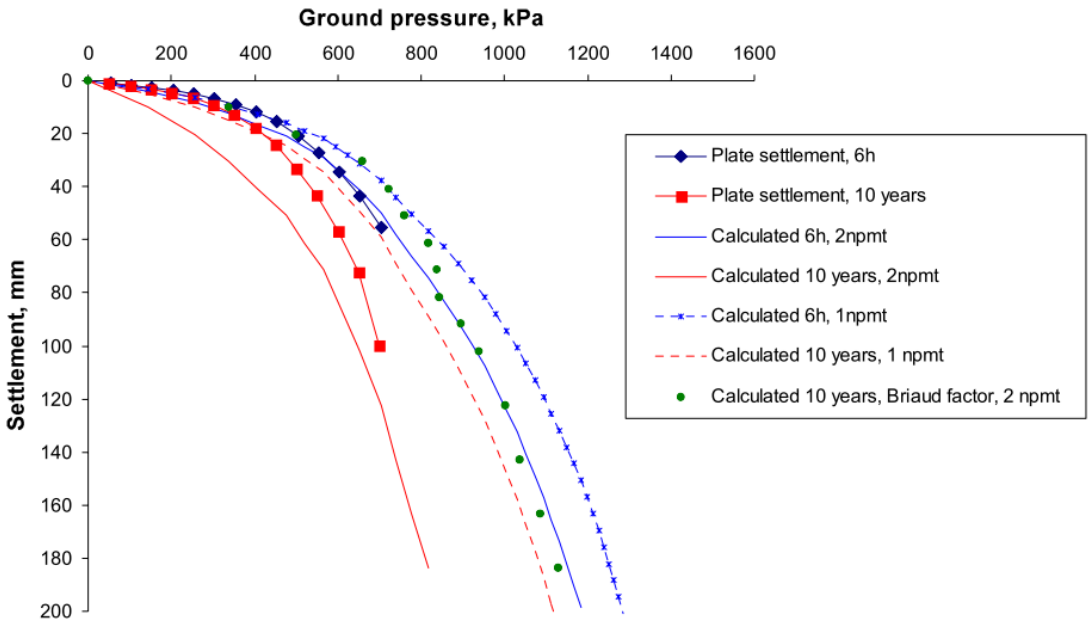

Figure 4.13 Comparison of calculated load-settlement curves to the results of plate load tests for 2.0 X 2.0 m plate at Tornhill footing load test site(Larsson 2001).

The bearing capacity is traditionally calculated as an ultimate load on the basis of the measured shear strength of the soil. In the current load tests, failure was obtained only for the smallest plate. Probable ranges for the failure load could be obtained by extrapolation of the load-settlement curves from the other two plates. It should be observed that the failure obtained in the load test on the smallest plate was a punching type failure and not the classical shear surface assumed in most bearing capacity theories. The detail regarding bearing capacity results was studied in (Larsson 2001). From the plate load tests, it was possible to estimate the approximate failure and creep ground pressures beneath the plates which are illustrated in Table 4.4.

Table 4.4 Estimated failure and creep pressures from the load tests at Tornhill footing load test site(Larsson 2001).

Plate	Ultimate failure kPa	s = 0.1b, load test, kPa	s = 0.1b, 10 years kPa	Creep pressure kPa
0.5 x 0.5	950	950	910	800
1.0 x 1.0	1600	1400	1150	700
2.0 x 2.0	950	950	780	800

4.1.2 Numerical modeling

The FEM analysis of reinforced concrete footings are modeled in FEM based package PLAXIS 2D. The 15 nodes element will result a more precise calculation of the stress and strains. A fine mesh is used for the models. The axi-symmetric circular footing has modeled as linear elastic element. The experimental load--displacement curves for shallow foundations obtained by (Larsson 2001) are compared with the numerical results obtained using

constitutive model, that is, Hardening Soil Model. The elastic modulus of soil has been considered based on the available correlation with the in-situ and laboratory test results e.g. CPT, CHT, DMT, PMT, oedometer and triaxial tests.

Three square footings with plane dimensions 0.5 X 0.5 m, 1 X 1 m, and 2 X 2 m are considered. The square footings can be approximated as circular footings with soil-foundation contact areas equivalent to those of the corresponding square footings, that is, with diameters of 0.56 m, 1.12 m and 2.26 m which is shown in Figure 4.14. (Lee and Salgado 2002) found that 'differences in stresses at the same depths due to the use of circular rather than square footings were less than 2%, based on linear elastic calculations'.

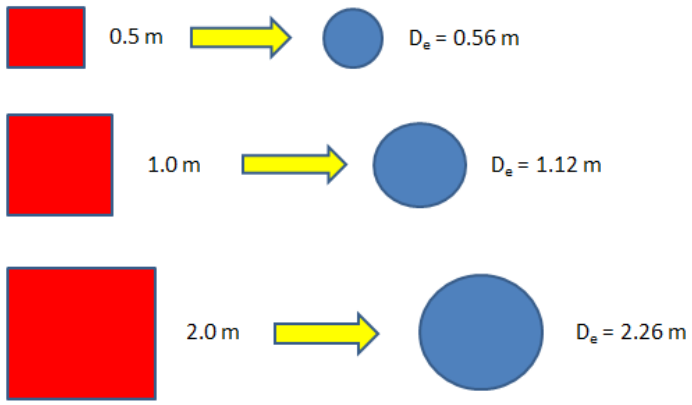

Figure 4.14 Examined square footings and equivalent circular footings at Tornhill footing load test site.

All three square footings were modeled numerically with number of simulations by changing the value of strength parameters c'_{ref} and ϕ'. The goal of these simulations is to validate our numerical analysis by comparison with existing load-settlement observations. In PLAXIS, based on the soil profile in Figure 4.1, the numerical model is created for the bearing capacity calculation which is shown in Figure 4.15.

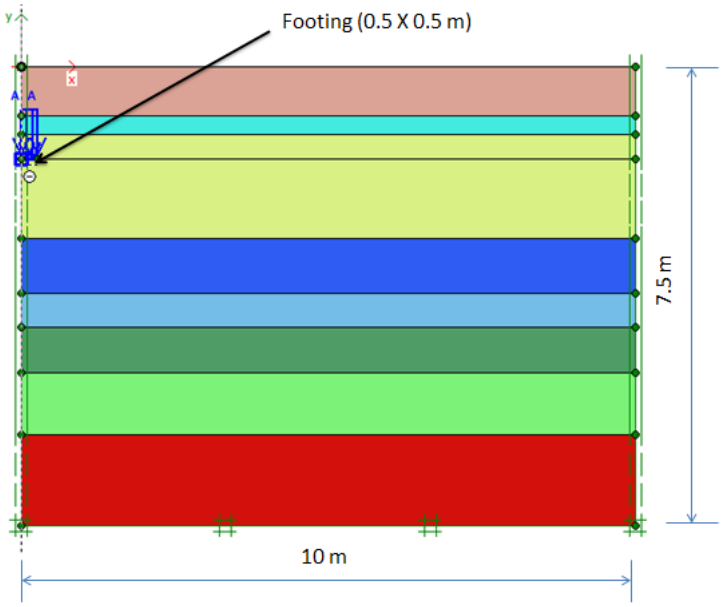

Figure 4.15 Typical Numerical model for simulation at Tornhill footing load test site.

A drained behavior is assumed for the materials for the bearing capacity calculations. The undrained behavior is assumed for north-east clay till due to very stiff clay till. Initial stresses in the soil are driven from the material weight and their historical of development. In the PLAXIS software the horizontal stress in static state is calculated using Jacky's formula;

$$k_o = 1 - \sin(\phi)$$

When the typical model for simulation is created with all material sets in it, the standard boundary conditions are set. As a result PLAXIS will automatically generate a full fixity at the base of the geometry and roller boundaries at the vertical sides (u_x = 0; u_y = free). In this project, in order to calculate the bearing capacity, the elastic footing was chosen with flexural rigidity (bending stiffness), EI and axial stiffness, EA.

A typical 2D meshes are shown in Figure 4.16. The bottom boundaries of the finite element models are located at a depth of 7.5 m and the lateral boundaries are located at a distance of 10 m from the center of the footings. 15-noded axisymmetric elements are used in the finite element meshes to model both the soil and the footings. The interface elements are also used between the footing base and the soil with a R_{inter} = 1.

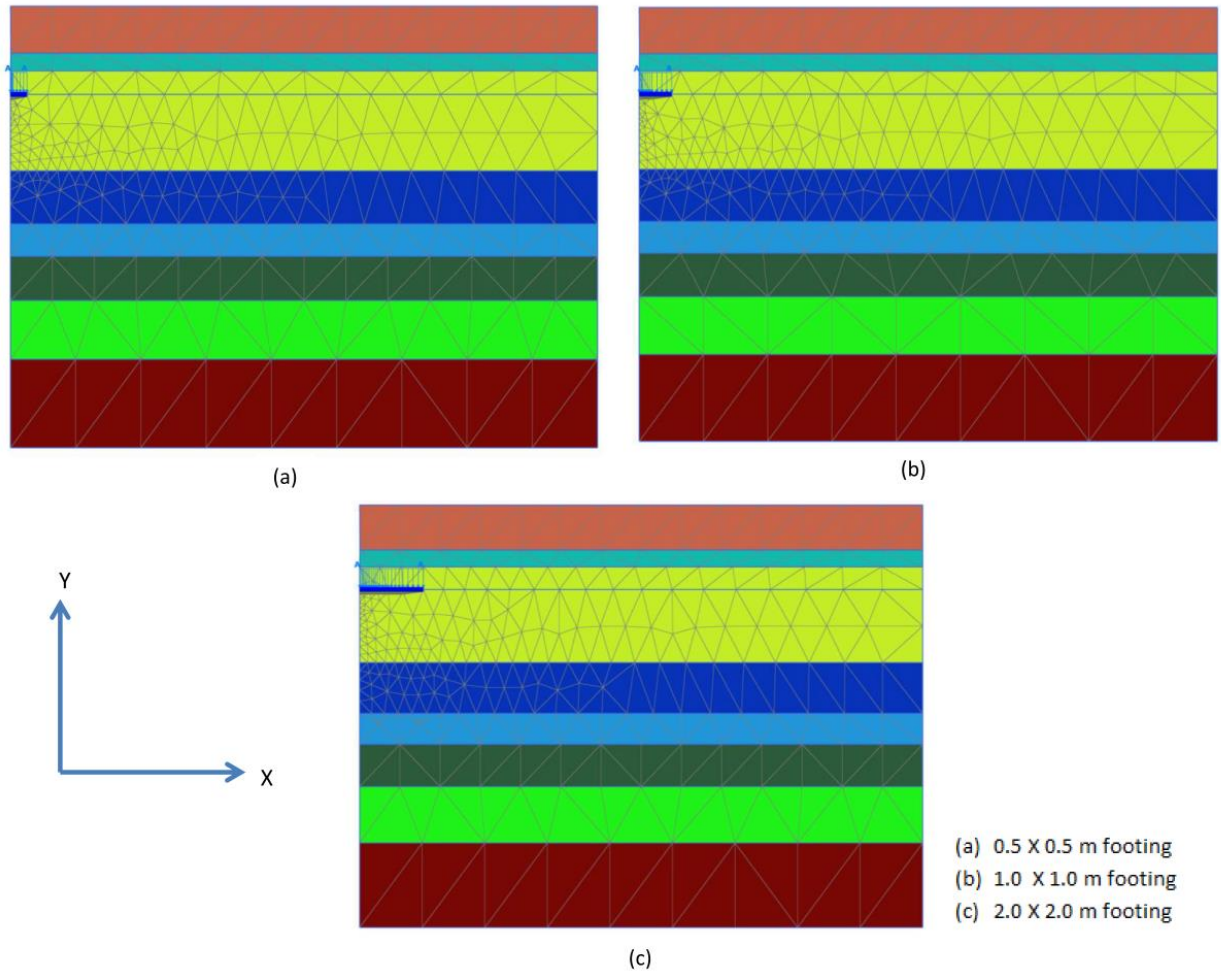

Figure 4.16 FEM mesh for the numerical simulation at Tornhill footing load test site.

Loading condition:

Distributed load – load system A is applied vertically over the footing without eccentricity. Initial stresses are developed in the input stage by deactivating the footing. It is assumed that the self-weight of the footing has added to the distributed load. Two staged construction are performed. In the first staged construction, the excavation is done and in the second staged construction, footing and loading are activated. Finally, incremental multiplier is applied for vertical load to failure. The footing model is shown in Figure 4.17.

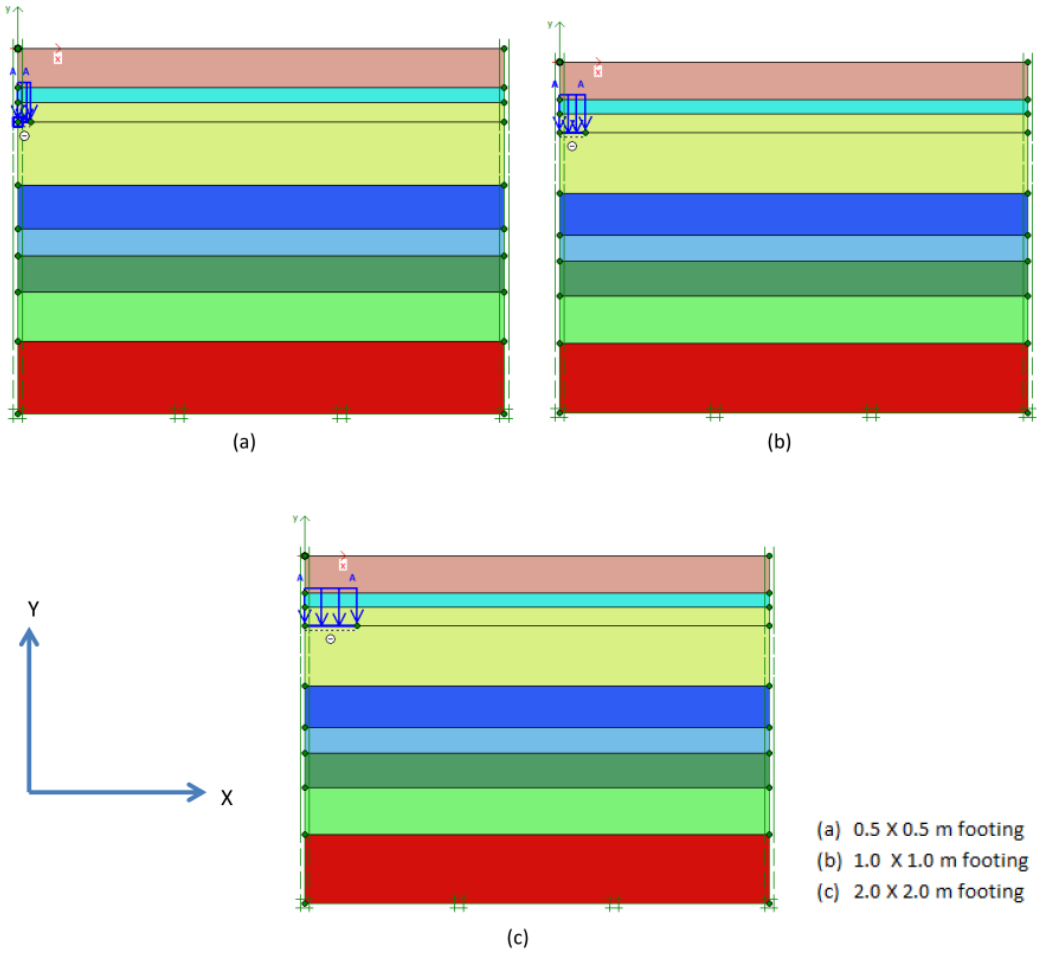

Figure 4.17 Footing model in PLAXIS at Tornhill footing load test site.

Deterministic results:

The simulations of different size of footings are carried out using Hardening Soil Model. Three square footings with plane dimensions 0.5 X 0.5 m, 1 X 1 m, and 2 X 2 m are considered. For each of the dimensions, numbers of simulations are done, for example, simulation 1, simulation 2 and simulation 3 to show consistency in the load-settlement curve between extrapolated 10 years plate loading test and simulated values. After the simulations are conducted, it can be seen that simulation 3 has load-settlement curve similar with extrapolated 10 years plate load tests. Then, only the deterministic results of simulation 3 are shown in Figure 4.18 to Figure 4.23.

Table 4.5 Number of simulations and strength parameters for different size footings at Tornhill footing load test site.

0.5 X 0.5 m footing			
Simulations	c'_{ref}	**ϕ'**	**Ψ'**
1	13.45	30	0
2	12.45	30	0
3	11.45	30	0
1.0 X 1.0 m footing			
1	13.45	30	0
2	12.45	30	0
3	14.45	30	0
2.0 X 2.0 m footing			
1	13.45	30	0
2	12.45	30	0
3	11.45	30	0

Total displacement, u_y:

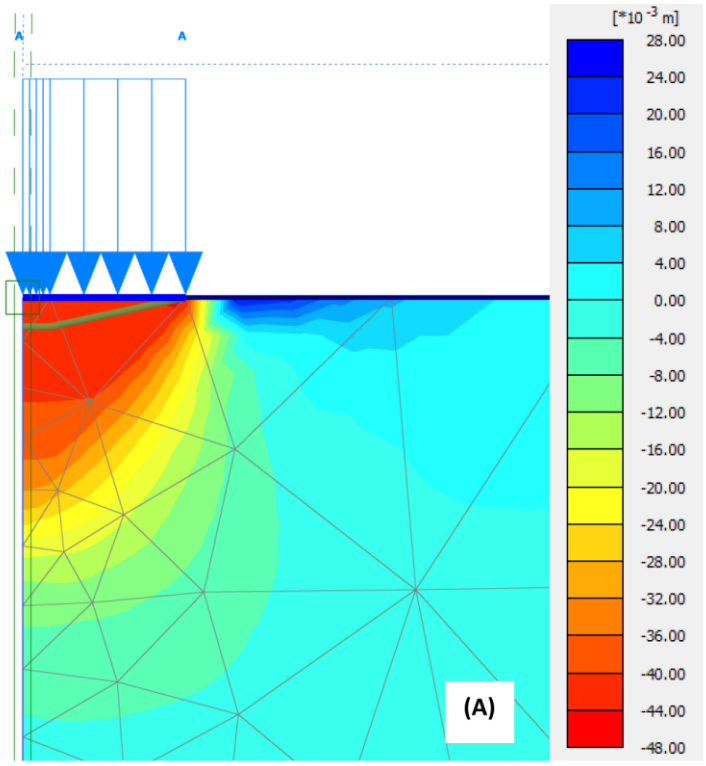

Figure 4.18 Vertical displacement transferred to the soil at Tornhill: 0.5 X 0.5 m footing.

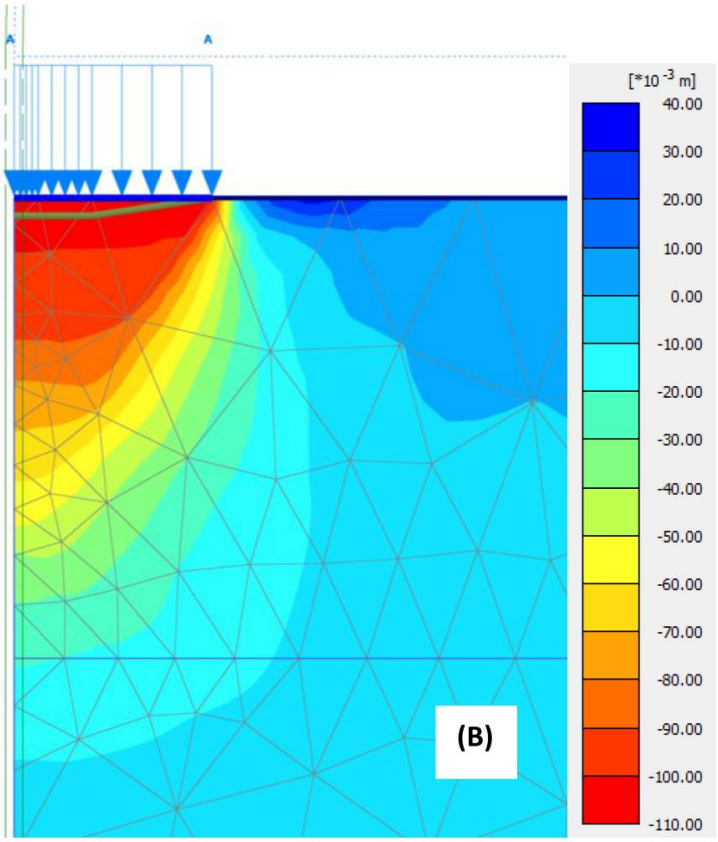

Figure 4.19 Vertical displacement transferred to the soil at Tornhill: 1.0 X 1.0 m footing.

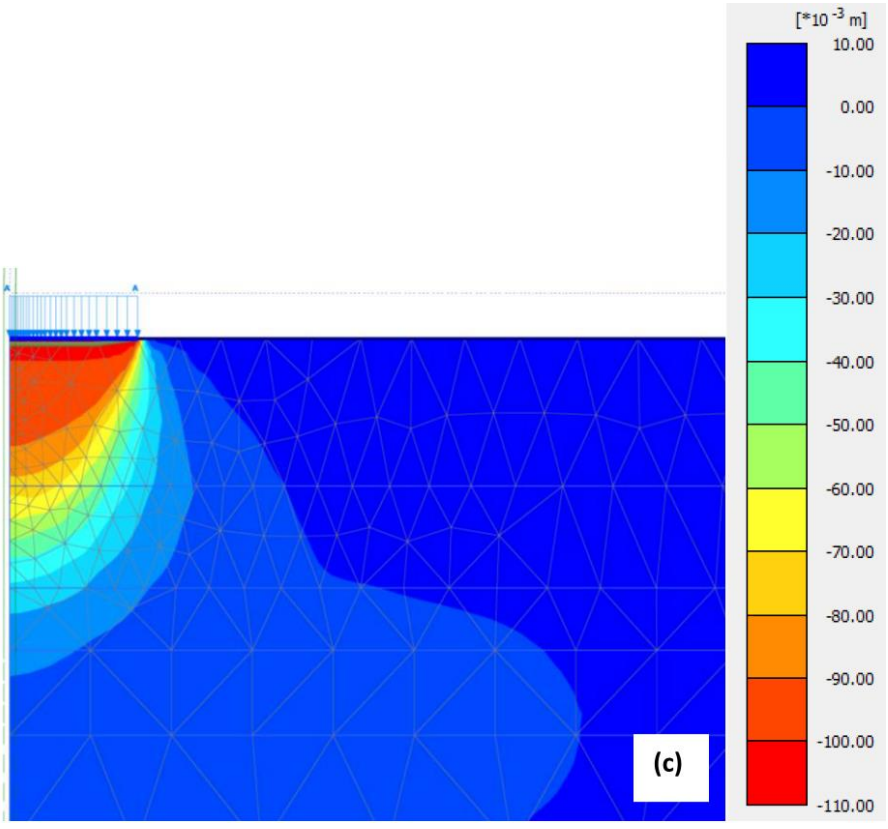

Figure 4.20 Vertical displacement transferred to the soil at Tornhill: 2.0 X 2.0 m footing.

Table 4.6 Showing maximum and minimum vertical displacement for total ground pressure below footing at Tornhill.

S/N	Total displacement, u_y (mm)	
	Maximum	Minimum
(A)	25.19	-44.31
(B)	35	-103.2
(C)	7.266	-102.4

Total deviatoric strain, γ_s:

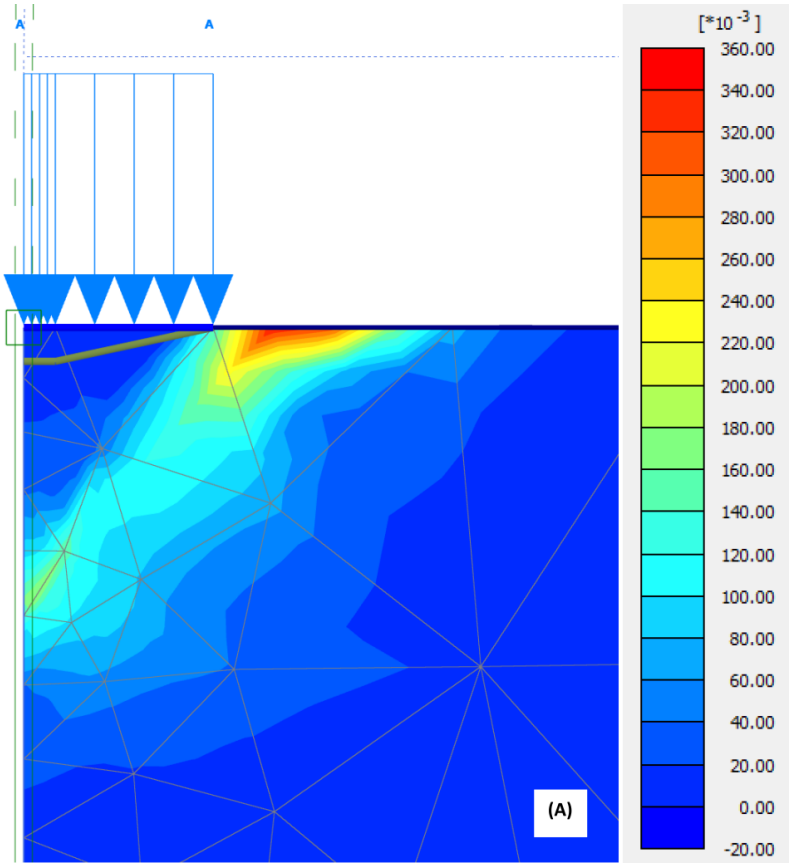

Figure 4.21 Total deviatoric strain for total ground pressure at Tornhill: 0.5 X 0.5 m footing.

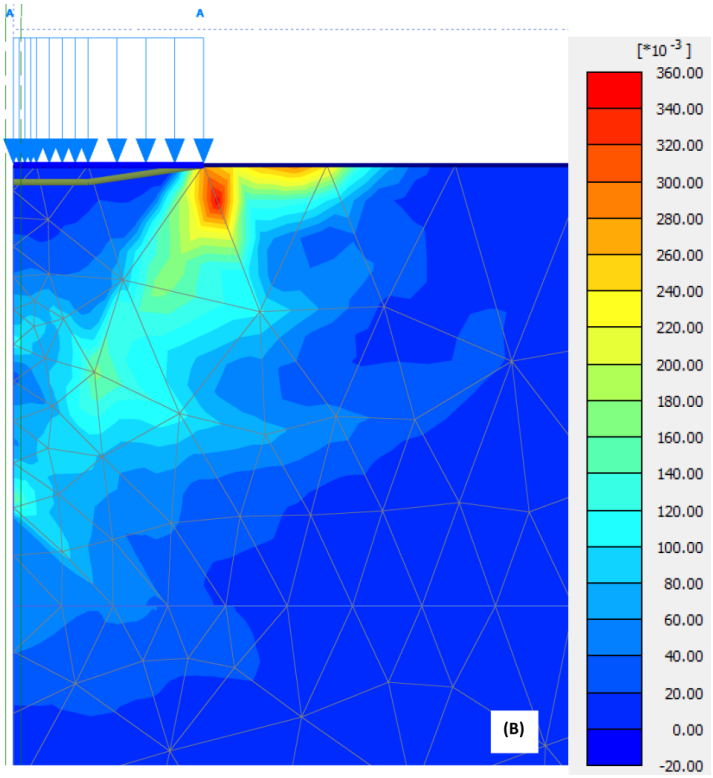

Figure 4.22 Total deviatoric strain for total ground pressure at Tornhill: 1.0 X 1.0 m footing.

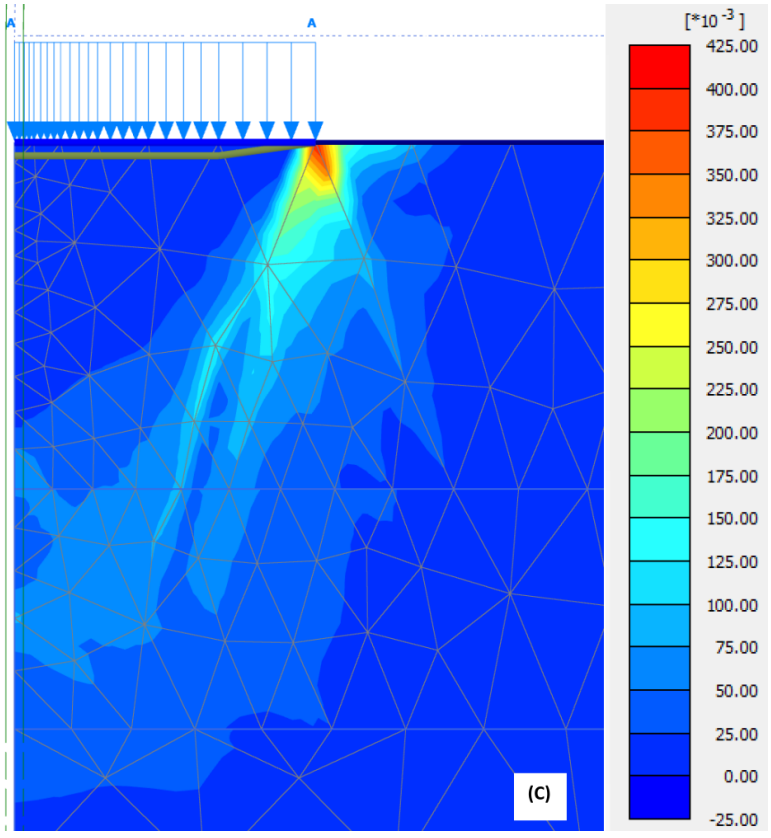

Figure 4.23 Total deviatoric strain for total ground pressure at Tornhill: 2.0 X 2.0 m footing.

Table 4.7 Showing maximum and minimum total deviatoric strain for total ground pressure below footing at Tornhill.

S/N	Total deviatoric strain, γ_s	
	Maximum	Minimum
(A)	0.3441	0.033E-6
(B)	0.3526	0.078E-6
(C)	0.4057	0.233E-6

The horizontal displacement of the soil from the edge of the 2.0 X2.0 m footing is shown in Figure 4.24. It is seen from the illustration that the maximum horizontal displacement is about 23.4 mm at a maximum load of about 780 kPa. This is the maximum load that is applied during plate loading test.

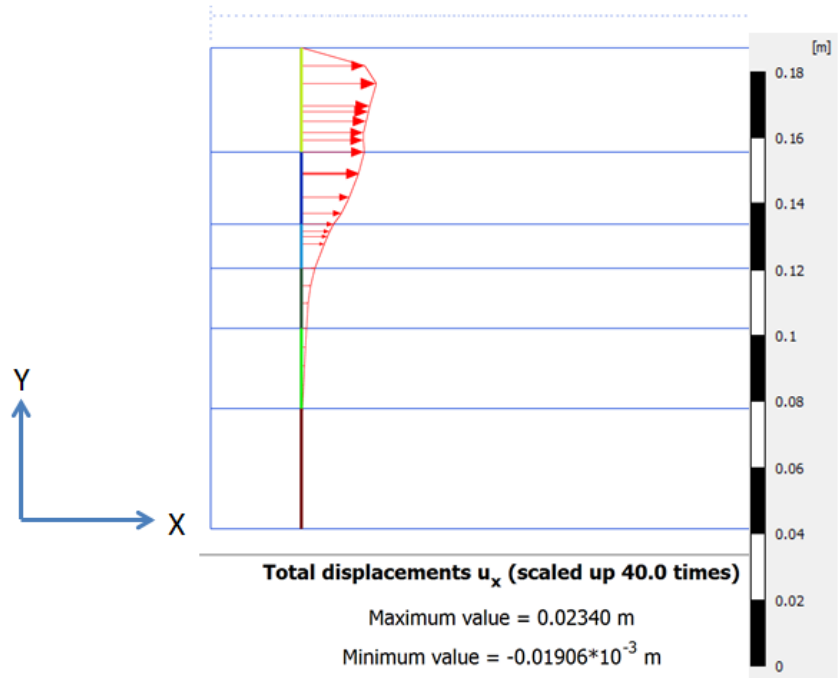

Figure 4.24 Horizontal displacement from the edge of footing at Tornhill: 2.0 X 2.0 m footing.

Stress paths show the change of stress states during loading or unloading. During this case, the stress paths at a depth of 2.8 m below the footing, below the edge of the footing and on the same line away from the footing at points K, L and M respectively are determined for 2.0 X 2.0 m footing. It is illustrated in Figure 4.25.

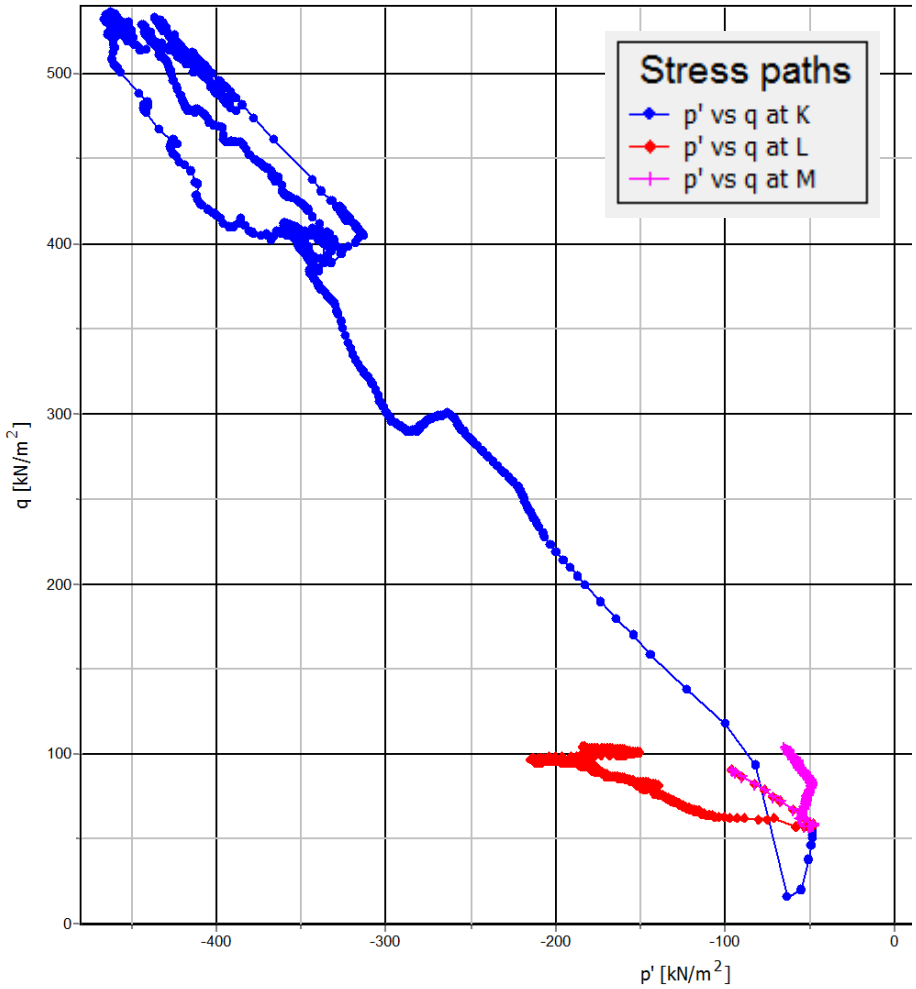

Figure 4.25 Stress paths at point K, L and M for 2.0 X 2.0 m footing at Tornhill.

4.1.3 Comparison of load-settlement curve from PLT and PLAXIS

It is instructive to compare the results of plate loading tests with those obtained from our numerical results. Figure 4.26,Figure 4.27 andFigure 4.28 show the measured and simulated load-settlement response for each footing. It can be seen that the measured load-settlement curves and the numerical curves obtained using the proposed numerical model are more or less similar for all the footings investigated. During the simulation, it is seen that three simulations are done for each footing. For each simulation, back-calculation was done for the values of c'_{ref} and ϕ' because the coefficient of bearing capacity depends on these two values. The simulation 3 for each footing provides very similar results.

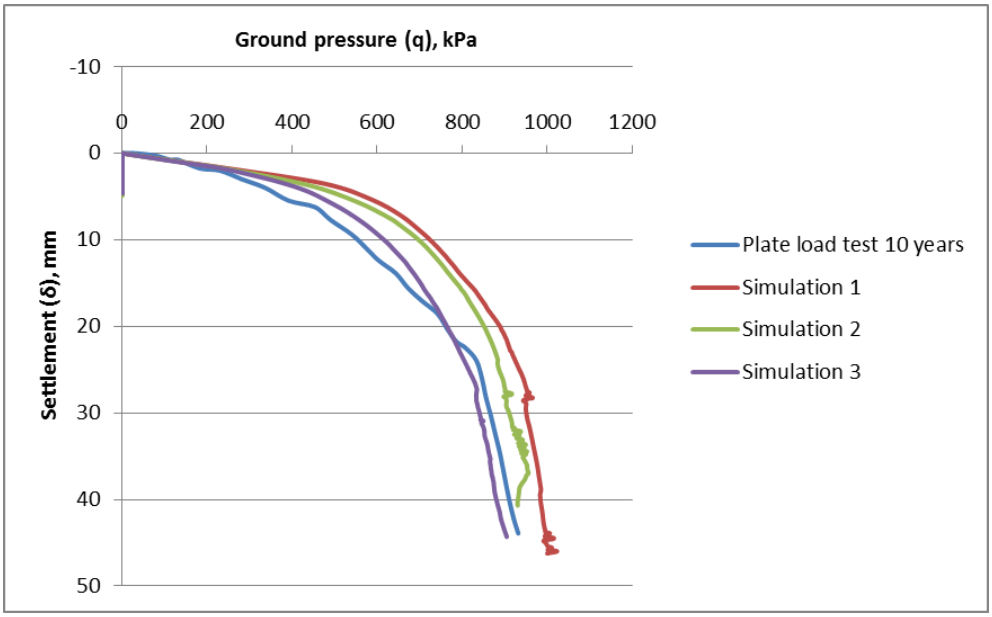

Figure 4.26 Comparison of experimental (Larsson 2001) and numerical load-settlement curve at Tornhill: 0.5 x0.5 m footing.

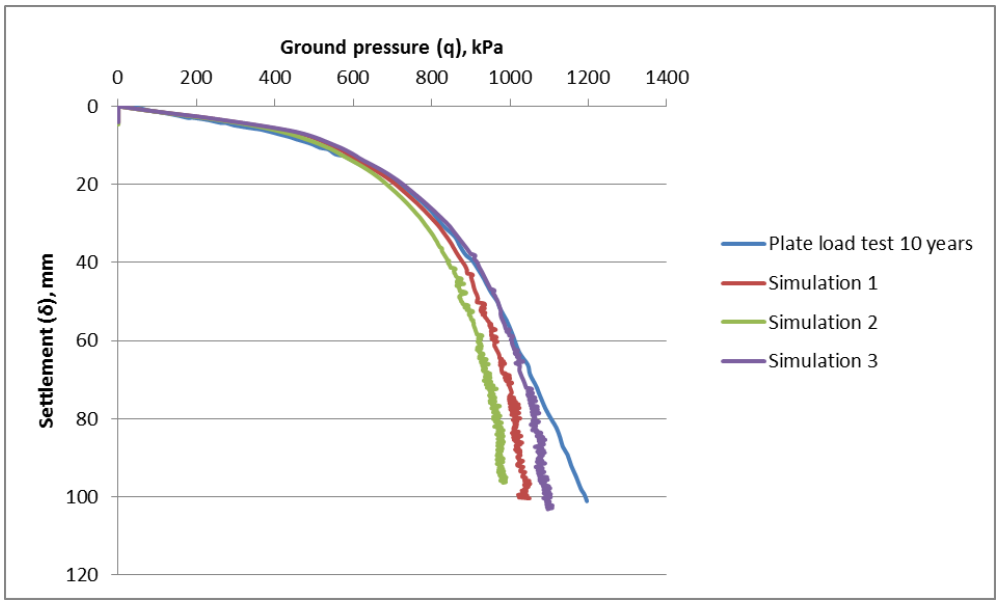

Figure 4.27 Comparison of experimental (Larsson 2001) and numerical load-settlement curve at Tornhill: 1.0 X 1.0 m footing.

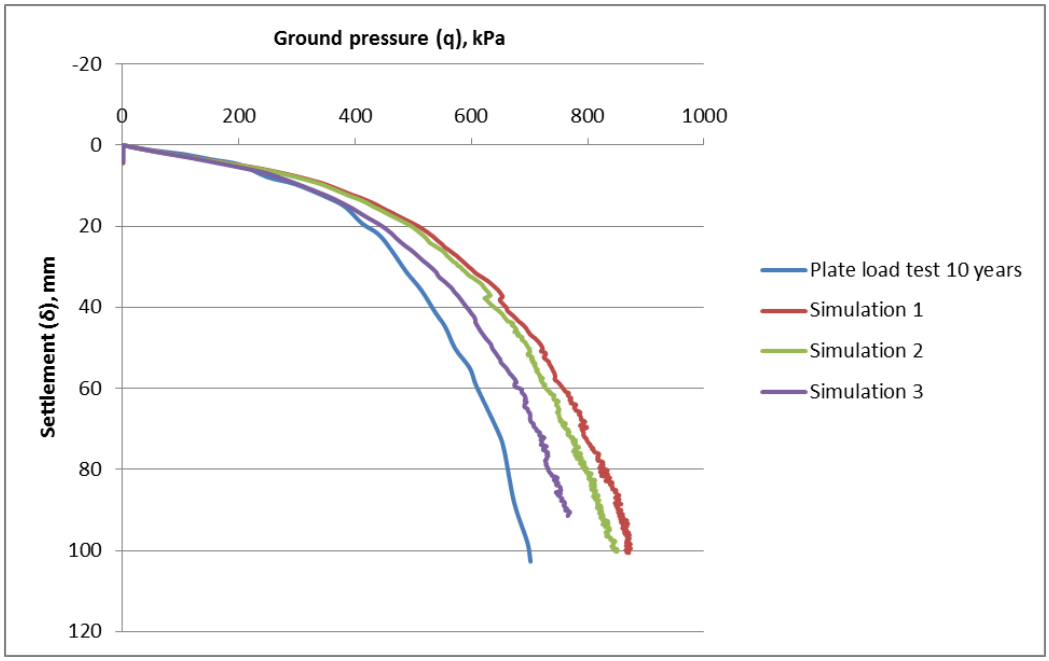

Figure 4.28 Comparison of experimental (Larsson 2001) and numerical load-settlement curve at Tornhill: 2.0 X 2.0 m footing.

4.1.4 Summary and conclusions

In this case, the load-settlement response of vertically loaded footings on clay till was investigated using non-linear finite element analysis. The FEM analysis is performed with Hardening Soil model which is and elasto-plastic hyperbolic constitutive model with isotropic hardening connected to two plastic yield surfaces, that is, one is cone and other is a cap. Hardening soil model is and advanced soil model for simulating the behavior of different types of soil. The results of oedometer as well as triaxial test were used to define parameters of Hardening soil model.

The Clay till is overconsolidated clay and stiffness increases with depth. The K_0 and OCR values obtained from dilatometer tests are used as input parameters in PLAXIS. The value of K_0 is very greater than 1. In this case due to $K_0 > 1$, the horizontal stresses are higher than the vertical stresses in soil. During simulation, at initial phase the plastic points were created in Sandy silty clay layer. Either size factors of elements below the footing can be reduced or reduce K_0 value during simulation until platic points are vanished.

The measured load-settlement curves were compared with back-calculated load-settlement curve numerically. The three full-scale shallow foundations of different sizes were used during simulation. After the simulation, the measured and numerically simulated load-settlement curves were compared. From Figure 4.26,Figure 4.27, and Figure 4.28, it is shown that the numerical curves obtained using finite element analyses are in reasonable agreement with the measured results. The curves obtained from third simulation were more similar though the ends of the curves show slight variation. Hence, the back-calculated results obtained from the simulations show that effective cohesion is between 11.45 to 14.45 kPa and friction angle is about 30^0.

4.2 A case study of Portugal on saprolitic soil

4.2.1 Geological and geotechnical studies

The experimental site was located in the north-western region of Portugal and in the test site dominant soils are residual soils from granite which is also very common in northern part of Portugal. The typical Porto granite is a leucocratic alkaline rock, with two micas and of medium to coarse grain size. The chemical and mineralogical constitution of this rock varies naturally, generating a fairly heterogeneous mass. In this region, climatic conditions with high temperatures and precipitation dominate are responsible for the development of chemical and mineralogical processes which gives rock weathering. The thickness of these regional saprolitic soils may sometimes attain 20 m, with more common values 5 – 10 m. The bonded structure and fabric of these soils have significant influence on engineering behaviors, and several particularities dominate foundation design in these materials (da Fonseca 2002).

To determine the characteristics of the soil, an extensive site investigation was made in a relatively homogeneous weathered profile of a typical saprolitic soil from granite of Porto region. A range of in situ tests including standard penetration tests (SPT), static cone penetration tests (CPT), dynamic probing (DP), Ménard pressuremeter tests (PMT), Marchetti dilatometer tests (DMT), self-boring pressuremeter tests (SBPT) and cross-hole tests (CH) were carried out. In addition, oedometer and triaxial tests in laboratory were carried out. After the investigations, a series of load test on shallow foundation were performed, a mojor part of the experimental work wwas carried out at a given site on which a fairly homogeneous saprolitic soil 6 m thick was encountered. To carry out the loading test plate loading test (PLT) were made with circular steel plates 30 and 60 cm in diameter. The main part of the experiment was the execution of a load test on a 1.2 m diameter rigid reinforced concrete footing. The detail description of in situ tests, laboratory tests and plate loading test as well as characteristics of residual soils was studied from (Da Fonseca, Fernandes et al. 1998, Fonseca 2001, da Fonseca 2002).

The classification of soil profile was done by (Robertson 1990) chart.

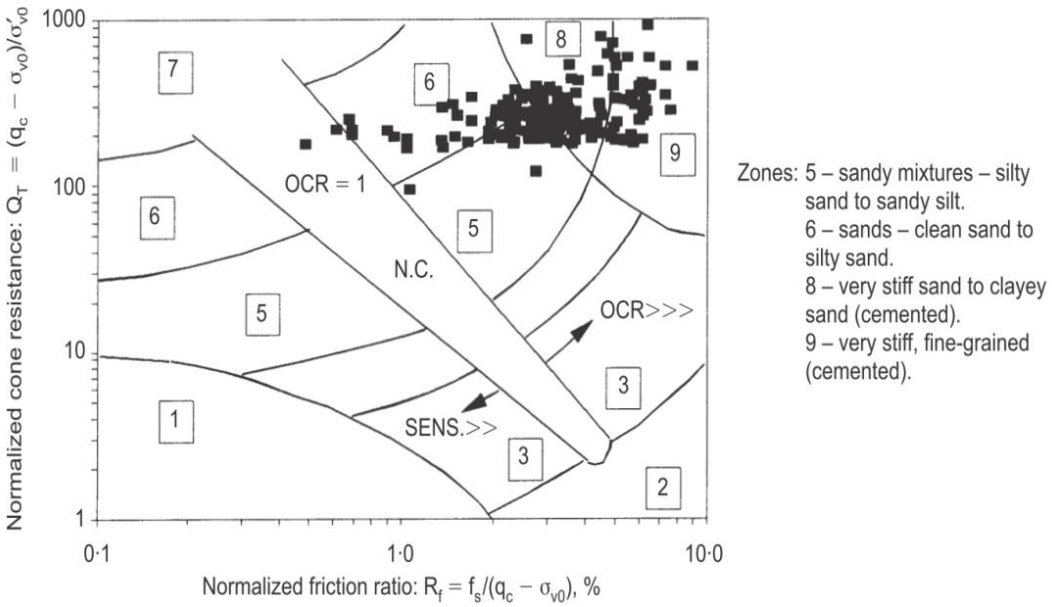

Figure 4.29 Soil classification by Robertson chart at Porto footing load test site (da Fonseca 2002).

After determining the values of R_f and Q_T from CPT tests results, the classification of soil profile in detail can be demonstrated in Table 4.8.

Table 4.8 Soil classification at Porto footing load test site on saprolitic soil.

Depth, m	Rf	Qt	Soi classification
1	6.241	274.00	very stiff, fine grained (cemented)
2	3.548	215.25	very stiff sand to clayey sand (cemented)
3	3.391	176.80	silty sand to sandy silt
4	2.249	179.92	silty sand to sandy silt
5	3.027	134.64	silty sand to sandy silt
6	4.273	163.08	silty sand to sandy silt
7	3.662	179.00	silty sand to sandy silt

From Table 4.8, the sub-soil profile for the study was determined. The water table was observed at a depth of 2 m from the ground surface. The sub-soil profile at the site is shown in Figure 4.30.

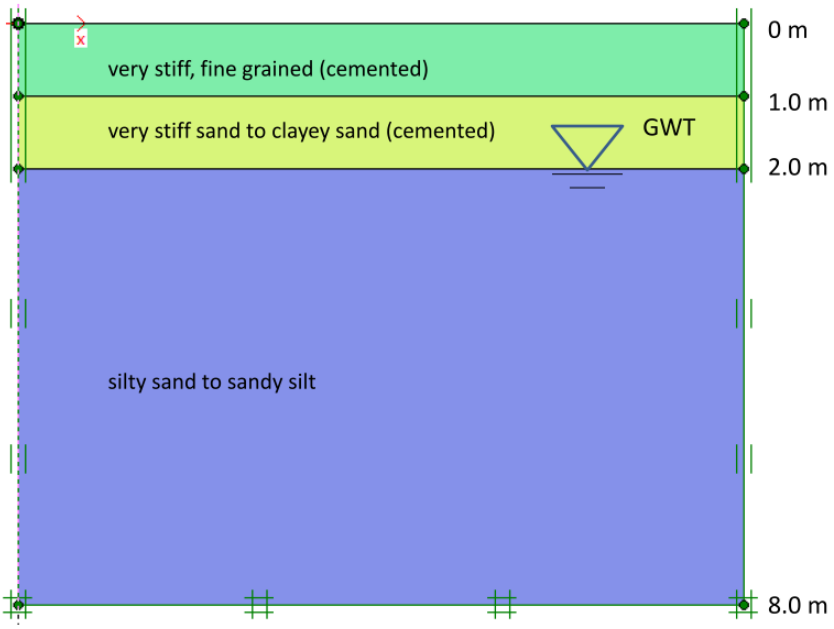

Figure 4.30 Soi profile for the test at Porto footing load test site on saprolitic soil.

The saprolitic soil is fairly homogeneous soil with SM (Silty sand) or SM-SC (Silty clay sand). Plotting of the CPT test results on the (Robertson 1990) classification chart, most values fall in zones with cementd, aged or very stiff natural soils which can be seen in Figure 4.29. The soil is lightly oveconsolidated.

4.2.1.1Laboratory tests

The undisturbed samples were taken out from large blocks in open ditches of 0.5 to 1 m depth below the level of footing base and the laboratory test for mechanical characterization was carried out. Oedometer and triaxial specimens were obtained by driving rings of tube samplers into the blocks with the help of a static thrust.

Though the parameters required for the Hardening soil model are studied throughout the report, the final parameters are derived mainly from the laboratory tests. The results from CID triaxial tests under three distinct consolidation stresses are available. The E_{50} and E_{ur} moduli for σ_c' = 10 kPa and σ_c' = 100 kPa were calculated. Then, E_{50}^{ref} and E_{ur}^{ref} were determined as follows;

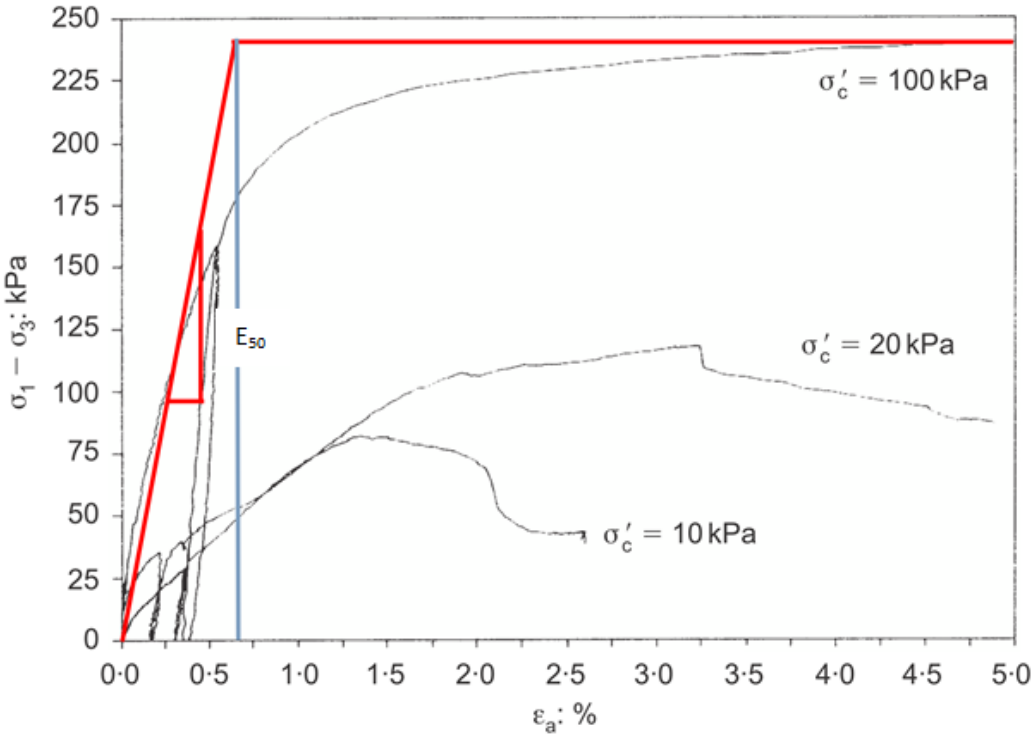

Figure 4.31 Determination of E_{50} modulus from CID triaxial test under consolidation stress, σ_c' = 100 kPa at Porto footing load test site(da Fonseca 2002).

E_{50} = (240/0.7) X 100 = 34285 kPa ≈ 35 MPa

$$E_{50} = E_{50}^{ref}\sqrt{\frac{\sigma_3^{'}+a}{p^{ref}+a}} \qquad @\ \sigma_3^{'} = 100\ \text{kPa};\ p^{ref} = 100\ \text{kPa}$$

Where, $a = \frac{c}{\tan\phi} = \frac{10}{\tan 38} \approx 13$ kPa

$$E_{50} = E_{50}^{ref}\sqrt{\frac{100+13}{100+13}} = 1\ \text{X}\ E_{50}^{ref}$$

Therefore,

E_{50}^{ref} = 1 X E_{50} = 35 MPa

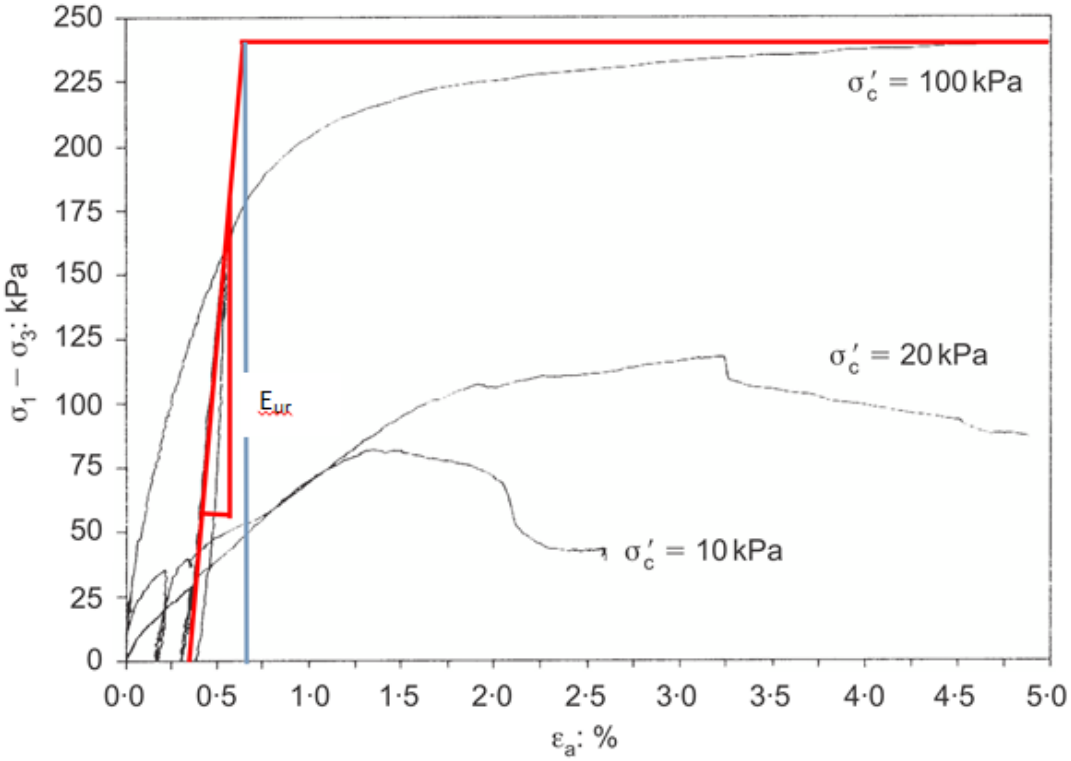

Figure 4.32 Determination of E_{ur} modulus from CID triaxial test under consolidation stress, σ_c' = 100 kPa ata Porto footing load test site(da Fonseca 2002).

E_{ur} = 240/(0.7-0.3) X 100 = 60000 kPa ≈ 60 MPa

$$E_{ur} = E_{ur}^{ref}\sqrt{\frac{\sigma_3^{'}+a}{p^{ref}+a}} \qquad @\ \sigma_3^{'} = 100\ \text{kPa};\ p^{ref} = 100\ \text{kPa}$$

Where, $a = \frac{c}{\tan\phi} = \frac{10}{\tan 38} \approx 13$ kPa

$$E_{ur} = E_{ur}^{ref}\sqrt{\frac{100+13}{100+13}} = 1\ \text{X}\ E_{50}^{ref}$$

Therefore,

E_{ur}^{ref} = 1 X E_{ur} = 60 MPa

The E_{ur}^{ref} as determined above is less than the double of E_{50}^{ref}. In the Hardening Soil Model, E_{ur}^{ref} = 3 X E_{50}^{ref}. Therefore, in Table 4.9 for σ_c' = 100 kPa the values of E_{ur}^{ref} were triple of E_{50}^{ref}.

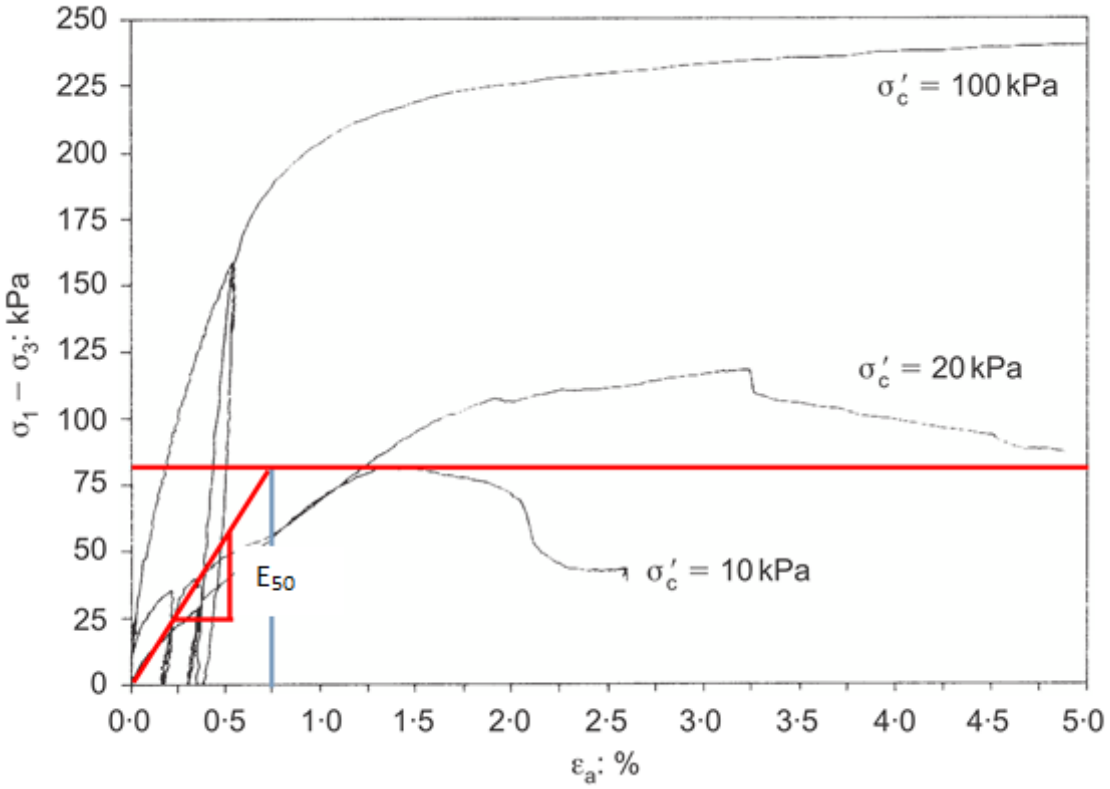

Figure 4.33 Determination of E_{50} modulus from CID triaxial test under consolidation stress, σ_c' = 10 kPa at Porto footing load test site(da Fonseca 2002).

E_{50} = 80/0.75 X 100 = 10667 kPa = 10.67 MPa

$$E_{50} = E_{50}^{ref}\sqrt{\frac{\sigma_3^{'}+a}{p^{ref}+a}} \qquad @\ \sigma_3^{'} = 10\ \text{kPa};\ p^{ref} = 100\ \text{kPa}$$

where, $a = \frac{c}{\tan\phi} = \frac{10}{\tan 38} \approx 13$ kPa

$$E_{50} = E_{50}^{ref}\sqrt{\frac{10+13}{100+13}} = 2\ \text{X}\ E_{50}^{ref}$$

Therefore,

E_{50}^{ref} = 2 X E_{50} = 2 X 10.67 ≈ 22 MPa

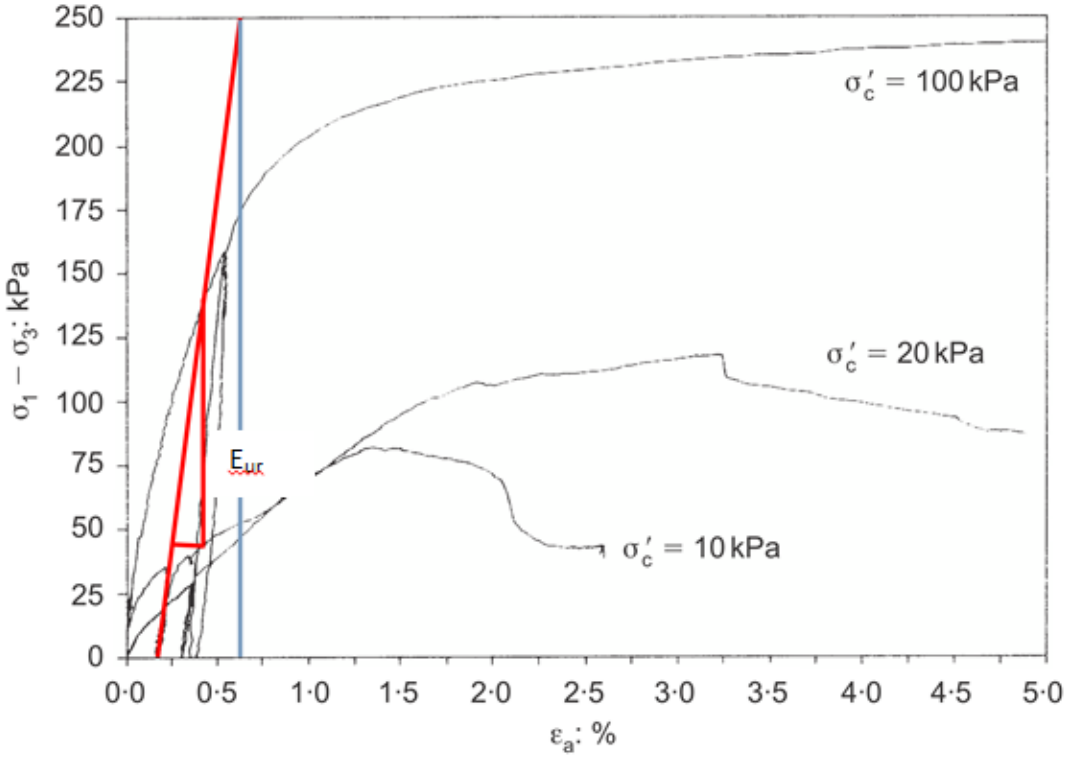

Figure 4.34 Determination of E_{ur} modulus from CID triaxial test under consolidation stress, σ'_c = 10 kPa at Porto footing load test site(da Fonseca 2002).

E_{ur} = 250/(0.75-0.20) X 100 = 45.45 MPa

$$E_{ur} = E_{ur}^{ref}\sqrt{\frac{\sigma_3^{'}+a}{p^{ref}+a}} \qquad @\ \sigma_3^{'} = 100\ \text{kPa};\ p^{ref} = 100\ \text{kPa}$$

Where, $a = \frac{c}{\tan\phi} = \frac{10}{\tan 38} \approx 13$ kPa

$$E_{ur} = E_{ur}^{ref}\sqrt{\frac{10+13}{100+13}} = 2\ \text{X}\ E_{50}^{ref}$$

Therefore,

E_{ur}^{ref} = 2 X E_{ur} = 2 X 45.45 ≈ 90 MPa

The drained and effective shear strength parameters, c'_{ref} and Φ' are determined from triaxial tests. The value of effective cohesion was between 9 to 12 kPa and friction angle was 37^0 and 38^0. The dry density was with an average value of 20 kN/m^3. The values of isotropic preconsolidation stress (σ'_{mp}) deduced from oedometer tests was 85 – 140 kPa. The evaluation of coefficient of earth pressure at rest, K_0, in saprolitic soils from granite is of vital importance for the application of well-defined constitutive laws in geotechnical analysis.

The values of K_0 determined from very well controlled SBPT curves ranged between 0.35 and 0.38. The detail description regarding laboratory test is given in (da Fonseca 2002).

The study of an extensive geological and geotechnical characterization was undertaken to determine the parameters required for Hardening Soil Model. The parameters are shown in Table 4.9.

Table 4.9 Parameters of saprolitic soil at Porto footing load test site.

σc' = 100 kPa													
Soil Type	E_{oed}^{ref}	E_{50}^{ref}	E_{ur}^{ref}	**m**	**c'**	**ϕ**	**Ψ**	**Ko**	**OCR**	K_0^{nc}	γ	**Model**	**Type**
	MPa	MPa	MPa		kPa						kN/m^2		
very stiff, fine grained sand (cemented)	31.5	31.5	99	0.5	9 to 12	37 to 38	7 to 8	0.38	10	0.38	20	HS	Drained
very stiff sand to clayey sand (cemented)	35	35	110	0.5	9 to 12	37 to 38	7 to 8	0.38	3.33	0.38	20	HS	Drained
silty sand to sandy silt	38.5	38.5	121	0.5	9 to 12	37 to 38	7 to 8	0.38	1.62	0.38	20	HS	Drained
σc' = 10 kPa													
Soil Type	E_{oed}^{ref}	E_{50}^{ref}	E_{ur}^{ref}	**m**	**c'**	**ϕ**	**Ψ**	**Ko**	**OCR**	K_0^{nc}	γ	**Model**	**Type**
	MPa	MPa	MPa		kPa						kN/m^2		
very stiff, fine grained sand (cemented)	19.80	19.80	81.00	0.5	9 to 12	37 to 38	7 to 8	0.38	7	0.38	20	HS	Drained
very stiff sand to clayey sand (cemented)	22	22	90	0.5	9 to 12	37 to 38	7 to 8	0.38	3.33	0.38	20	HS	Drained
silty sand to sandy silt	24.2	24.20	99.00	0.5	9 to 12	37 to 38	7 to 8	0.38	1.62	0.38	20	HS	Drained

Table 4.10 Material properties of the footing at Porto footing load test site.

Parameter	Name	Steel plate	Reinforced concrete footing	Unit
Thickness	d	0.5	0.5	m
Weight	w	39	12.5	kN/m/m
Poisson's ratio	υ	0.3	0.15	-
Type of behavior	Type	Elastic, isotropic	Elastic, isotropic	-
Normal stiffness	EA	1.00E+08	1.50E+07	kN/m
Flexural rigidity	EI	2.08E+06	3.13E+05	kNm^2/m

4.2.1.2 Loading tests

A full scale loading test was carried out on a 1.2 m diameter reinforced concrete foundation of 0.5 m thick. Before the loading was conducted, the instrumentation was done which consisted of:

(i) 3 displacement dial gauges with 50 mm travel and 0.01 mm divisions connected to the footing to record its settlement;

(ii) 9 reference pins to survey the deflection of the ground surface around the footing by means of topographic electronic equipment;

(iii) 4 vertical inclinometer tubes sealed at 6 m depth to measure horizontal displacements in the ground, these tubes also being used to observe the water table.

The layout of the measuring instruments is given in Figure 4.35. The water level was at a depth of 1 m below the footing base, when the test was conducted. The main test was loaded from kentledge by a hydraulic jack. The kentledge of 140 tons was provided by a water tank 11.2 m in diameter supported by found steel beams resting on concrete bases placed 4.6 m from the center of the test area. The middle two beams were spaced 1.2 m apart to give room for the hydraulic jack. The layout for the main test and views of the site are given in Figure 4.36.

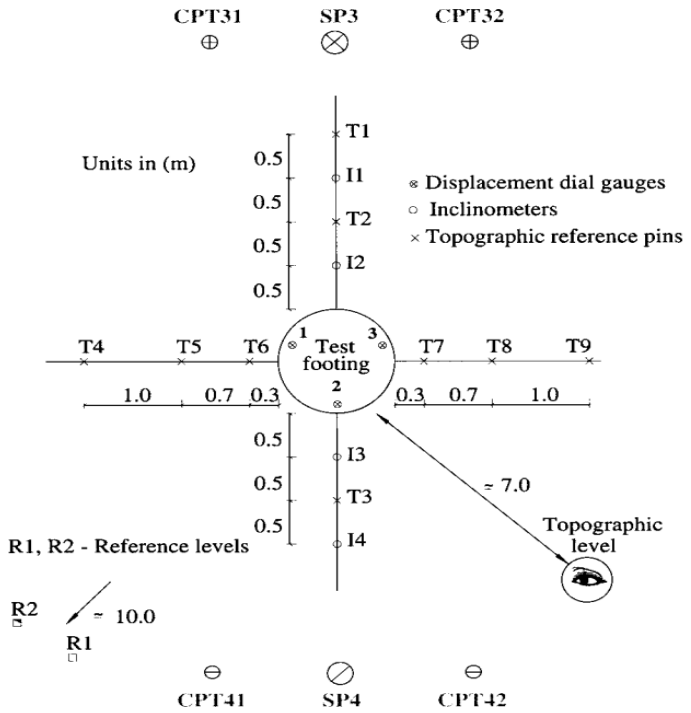

⊗ - 3 displacement dial gauges with 50mm travel and 0.01mm divisions connected to the footing to record its settlement
× - 9 reference pins to survey the deflection of the ground surface around the footing by means of topographic electronic equipment
○ - 4 vertical inclinometer tubes sealed at 6m depth to measure horizontal displacements in the ground; the inclinometer tubes were also used to observe the position of the water table;
□ - fixed reference topographic pins;

Note: distances in cm.

Figure 4.35 Layout of Instruments to Measure Foundation Settlements and Movements of Ground at Porto footing load test site(Fonseca 2001).

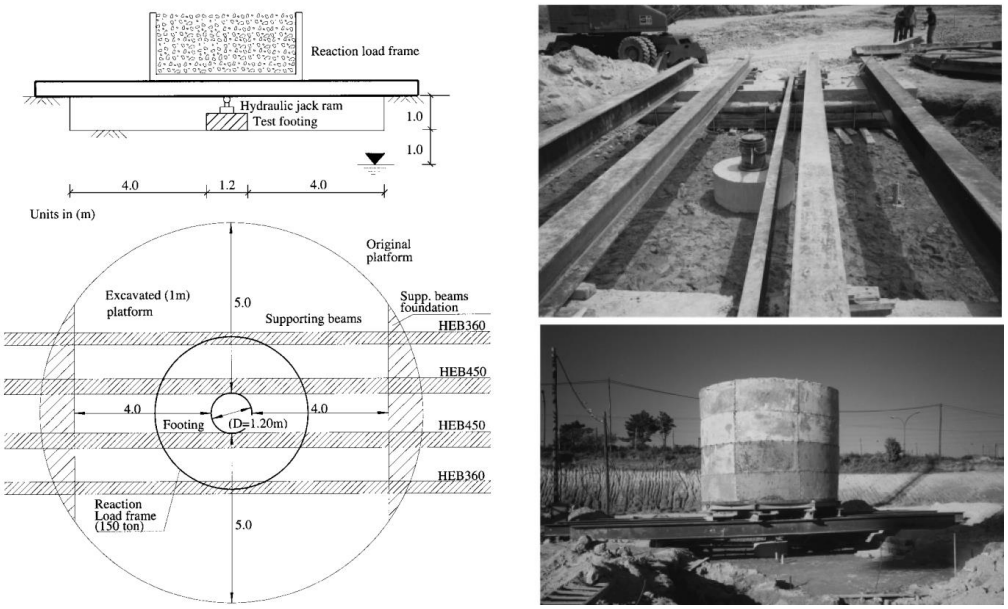

Figure 4.36 Layout for the main test and views of the site at Porto footing load test site(Fonseca 2001).

The duration for full scale loading test was about 15 days, using 35 increments of load with each load maintained for 4 hours including four unload-reload cycles. The detail of the test is given in Table 4.11.

Table 4.11 Full Details of Loading Tests at Porto footing load test site(Fonseca 2001).

Main Cycles	Loading Type	Pressure (kPa)	Stabilization (hours)	Number of executed registers			
				dial gauges	Top. pins	Inclinom.	Water level
1st cycle	1st load	0	---	1	1	1	1
		11	4	10	1	1	1
		27	4	10	1	1	1
		49	4	10	1	1	1
		76	4	10	1	1	---
		98	4	10	1	2	1
	Unload - - reload	49	2	8	1	---	---
		0	10	5	1	1	1
2nd cycle		49	2	8	1	---	---
		98	2	8	1	1	1
	1st load	152	4	10	1	1	---
		201	6	12	1	1	1
		250	6	12	1	1	---
		300	8	14	1	1	1
		349	6	12	1	---	---
		398	6	12	1	1	1
	Unload- - reload	201	2	8	1	---	---
		0	16	6	1	1	1
3rd cycle		201	2	8	1	---	---
		398	2	8	1	1	1
	1st load	452	8	14	1	---	---
		501	8	14	1	1	1
		550	12	18	3	1	---
		599	10	16	2	1	1
		648	10	16	2	1	---
		702	20	26	1	1	---
		751	24	30	3	1	1
		800	24	30	2	2	---
		849	24	30	1	1	1
	Unload - - reload	0	12	18	1	1	---
		849	12	18	1	1	1
4th cycle	1st load	904	24	30	2	2	---
		953	24	30	2	2	1
		1002	36	42	2	1	1
	Final Unload	501	2	8	---	---	---
		0	14	20	1	1	1

The complete load-settlement curve from the footing loading test is shown in Figure 4.37 which shows that at a maximum footing pressure of 1000 kPa, settlement of footing was about 100 mm. The figure in the left is the enlargement where a clear increase of the settlement rate with load for pressure values exceeding around 125 kPa can be seen.

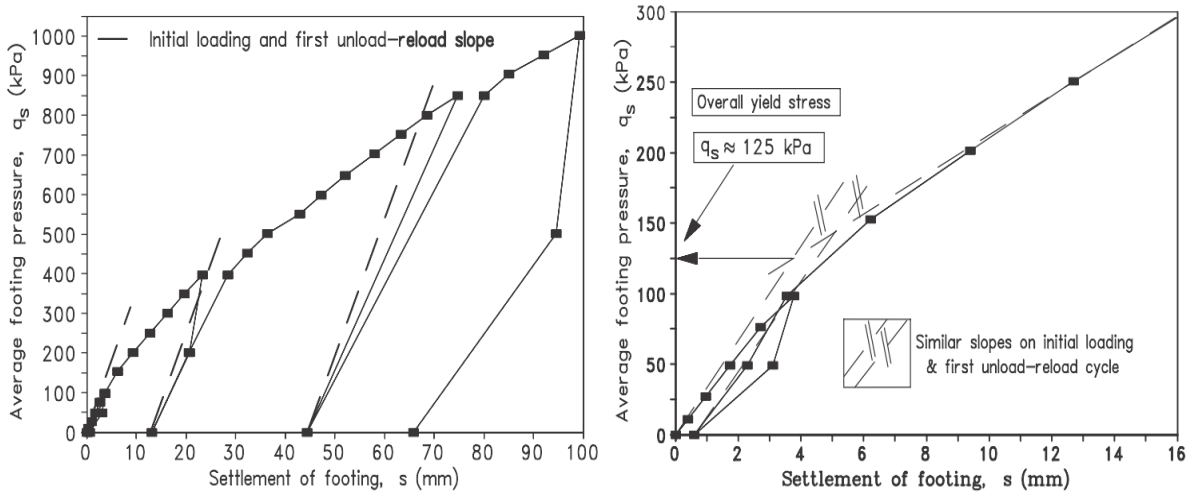

Figure 4.37 Load-settlement curve for main loading test at Porto footing load test site on Saprolitic soil(da Fonseca 2002).

On the same zone of the footing loading test, plate loading test (PLT) were made with circular steel plates 30 and 60 cm in diameter. Plate loading tests were carried out with a hydraulic jack reacting against the two outer beams. The settlements of the plates were measured from the independently supported beam by use of Benkelmann beams. The position and test of PLT is shown in Figure 4.38. The incremental loading was applied with the same stress level as those of the main footing test. The load-settlement curve for the plate loading test is shown together in Figure 4.39.

From the main loading test it can be seen that the settlement reached to 100 mm at highest pressure while the ground surface pins situated at 0.3 m from its border gives only about 10 mm settlement. It can be illustrious that the shape of the load-settlement curve is typical of a punching shear failure mode. When this type of failure mode occurs, the ultimate bearing capacity is not well defined. In order to establish the serviceability limit state pressure the criterion proposed by (Décourt 1992) was adopted as a reference. This stipulates that the allowable pressure on a shallow foundation on residual soil should correspond in its effect to a settlement of 6.0 mm for a 0.8 m diameter plate load test. This represents a settlement of 0.75% of the diameter of the loading surface, which gives a settlement of 9 mm in the present case. A 9 mm settlement corresponds to an applied pressure of about 195 kPa which can be seen in Figure 4.37.

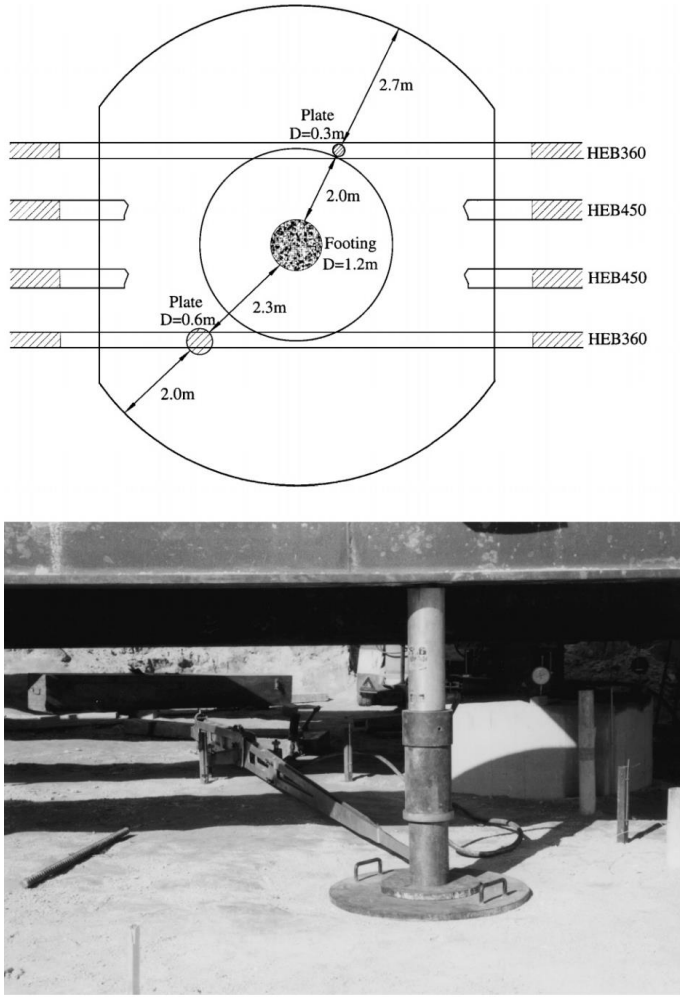

Figure 4.38 Position and Photo of PLT: 30 and 60 cm diameter at Porto footing load test site on Saprolitic soil(Fonseca 2001).

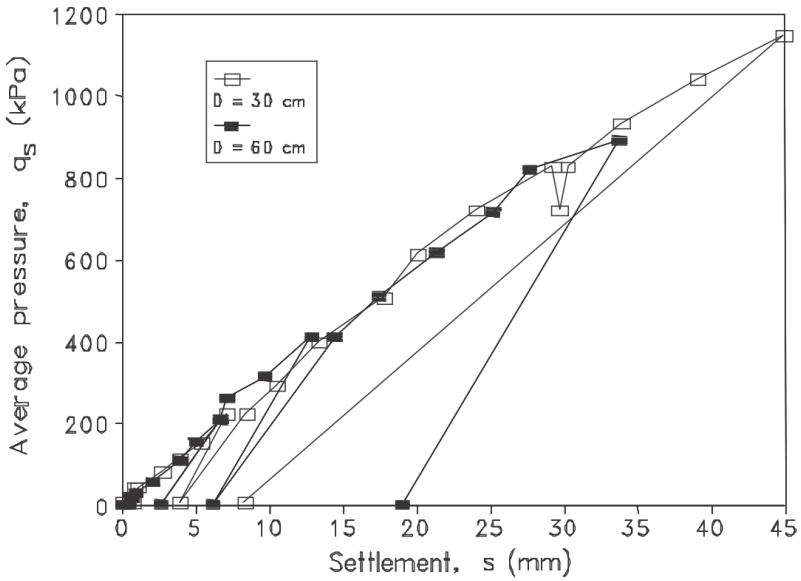

Figure 4.39 Load-settlement curve of the plate loading test (D = 30 and 60 cm) at Porto footing load test site on saprolitic soil(da Fonseca 2002).

4.2.2 Numerical modeling

The FEM analysis of reinforced concrete footing and steel plates are modeled in FEM based package PLAXIS 2D. The 15 nodes element will result a more precise calculation of the stress and strains. A fine mesh is used for the models. The axi-symmetric circular footing and steel plates are modeled as linear elastic element. The experimental load-displacement curves for shallow foundations obtained by (da Fonseca 2002) are compared with the numerical results obtained using constitutive model, that is, Hardening Soil Model. The elastic modulus of soil has been considered based on the available correlation with the in-situ and laboratory test results e.g. CPT, CHT, DMT, PMT, oedometer and triaxial tests.

The dimension of main footing is 1.2 m diameter which is reinforced concrete and the two steel plates of 30 and 60 cm diameter are considered as supplementary analysis. Both the plates and the main footing were modeled numerically with the number of simulations by changing the value of c'_{ref} and ϕ' because the coefficient of bearing capacity depends on these values. The goal of these simulations is to validate our numerical analysis by comparison with existing load-settlement observations. In PLAXIS, based on the soil profile in Figure 4.30, the numerical model is created for the bearing capacity calculation which is shown in Figure 4.40.

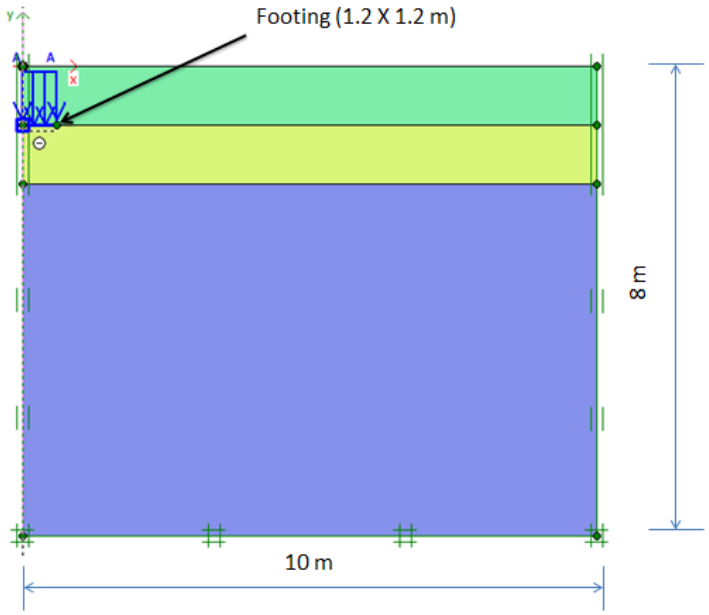

Figure 4.40 Typical Numerical model for simulation at Porto footing load test site.on saprolitic soil.

A drained behavior is assumed for the materials for the bearing capacity calculations. The undrained behavior is assumed for north-east clay till due to very stiff clay till. Initial stresses in the soil are driven from the material weight and their historical of development. In the PLAXIS software the horizontal stress in static state is calculated using Jacky's formula;

$$k_o = 1 - \sin(\phi)$$

When the typical model for simulation is created with all material sets in it, the standard boundary conditions are set. As a result, PLAXIS will automatically generate a full fixity at

the base of the geometry and roller boundaries at the vertical sides (u_x = 0; u_y = free). In this project, in order to calculate the bearing capacity, the elastic footing was chosen with flexural rigidity (bending stiffness), EI and axial stiffness, EA.

A typical 2D meshes are shown in Figure 4.41. The bottom boundaries of the finite element models are located at a depth of 8 m and the lateral boundaries are located at a distance of 10 m from the center of the footings. 15-noded axisymmetric elements are used in the finite element meshes to model both the soil and the footings. The interface elements are also used between the footing base and the soil with a R_{inter} = 1. The numbers of simulations are performed by using stiffness parameters determined from both consolidation stresses at σ_c' = 10 kPa and σ_c' = 100 kPa.

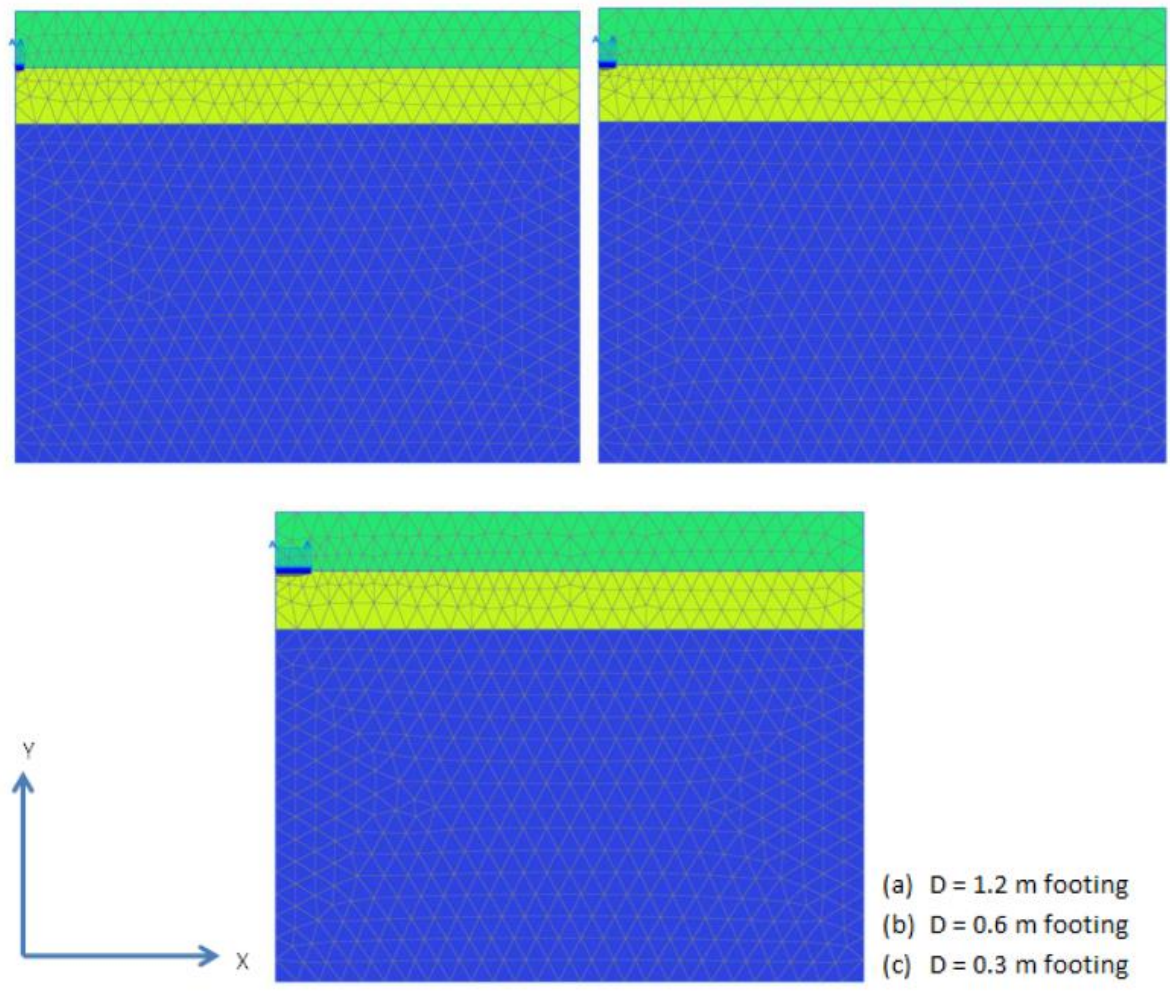

Figure 4.41 FEM mesh for the numerical simulation at Porto footing load test site on Saprolitic soil.

Loading-condition:

Distributed load – load system A is applied vertically over the footing without eccentricity. Initial stresses are developed in the input stage by deactivating the footing. It is assumed that the self-weight of the footing has added to the distributed load. Two staged construction are performed. In the first staged construction, the excavation is done and in the second staged construction, footing and loading are activated. Finally, incremental multiplier is applied for vertical load to failure. The footing model is shown in Figure 4.42.

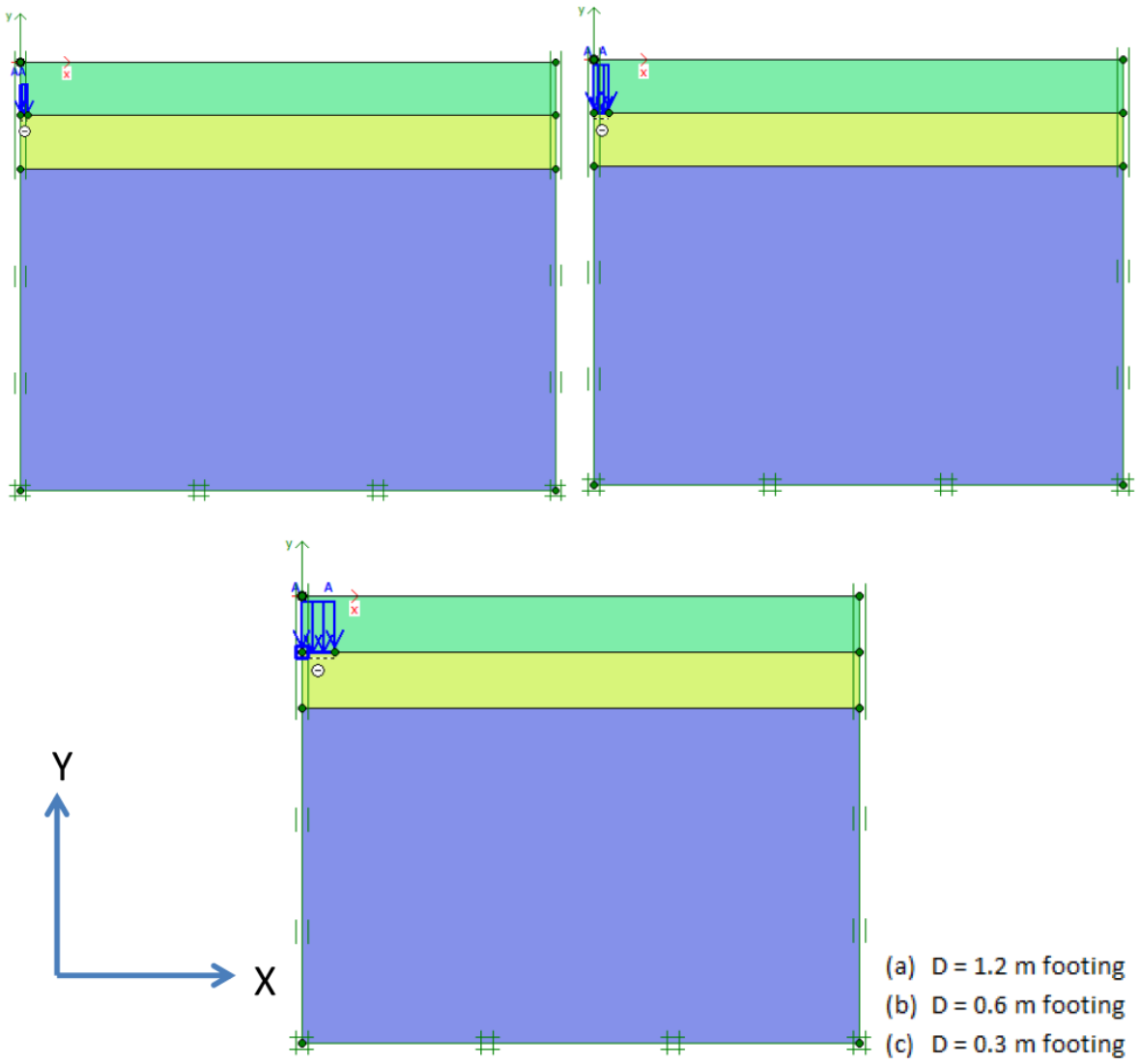

Figure 4.42 Footing model in Plaxis at Porto footing load test site at Porto footing load test site on Saprolitic soil.

Deterministic results:

The simulations of different size of footings are performed using Hardening Soil Model. The square footings with plane dimensions 1.2 m diameter, 0.6 m diameter and 0.3 m diameter are considered. The number of simulations were performed by using stiffness parameters determined from both consolidations stresses σ_c' = 10 kPa and σ_c' = 100 kPa. After the simulations were carried out, comparison of load-settlement curve between measured and PLAXIS analysis was done. From the simulations performed and compared with the measured ones, there was good consistency with the results of σ_c' = 10 kPa. Therefore, the results of this case are only shown in this chapter. The results for σ_c' = 100 kPa are shown in Appendix C.

Table 4.12 Number of simulations and strength paramters for different size footings at Porto footing load test site.

D = 1.2 m			
Simulations	c'_{ref}	**ϕ'**	**Ψ'**
1	10	37	7
2	9	38	8
3	11	37	7
D = 0.6 m			
1	11	37	7
2	12	38	8
3	15	37	7
D = 0.3 m			
1	10	37	7
2	9	37	7
3	8	37	7

The simulations for different sizes footings were performed as shown in Table 4.12 whereas the detail parameters is already illustrated in Table 4.9. For each of the dimensions, three simulations are carried out, that is, simulation 1, simulation 2 and simulation 3 with their respective strength parameters. After the simulations are conducted, it can be seen from 4.2.3 that simulation 3 has load-settlement curve similar with the measured results. Therefore, only the deterministic results of simulation 3 are shown in Figure 4.43 to Figure 4.48.

Total displacement, u_y:

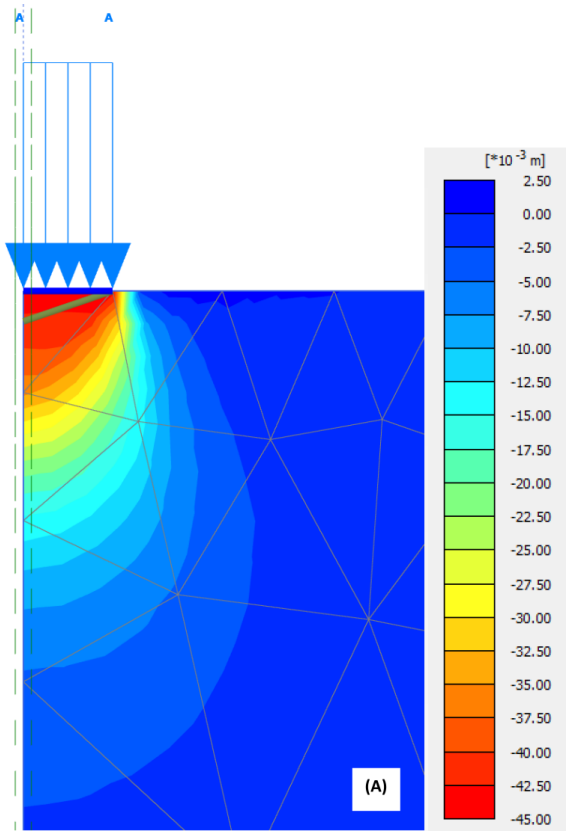

Figure 4.43 Vertical displacement transferred to the soil on saprolitic soil: 0.3 m diameter plate.

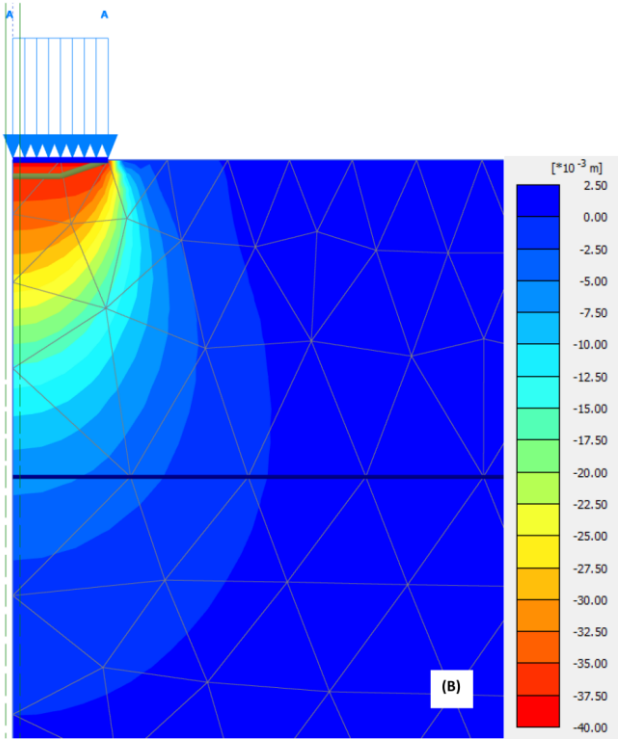

Figure 4.44 Vertical displacement transferred to the soil on saprolitic soil: 0.6 m diameter plate.

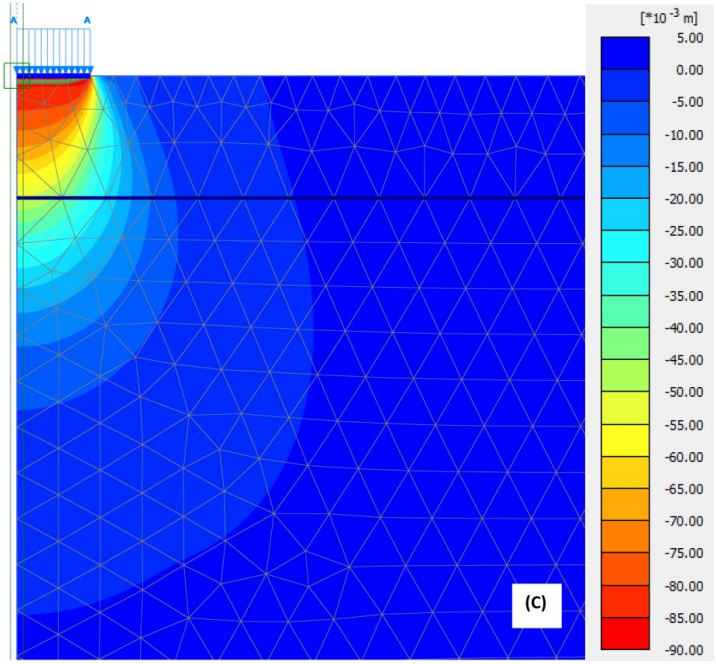

Figure 4.45 Vertical displacement transferred to the soil on saprolitic soil: 1.2 m diameter reinforced footing.

Table 4.13 Showing maximum and minimum vertical displacement for total ground pressure below footing on saprolitic soil.

S/N	Total displacement, u_y (mm)	
	Maximum	Minimum
(A)	0.9081	-43.88
(B)	2.223	-38.19
(C)	2.342	-87.49

Total deviatoric strain, γ_s:

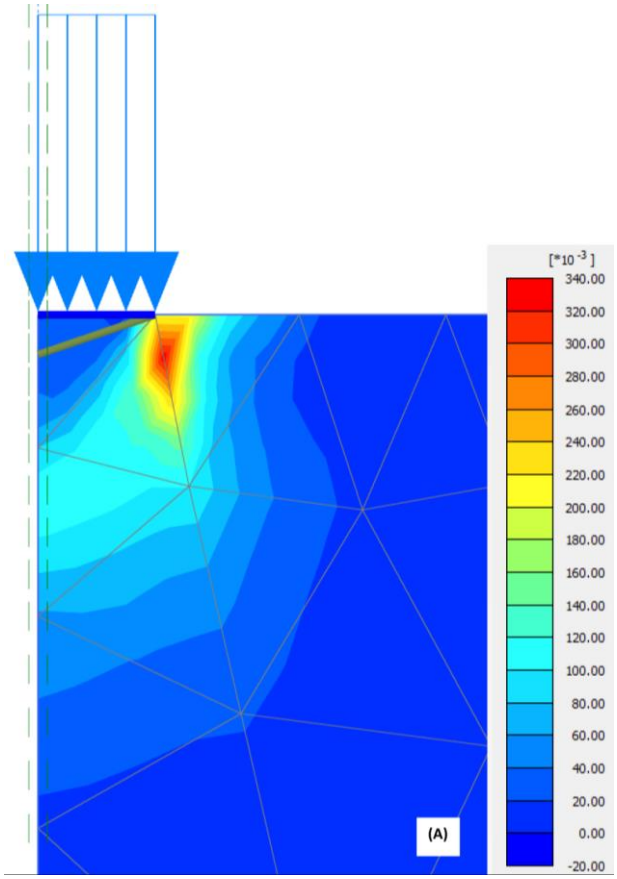

Figure 4.46 Total deviatoric strain for total ground pressure on saprolitic soil: 0.3 m diameter plate.

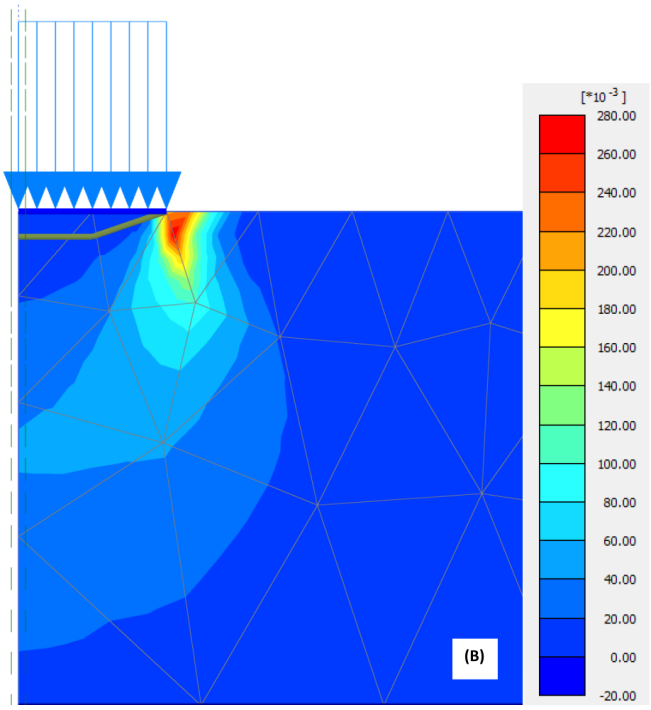

Figure 4.47 Total deviatoric strain for total ground pressure on saprolitic soil: 0.6 m diameter plate.

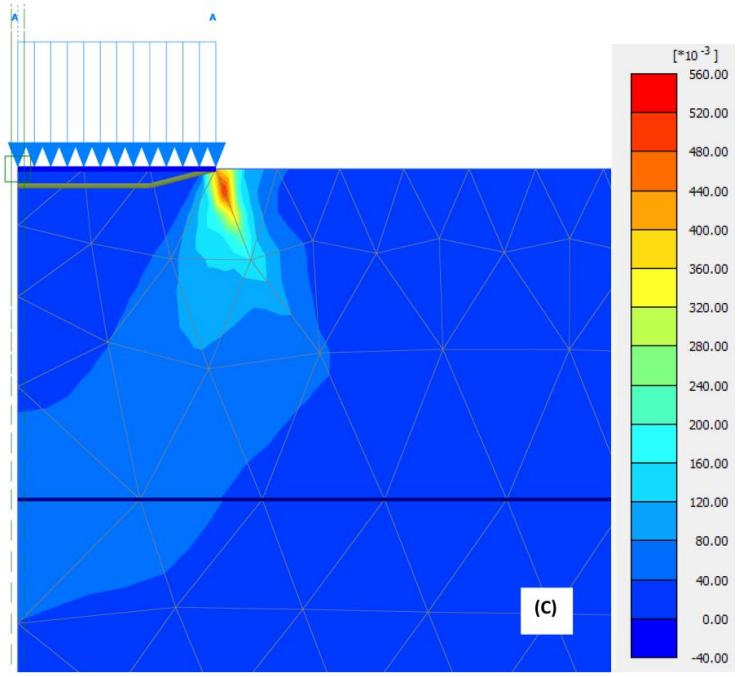

Figure 4.48 Total deviatoric strain for total ground pressure on saprolitic soil: 1.2 m diameter reinforced footing.

Table 4.14 Showing maximum and minimum total deviatoric strain for total ground pressure below footing on saprolitic soil.

S/N	Total deviatoric strain, γ_s	
	Maximum	Minimum
(A)	0.3441	1.08E-9
(B)	0.2784	0.02647E-3
(C)	0.5262	0.01959E-3

4.2.3 Comparison of load-settlement curve from PLT and PLAXIS

It is instructive to compare the results of plate loading tests with those obtained from our numerical results. Figure 4.49, Figure 4.50 and Figure 4.51 show the measured and simulated load-settlement response for each footing. It can be seen that the measured load-settlement curves and the numerical curves obtained using the proposed numerical model are more or less similar for all the footings investigated. During the simulation, it is seen that three simulations are done for each footing. For each simulation, back-calculation was done for the values of c'_{ref}, ϕ' because the coefficient of bearing capacity depends on these two values. The simulation 3 for each footing provides very similar results.

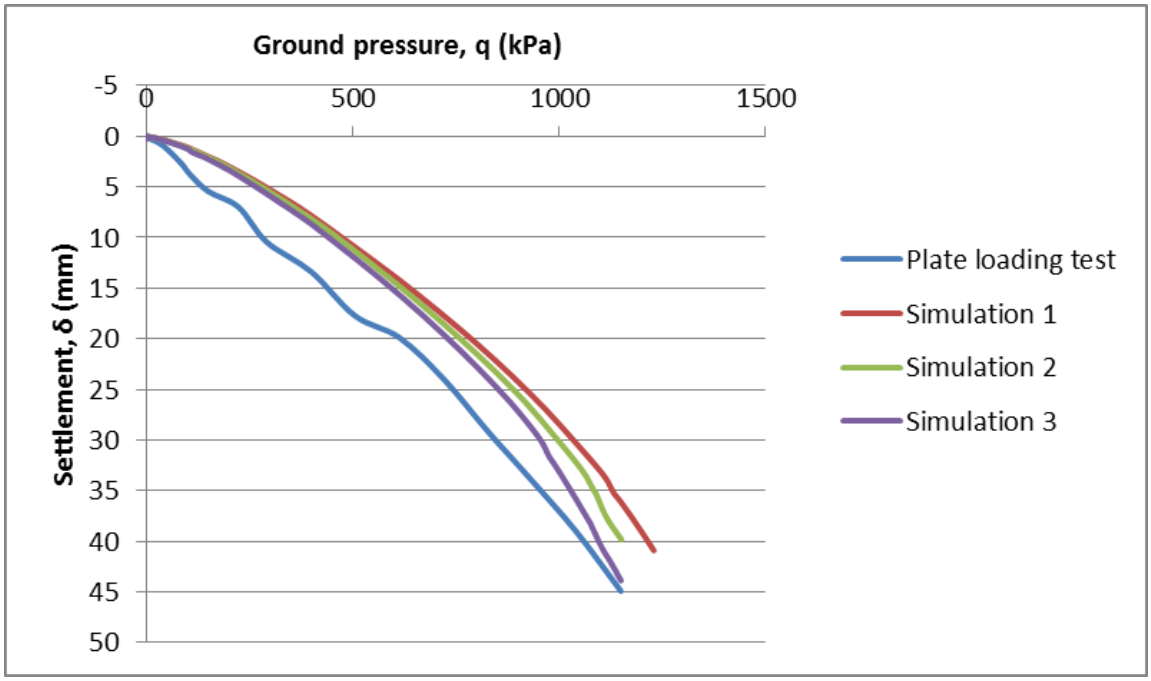

Figure 4.49 Comparison of experimental(da Fonseca 2002) and numerical load-settlement curve on saprolitic soil: 0.3 m diameter steel plate.

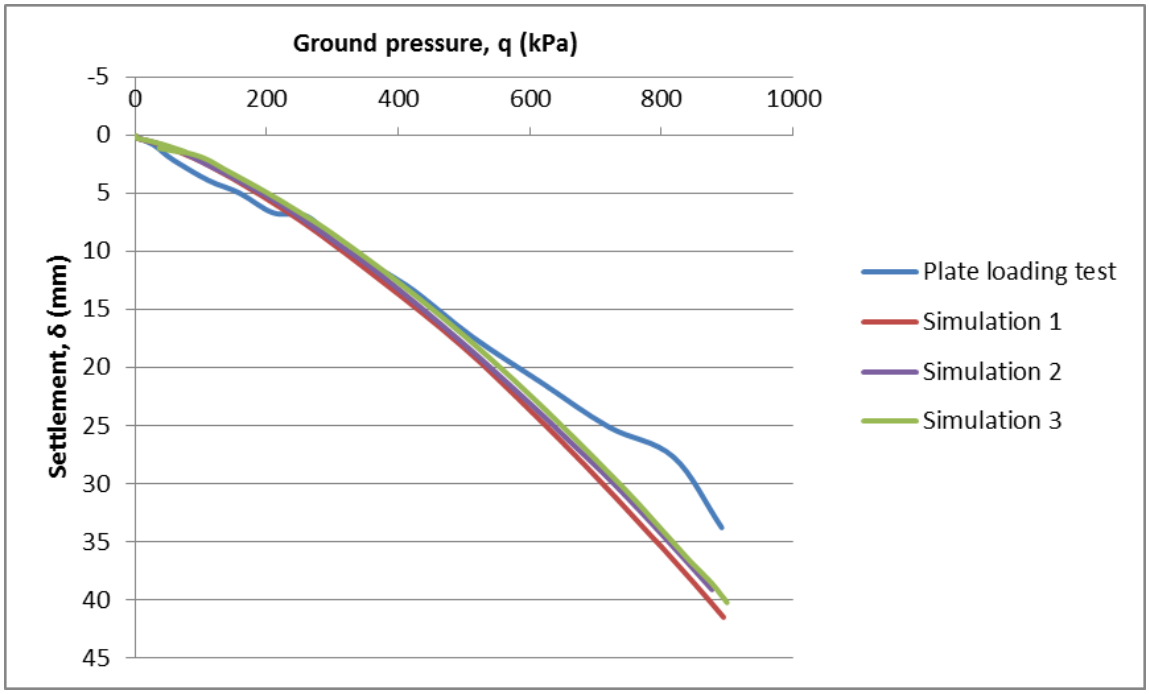

Figure 4.50 Comparison of experimental(da Fonseca 2002) and numerical load-settlement curve on saprolitic soil: 0.6 m diameter steel plate.

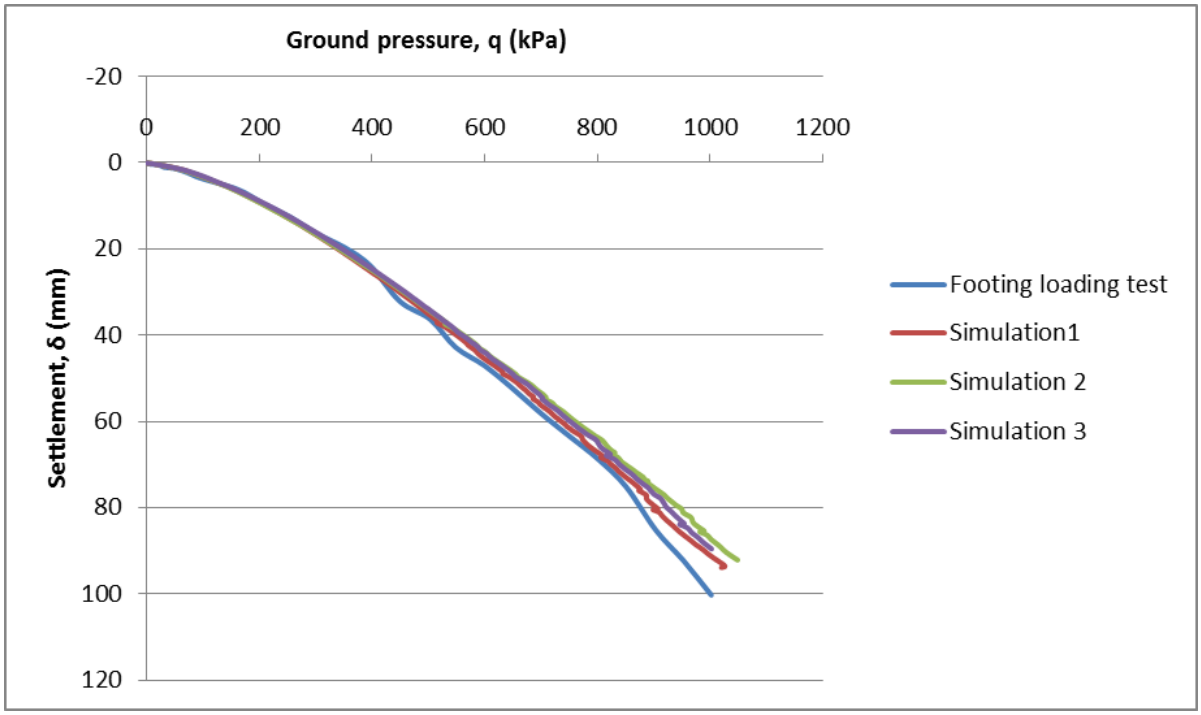

Figure 4.51 Comparison of experimental(da Fonseca 2002) and numerical load-settlement curve on saprolitic soil: 1.2 m diameter reinforced footing.

4.2.4 Summary and conclusions

In this case, the load-settlement response of vertically loaded footings on saprolitic soil was investigated using non-linear finite element analysis. The FEM analysis is performed with Hardening Soil model which is an elasto-plastic hyperbolic constitutive model with isotropic hardening connected to two plastic yield surfaces, that is, one is cone and other is a cap. Hardening soil model is and advanced soil model for simulating the behavior of different types of soil. The results of oedometer as well as triaxial test were used to define parameters of Hardening soil model.

The saprolitic soil is slightly overconsolidated clay. The soil was classified according to Robertson chart. The extensive study on field and laboratory tests was made to determine parameters needed for Hardening Soil model. Especially, stiffness parameters determined from the CID triaxial tests results with different consolidation stresses are used in the model. The strength paramteters as well as coefficients of earth pressure at rest are found in triaxial tests. In this case, the value of K_0 is about 0.38.

The measured load-settlement curves were compared with back-calculated load-settlement curve numerically. A full scale loading test was performed on a 1.2 m diameter reinforced concrete footing with additional plate loading test with circular steel plates. These three different sizes footings were analysed numerically. After the simulation, the measured and numerically simulated load-settlement curves were compared. From Figure 4.49, Figure 4.50, and Figure 4.51 it is shown that the numerical curves obtained using finite element analysis are in reasonable agreement with the measured results. The load-settlement curve with 0.3 m diameter plate is little underprediction. The curve are not coinciding though the

cohesion and angle of friction was reduced to 8 kPa and 37^0 for third simulation. But for 0.6 m diameter plate, the curves are consistent with measured results thought at the end there is some variation. Simulation 3 is very similar to the measured load-settlement curve with effective cohesion and friction angle of 15 kPa and 37^0 respectively. The main loading test is 1.2 m diameter footing and the comparisons between measured and simulated load-settlement curves are very consistent. For this footing also, simulation 3 gives the very similar result at effective cohesion of 11 kPa and friction angle at 37^0. Therefore, from the back-calculation it can be concluded that the effective cohesion is between 8 to 13 kPa and friction angle between 37^0 to 38^0.

4.3 A case study of Texas A & M University on sand

4.3.1 Geological and geotechnical studies

The experimental site was located on the Texas A & M University National Geotechnical Experimentation Site (NGES). The soil in the upper layer, that is, to a depth of 11 m is medium dense silty fine silica sand. Grain size analysis showed the amount of fines content to vary with depth. At 3 m depth fines contents are from 2 to 8% and at 9 m depths fines contents are from 5 to 30%. The mean grain size D_{50} = 0.2mm. Below the sand layer is clay layer which exists until a depth of at least 33 m. The geological condition of the site suggests that the sand is slightly overconsolidated by dessication of the fines. The focus of the investigations mainly lies on the upper soil (Briaud and Gibbens 1997).

Geologically, the top layer of sand is a flood plain deposit of Pleistocene age about 3 m thick with a high fine content. The next layer of sand is a river channel deposit of Pleistocene age about 3 m thick, clean and uniform. The third layer is a mixed unit with an increasing amount of clay seams and gravel layers; it is also of Pleistocene age and was deposited by a stream of fluctuating energy. Below these 200,000-year-old sand layers and about 10 m below the ground surface is the 45-million-year-old Eocene bedrock; this bedrock is a dark gray clay shale that was deposited in a series of marine transgressions and regressions. Erosion of the Eocene marine clay took place before the Pleistocene river sediments were deposited (Briaud and Gibbens 1999).

A series of field and laboratory tests were performed in order to characterize the material on site. A number of tests such as PiezoCone Penetration tests (CPT), Standard Penetration tests (SPT), Dilatometer tests (DMT), Pressuremeter tests (PMT), Borehole Shear tests (BHST), Cross-Hole Wave tests (CH), triaxial tests were carried out. A series of five spread footings were performed at the sand site with dimensions of two 3 X 3 m footings (south and north sides), one 2.5 X 2.5 m footing, one 1.5 X 1.5 m footing, and one 1 X 1 m footing. The detail description of the field tests and laboratory tests was studied from the technical report entitled, 'Large-Scale Load Tests and Data Base of Spread Footings on Sand'(Briaud and Gibbens 1997).

The general sub-soil profile was determined from extensive site characterization. The water table is 4.9 m deep from the ground surface. Figure 4.52 shows the sub-soil profile for test site.

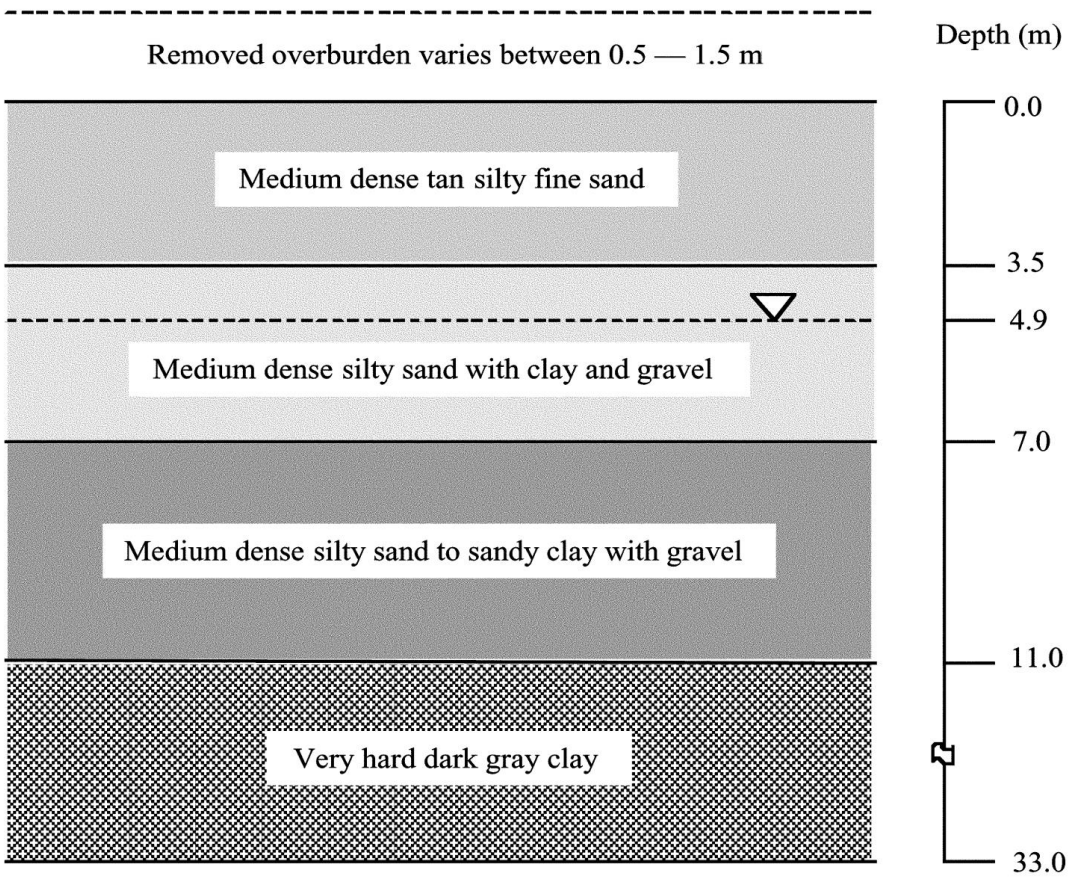

Figure 4.52 Soil profile at Texas A & M footing load test site(Lee and Salgado 2002).

4.3.1.1 Field and laboratory tests

The field and laboratory tests were conducted to study the characteristics of soil in the experimental test site. The plots of different field tests with depth are illustrated in Figure 4.53 to Figure 4.56 with their respective average values. From the respective figures it shows the SPT (standard penetration test) blow count 18 blows per 0.3m, CPT (cone penetrometer test) point resistance 6 MPa, PMT (pressuremeter test) limit pressure 800 kPa, PMT modulus 8.5 MPa, DMT (dilatometer test) modulus 30 MPa The detail results of the field tests were studied from (Briaud and Gibbens 1997).

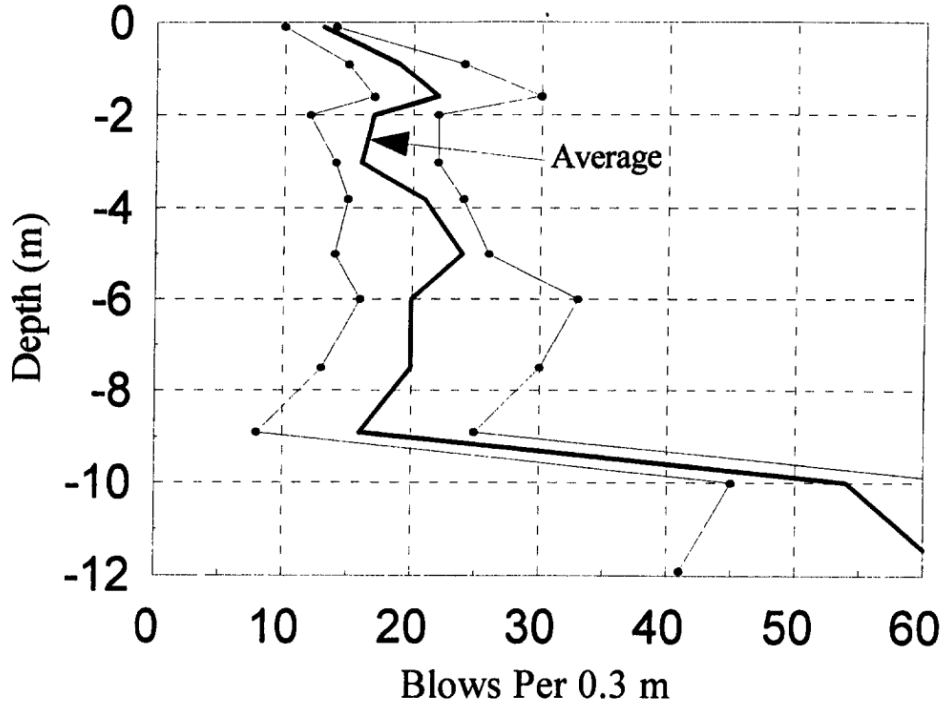

Figure 4.53 SPT results at Texas A & M footing load test site(Briaud and Gibbens 1997).

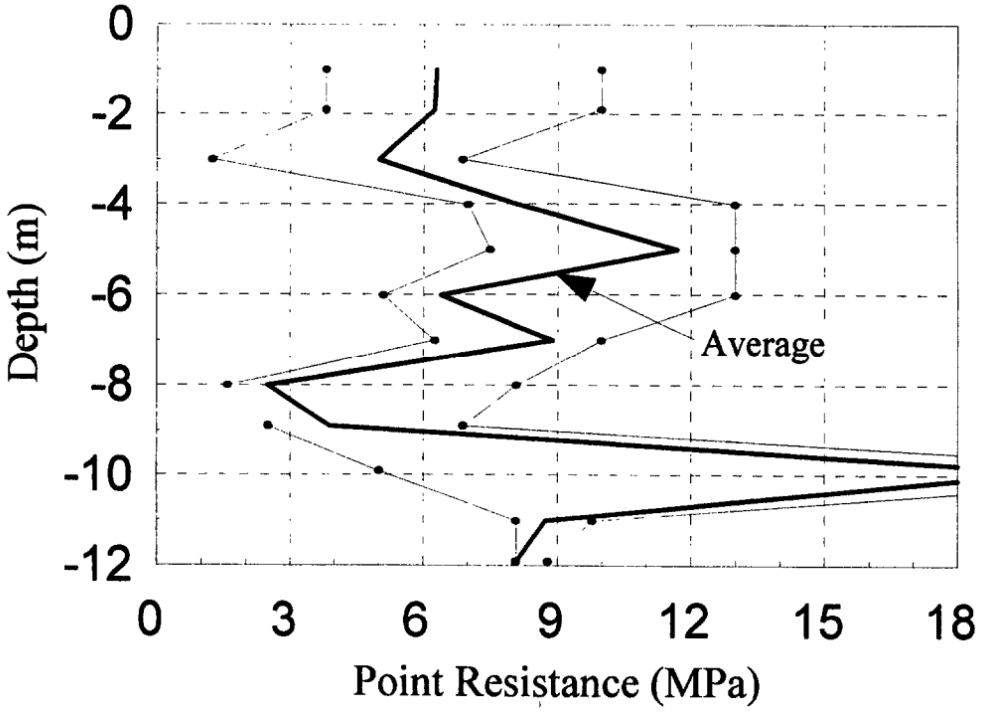

Figure 4.54 CPT results at Texas A & M footing load test site(Briaud and Gibbens 1997).

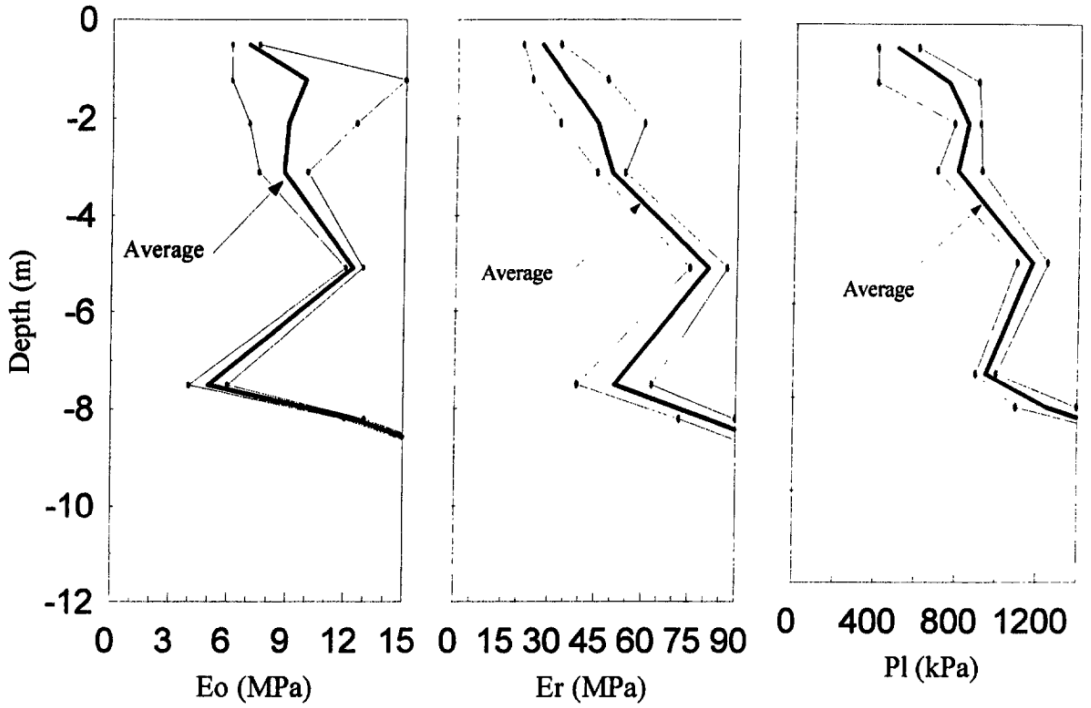

Figure 4.55 PMT results at Texas A & M footing load test site(Briaud and Gibbens 1997).

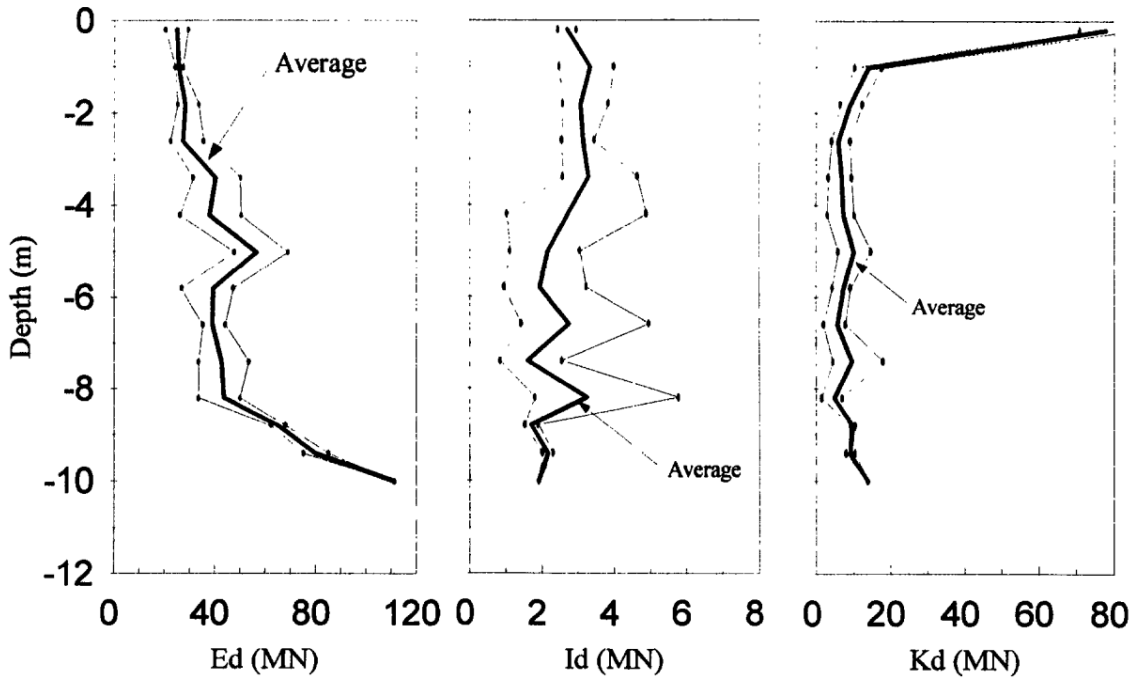

Figure 4.56 DMT results at Texas A&M footing load test site(Briaud and Gibbens 1997).

The routine tests and consolidated/drained triaxial tests were performed at Texas A&M University. The triaxial tests were conducted for samples at 0.6 m and 3.0 m. The results obtained from triaxial tests are illustrated in

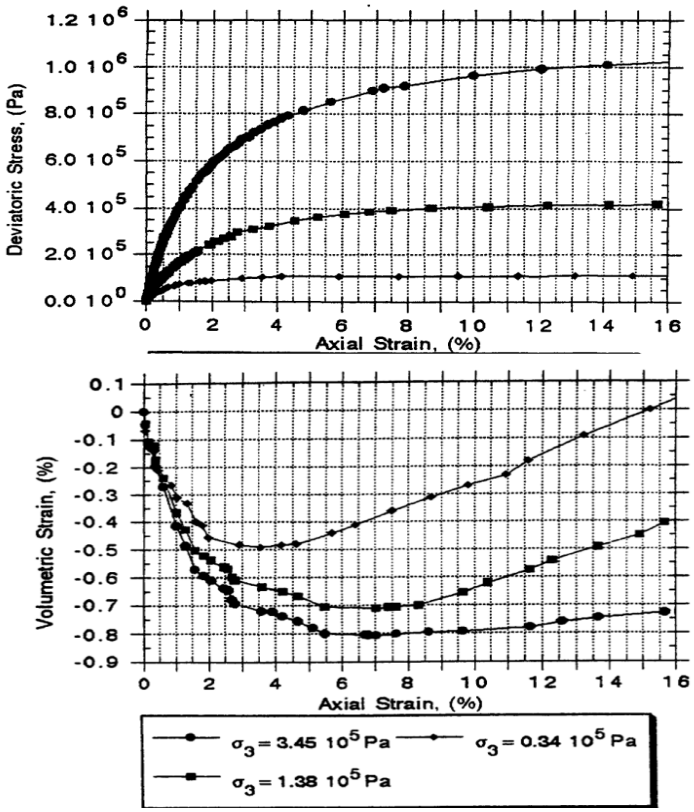

Figure 4.57 Strain-strain and volume change curve for 0.6 m sample at Texas A&M footing load test site(Briaud and Gibbens 1997).

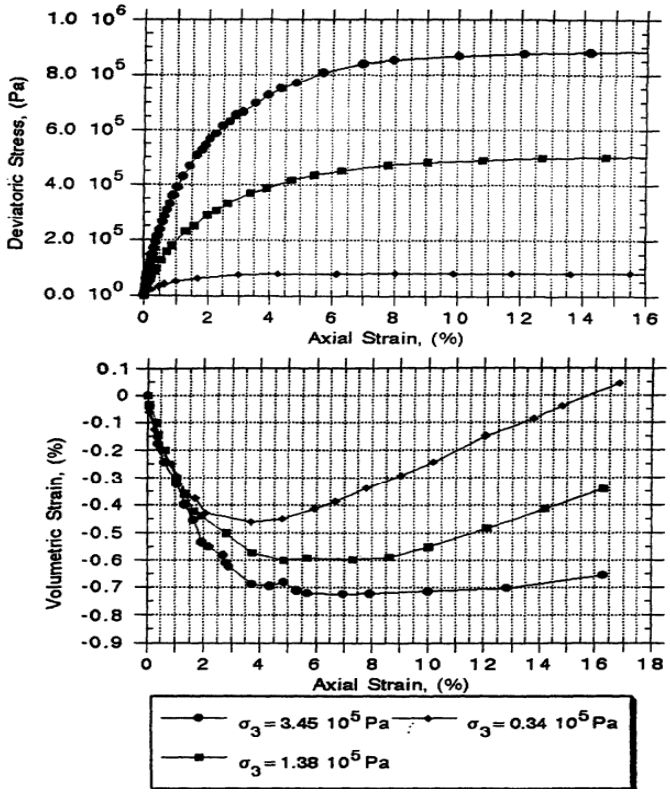

Figure 4.58 Strain-strain and volume change curve for 3.0 m sample at Texas A&M footing load test site(Briaud and Gibbens 1997).

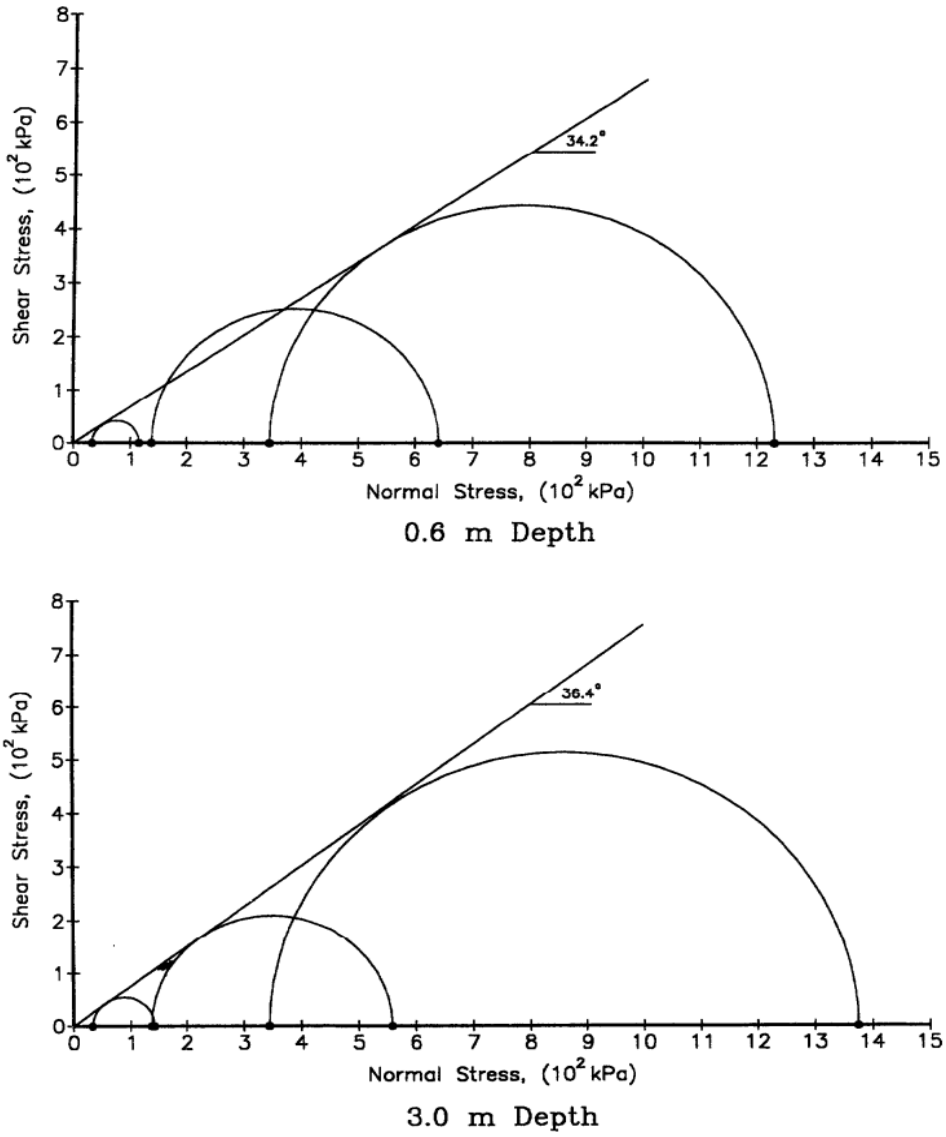

Figure 4.59 Mohr's Circles From Triaxial test at Texas A&M footing load test site(Briaud and Gibbens 1997).

From the results of triaxial tests, the average stiffness, E_{50} is determined using the graphs in Figure 4.57 and Figure 4.58. Hence, the E_{50}^{ref} can be determined as follows;

Sample from 3.0 m depth

For σ_3 = 345 kPa:

E_{50} = (830/2.7) X 100 = 30741 kPa = 30.7 MPa ≈ 31 MPa

$$E_{50} = E_{50}^{ref}\sqrt{\frac{\sigma_3^{'} + a}{p^{ref} + a}} \qquad @\ \sigma_3^{'} = 345 \text{ kPa}$$

Here, a = 0 since c = 0 for sand.

$$E_{50} = E_{50}^{ref}\sqrt{\frac{345}{100}} = 1.86 \text{ X } E_{50}^{ref}$$

Therefore,

E_{50}^{ref} = E_{50} /1.86 = 31/1.86 = 16.67 MPa ≈ 17 MPa @ 3.0 m depth

For σ_3 = 138 kPa:

E_{50} = (500/3.5) X 100 = 14285.7 kPa ≈ 14 MPa

$$E_{50} = E_{50}^{ref} \sqrt{\frac{\sigma_3^{'} + a}{p^{ref} + a}}$$ @ $\sigma_3^{'}$ = 138 kPa

Here, a = 0 since c = 0 for sand.

$$E_{50} = E_{50}^{ref} \sqrt{\frac{138}{100}} = 1.17 \text{ X } E_{50}^{ref}$$

Therefore,

E_{50}^{ref} = E_{50} /1.17 = 14/1.17 = 11.97 MPa ≈ 12 MPa @ 3.0 m depth

Sample from 0.6 m depth

For σ_3 = 345 kPa:

E_{50} = (1000/3) X 100 = 33333 kPa = 33.33 MPa ≈ 33 MPa

$$E_{50} = E_{50}^{ref} \sqrt{\frac{\sigma_3^{'} + a}{p^{ref} + a}}$$ @ $\sigma_3^{'}$ = 345 kPa

Here, a = 0 since c = 0 for sand.

$$E_{50} = E_{50}^{ref} \sqrt{\frac{345}{100}} = 1.86 \text{ X } E_{50}^{ref}$$

Therefore,

E_{50}^{ref} = E_{50} /1.86 = 33/1.86 = 17.74 MPa ≈ 18 MPa @ 0.6 m depth

For σ_3 = 138 kPa:

E_{50} = (400/2.5) X 100 = 16000 kPa ≈ 16 MPa

$$E_{50} = E_{50}^{ref} \sqrt{\frac{\sigma_3^{'} + a}{p^{ref} + a}}$$ @ $\sigma_3^{'}$ = 138 kPa

$$E_{50} = E_{50}^{ref} \sqrt{\frac{138}{100}} = 1.17 \text{ X } E_{50}^{ref}$$

Therefore,

E_{50}^{ref} = E_{50} /1.17 = 16/1.17 = 13.67 MPa ≈ 14 MPa @ 0.6 m depth

The stiffness parameters are determined above using two cell pressures, that is, σ_3 = 345 kPa and 138 kPa. Most of the sands show a reference stiffness, E_{50}^{ref}, in the range of 15 to 50 MPa. In this report the stiffness parameters calculated at σ_3 = 345 kPa are used for Hardening soil model.

The Poisson's ratio, υ, can be determined from the graph of volumetric strain versus axial strain. So, from the graph in Figure 4.57 and Figure 4.58, Poisson's ration at σ_3 = 345 kPa are calculated using the equation;

$$\frac{\Delta\varepsilon_v}{\Delta\varepsilon_y} = 1 - 2\upsilon$$

where,

$\Delta\varepsilon_v$ = volumetric strain

$\Delta\varepsilon_y$ = axial strain

Sample from 3.0 m depth

$$\frac{0.3}{(3.5-1.75)} = 1 - 2\upsilon$$

$\Rightarrow$ υ = 0.4

Sample from 0.6 m depth

$$\frac{0.1}{0.5} = 1 - 2\upsilon$$

$\Rightarrow$ υ = 0.4

The values of ϕ' calculated from triaxial tests are:

At 0.6 m depth: ϕ' = 34.2 degrees

At 3.0 m depth: ϕ' = 36.4 degrees

The dry density can be found in the technical report at Texas A&M University footing load test site with an average value of 15.28 and 16.65 kN/m^2 at 0.6 m and 0.3 m depth respectively. Taking one typical value of CPT, that is, 3.0 X 3.0 m footing (North), the range of OCR is determined in Figure 4.60.

Depth, m	Friction, fs (tsf)	fs, kPa	Tip resistanc, qc (tsf)	qc, kPa	sigma_vo	sigma_vo'	Rf	QT
1.75	0.8	76.64	125	11975	26.25	26.25	0.641406	455.1905
5.25	1.5	143.7	50	4790	78.75	75.25	3.050146	62.60797
9	1.5	143.7	35	3353	135	94	4.465507	34.23404
14.5	2.2	210.76	98	9388.4	228	132	2.300773	69.39697

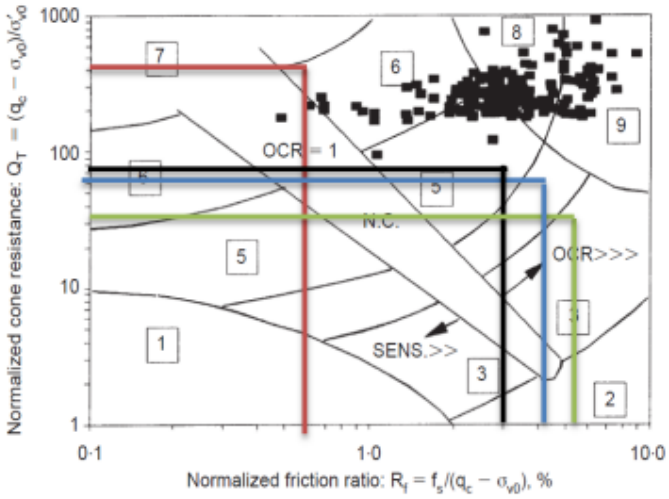

Figure 4.60 Range of OCR at Texas A&M footing load test site.

The range of OCR is estimated and iterated using the following two equations. The OCR is iterated until K_o values from both equations are similar. It is shown in Table 4.15.

$$K_o = 0.192(q_c / p_a)^{0.22}(\sigma'_{vo} / p_a)^{-0.31} OCR^{0.27}$$ by Mayne, CPT'95

$$K_o = [1 - \sin(\phi')] OCR^{\sin\phi'}$$ by Mayne & Kulhawy, 1982

Table 4.15 Determintion of OCR and K_o by iteration at Texas A&M footing load test site.

Depth m	Tip resistance, q_c (tsf)	q_c kPa	σ_{vo}	σ'_{vo}	P_a	OCR	Φ'	K_0	K_0
1.75	125	11975	26.25	26.25	100	8.95	36	1.5052	1.4948
5.25	50	4790	78.75	75.25	100	1.75	36	0.5713	0.5728
9.0	35	3353	135	94	100	1.16	36	0.4412	0.4498
14.5	98	9388.4	228	132	100	1.54	36	0.5377	0.5313

After extensive study of the geotechnical report of five large scale load tests, the parameters required for Hardening Soil model are determined. Especially, the triaxial test results are used as a basis for the necessary parameters. The stiffness parameters determined at σ_3 = 345 kPa are used and Table 4.16 illustrates the parameters. The subsoil

profile shows that the sand is medium dense and for this type of sand the reference stiffness is in the range of 30 to 35 MPa. But the reference stiffness found from the triaxial test is of the loose sand. The reason behind this may be due to the triaxial test performed on remolded samples of material taken from a hand auger.

Table 4.16 Parameters of Texas A&M footing load test site.

S/N	Soil Type	E_{50}^{ref}	E_{oed}^{ref}	E_{ur}^{ref}	m	c'	ϕ'	Ψ'	K_o	OCR	γ	Model	Type
		MPa	MPa	MPa		kPa					kN/m^2		
1	Medium dense tan silty fine sand	18	18	54	0.5	0	36	6	1.5	8.95	16	HS	Drained
2	Medium dense silty sand with clay and gravel	20	20	60	0.5	0	36	6	0.57	1.75	16	HS	Drained
3	Medium dense silty sand to sandy clay with gravel	22	22	66	0.5	0	36	6	0.44	1.16	16	HS	Drained
4	Very hard dark gray clay	28	28	84	0.5	0	36	6	0.44	0.54	1.54	HS	Drained

Table 4.17 Material properties for footing at Texas A&M footing load test site.

Parameters	Name	Reinforced concrete footing	Unit
Thickness	d	1.2	m
Weight	w	28.8	kN/m/m
Poisson's ratio	υ	0.15	-
Type of behavior	Type	Elastic, isotropic	-
Normal stiffness	EA	3.60E+07	kN/m
Flexural rigidity	EI	4.32E+06	kNm^2/m

4.3.1.2 Plate loading test

The five spread footing tests were performed at the National Geotechnical Experimentation Site on the Texas A&M University Riverside Campus near college station. The plane dimensions of the footings are: two 3.0 X 3.0 m footing (south and north sides), one 2.5 X 2.5 m footing, one 1.5 X 1.5 m footing, and one 1.0 X 1.0 m footing. The plan view of the footings arrangement is presented in Figure 4.61. Four 0.91 m diameter, 21.3 m long drilled shafts with 2.7 m 60^0 underreamed bells and on 0.91 m diameter, 5 m long straight drilled shaft were built. The four drilled and belled shafts were founded at depths ranging from 19.6 to 20.6 m. The exact as-built dimensions are shown in Table 4.18.

Table 4.18 As-Built Footing Dimensions at Texas A&M footing load test site(Briaud and Gibbens 1997).

Footing No.	Length by Width	Thickness	Embedment Depth	In Text, Referred to as
1	3.004 by 3.004	1.219	0.762	3-m North footing
2	1.505 by 1.492	1.219	0.762	1.5-m footing
3	3.023 by 3.016	1.346	0.889	3-m South footing
4	2.489 by 2.496	1.219	0.762	2.5-m footing
5	0.991 by 0.991	1.168	0.711	1.0-m footing

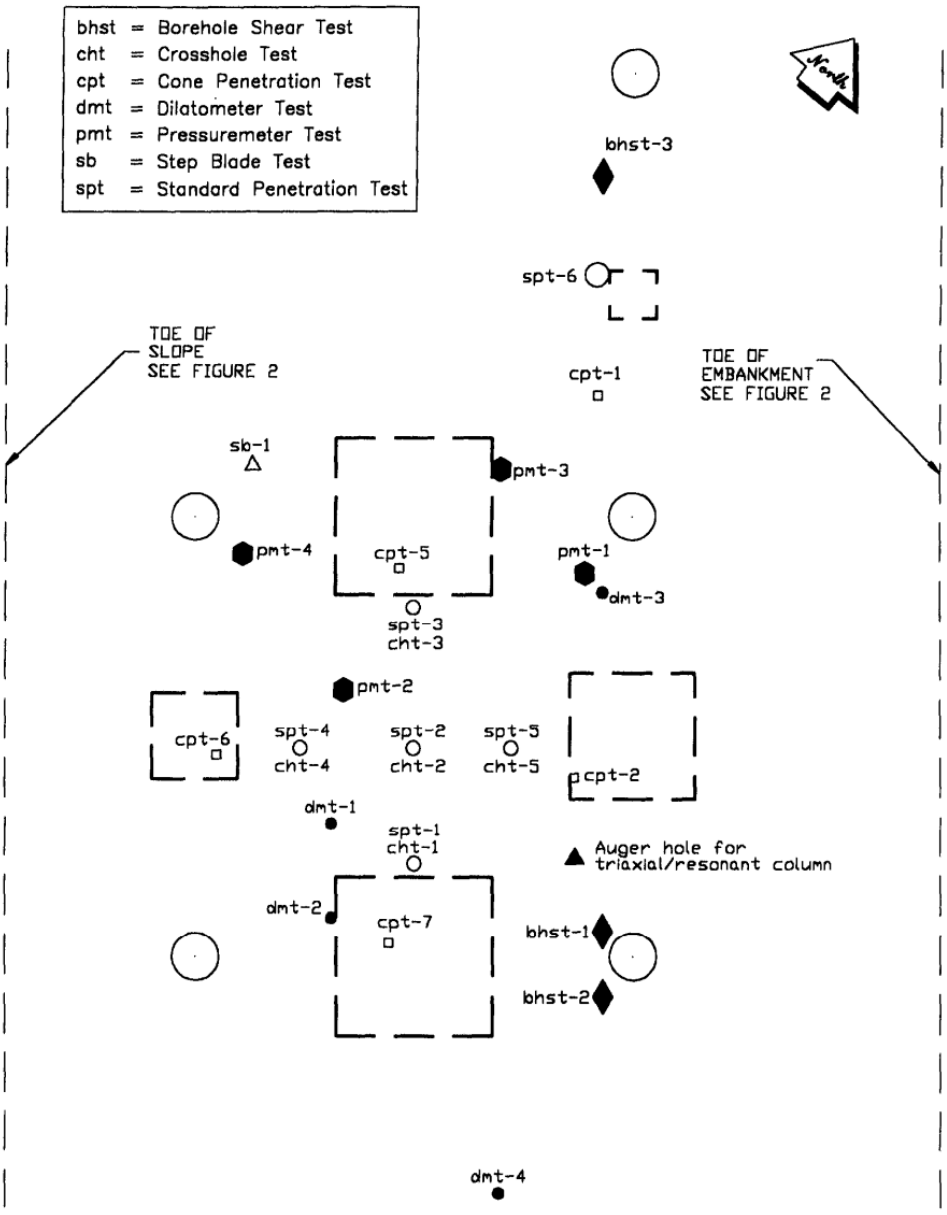

Figure 4.61 A plan view of footing arrangement at Texas A&M footing load test site(Briaud and Gibbens 1997).

After excavating the holes with a backhoe and hand finishing with shovels, a mat type reinforcement cage was placed just off the bottom of the footing excavation using #11 rebar, 150 mm center to center in both directions. Prior to concrete placement, three 120 mm diameter PVC sleeves were placed within the footing to serve as conduits through which the drilling of the telltales would take place. The footings were formed and poured at a rate of approximately two footings per day. A typical load test is shown in Figure 4.62.

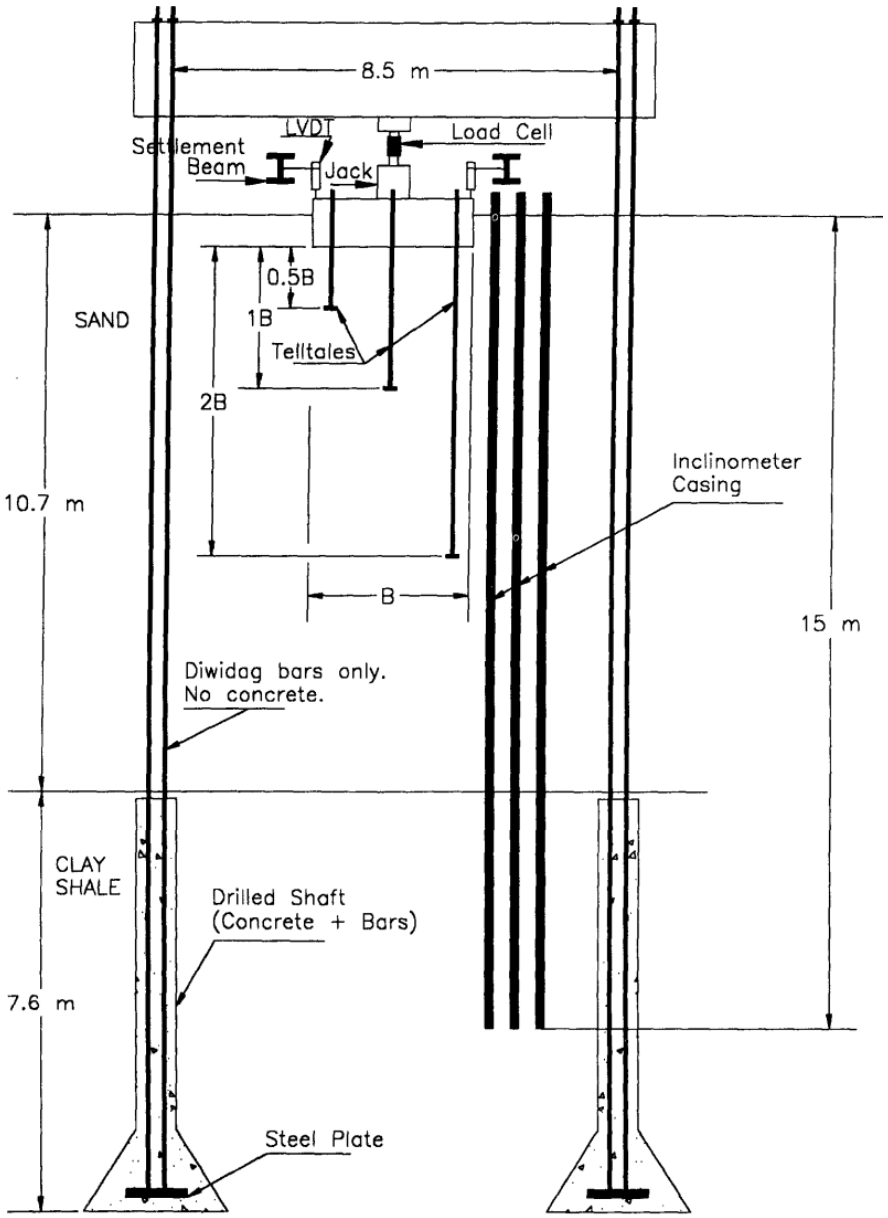

Figure 4.62 A typical load setup at Texas A&M footing load test site(Briaud and Gibbens 1997).

Reaction shafts were installed to resist the 12 MN load applied vertically to each of the footings. The dywidag bars went from the reaction beam down to the bottom of the shaft, but only the portion of the shaft in the shale was filled with concrete. The portion of the shaft in the sand was filled with sand to minimize the influence of the reaction shaft on the footing and soil behavior. Construction of the shafts was completed at a rate of one shaft

per day. Six vertical inclinometer casings were installed in order to evaluate the horizontal displacement of the soil surrounding the footing group which is shown in Figure 4.62. In addition, extensometer type telltales were designed and constructed and measurement of vertical displacement was taken at 0.5B, 1.0B and 2.0B depths for each footing (Figure 4.62).

The load was measured with a 12-MN load cell resting between the jack and the load frame. To measure the vertical displacement the average reading of four LVDTs (linear variable displacement transducers) was used which were placed at the corners of the footings and tied to two reference beams. The testing procedure consisted of applying the load in increments equal to one-tenth of the estimated footing capacity as determined by commonly used bearing capacity calculation methods. Each load step lasted 30 min, with settlement readings at 1, 3, 5, 7, 10, 20, and 30 min. This 30-min period was considered sufficiently long to bring the settlement rate at the end of each load step to a very small value and to calibrate the creep settlement model while deeping the load-test duration reasonable. The load-settlement curves are shown in taken during 30 min under each load. Unload-reload cycles were necessary in order to install shims above the jack.

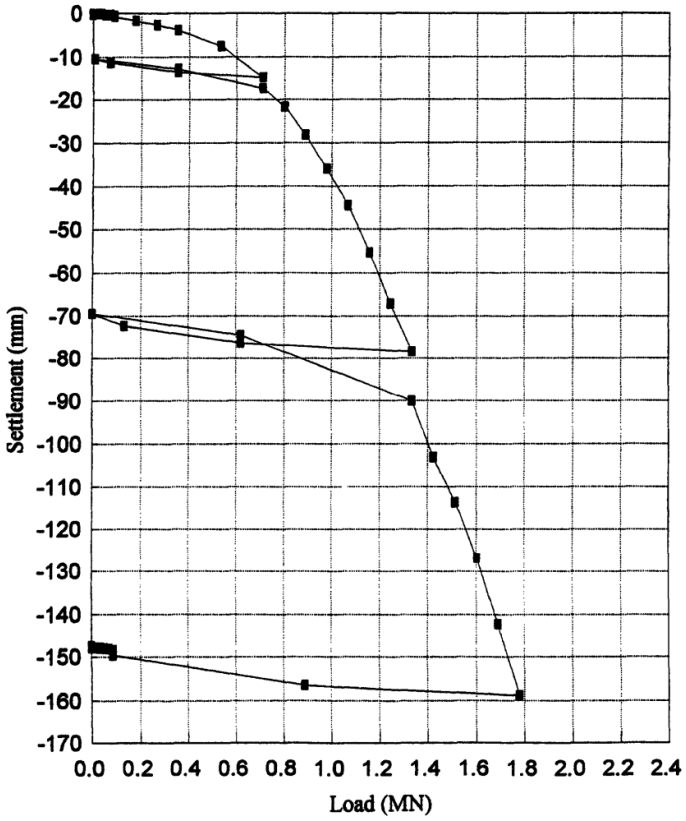

Figure 4.63 Load-settlement curve for 1.0 m footing at Texas A&M footing load test site(Briaud and Gibbens 1997).

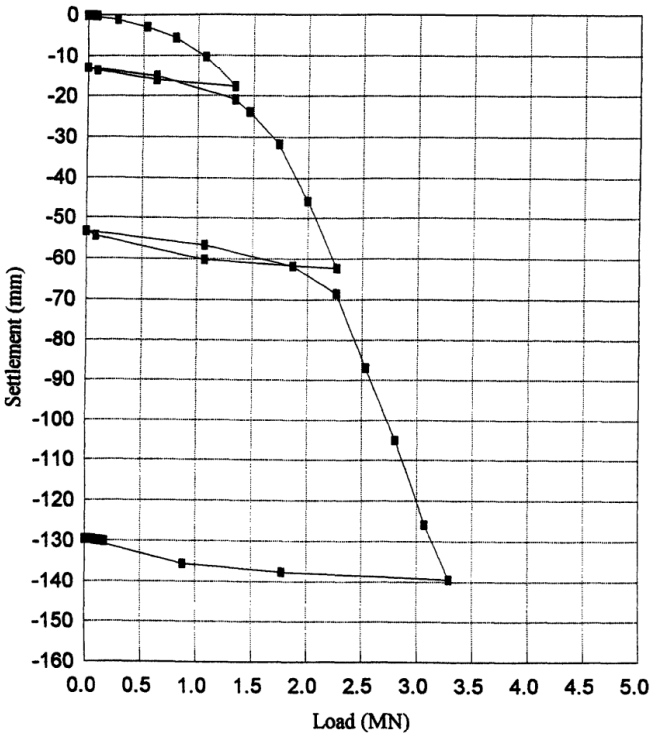

Figure 4.64 Load-settlement curve for 1.5 m footing at Texam A&M footing load test site(Briaud and Gibbens 1997).

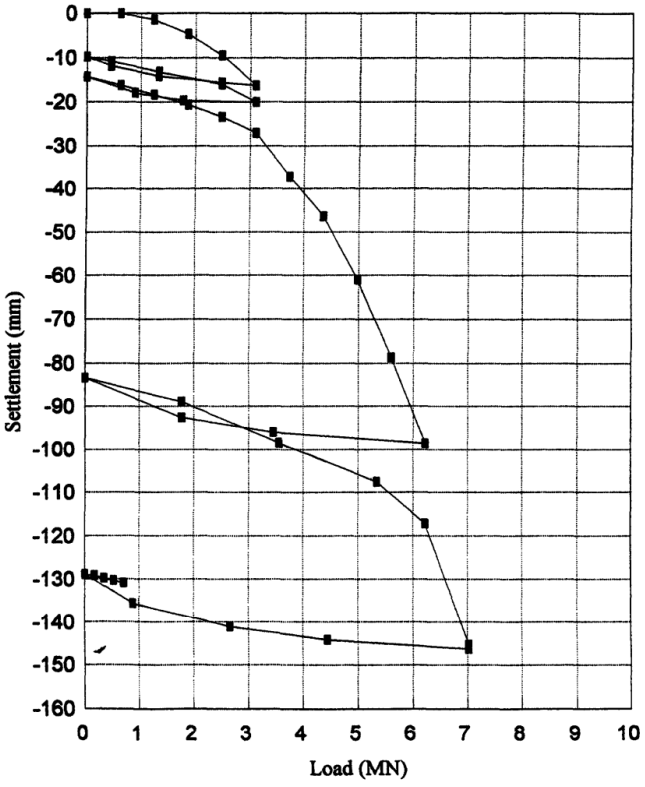

Figure 4.65 Load-settlement curve for 2.5 m footing at Texas A&M footing load test site(Briaud and Gibbens 1997).

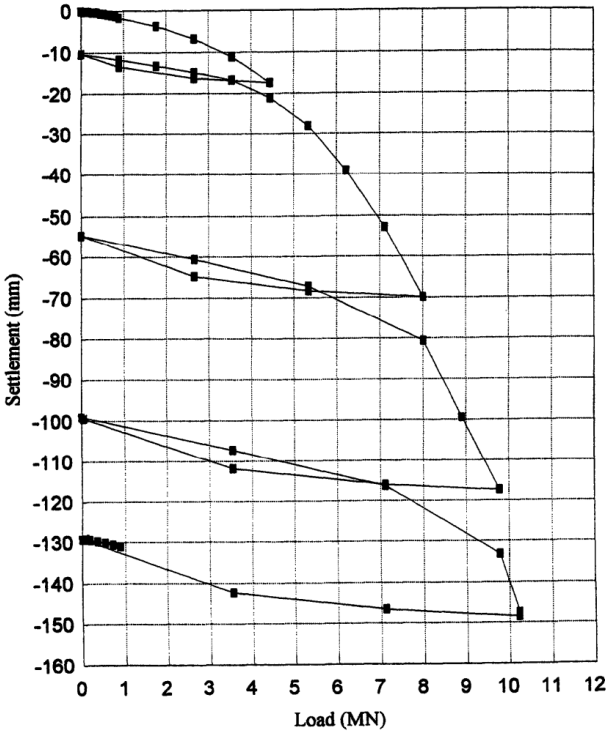

Figure 4.66 Load-settlement curve for 3.0 m north footing at Texas A&M footing load test site(Briaud and Gibbens 1997).

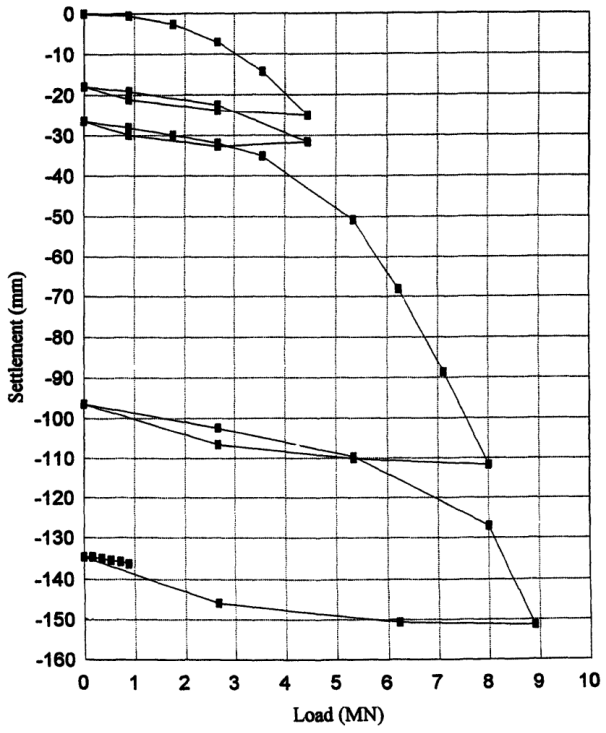

Figure 4.67 Load-settlement curve for 3.0 m south footing at Texas A&M footing load test site(Briaud and Gibbens 1997).

4.3.2 Numerical modeling

The FEM analysis of reinforced concrete footing and steel plates are modeled in FEM based package PLAXIS 2D. The 15 nodes element will result a more precise calculation of the stress and strains. A fine mesh is used for the models. The axi-symmetric circular footing and steel plates are modeled as linear elastic element. The experimental load-displacement curves for shallow foundations obtained by (Briaud and Gibbens 1997) are compared with the numerical results obtained using constitutive model, that is, Hardening Soil Model. The elastic modulus of soil has been considered based on the available correlation with the in-situ and laboratory test results e.g. SPT, CPT, CHT, DMT, PMT, BHST and triaxial tests.

Four square footings with plane dimensions 1.0 X 1.0 m, 1.5 X 1.5 m, 2.5 X 2.5 m, and 3.0 X 3.0 m are considered. The square footings can be approximated as circular footings with soil-foundation contact areas equivalent to those of the corresponding square footings, that is, with diameters of 1.13 m, 1.69 m, 2.80 m, and 3.40 m which is shown in Figure 4.68. (Lee and Salgado 2002) found that 'differences in stresses at the same depths due to the use of circular rather than square footings were less than 2%, based on linear elastic calculations'.

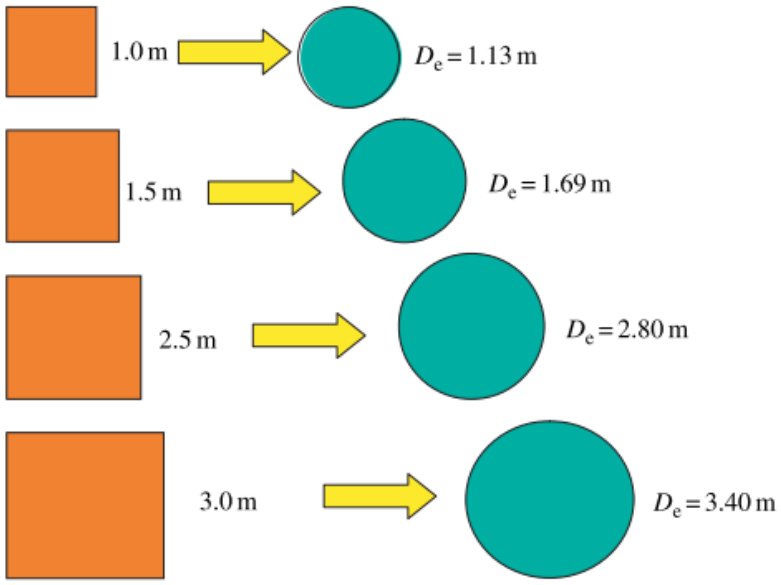

Figure 4.68 Examined square footings and equivalent circular footings at Texas A&M footing load test site.

All three square footings were modeled numerically with number of simulations by changing the value of strength parameters c'_{ref} and ϕ'. The goal of these simulations is to validate our numerical analysis by comparison with existing load-settlement observations. In PLAXIS, based on the soil profile in Figure 4.52, the numerical model is created for the bearing capacity calculation which is shown in Figure 4.69.

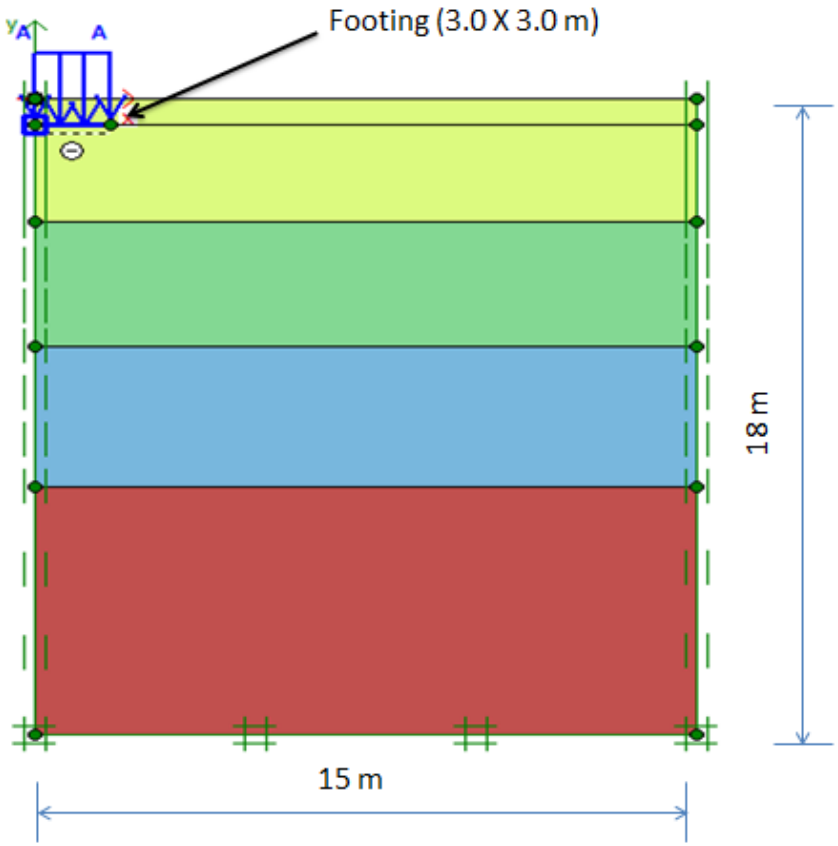

Figure 4.69 Typical numerical model for simulation at Texas A&M footing load test site.

A drained behavior is assumed for the materials for the bearing capacity calculations. Initial stresses in the soil are driven from the material weight and their historical of development. In the Plaxis software the horizontal stress in static state is calculated using Jacky's formula;

$$k_o = 1 - \sin(\phi)$$

When the typical model for simulation is created with all material sets in it, the standard boundary conditions are set. As a result Plaxis will automatically generate a full fixity at the base of the geometry and roller boundaries at the vertical sides (u_x = 0; u_y = free). In this project, in order to calculate the bearing capacity, the elastic footing was chosen with flexural rigidity (bending stiffness), EI and axial stiffness, EA.

A typical 2D meshes are shown in Figure 4.70. The bottom boundaries of the finite element models are located at a depth of 18 m and the lateral boundaries are located at a distance of 15 m from the center of the footings. 15-noded axisymmetric elements are used in the finite element meshes to model both the soil and the footings. The interface elements are also used between the footing base and the soil with a R_{inter} = 1.

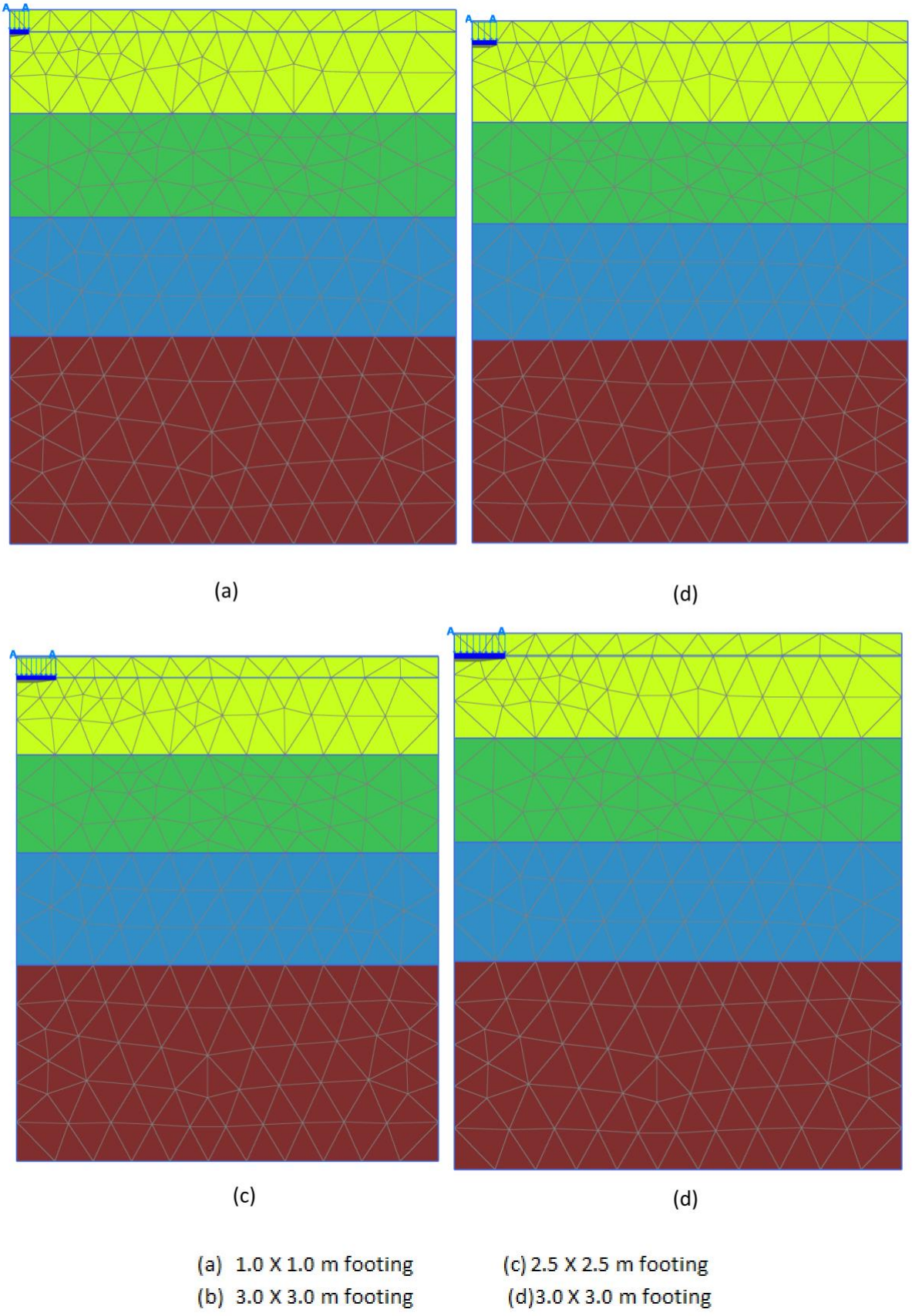

Figure 4.70 FEM mesh for the numerical simulation at Texas A&M footing load test site.

Loading condition:

Distributed load – load system A is applied vertically over the footing without eccentricity. Initial stresses are developed in the input stage by deactivating the footing. It is assumed that the self-weight of the footing has added to the distributed load. Three staged construction are performed. In the first staged construction, the excavation is done; in the second staged construction, footing is placed; and in the third staged construction, loading is activated. Finally, incremental multiplier is applied for vertical load to failure. The footing model is shown in Figure 4.71.

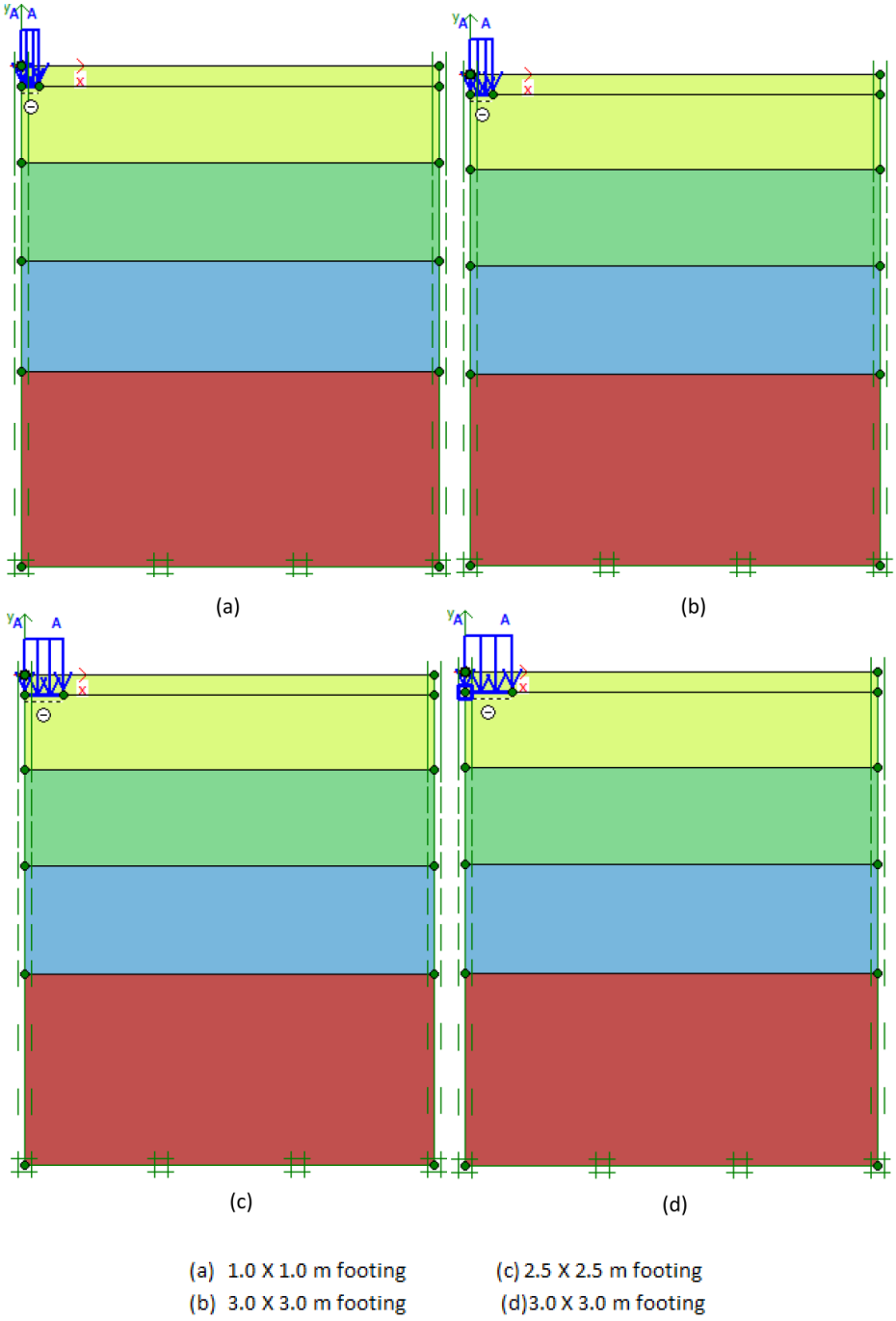

Figure 4.71 FEM footing model for the numerical simulation at Texas A&M footing load test site.

Deterministic results:

The simulations of different size of footings are performed using Hardening Soil model. the square footings with plane dimensions 1.0 X 1.0 m, 1.5 X 1.5 m, 2.5 X2.5 m and 3.0 X 3.0 m are considered. Three simulations are conducted for each of the footings, such as, simulation 1, simulation 2 and simulation 3. The simulations for different size of footings are shown in Table 4.21, Table 4.22, and Table 4.23.

After the simulation, outputs are observed as well as compare the load-settlement curves between simulated and measured. The deterministic results of only one simulation for each footing is shown here. In 4.3.3, it can be seen that simulation 2 has similar results for 1.5 X 1.5 m, 2.5 X 2.5 m and 3.0 X 3.0 m footings and for 1.0 X 1.0 m footing simulations 3 gives satisfactory results. Hence, the deterministic results are illustrated in Figure 4.72Figure 4.79.

Total displacement, u_y:

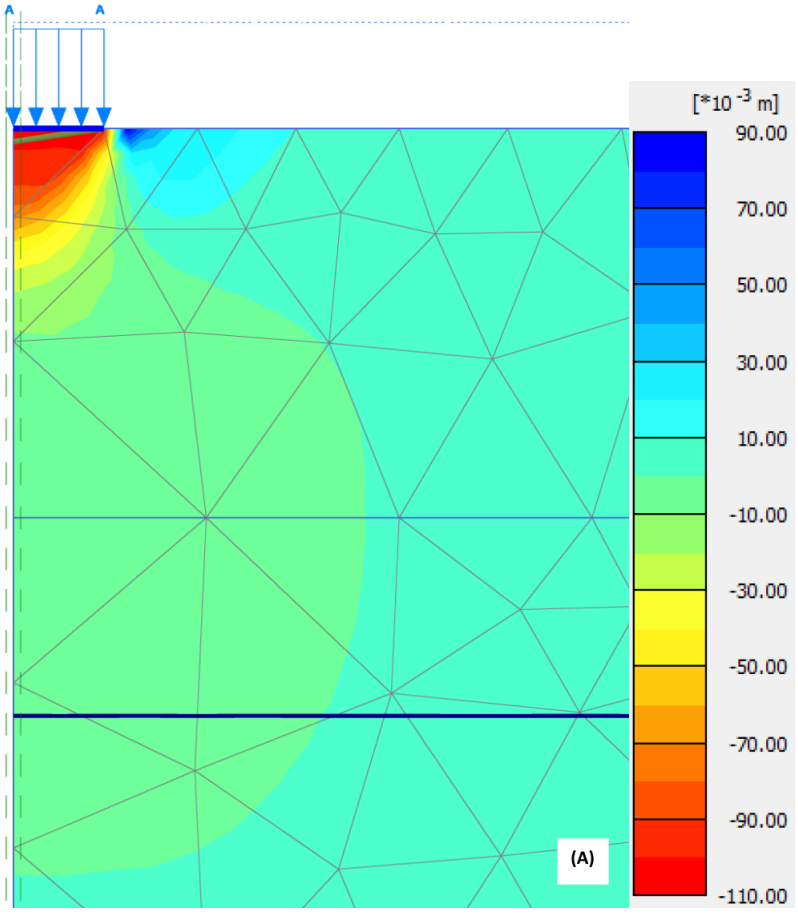

Figure 4.72 Vertical displacement transferred to the soil at Texas A&M footing load test site: 1.0 X 1.0 m footing.

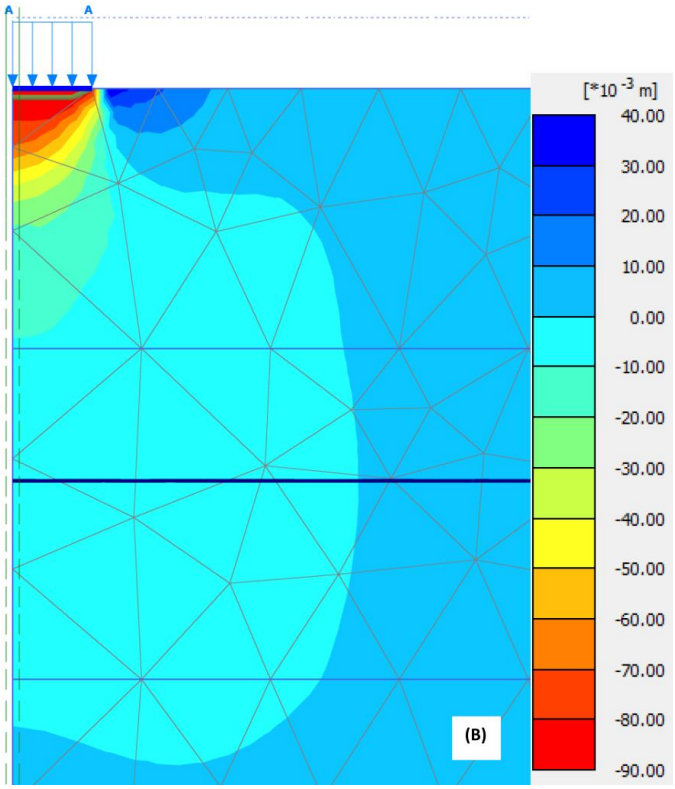

Figure 4.73 Vertical displacement transferred to the soil at Texas A&M footing load test site: 1.5 X 1.5 m footing.

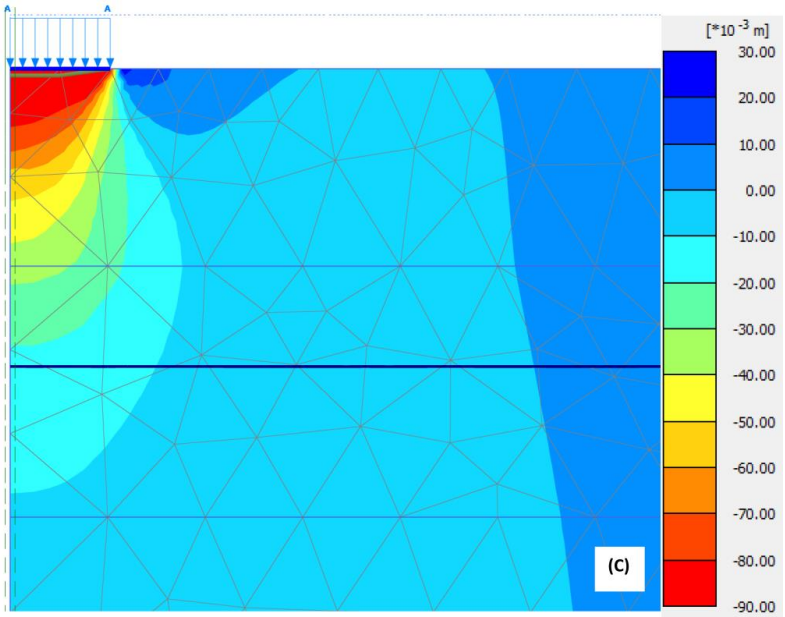

Figure 4.74 Vertical displacement transferred to the soil at Texas A&M footing load test site: 2.5 X 2.5 m footing.

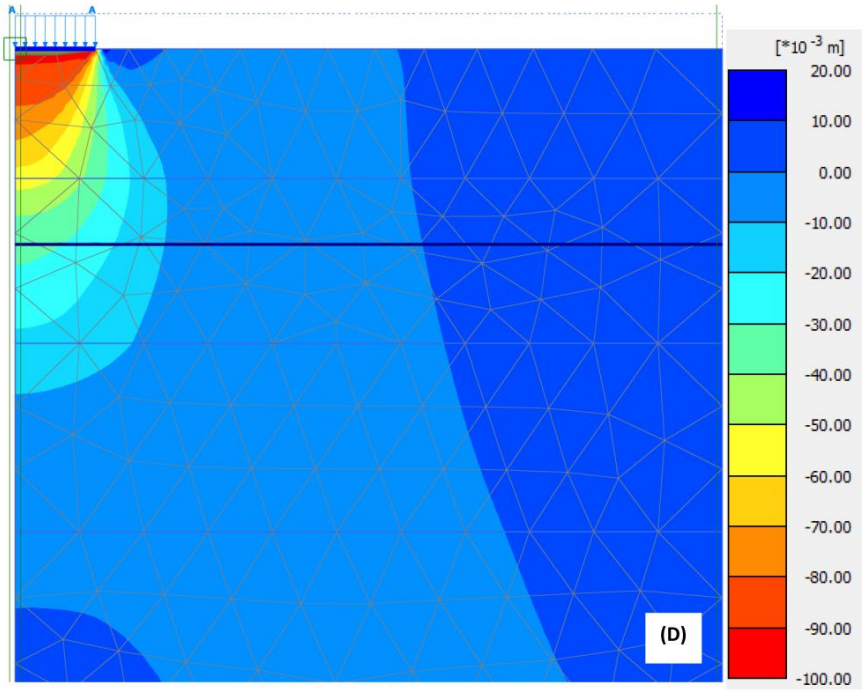

Figure 4.75 Vertical displacement transferred to the soil at Texas A&M footing load test site: 3.0 X 3.0 m footing.

Table 4.19 Showing maximum and minimum vertical displacement for total ground pressure below footing at Texas A&M footing load test site.

S/N	Total displacement, u_y (mm)	
	Maximum	Minimum
(A)	88.73	-103.00
(B)	41.61	-88.96
(C)	26.54	-89.52
(D)	17.58	-92.04

Total deviatoric strain:

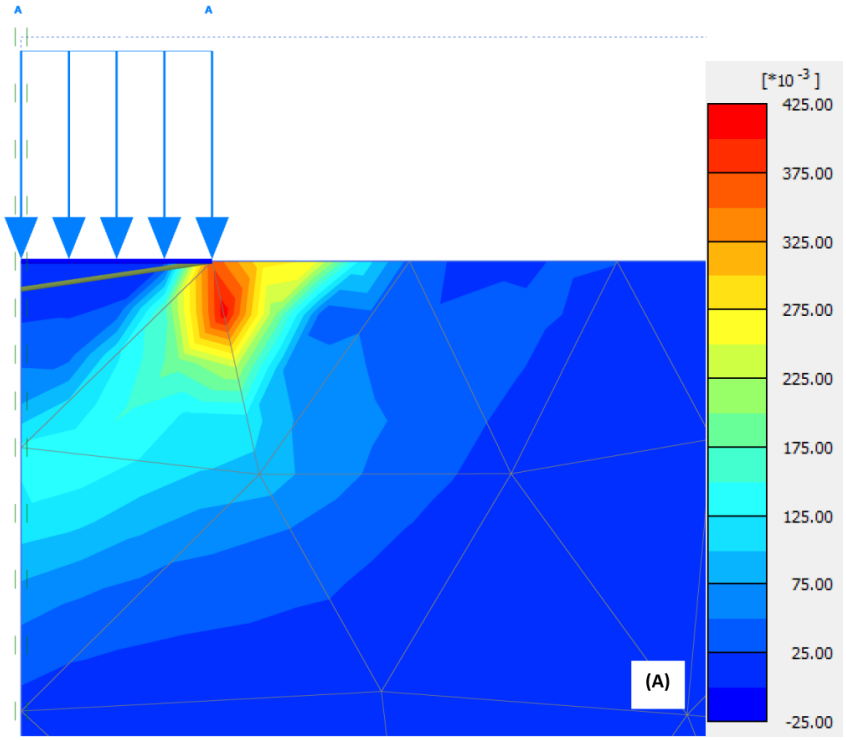

Figure 4.76 Total deviatoric strain for the total ground pressure in sand at Texas A&M footing load test site: 1.0 X 1.0 m footing.

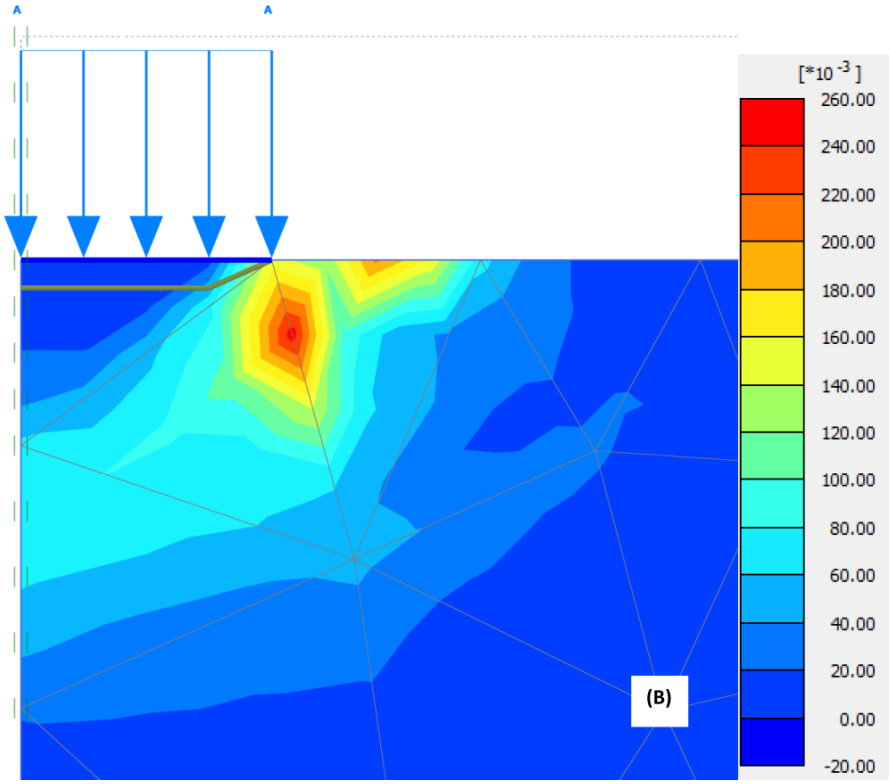

Figure 4.77 Total deviatoric strain for the total ground pressure in sand at Texas A&M footing load test site: 1.5 X 1.5 m footing.

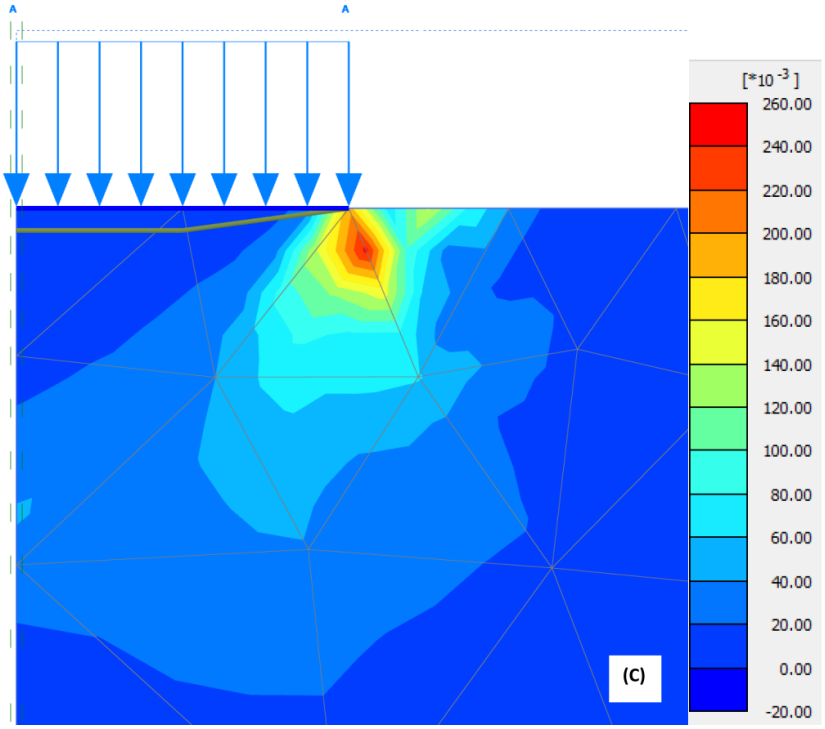

Figure 4.78 Total deviatoric strain for the total ground pressure in sand at Texas A&M footing load test site: 2.5 X 2.5 m footing.

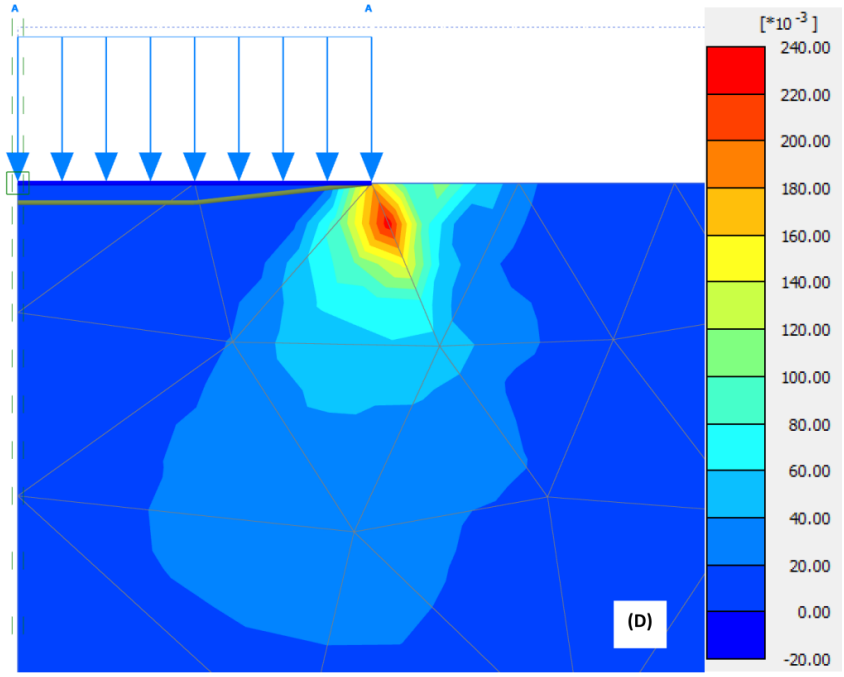

Figure 4.79 Total deviatoric strain for the total ground pressure in sand at Texas A&M footing load test site: 3.0 X 3.0 m footing.

Table 4.20 Showing maximum and minimum the total deviatoric strain for total ground pressure below footing in sand at Texas A&M footing load test site.

S/N	Total deviatoric strain, γ_s	
	Maximum	Minimum
(A)	0.4140	0.4954E-6
(B)	0.2595	0.3954E-6
(C)	0.2466	0.6054E-6
(D)	0.2330	1.991E-6

4.3.3 Comparison of load-settlement curve from PLT and PLAXIS

For sand at Texas A&M footing load test site, the stiffness parameters show some varying behavior. The load-settlement curve obtained using the stiffness parameters determined from triaxial test give an inconsistent result. The measured curves vary by a factor of 4 to 5 which can be seen in Figure 4.80. The reason is that the samples for triaxial test was taken from a hand auger which is not an undisturbed sample and gives stiffness compare to loose sand. The comparison with measured curve so that in real field the sand is very stiff. Hence, the back-calculation was done to find the well fitted curve.

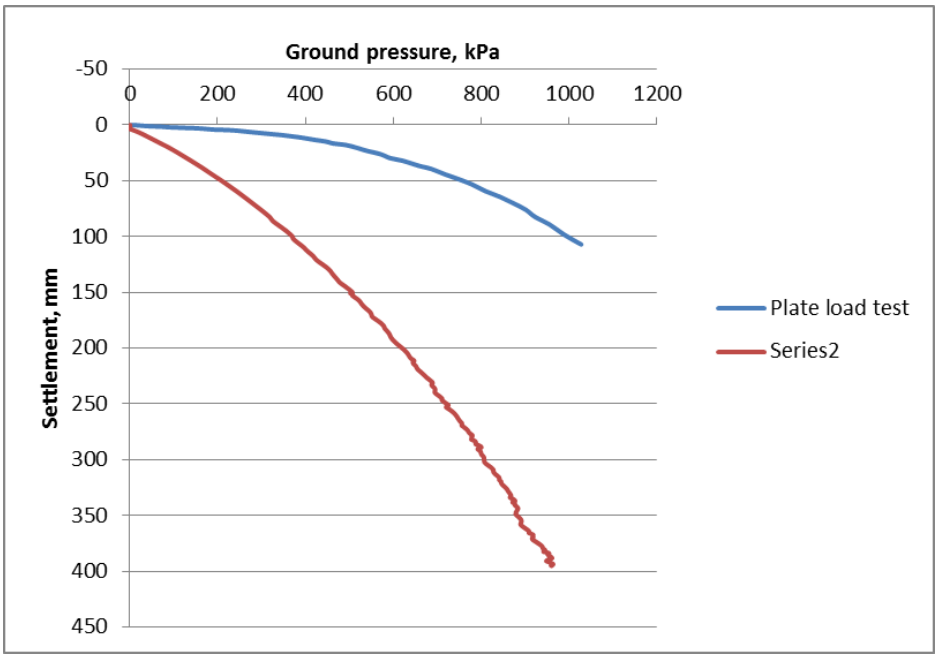

Figure 4.80 Load-settlement curve of simulation performed using stiffness parameters determined from triaxial test at Texas A&M footing load test site: 3.0 X 3.0 m footing.

It is instructive to compare the results of plate loading tests with those obtained from our numerical results. Figure 4.81 toFigure 4.85 show the measured and simulated load-settlement response for each footing. It can be seen that the measured load-settlement

curves and the numerical curves obtained using the proposed numerical model are more or less similar for all the footings investigated. During the simulation, it is seen that three simulations are done for each footing. From the load-settlement curve it is seen that simulation 2 gives consistent result for 1.5 X 1.5 m, 2.5 X 2.5 m and 3.0 X 3.0 m footing and for 1.0 X 1.0 m footing simulation 3 is well fitted.

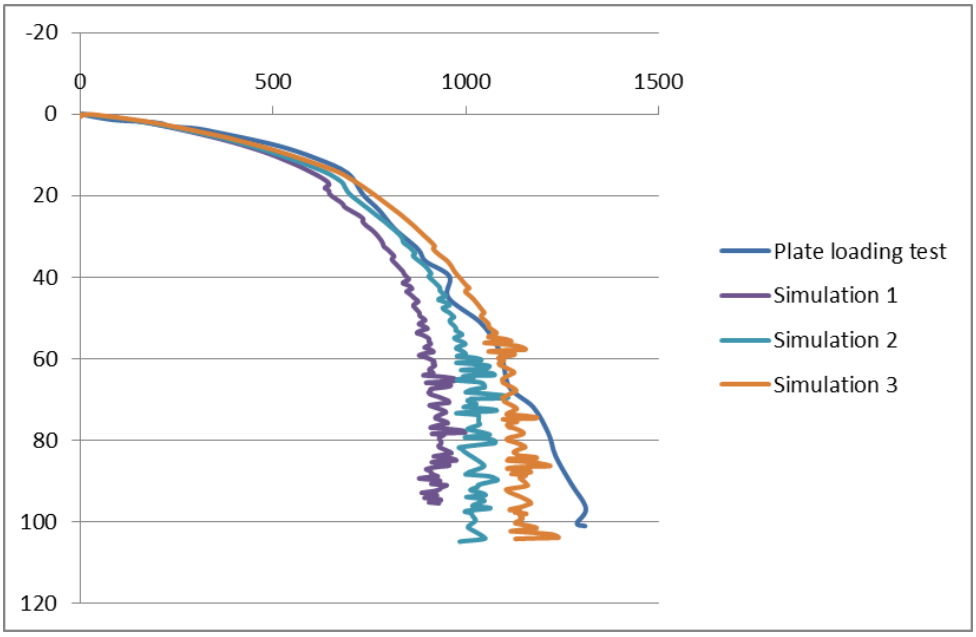

Figure 4.81 Comparison of experimental(Briaud and Gibbens 1997) and numerical load settlement curve at Texas A&M footing load test site: 1.0 X1.0 m footing.

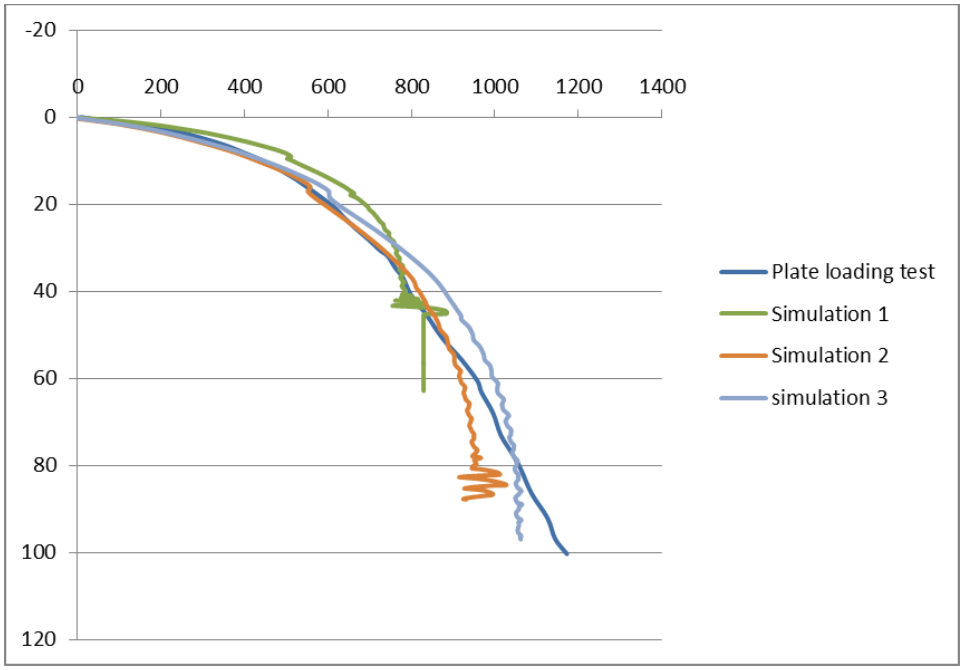

Figure 4.82 Comparison of experimental(Briaud and Gibbens 1997) and numerical load settlement curve at Texas A&M footing load test site: 1.5 X 1.5 m footing.

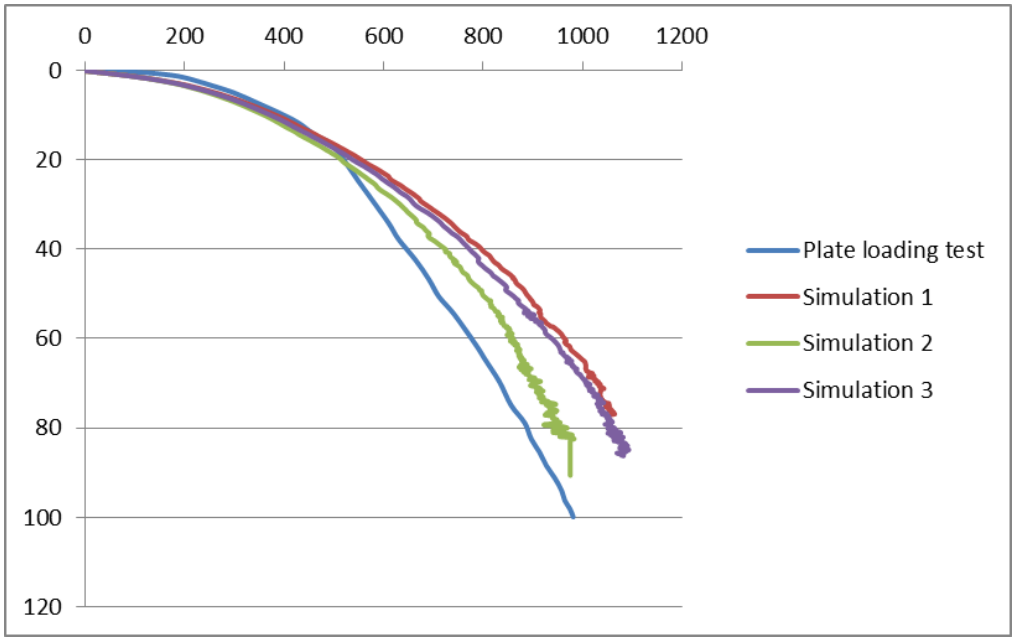

Figure 4.83 Comparison of experimental(Briaud and Gibbens 1997) and numerical load settlement curve at Texas A&M footing load test site: 2.5 X2.5 m footing.

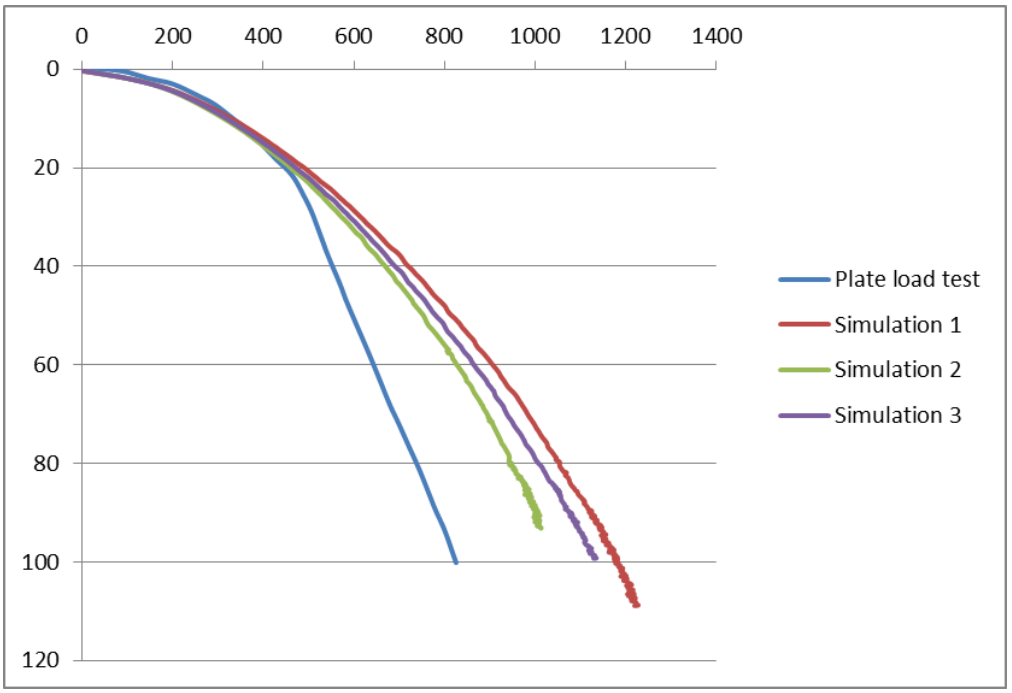

Figure 4.84 Comparison of experimental(Briaud and Gibbens 1997) and numerical load settlement curve at Texas A&M footing load test site: 3.0 X3.0 m south footing.

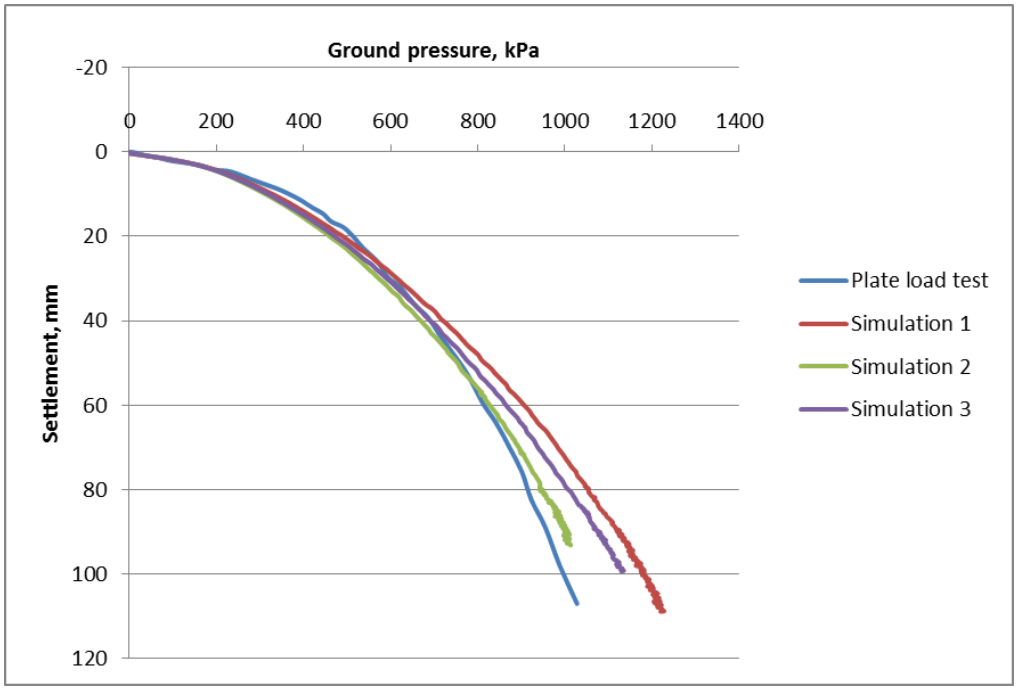

Figure 4.85 Comparison of experimental(Briaud and Gibbens 1997) and numerical load settlement curve at Texas A&M footing load test site: 3.0 X3.0 m north footing.

4.3.4 Summary and conclusions

In this case, the load-settlement response of vertically loaded footings on sand at Texas A&M footing load test site was investigated using non-linear finite element analysis. The FEM analysis is performed with Hardening Soil model which is an elasto-plastic hyperbolic constitutive model with isotropic hardening connected to two plastic yield surfaces, that is, one is cone and other is a cap. Hardening soil model is an advanced soil model for simulating the behavior of different types of soil. The results of insitu as well as triaxial test were used to define parameters of Hardening soil model.

The site contains medium dense silty fine silica sand which is slightly overconsolidated by desiccation of the fines. A series of field and laboratory tests were performed in order to characterize the material on site. The triaxial test results were used to find the stiffness parameters as well as strength parameters required for Hardening Soil model. For determination of K_0 and OCR values, the iteration was done between empirical formulae.

The measured load-settlement curves were compared with back-calculated load-settlement curve numerically. The five spread footings were performed at the site and those different sizes footing were analysed numerically using PLAXIS 2D. After the simulations were executed, the load-settlement curves obtained using finite element analysis was compared with those obtained from measured plate loading test. Initially, the simulation was performed using stiffness parameters determined from triaxial test results (Table 4.16). The simulations gave load-settlement curve that vary by a factor of 4 to 5 which is illustrated in Figure 4.80. The reason behind this vast variation may be due to the samples for triaxial test

taken from a hand auger which is a disturbed sample and behaves as loose sand. The curve obtained shows that the sand is real field may be very stiff.

Table 4.21 Back-calculated stiffness parameters at Texas A&M footing load test site: 2.5 X 2.5 m and 3.0 X 3.0 m footings.

2.5 X 2.5 m and 3.0 X 3.0 m footings												
	Simulation 1				Simulation 2				Simulation 2			
Soil Type	E_{50}^{ref}	E_{oed}^{ref}	E_{ur}^{ref}	ϕ'	E_{50}^{ref}	E_{oed}^{ref}	E_{ur}^{ref}	ϕ'	E_{50}^{ref}	E_{oed}^{ref}	E_{ur}^{ref}	ϕ'
	MPa	MPa	MPa		MPa	MPa	MPa		MPa	MPa	MPa	
Medium dense tan silty fine sand	150	150	450	36	150	150	450	35	150	150	450	36
Medium dense silty sand with clay & gravel	75	75	225	36	75	75	225	35	70	70	210	36
Medium dense silty sand to sandy clay with gravel	40	40	120	36	40	40	120	35	35	35	105	36
Very hard dark gray clay	55	55	165	30	55	55	165	30	45	45	135	30

For the load-settlement to be fitted some back-calculations were carried out. The numbers of simulations were executed for different sizes of footings. While the simulations were performed, the parameters demonstrated in Table 4.21 provide consistency between simulated and measured load-settlement curves. The CPT results in 3.0 X 3.0 m footing (south side) gives that the cone resistance at about 3.0 m is very low and might be due to this low value some underpredicted results are obtained during simulation. Similarly, the parameters in Table 4.22 and Table 4.23 are for 1.5 X 1.5 m and 1.0 X 1.0 m footings. The back-calculation is done to get the load-settlement curves are well fitted. It is seen that the curves are similar to the footings.

Table 4.22 Back-calculated stiffness parameters at Texas A&M footing load test site: 1.5 X 1.5 m footing.

1.5 X 1.5 m footing												
	Simulation 1				Simulation 2				Simulation 2			
Soil Type	E_{50}^{ref}	E_{oed}^{ref}	E_{ur}^{ref}	ϕ'	E_{50}^{ref}	E_{oed}^{ref}	E_{ur}^{ref}	ϕ'	E_{50}^{ref}	E_{oed}^{ref}	E_{ur}^{ref}	ϕ'
	MPa	MPa	MPa		MPa	MPa	MPa		MPa	MPa	MPa	
Medium dense tan silty fine sand	150	150	450	36	80	80	240	37	80	80	240	37.5
Medium dense silty sand with clay & gravel	75	75	225	36	50	50	150	37	50	50	150	37.5
Medium dense silty sand to sandy clay with gravel	40	40	120	36	30	30	90	37	30	30	90	37.5
Very hard dark gray clay	55	55	165	30	45	45	135	32	45	45	135	32

Table 4.23 Back-calculated stiffness parameters at Texas A&M footing load test site: 1.0 X 1.0 m footing.

1.0 X 1.0 m footing						
				Simulation 1	Simulation2	Simulation3
Soil Type	E_{50}^{ref}	E_{oed}^{ref}	E_{ur}^{ref}	**ϕ'**	**ϕ'**	**ϕ'**
	MPa	MPa	MPa			
Medium dense tan silty fine sand	150	150	450	38	38.5	39
Medium dense silty sand with clay & gravel	75	75	225	38	38.5	39
Medium dense silty sand to sandy clay with gravel	40	40	120	38	38.5	39
Very hard dark gray clay	55	55	165	35	36	37

The back-calculates results provide that the sand at the site is stiff and gives some high stiffness parameters. It can be concluded that the reference stiffness, E_{50}^{ref}, vary from 150 MPa at the top layer to 55 MPa at the bottom layer. The sand at the site is medium dense and the range of reference stiffness, E_{50}^{ref}, is from 30 to 35 MPa but in this case, it is higher at a factor of 3 to 8 which is a quite interesting behavior to be studied.

5 CONCLUSION AND RECOMMENDATION

5.1 Conclusion

In the present study, back-calculation of plate loading tests of shallow foundations has been done using PLAXIS 2D and the Hardening Soil model.

Initial part of the study was to identify high quality, relevant, well documented plate loading tests with recorded load-settlement curves. The relevant soil profiles and soil parameters were identified and calculated from the existing reports. Three case studies with full scale load tests were selected to back-calculate using advanced soil model in PLAXIS 2D in order to gather experience on soil behavior of shallow foundations.

The first case study was on clay till at Tornhill, Sweden. The measured load-settlement curves were compared with back-calculated load-settlement curves numerically for three full-scale shallow foundations of different sizes. From the result, it was seen that the numerical curves obtained using finite element analysis are in reasonable agreement with the measured results. The curves obtained from third simulation were more similar though the ends of the curves show slight variation. Hence, the back-calculated results obtained from the simulations show that effective cohesion is between 11.45 to 14.45 kPa and friction angle is about 30^0.

The second case study was on saprolitic soil from Portugal. The load-settlement curves obtained numerically using the proposed numerical model for three plates were compared with measured curves. From the result, it was seen that the curves were very similar for all the footings investigated except for 0.3 m diameter plate which shows little underprediction. Therefore, from the back-calculation it can be concluded that the effective cohesion is between 8 to 13 kPa and friction angle between 37^0 to 38^0.

The third case study was on sand at Texas A&M footing load site, USA. The site contains slightly overconsolidated sand. Initially, the back-calculation using proposed numerical model was performed from the parameters obtained from the triaxial test which gave load-settlement curve that vary by a factor of 4 to 5. It was seen that the sand in the field was stiffer. Then, the back-calculation was carried out to obtain the numerical curves get fitted with the measured load-settlement curves. Finally, back-calculation results provide that the sand at the site is stiff and gives some high stiffness parameters. It can be concluded that the reference stiffness, E_{50}^{ref}, vary from 150 MPa at the top layer to 55 MPa at the bottom layer. The sand at the site is medium dense and the range of reference stiffness, E_{50}^{ref}, is from 30 to 35 MPa but in this case, it is higher at a factor of 3 to 8 which is rather attention-grabbing behavior to be studied.

5.2 Recommendation

The behavior of shallow foundation has been studied during this whole thesis from the back-calculation of plate load tests. Though, the finite element analysis provides efficient results, the programs need many input parameters and may be complicated to use. Analysis should be performed with high care as back-analysing the parameter are very sensitive due to small value.

For further study, ore case studies could be searched, selected and studied extensively for the back-calculation using advanced soil models. In addition, the soil behavior could be studied by using other constitutive models, such as, Hardening Soil Small model, Soft Soil Creep model or Cam Clay model. I would suggest providing more time and study to compare results from different constitutive models.

REFERENCES

Abate, G., C. Caruso, M. Massimino and M. Maugeri (2008). "Evaluation of shallow foundation settlements by an elasto-plastic kinematic-isotropic hardening numerical model for granular soil." Geomechanics and Geoengineering: An International Journal **3**(1): 27-40.

Bowles, J. E. 1977. Foundation Analysis and Design, McGraw-Hill, Inc.

Bowles, J. E. (1988). Foundation analysis and design.

Briaud, J.-L. and R. Gibbens (1999). "Behavior of five large spread footings in sand." Journal of Geotechnical and Geoenvironmental Engineering **125**(9): 787-796.

Briaud, J. and R. Gibbens (1997). Large scale load tests and data base of spread footings on sand.

Brinkgreve, R., W. Broere and D. Waterman (2012). PLAXIS 2D 2012. R. Brinkgreve, E. Engin and W.M.Swolfs, Delft University of Technology & PLAXIS bv, The Netherlands

Burd, H. (1999). The history of PLAXIS. Beyond 2000 in Computational Geotechnics: 10 Years of PLAXIS International; Proceedings of the International Symposium Beyond 2000 in Computational Geotechnics, Amsterdam, The Netherlands, 18-20 March 1999, Taylor & Francis Group.

Christian, J. T. and W. David Carrier III (1978). "Janbu, Bjerrum and Kjaernsli's chart reinterpreted." Canadian Geotechnical Journal **15**(1): 123-128.

da Fonseca, A. V. (2002). "Characterising and deriving engineering properties of a saprolitic soil from granite, in Porto." Characterisation and Engineering Properties of Natural Soils.

Da Fonseca, A. V., M. M. Fernandes and A. S. Cardoso (1998). "Interpretation of a footing load test on a saprolitic soil from granite." Pre-Failure Deformation Behaviour of Geomaterials: 247.

Das, B. M. (2009). Settlement and Allowable Bearing Capacity. Shallow Foundations, CRC Press**:** 165-228.

Das, B. M. (2009). Ultimate Bearing Capacity Theories? Centric Vertical Loading. Shallow Foundations, CRC Press**:** 11-75.

Décourt, L. (1992). SPT in non classical material. Proceedings of US-Brazil Geotechnical Workshop on Applicability of Classical Soil Mechanics Principles in Structured Soil, Belo Horizonte.

Duncan, J. M. and C.-Y. Chang (1970). "Nonlinear analysis of stress and strain in soils." Journal of the Soil Mechanics and Foundations Division **96**(5): 1629-1653.

Dunn, I. S., L. R. Anderson and F. W. Kiefer (1980). Fundamentals of geotechnical analysis, Wiley New York.

Erickson, H. L. and A. Drescher (2002). "Bearing capacity of circular footings." Journal of geotechnical and geoenvironmental engineering **128**(1): 38-43.

Fonseca, A. (2001). "Load Tests on Residual Soil and Settlement Prediction on Shallow Foundation." Journal of Geotechnical and Geoenvironmental Engineering **127**(10): 869-883.

Fonseca, A. V. d. (2001). "Load Tests on residual soil and settlement prediction on shallow foundation." Journal of geotechnical and geoenvironmental engineering **127**(10): 869-883.

Frydman, S. and H. J. Burd (1997). "Numerical studies of bearing-capacity factor N γ." Journal of geotechnical and geoenvironmental engineering **123**(1): 20-29.

Griffiths, D. (1989). "Computation of collapse loads in geomechanics by finite elements." Ingenieur-Archiv **59**(3): 237-244.

Griffiths, D., G. A. Fenton and N. Manoharan (2002). "Bearing capacity of rough rigid strip footing on cohesive soil: probabilistic study." Journal of geotechnical and geoenvironmental engineering **128**(9): 743-755.

Hansen, J. B. (1970). "A revised and extended formula for bearing capacity."

Janbu, N., E. Hjeldnes, K. Senneset, L. Grande, S. Nordal and A. Skotheim TBA 5100 Theoretical Soil Mechanics. Manual

L. Grande and A. Emdal, Department of Civil and Transport Engineering, NTNU; 139 - 172.

Larsson, R. (2001). "Investigations and load tests in clay till." Statens geotekniska institut, Rapport(59).

Lee, J. and R. Salgado (2002). "Estimation of footing settlement in sand." The International Journal Geomechanics **2**(1): 1-28.

Meyerhof, G. (1951). "The Ultimate Bearing Capacity of Foudations." Geotechnique **2**(4): 301-332.

Meyerhof, G. (1955). "Influence of roughness of base and ground-water conditions on the ultimate bearing capacity of foundations." Geotechnique **5**(3): 227-242.

Meyerhof, G. (1956). "Penetration tests and bearing capacity of cohesionless soils." Journal of the Soil Mechanics and Foundation Division **82**(1): 1-19.

Meyerhof, G. G. (1963). "Some recent research on the bearing capacity of foundations." Canadian Geotechnical Journal **1**(1): 16-26.

Meyerhof, G. G. (1965). "Shallow foundations." Journal of Soil Mechanics & Foundations Div **91**(Proc. Paper 4275).

Murthy, V. (2007). Textbook of Soil Mechanics and Foundation Engineering.

Peck, R. B., W. E. Hanson and T. H. Thornburn (1974). Foundation engineering, Wiley New York.

Prandtl, L. (1920). "Über die härte plastischer körper." Nachrichten von der Gesellschaft der Wissenschaften zu Goettingen, Mathematisch-Physikalische Klasse **1920**: 74-85.

Robertson, P. (1990). "Soil classification using the cone penetration test." Canadian Geotechnical Journal **27**(1): 151-158.

Schanz, T., P. Vermeer and P. Bonnier (1999). The hardening soil model: formulation and verification. Beyond 2000 in computational geotechnics: 10 years of PLAXIS International; proceedings of the International Symposium beyond 2000 in Computational Geotechnics, Amsterdam, The Netherlands, 18-20 March 1999, Rotterdam: Taylor & Francis.

Skempton, A. (1951). "The bearing capacity of clays."

Sloan, S. and M. F. Randolph (1982). "Numerical prediction of collapse loads using finite element methods." International Journal for Numerical and Analytical Methods in Geomechanics **6**(1): 47-76.

Taiebat, H. A. and J. P. Carter (2000). "Numerical studies of the bearing capacity of shallow foundations on cohesive soil subjected to combined loading." Geotechnique **50**(4): 409-418.

Terzaghi, K. (1943). "Theoretical soil mechanics."

Terzaghi, K., R. B. Peck and G. Mesri (1996). Soil mechanics in engineering practice, Wiley-Interscience.

Vesic, A. S. (1973). "ANALYSIS OF ULTIMATE LOADS OF SHALLOW FOUNDATIONS." ASCE J Soil Mech Found Div **99**(SM1): 45-73.

Wood, D. M. (2004). Geotechnical modelling, Taylor & Francis.

APPENDICES

APPENDIX A – SOME INFORMATIVE TABLES AND FIGURES

Table A.1 Soil models and model parameters used in PLAXIS program.

Category	Index/Physical		Strength			Compressibility and Consolidation						Permeability	
	γ_{wet}	γ_{dry}	c'	ϕ'	ψ	E'_{ref}	ν'	λ^*	κ^*	OCR	m	k_v	k_h
Name of Symbol	Wet unit weight	Dry unit weight	Soil cohesion (CID Test)	Friction angle (CID Test)	Dilatancy angle	Drained Modulus (CID, 50% cut)	Poison's ratio	See legend	See legend	Overconsolation ratio	Power for stress level dependency	Coefficient of vertical permeability	Coefficient of horizontal permeability
Unit	kN/m^3	kN/m^3	kPa	Degree	Degree	kPa							
												m/day	m/day
Model Symbol													
SSM	R	R	R	R	R	R	R	R	R	R		R	R
HSM	R	R	R	R	R	R	R			R	R	R	R
MCM	R	R	R	R	R	R	R			R		R	R
SSCM+	R	R	R	R	R	R	R	R	R	R		R	R
EM	R	R				R	R					R	R

Legend:
SSM = Soft Soil Model
HSM = Hardening Soil Model
MCM = Mohr Coulomb Model
SSCM = Soft Soil Creep Model
EM = Elastic Model
$\lambda^* = CR/2.303$
$\kappa^* = RR/2.303$
R = Required
+ = Additional parameter is μ^*, which is called the modified creep index

Table A.2 Equations for computing E_s by making use of SPT and CPT values in kPa.

Soil	SPT	CPT
Sand (normally consolidated)	500 (N_{cor} + 100) (35000 to 50000) log (N_{cor} (USSR Practice)	2 to 4 q_c (1+D_r^2) q_c
Sand (saturated)	250 ((N_{cor} +15)	---
Sand (overconsolidated)	---	6 to 30 q_c
Gravelly sand and gravel	1200 ((N_{cor} + 6)	
Clayey sand	320 ((N_{cor} + 15)	3 to 6 q_c
Silty sand	300 ((N_{cor} + 6)	1 to 2 q_c
Soft clay	---	3 to 8 q_c

Table A.3 Typical range of values for Poisson's ratio.

Type of soil	μ
Clay, saturated	0.4 – 0.5
Clay, unsaturated	0.1 – 0.3
Sandy clay	0.2 – 0.3
Silt	0.3 – 0.35
Sand (dense)	0.2 – 0.4
Coarse (void ratio = 0.4 to 0.7)	0.15
Fine grained (void ratio = 0.4 to 0.7)	0.25
Rock	0.1 – 0.4

5.3 Clay strength from SPT data

- As a first approximation $C_u = 5$ SPT is commonly used. However this correlation is known to vary from 2 to 8.
- The overburden correction is not required for SPT values in clays.
- Sensitivity of clay affects the results.

Table 5.3 Clay strength from SPT data.

Material	*Description*	*SPT – N (blows/300 mm)*	*Strength*
Clay	V. Soft	≤2	0–12 kPa
	Soft	2–5	12–25 kPa
	Firm	5–10	25–50 kPa
	Stiff	10–20	50–100 kPa
	V. Stiff	20–40	100–200 kPa
	Hard	>40	>200 kPa

- An indication of the variability of the correlation in the literature is as follows
  - Sower's graphs uses $C_u = 4$ N for high plasticity clays and increasing to about 15 N for low plasticity clays.
  - Contrast with Stroud and Butler's (1975) graph which shows Cu = 4.5 N for PI > 30%, and increasing to Cu = 8 N for low plasticity clays (PI = 15%).
- Therefore use with caution, and with some local correlations.

Figure A.1 Strength parameters from SPT-value in clay.

5.4 Clean sand strength from SPT data

- The values vary from corrected to uncorrected N values and type of sand.
- The SPT – value can be used to determine the degree of compactness of a cohesionless soil. However, it is the soil friction angle that is used as the strength parameter.

Table 5.4 Strength from SPT on clean medium size sands only.

Description	*Relative density D_r*	*SPT – N (blows/300 mm)*		*Strength*
		Uncorrected field value	*Corrected value*	*Friction angle*
V. Loose	<15%	$N \leq 4$	$(N_o)_{60} \leq 3$	$\phi < 28°$
Loose	15–35%	$N = 4–10$	$(N_o)_{60} = 3–8$	$\phi = 28–30°$
Med dense	35–65%	$N = 10–30$	$(N_o)_{60} = 8–25$	$\phi = 30–40°$
Dense	65–85%	$N = 30–50$	$(N_o)_{60} = 25–42$	$\phi = 40–45°$
V. Dense	>85%	$N > 50$	$(N_o)_{60} > 42$	$\phi = 45°–50°$
	100%		$(N_o)_{60} = 60$	$\phi = 50°$

- Reduce ϕ by 5° for clayey sand.
- Increase ϕ by 5° for gravely sand.

5.5 Fine and coarse sand strength from SPT data

- Fine sands have reduced values from the table above while coarse sand has an increased strength value.
- The corrected N value is used in the table below.

Table 5.5 Strength from corrected SPT value on clean fine and coarse size sands.

Description	*Relative density D_r*	*Corrected SPT – N (blows/300 mm)*			*Strength*
		Fine sand	*Medium*	*Coarse sand*	
V. Loose	<15%	$(N_o)_{60} \leq 3$	$(N_o)_{60} \leq 3$	$(N_o)_{60} \leq 3$	$\phi < 28°$
Loose	15–35%	$(N_o)_{60} = 3–7$	$(N_o)_{60} = 3–8$	$(N_o)_{60} = 3–8$	$\phi = 28–30°$
Med dense	35–65%	$(N_o)_{60} = 7–23$	$(N_o)_{60} = 8–25$	$(N_o)_{60} = 8–27$	$\phi = 30–40°$
Dense	65–85%	$(N_o)_{60} = 23–40$	$(N_o)_{60} = 25-43$	$(N_o)_{60} = 27–47$	$\phi = 40–45°$
V. Dense	>85%	$(N_o)_{60} > 40$	$(N_o)_{60} > 43$	$(N_o)_{60} > 47$	$\phi = 45–50°$
	100%	$(N_o)_{60} = 55$	$(N_o)_{60} = 60$	$(N_o)_{60} = 65$	$\phi = 50°$

Figure A.2 Strength parameters from SPT-value in sand.

7.9 Effective strength of cohesive soils

- The typical peak strength is shown in the table.
- Allowance should be made for long term softening of the clay, with loss of effective cohesion.
- Remoulded strength and residual strength values would have a reduction in both cohesion and friction.

Table 7.9 Effective strength of cohesive soils

Type	*Soil description/state*	*Effective cohesion (kPa)*	*Friction angle (degrees)*
Cohesive	Soft – organic	5–10	10–20
	Soft – non organic	10–20	15–25
	Stiff	20–50	20–30
	Hard	50–100	25–30

Figure A.3 Strength parameters in cohesive soils

Table 11.7 Elastic parameters of various soils.

Type	*Strength of soil*	*Elastic modulus, E (MPa)*	
		Short term	*Long term*
Gravel	Loose	25–50	
	Medium	50–100	
	Dense	100–200	
Medium to coarse sand	Very loose	<5	
	Loose	3–10	
	Medium dense	8–30	
	Dense	25–50	
	Very dense	40–100	
Fine sand	Loose	5–10	
	Medium	10–25	
	Dense	25–50	
Silt	Soft	<10	<8
	Stiff	10–20	8–15
	Hard	>20	>15
Clay	Very soft	<3	<2
	Soft	2–7	1–5
	Firm	5–12	4–8
	Stiff	10–25	7–20
	Very stiff	20–50	15–35
	Hard	40–80	30–60

Figure A.4 Elastic modulus of various soils.

APPENDIX B – SOIL DATA AT TORNHILL SITE

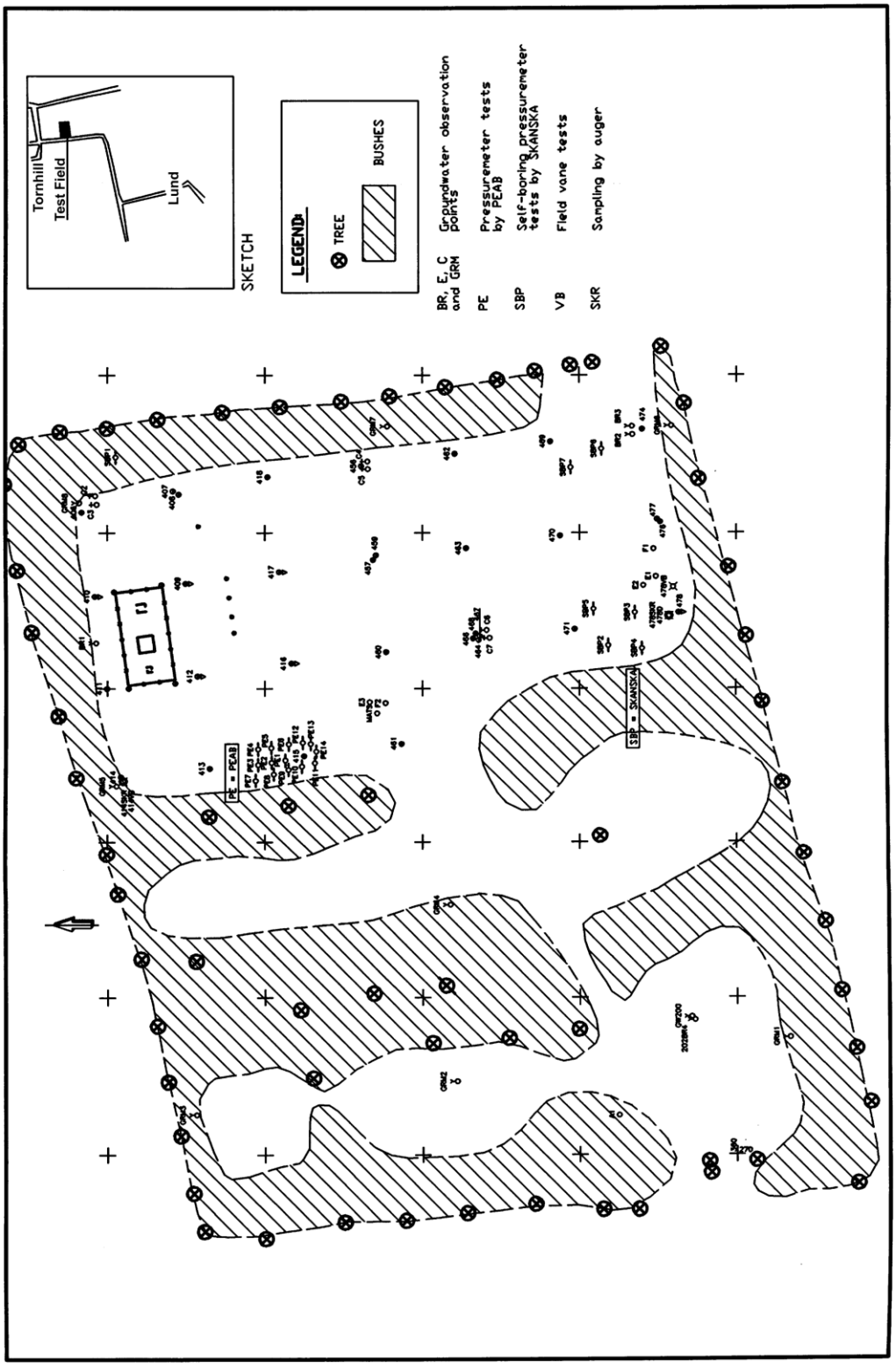

Figure B.1 Layout of the test field and the investigation points.

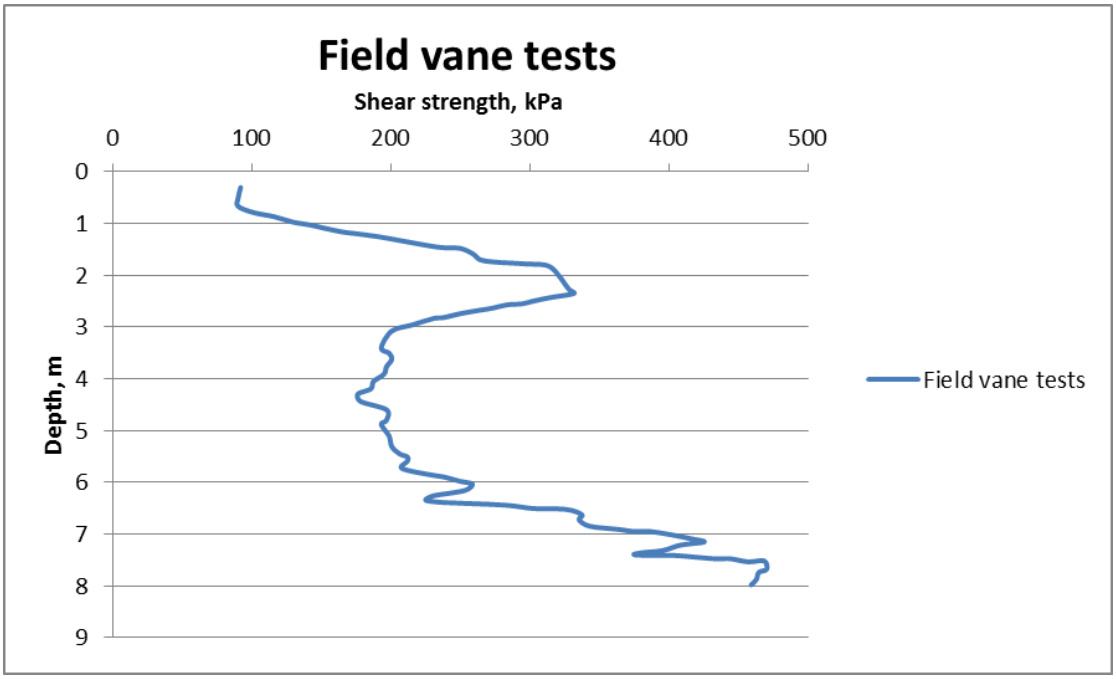

Figure B.2 Results of the field vane test.

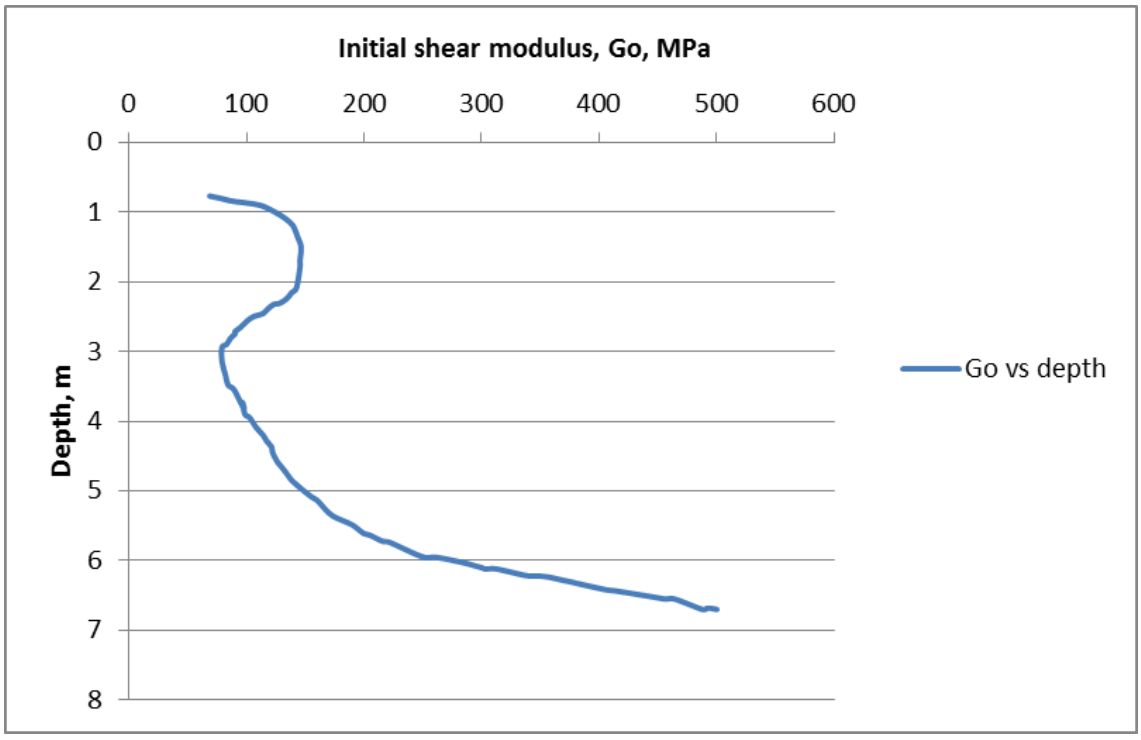

Figure B.3 Initial shear modulus with depth from seismic CPT tests at Tornhill.

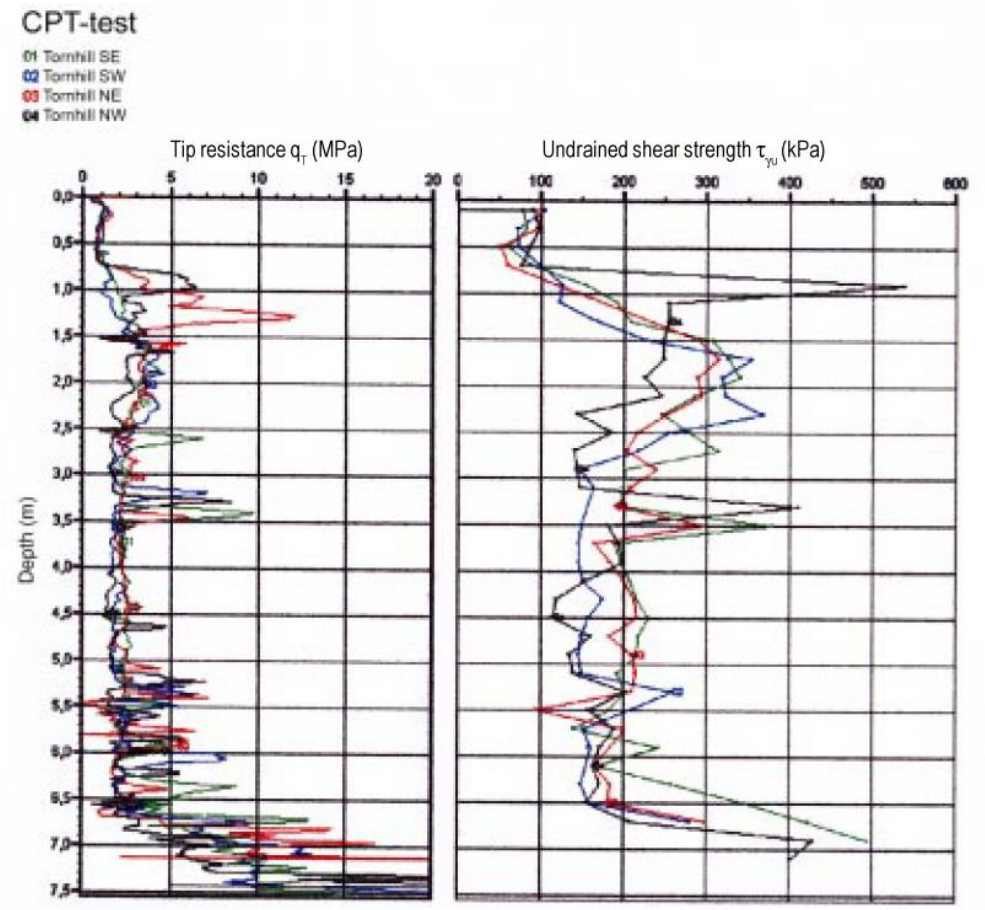

Figure B.4 Results from CPT-tests.

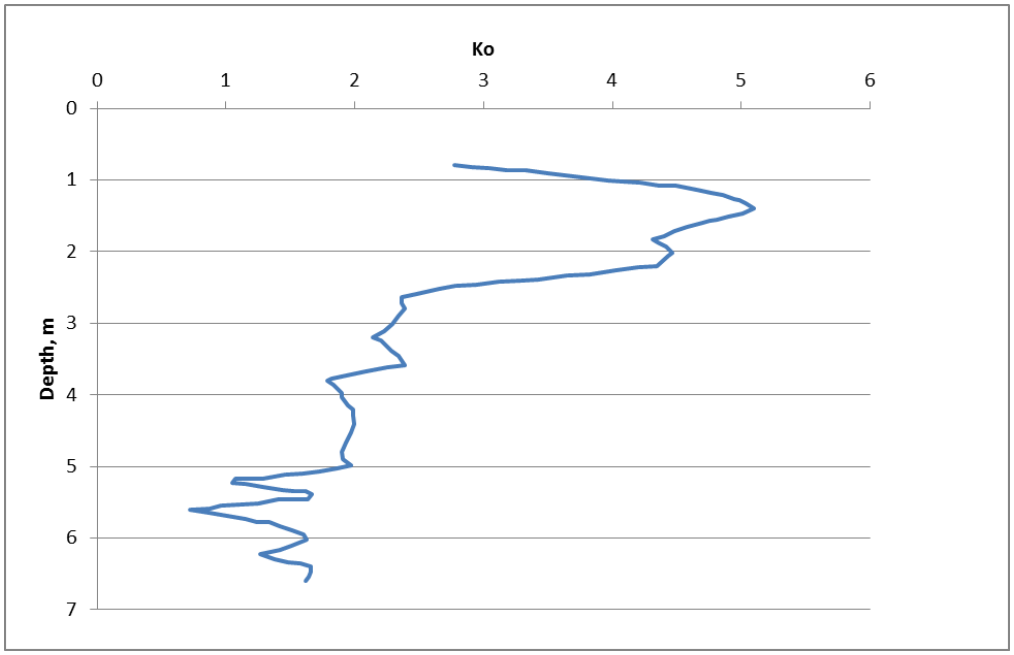

Figure B.5 Coefficient of horizontal earth pressure from the horizontal index measured in the dilatometer test at Tornhill.

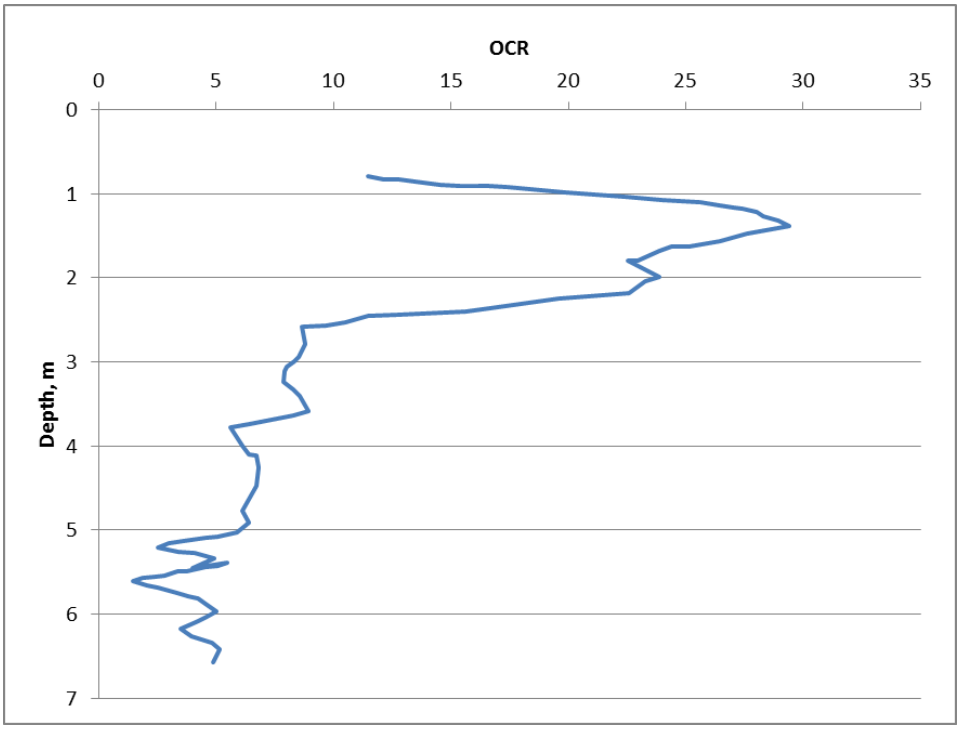

Figure B.6 Overconsolidation ratio (OCR) from the horizontal index measured in the dilatometer test at Tornhill.

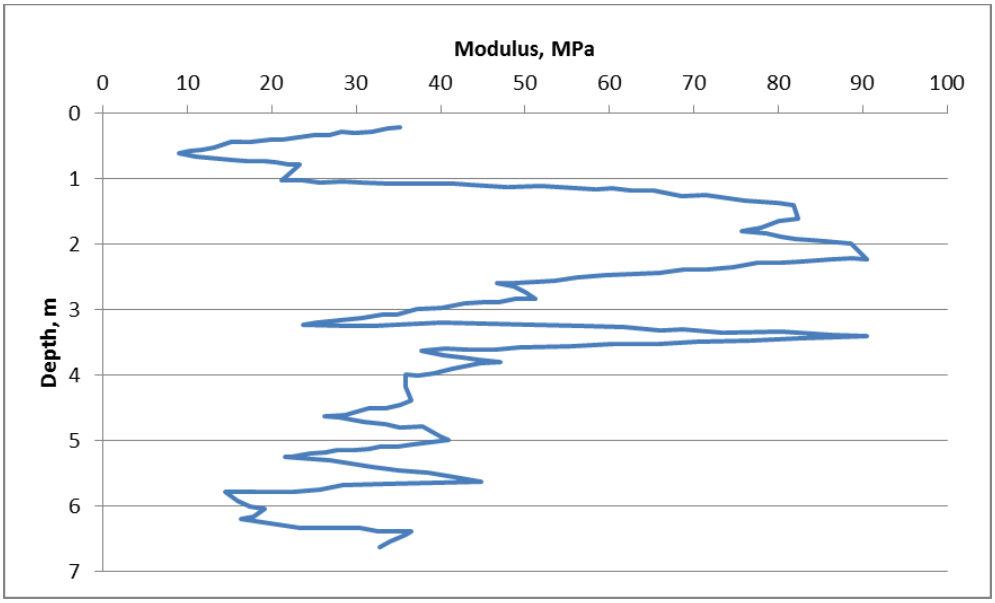

Figure B.7 Evaluated modulus from the dilatometer test at Tornhill.

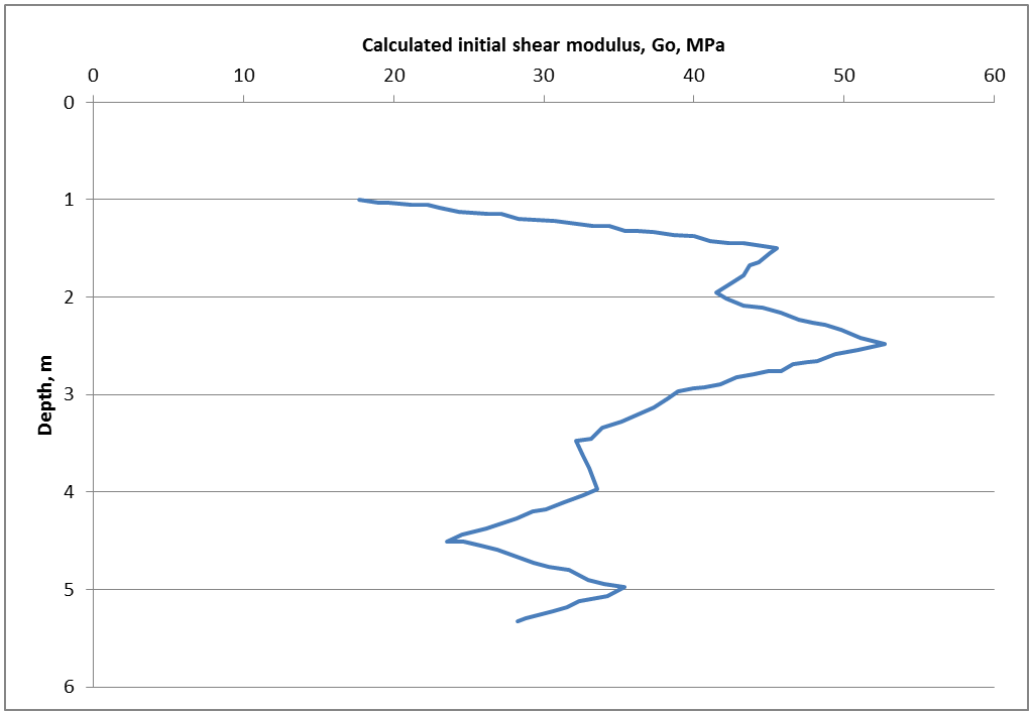

Figure B.8 Initial shear modulus at in situ stresses calculated from the pressuremeter tests.

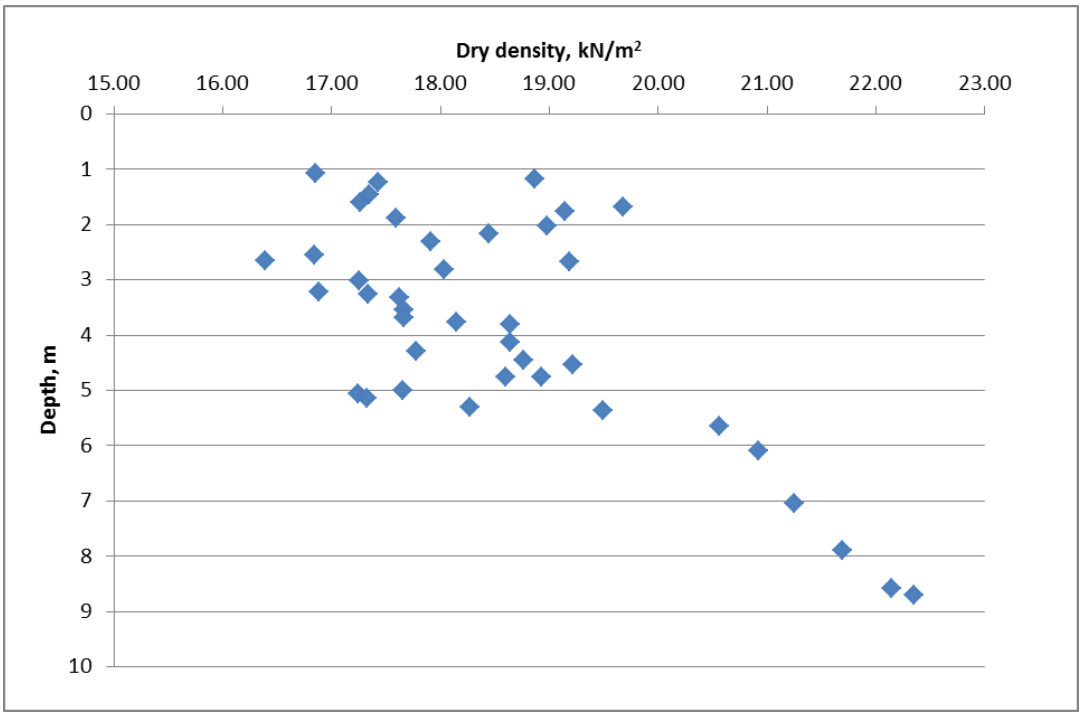

Figure B.9 Measured dry densities from the test field.

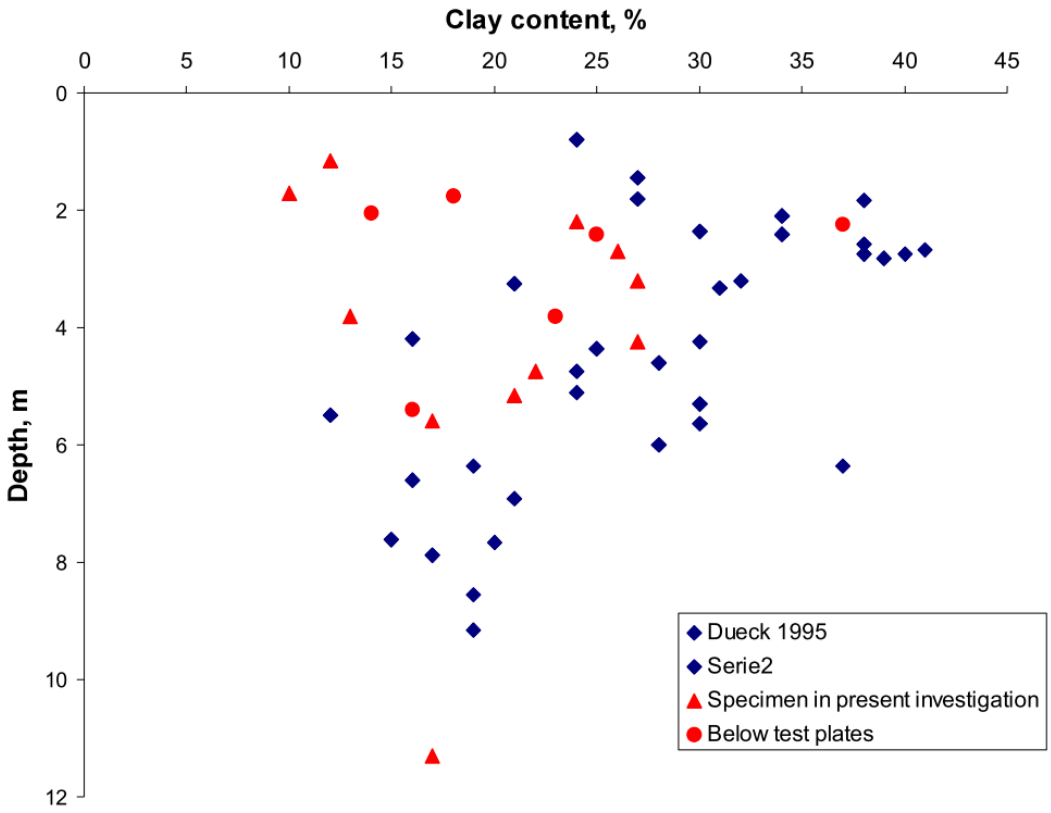

Figure B.10 Measured clay contents from the test field.

APPENDIX C – SOIL DATA AND PLAXIS RESULTS ON SAPROLITIC SOIL

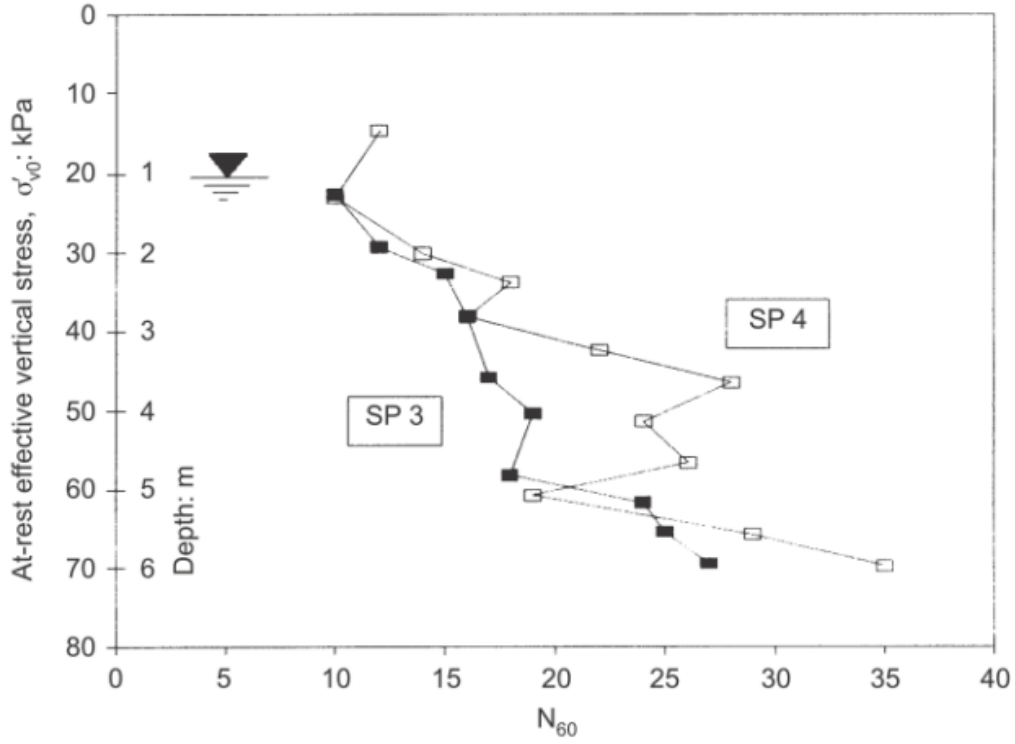

Figure C.1 SPT test results versus the at-rest effective vertical stress.

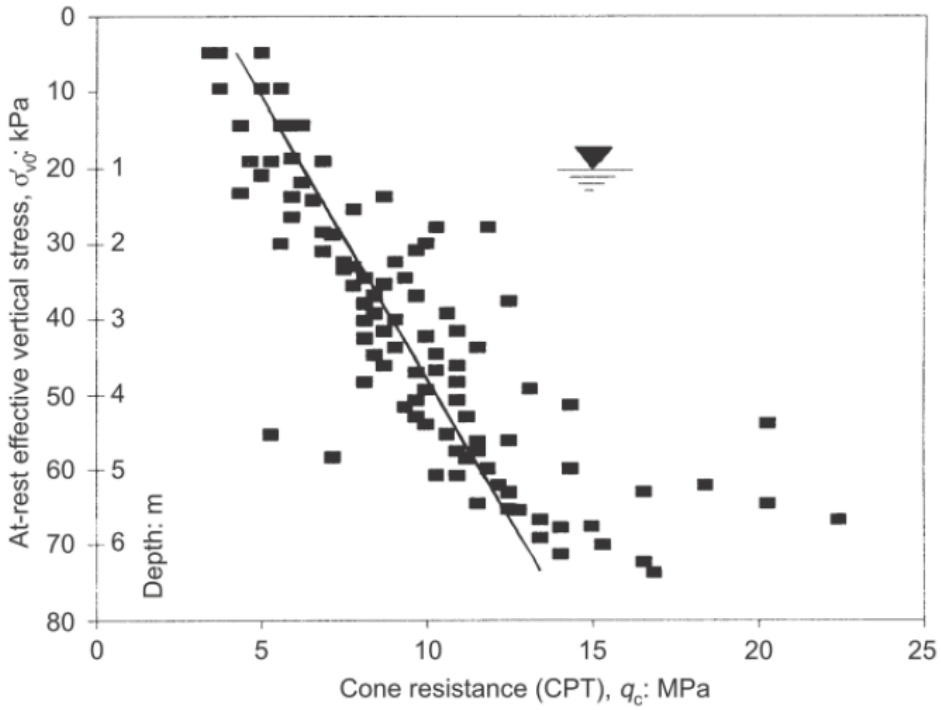

Figure C.2 CPT test results versus the at-rest effective vertical stress.

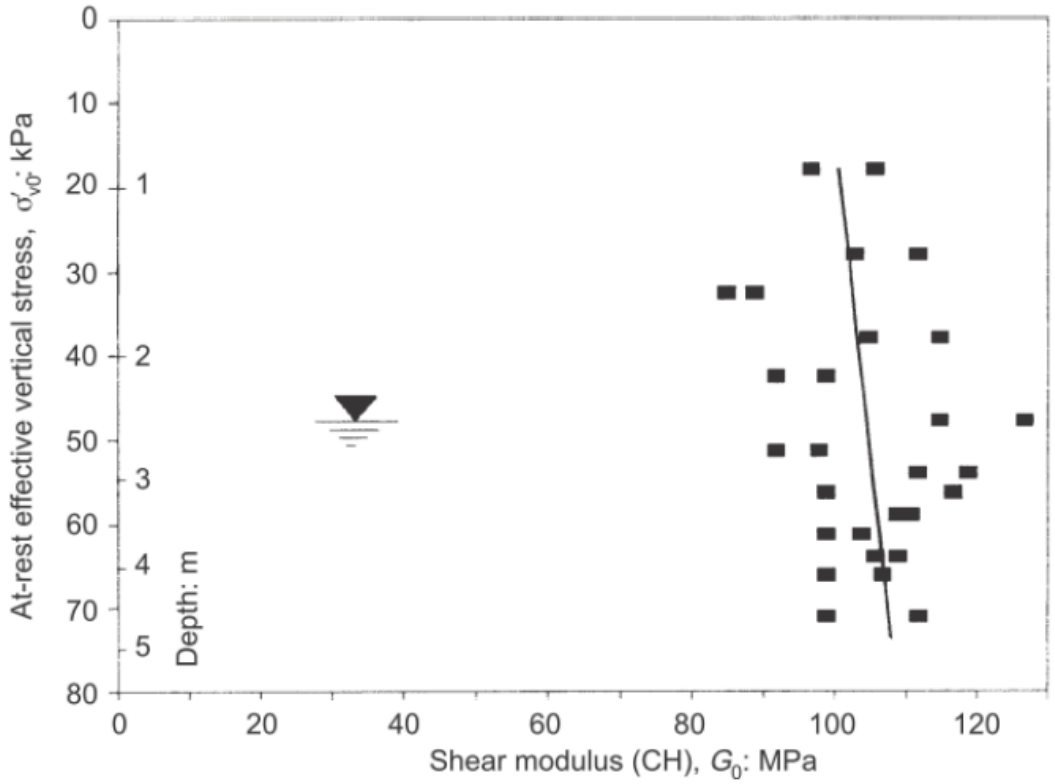

Figure C.3 CH test results versus the at-rest effective vertical stress.

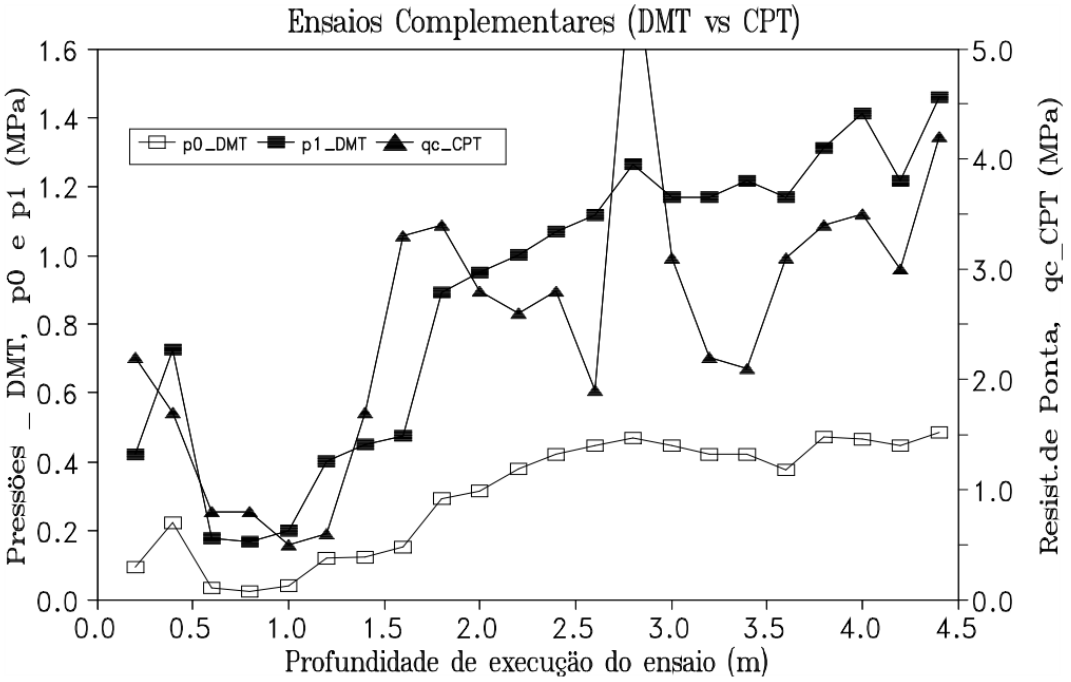

Figure C.4 DMT together with CPT with depth.

PMT tests (WL at 2,55 m)

z (m)	E_{pm} (MPa) ν=0,33	p'_0 (kPa)	p_f (kPa)	p_L (kPa)
1,55	9,4	10,0	570	980
3,00	8,2	18,4	580	1000
4,70	5,9	22,6	680	1000
5,85	13,3	27,6	1220	1555

Figure C.5 PMT test results.

Shera wave velocities

Cross-hole tetst ***Vs* (CH)**

Prof. (m)	Vs (m/s)	
1,0	220	230
1,5	227	237
2,0	229	240
2,5	240	252
3,0	244	237
3,5	236	233
4,0	233	230
4,5	309	312
5,0	303	300

$\gamma = 20$ kN/m^3

Figure C.6 Shear wave velocities.

For σ_c' = 100 kPa:

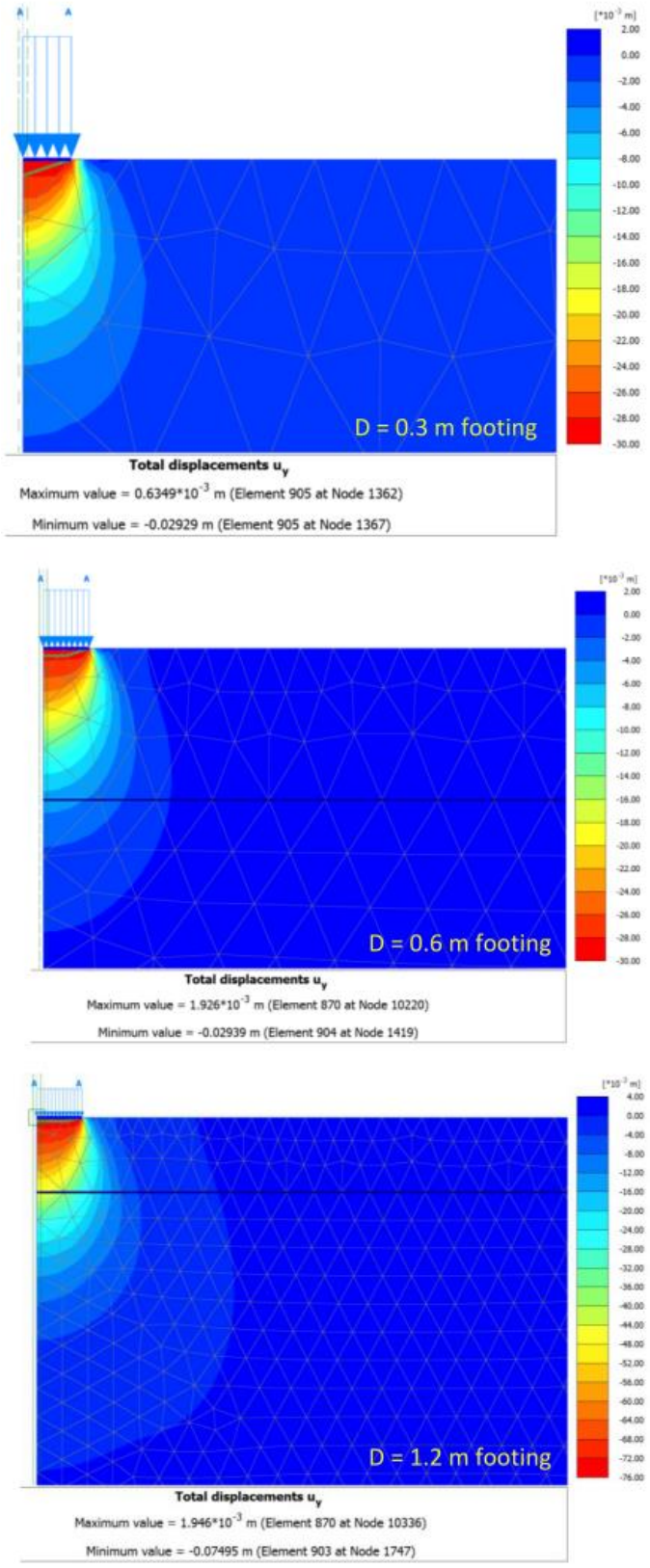

Figure C.7 Vertical displacements transferred to the soil at Porto site in saprolitic soil for σ_c' = 100 kPa.

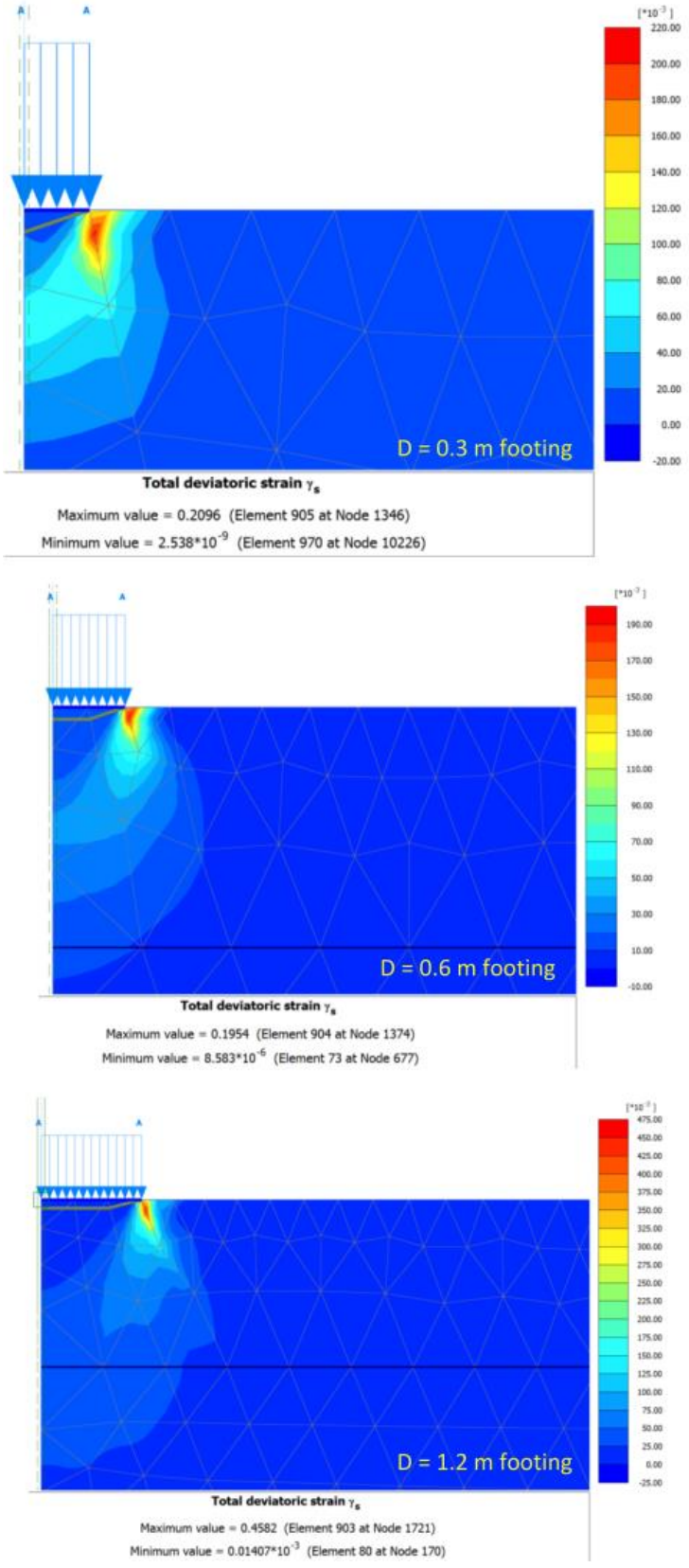

Figure C.8 Total deviatoric strains for the total ground pressure at Porto site in saprolitic soil for σ'_c = 100 kPa.

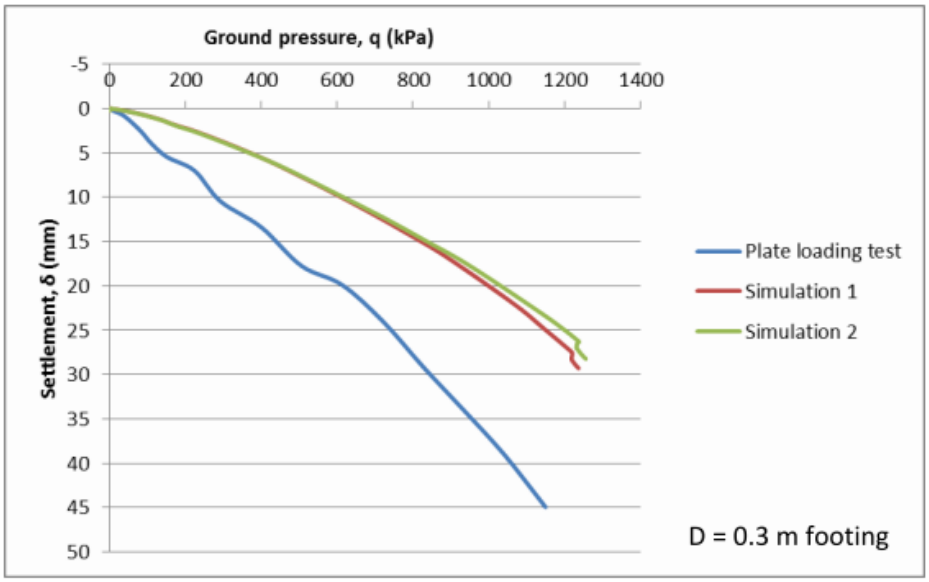

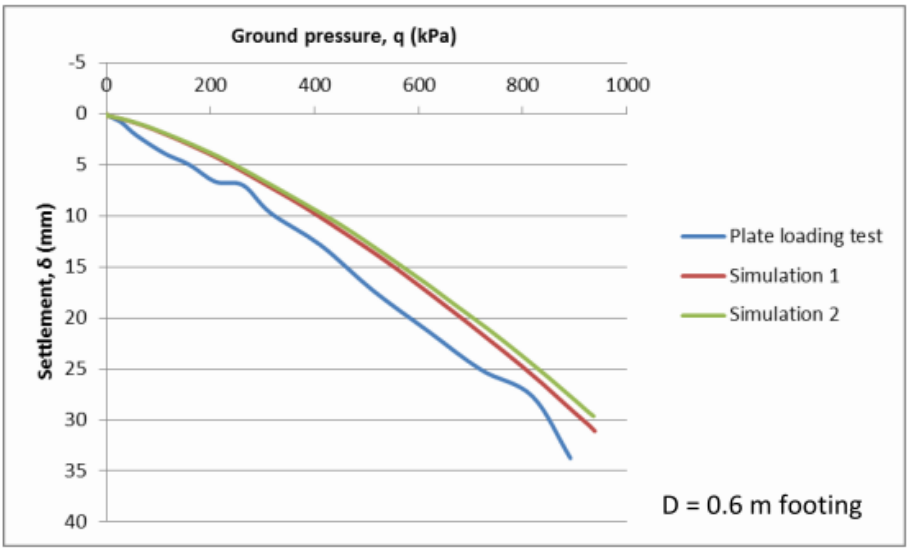

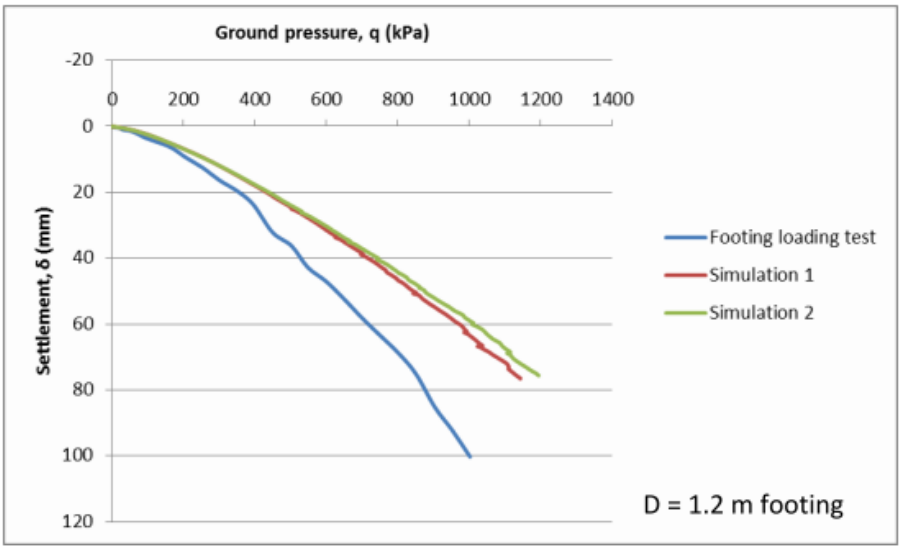

Figure C.9 Comparision of experimental and numerical load-settlement curves at Porto site in saprolitic soil for σ'_c = 100 kPa.

APPENDIX D – SOIL DATA AT TEXAS A&M FOOTING LOAD TEST SITE

SPT test results:

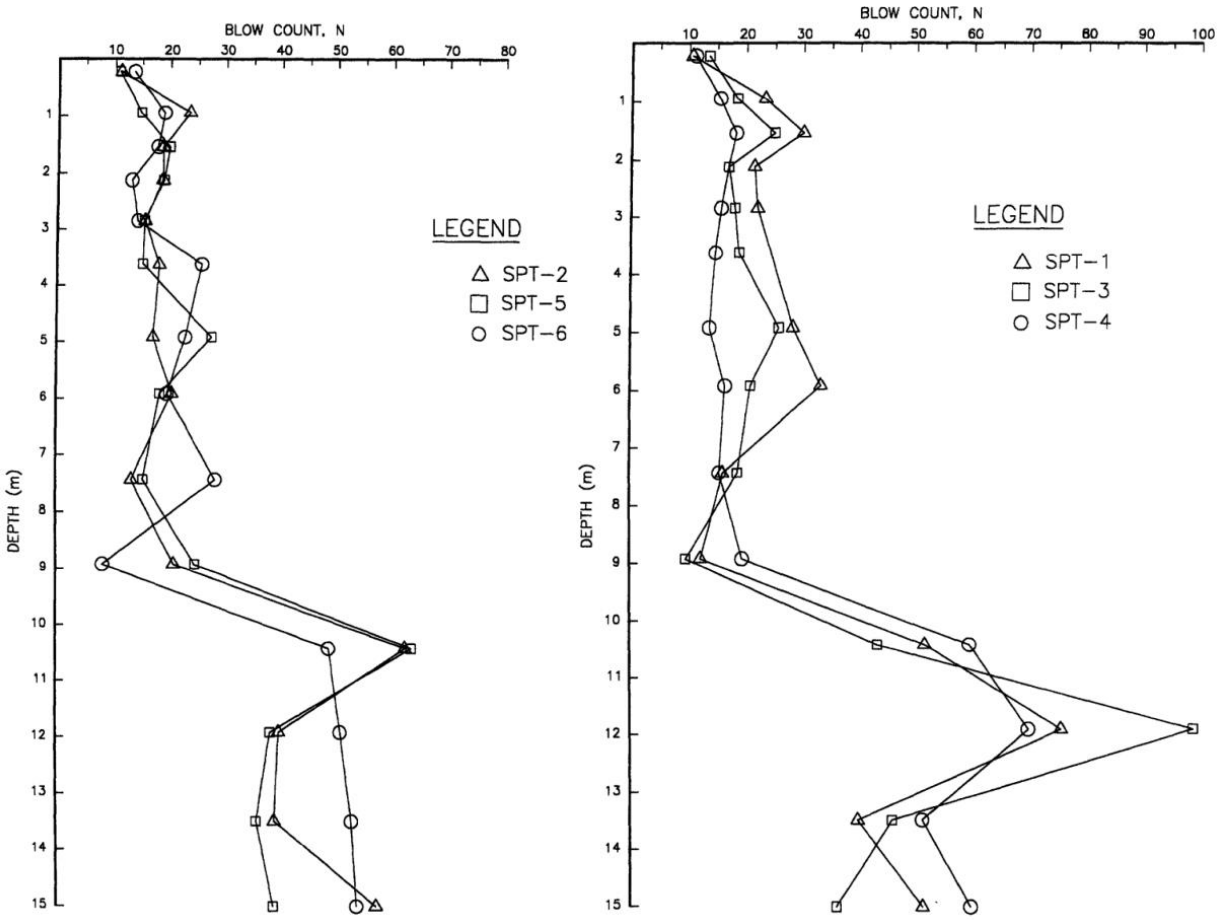

CPT test results:

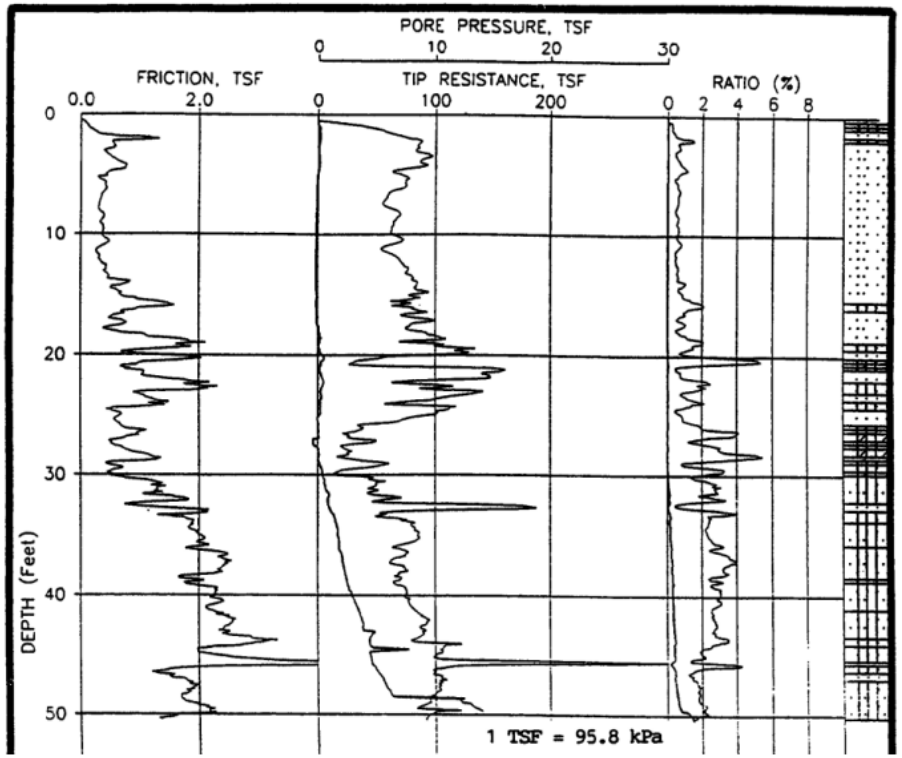

CPT 1

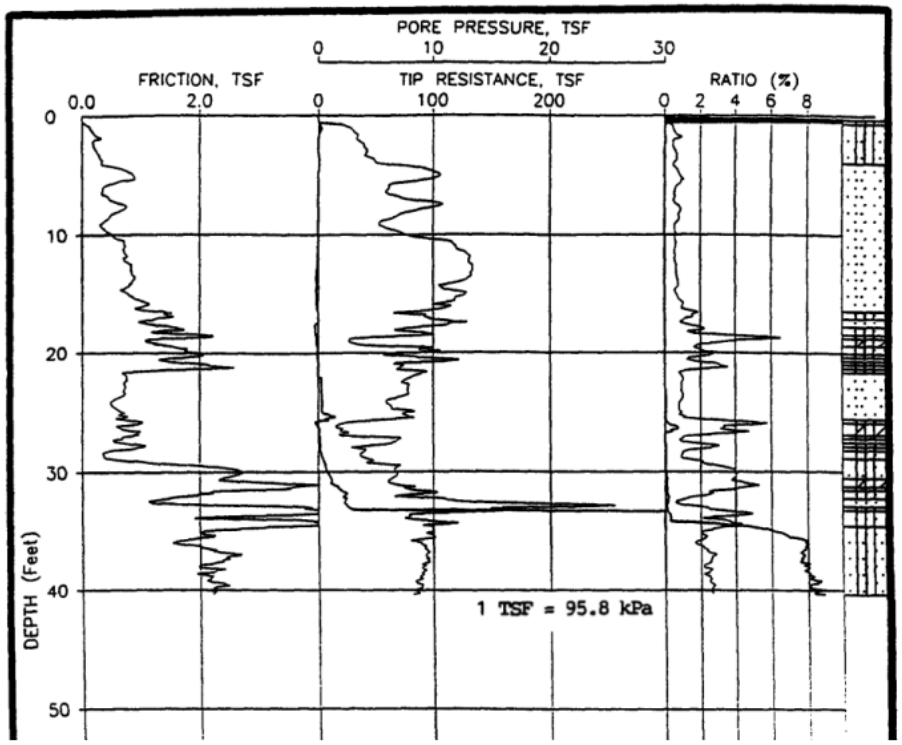

CPT 2

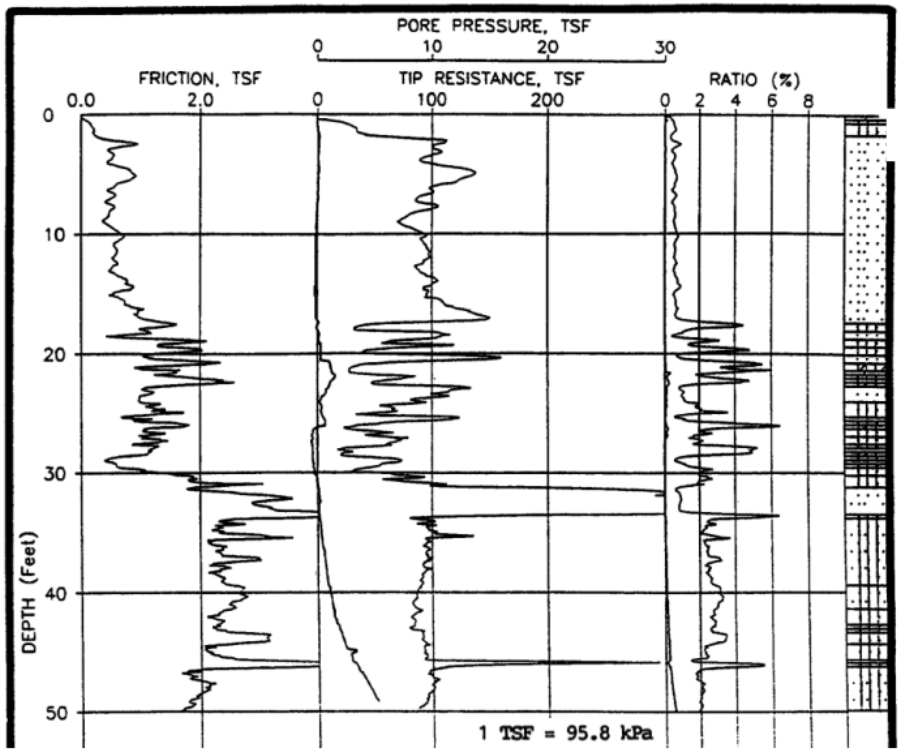

CPT 5

CPT 6

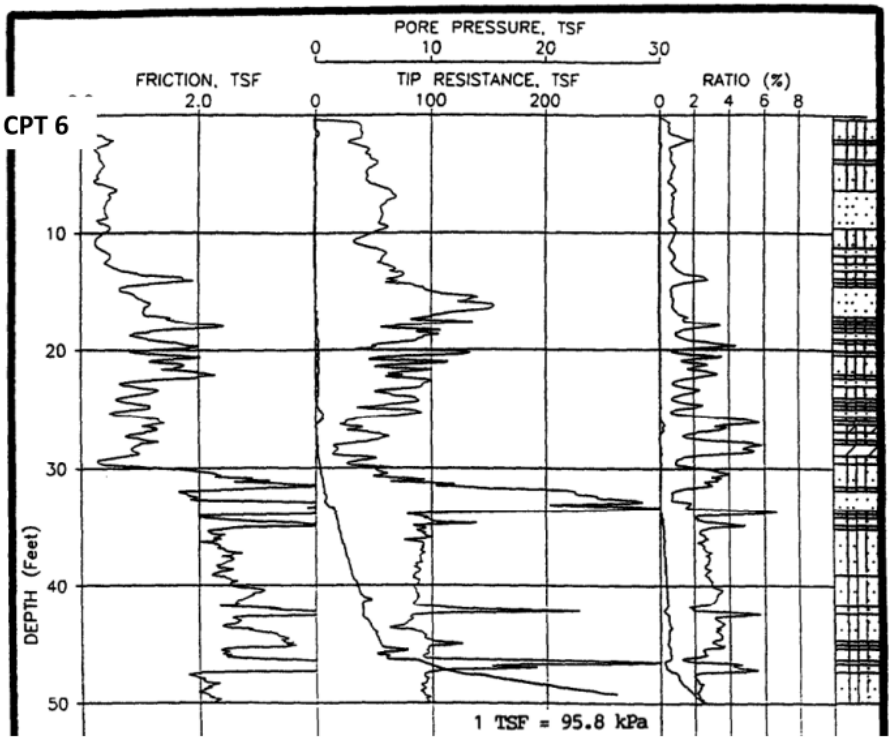

CPT 6

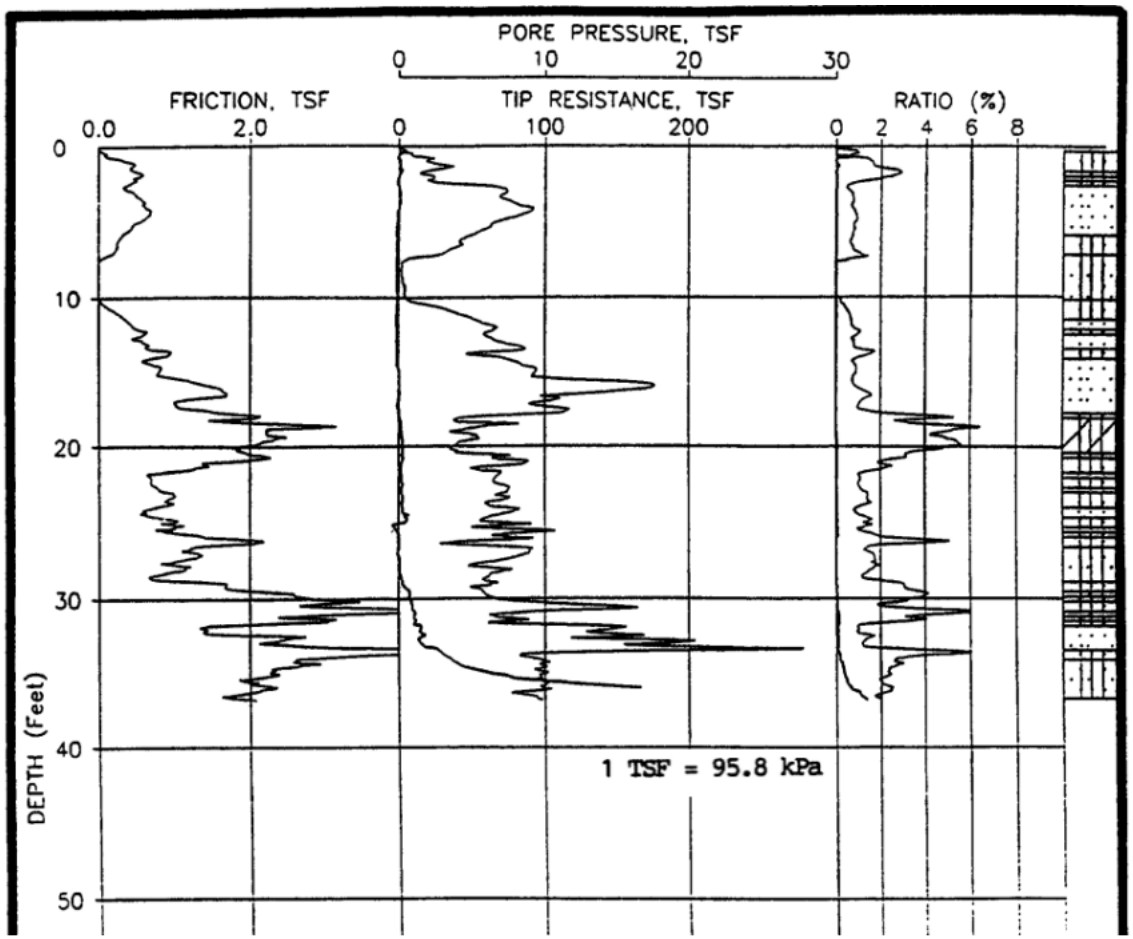
PORE PRESSURE, TSF
0
10
20
30
FRICTION, TSF
0.0
2.0
TIP RESISTANCE, TSF
0
100
200
RATIO (%)
0
2
4
6
8
0
10
20
30
40
50
DEPTH (Feet)
1 TSF = 95.8 kPa

CPT 7

APPENDIX E - CD

The CD contains:

- Numerical simulations of three case studies
- Excel files of load-settlement curves from simulations
- The master thesis